Mechanistic Investigation of Skin Barrier Perturbation Induced by Surfactants in the Presence of Humectants

by

Saswata Ghosh

Submitted to the Department of Chemical Engineering
In partial fulfillment of the requirements for the degree of

Doctor of Philosophy in Chemical Engineering

at the

MASSACHUSETTS INSTITUTE OF TECHNOLOGY

January 2007

[February 2007]

Author.....
Department of Chemical Engineering
January 8, 2007

Certified by.....
Daniel Blankschtein
Professor of Chemical Engineering
Thesis Supervisor

Accepted by.....
William Deen
Professor of Chemical Engineering
Chairman, Committee for Graduate Students

Mechanistic Investigation of Skin Barrier Perturbation Induced by Surfactants in the Presence of Humectants

by

Saswata Ghosh

Submitted to the Department of Chemical Engineering on
January 8, 2007 in Partial Fulfillment of the
Requirements for the Degree of
Doctor of Philosophy in Chemical Engineering

Abstract

The stratum corneum (SC) of the skin functions as a barrier between the body and the environment. Surfactants such as Sodium Dodecyl Sulfate (SDS) are used in skin cleansers and in skin-care formulations because of their ability to stabilize oil-water emulsions and clean the surface of the skin. However, they also have adverse effects on the skin barrier, including enhancing skin barrier perturbation which may lead to a disruption of the protective functions carried out by the skin barrier. On the other hand, humectants, such as Glycerol, which maintain the natural water content of the skin and preserve the skin barrier, have been shown to mitigate surfactant-induced skin barrier perturbation. The primary objective of this thesis was to develop a mechanistic understanding, including visualization and quantification, of: (i) how aqueous surfactant solutions, once in contact with the skin, can induce skin barrier perturbation, and (ii) how surfactant-induced skin barrier perturbation can be effectively mitigated through the addition of humectants to the aqueous surfactant contacting solutions.

SDS monomers self-assemble to form micelles at a SDS concentration above the Critical Micelle Concentration (CMC). The SDS skin penetration and associated skin barrier perturbation is dose-dependent, that is, it increases with an increase in the total SDS concentration above the CMC of SDS. However, when Glycerol was added to the aqueous SDS contacting solution, through in vitro quantitative skin radioactivity assays using ^{14}C radiolabeled SDS, I found that the dose-dependence in SDS skin penetration was almost completely eliminated. This is because the addition of Glycerol hinders the ability of the SDS micelles to penetrate into the skin barrier through aqueous pores that exist in the SC. In vitro Mannitol skin permeability and average skin electrical resistivity measurements, in the context of a hindered-transport aqueous porous pathway model of the SC, demonstrated that the addition of 10 wt% Glycerol: (1) reduces the average aqueous pore radius resulting from exposure of the skin to the aqueous SDS contacting solution from 33±5Å to 20±5Å, such that a SDS micelle of radius 18.5±1Å (as determined using dynamic light scattering (DLS) measurements) experiences significant steric hindrance and cannot penetrate into the SC, and (2) reduces the porosity-to-tortuosity ratio of the aqueous pores in the SC by more than 50%, thereby further reducing the ability of the SDS micelles to penetrate into the SC and perturb the skin barrier.

In vitro skin electrical current measurements can be used effectively to *rank* aqueous contacting solutions containing surfactants and humectants (the enhancer), relative to a PBS aqueous contacting solution (the control), based on their ability to perturb the skin aqueous pores. Specifically, an in vitro ranking metric was introduced using the enhancement in the skin electrical current induced by an enhancer relative to the control. For this study, I considered aqueous contacting solutions of the following chemicals: (1) humectants – Glycerol and Propylene Glycol, (2) surfactants – SDS and $C_{12}E_6$ (Dodecyl Hexa (Ethylene Oxide)), and (3) a

control – PBS. Utilizing the in vitro ranking metric, the aqueous solutions above contacting the skin were ranked as follows (from the mildest to the harshest): Glycerol < Propylene Glycol < PBS < $C_{12}E_6$ < SDS. In order to further develop this ranking methodology, which can potentially lead to the reduction of several costly operations associated with identifying surfactant/humectant systems which are mild to the skin, such as, in vivo clinical testing and trial-and-error screening, it was important to correlate the in vitro ranking metric findings with direct in vivo skin barrier measurements. For this purpose, in vivo *soap chamber* measurements were carried out on human subjects, using the aqueous surfactant/humectant solutions described above. The results of these in vivo measurements of skin barrier perturbation were found to be consistent with the ranking results obtained using the in vitro ranking metric for the aqueous surfactant and humectant contacting solutions considered. In addition, in vivo soap chamber measurements were carried out for aqueous SDS+Glycerol contacting solutions. These in vivo measurements indicated that adding Glycerol to a SDS aqueous contacting solution significantly mitigates SDS-induced in vivo skin barrier perturbation, which is consistent with the results of my in vitro skin electrical current and Mannitol skin permeability measurements.

In order to *visualize* the effects of aqueous surfactant/humectant systems on the skin barrier, an in vitro dual-channel two-photon fluorescence microscopy (TPM) visualization study was carried out. TPM is a non-invasive imaging technique based on two-photon induced nonlinear excitations of fluorophores, with the capability for deep-tissue imaging (up to several hundred micrometers). The following aqueous surfactant and humectant contacting solutions were studied: (i) SDS, (ii) SDS+Glycerol, (iii) SCI (a mild surfactant), (iv) PBS control, and (v) Glycerol. Sulforhodamine B (SRB), which is a hydrophilic fluorescent probe, was used to probe the effect of aqueous contacting solutions (i)-(v) on the skin barrier morphology. The results of this TPM visualization study revealed that SDS induces corneocyte damage by denaturing keratins and creating intra-corneocyte penetration pathways. On the other hand, SDS+Glycerol did not significantly induce corneocyte damage. The dual-channel TPM images corresponding to aqueous contacting solutions (iii)-(v) showed low SRB penetration into the corneocytes, as well as localization of the SRB probe within the lipid bilayers surrounding the corneocytes of the SC. Through a quantification of the amount of SRB that penetrated into the skin as a function of the skin depth, I found that adding Glycerol to SDS could significantly reduce the SDS-induced penetration depth of SRB, which provides evidence of the ability of Glycerol to mitigate SDS-induced skin barrier perturbation.

The fundamental understanding of surfactant-induced skin barrier perturbation in the presence of humectants developed in this thesis is of particular relevance to the cosmetic industry in enabling the formulation of mild, non-drying, skin-care products that contain surfactants and humectants. The novel TPM studies that visualize, as well as quantify, skin morphology upon exposure of the skin to surfactant/humectant systems, has the potential to be developed into a high-throughput imaging tool for the screening of new skin-care formulations. Such a strategy can simultaneously screen the skin-mildness potential of many skin-care formulations, thereby significantly speeding up the effort and time required to bring new skin-care formulations to the market. In addition to the practical impact on the formulation of mild skin-care products, this thesis has also advanced fundamental research carried out in the investigative dermatology and related health disciplines.

Thesis Advisor: Daniel Blankschtein
Title: Professor of Chemical Engineering

Acknowledgements

This thesis represents the culmination of a long-cherished dream of my mother, Madhusree Ghosh, who can only experience this from her heavenly abode. I remember her encouragement and inspiration every step of the long journey without which none of this would have been possible. I also dedicate this thesis to my father, Subrata Ghosh, who has and will always be there for me, during the crests as well as the troughs of life's experiences.

I would like to acknowledge my thesis advisor, Professor Daniel Blankschtein, for helping me focus on an important practical problem relevant to the skin-care and cosmetic industry. I have very much enjoyed our research discussions during the time spent at MIT, and also admire his incredible efforts in keeping the thesis on track, challenging me to set and exceed goals. I have learnt a lot from him that not only has stood me in good stead during this research experience, but should in the future as well. I am grateful for the guidance of my thesis committee: Professor William Deen and Professor Tania Phillips. The research meetings with them over the years yielded valuable insight for some of the experimental and theoretical investigations pursued in this thesis.

I would also like to acknowledge Dr. Sidney Hornby and Dr. Yohini Appa of Neutrogena Corporation for organizing clinical tests in association with Dr. Gary Grove of CyberDERM. It is always exciting to see correlation between lab studies and clinical tests, which lends validation to the key ideas developed in this thesis. I would also like to acknowledge past and present colleagues of the Blankschtein Lab at MIT, who have all been gracious friends and wonderful co-workers. Without them, much of the cheer and camaraderie that I enjoyed during this experience would be missng. The collaboration with the lab of Professor Peter So at MIT was instrumental in helping me obtain microscopy images of skin that yielded visual evidence for some of the ideas developed in this thesis. I am also grateful to Professor Alan Hatton's lab at MIT for introducing me to the light scattering equipment used for conducting light scattering studies reported in this thesis.

Finally, in addition to my parents, I would like to dedicate this thesis to my wife, Ankita Roy, who is also my closest friend. Pursuing a PhD thesis herself, her understanding of the sacrifices, efforts and commitment involved has always been perfect. Her patience and good humor have been an exceptional source of strength, and I wish her the very best as she completes her research voyage successfully.

Table of Contents

List of Figures

List of Tables

Chapter 1

1. Introduction

1.1. Research Motivation and Goals

Surfactants are used in skin care formulations because: (1) they can stabilize oil-in-water emulsions, and (2) being surface active, they can cleanse the surface of the skin. However, surfactants commonly encountered in skin care formulations can interact with the skin barrier in a variety of ways. They may first act on the skin surface, then penetrate into the deeper skin layers, and finally enter the general body circulation through blood capillaries in the dermis (see Section 1.5 for a discussion of the effects of surfactants on the skin). Since people use skin cleansers and skin care formulations repeatedly, and at times, very frequently, skin barrier insults due to surfactants are repetitive and frequent, and can induce a significant extent of skin barrier perturbation (1-5). A significant extent of skin barrier perturbation can, in turn, lead to a loss of the skin barrier protective functions, which can lead to various pathophysiological consequences (see Section 1.5). According to an estimate of the US Department of Labor, compensation benefits from skin diseases accounted for almost $200 million in California alone in 1990, and this figure has increased steadily in recent years (2). In a separate study, the economic burden of diseases pertaining to the skin and the skin barrier in the United States alone was estimated to be $35.9 billion in 1997 (3). In fact, it is widely accepted that skin diseases and disorders are the second highest of all occupational illnesses reported in the United States (3). However, it is also believed that skin diseases can, and should, be prevented (1-5). One possible way to achieve this

goal is to develop a fundamental, mechanistic understanding of the skin barrier responsible for the protective functions of the skin, whose disruption, for example, by surfactants in skin care products, may lead to various pathological and health conditions associated with the skin. In this thesis, I have carried out a mechanistic investigation of how surfactants may perturb the skin barrier, which may be of particular relevance to the cosmetic industry in enabling the formulation of milder, non-drying, skin care products that contain surfactants.

Research aimed at pursing the goal of minimizing surfactant-induced skin barrier perturbation has shown that humectants,[1] when present in a formulation with surfactants, can mitigate deleterious effects of surfactants on the skin barrier (6-15). Such a strategy is of tremendous practical relevance to a formulator interested in the formulation of milder surfactant-based skin care products. In order to create surfactant formulations containing humectants that are milder, or less irritating, to the skin, a fundamental understanding of surfactant-induced skin barrier perturbation and its mitigation in the presence of humectants must be developed. In this thesis, I have investigated the mechanism through which aqueous surfactant/humectant systems may induce a lower extent of skin barrier perturbation when compared to an aqueous contacting solution containing the surfactant at a similar concentration. Such an understanding will allow the rational design of new skin care formulations containing appropriate amounts of surfactants and humectants, or the modification of existing ones, based on fundamental knowledge of what will induce skin barrier perturbation, and how a surfactant/humectant system can be tuned to increase the mildness of the formulation.

[1] Humectants are small molecular weight poly-hydroxy compounds that have the ability to maintain, as well as to enhance, the water-holding capacity of the skin (13). Typical examples of humectants used in skin care formulations include Glycerol and Propylene Glycol, whose effects on the skin barrier have been studied in this thesis.

The central objective of my thesis involves investigating the physical modification of the morphology of the skin barrier induced by surfactants, humectants, and their mixtures. In this thesis, I have developed quantitative and visual criteria to assess the physical state of the skin barrier and its modification upon exposure to surfactants, humectants, and their mixtures (see Section 1.7.1). Surfactants, such as Sodium Dodecyl Sulfate (SDS), have been shown to promote a *clinically harsh* reaction (erythema, or skin redness) in the skin, while other surfactants, such as Dodecyl Hexa (Ethylene Oxide) $C_{12}E_6$, promote a *clinically mild* reaction (skin dryness) in the skin. In addition, other surfactants, such as Sodium Cocoyl Isethionate (SCI), have been shown to induce minimal erythema and skin dryness. On the other hand, humectants, which aid in maintaining the water-holding capacity of the skin, have been shown to mitigate surfactant-induced biological epidermal injury response, that is, erythema and skin dryness, in vivo. Presently, no clear mechanisms exist that can unambiguously explain the observed surfactant-skin and humectant-skin interactions. This lack of understanding can be attributed to the very complex biochemical reactions that surfactants and humectants may trigger once they are able to penetrate the skin barrier. However, if one was to analyze the simpler process of skin penetration by surfactants in the presence/absence of humectants (which is *upstream* to the more complex biological epidermal injury response), then, more clear mechanisms may be identified to describe and rationalize the skin penetration of these chemicals. The identification of such mechanisms, which would involve understanding how these chemicals affect the transport properties of the skin barrier in addition to understanding the solution properties of the chemicals themselves, would then allow: (i) predicting if a particular surfactant in the presence of a humectant can potentially penetrate into the skin barrier and induce a biological epidermal injury response, and

(ii) devising strategies to minimize skin penetration of surfactants, thereby also mitigating the biological epidermal injury response.

Because a chemical has to first penetrate into the stratum corneum (SC),[2] and at times, across it, before it can induce biological epidermal injury to the skin, I have focused my investigation on the skin penetration process of these chemicals. My investigation has also involved visualization of skin morphological modifications induced by these chemicals, on the corneocytes and the lipid bilayers which comprise the SC, using two-photon fluorescence microscopy (TPM) (see Chapter 5). In addition, as part of this thesis, I will present in vivo *patch* tests on human volunteers (see Chapter 4) to substantiate the results of the in vitro studies presented in Chapters 2, 3, and 5.

The central goal of this thesis requires pursuing the following sub-goals:

a) Investigation of the role of the surfactant solution physical chemistry, in the absence and in the presence of a humectant, in inducing skin barrier perturbation (see Chapter 2).
b) Development of an experimental and a theoretical framework for analyzing the skin barrier perturbation potential of a mild surfactant, and comparing it to those of a harsh surfactant and of an appropriate control (see Chapter 3).
c) Ranking of surfactants and humectants relative to an appropriate control based on an in vitro metric that quantifies the ability of these chemicals to perturb the skin barrier, and comparing these in vitro ranking results to the ranking obtained using in vivo patch measurements (see Chapter 4).
d) Visualization of skin barrier perturbation induced by surfactants in the presence/absence of a humectant using Two-Photon Fluorescence Microscopy (TPM) (see Chapter 5).

[2] The stratum corneum is the primary constituent of the skin barrier, as discussed in Section 1.4.

e) Development of a theoretical pore size distribution model to quantify the modification of the inherent skin barrier morphology induced by a surfactant in the presence/absence of a humectant (see Chapter 6).

In order to understand the following arguments concerning how humectants may modify the skin barrier perturbation potential of surfactant solutions, a brief review of the physico-chemical characteristics of aqueous surfactant and humectant solutions is presented in Sections 1.2 and 1.3 respectively. Section 1.4 provides a description of the morphology of the skin barrier where transdermal aqueous porous pathways exist to allow passage of hydrophilic permeants, including a brick-and-mortar representation of this barrier. Subsequently, in Sections 1.5 and 1.6, I discuss what is known about the effects of surfactants and humectants on the skin barrier, both in vitro and in vivo. Finally, in Section 1.7, I present an overview of the thesis, specifically, of: (i) the experiments conducted (see Section 1.7.1), (ii) the theoretical framework developed (see Section 1.7.2), and (iii) an outline of the remaining chapters of the thesis (see Section 1.7.3).

1.2. Surfactant Physico-Chemical Characteristics

Surfactants belong to a class of molecules called amphiphiles (16, 17). These molecules consist of a hydrophilic, or 'water-loving', head, and a hydrophobic, or 'water-fearing', tail (see *Figure 1-1*). The hydrophobic tail of surfactants is typically a hydrocarbon, such as an alkyl chain or an alkyl-phenyl chain. Common tails include straight chain alkanes, benzyl-alkanes, and methyl-branched alkanes. The tails typically consist of at least 8 carbon atoms, resulting in a distinct domain that is poorly soluble in water (16, 17, 48). *Figure 1-1* shows a schematic representation of the surfactant Sodium Dodecyl Sulfate (SDS), with a tail containing 12 carbon atoms, and an anionic sulfate head.

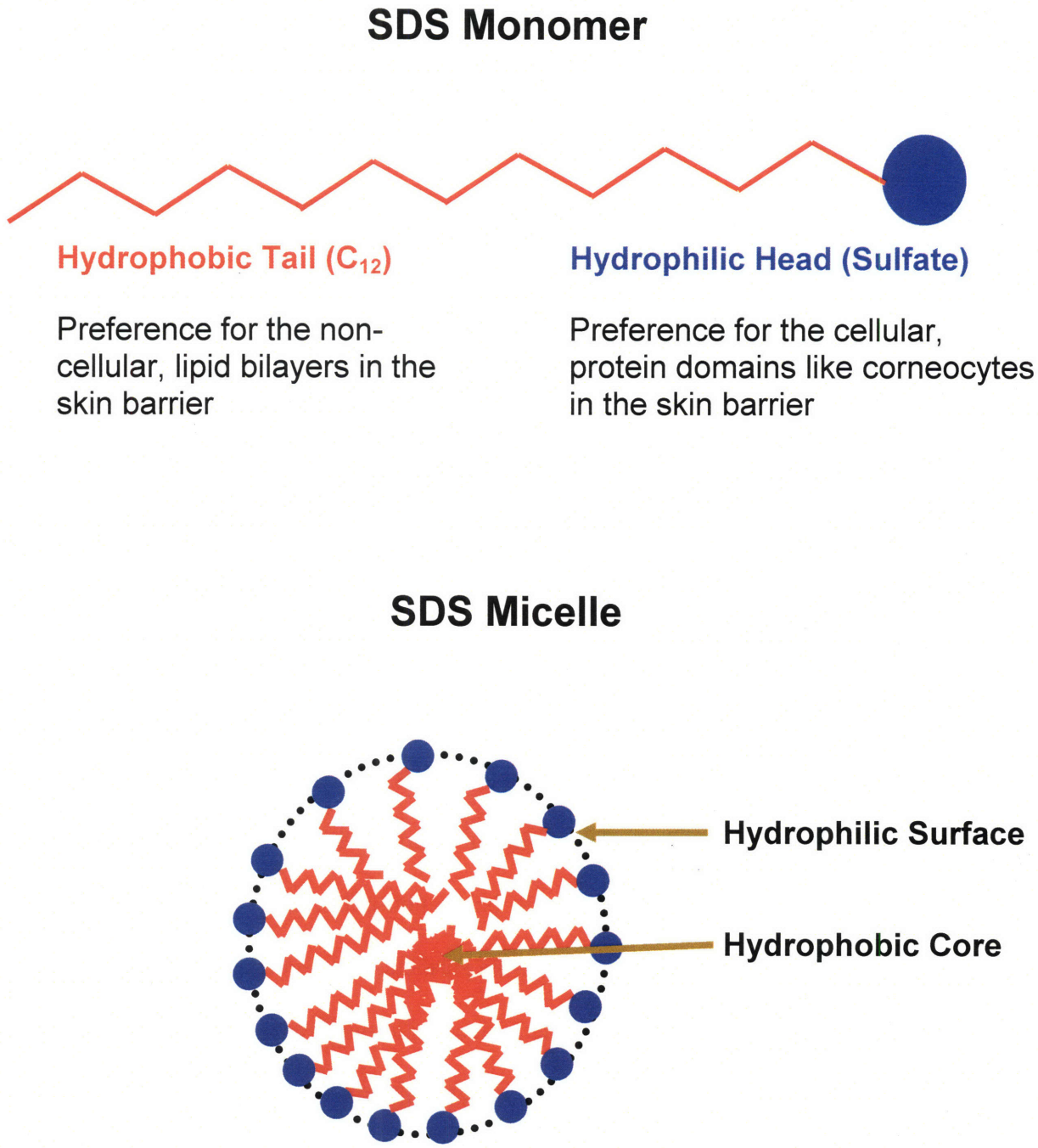

Figure 1-1. Schematic representation of a Sodium Dodecyl Sulfate (SDS) surfactant monomer and a SDS micelle.

In this thesis, in addition to SDS, I have studied the effect of Sodium Cocoyl Isethionate (SCI), which is also an anionic surfactant, on the skin barrier (see Chapter 3). Other types of hydrophilic heads for surfactants include: (i) cationic, (ii) nonionic, and (iii) amphoteric or zwitterionic (16, 17, 48). Cationic surfactants have a positively-charged head, such as an ammonium ion, bonded to the tail. Nonionic surfactants, such as Dodecyl Hexa (Ethylene Oxide) or $C_{12}E_6$ studied in this thesis, have a polar group that is soluble in water, such as a poly (ethylene oxide) group, as their head (48). Amphoteric, or zwitterionic, surfactants have no net charge, but have an internal charge separation. For example, in a betaine head, there is a negatively-charged carboxylate group separated from a positively-charged quaternary ammonium group that is covalently bonded to the surfactant tail (16, 48). As shown in *Figure 1-1*, the surfactant head, being hydrophilic in nature, has an affinity for the hydrophilic cellular protein domains of the skin barrier, while the surfactant tail, being hydrophobic in nature, binds to the hydrophobic lipoidal domains of the skin barrier (see Section 1.4 for a description of the morphology of the skin barrier). The surfactant heads, being ionic or polar in character, are soluble in water while the surfactant tails, being non-polar, are not. Accordingly, there are competing aqueous solubility tendencies for the surfactant molecules. These competing aqueous solubility tendencies cause the amphiphilic molecules to display interesting solution behavior in water (17). Our group has developed molecular-thermodynamic theories to describe and quantitatively predict the effects of the surfactant chemical structure and the solution conditions on the surfactant solution physical chemistry for both single and mixed surfactant systems (18, 20), as well as for surfactants mixed with nonionic polymers (21). These theories can predict the behavior of aqueous solutions containing ionic, nonionic, and even amphoteric linear-chain surfactants. Of particular relevance to this thesis is the ability to predict the concentrations and

compositions of the surfactant monomers and of the micelles, for ionic surfactants (SDS, SCI) as well as for nonionic surfactants ($C_{12}E_6$), requiring only the molecular structures of the surfactants involved and the solution conditions as inputs. Throughout the research presented in this thesis, our surfactant modeling capabilities were used as a tool to predict the surfactant solution conditions, such as the monomer concentrations and compositions, and these conditions were then related to the results of *in vitro* and *in vivo* skin barrier perturbation measurements.

One of the most important characteristics of surfactants is the formation of aggregates of surfactant molecules, called micelles, above a threshold surfactant concentration, known as the critical micelle concentration or CMC (see *Figure 1-2*). At concentrations below the CMC, the surfactant molecules do not aggregate with each other, and are instead free in solution. These free surfactant molecules are referred to as surfactant monomers. When the surfactant concentration exceeds the CMC, it becomes more free-energetically favorable for the surfactant molecules to aggregate into micelles than to remain in solution as surfactant monomers (16, 17). The onset of micellization occurs in a fairly sharp manner at the CMC, shown in *Figure 1-2*, such that below the CMC there are essentially no micellar species, while above the CMC micelles coexist with surfactant monomers, with the surfactant monomer concentration remaining approximately constant. Accordingly, as the total surfactant concentration is increased beyond the CMC, the concentration of the surfactant monomers remains essentially flat, while the concentration of the micellar surfactant increases steadily, as depicted schematically in *Figure 1-2.*

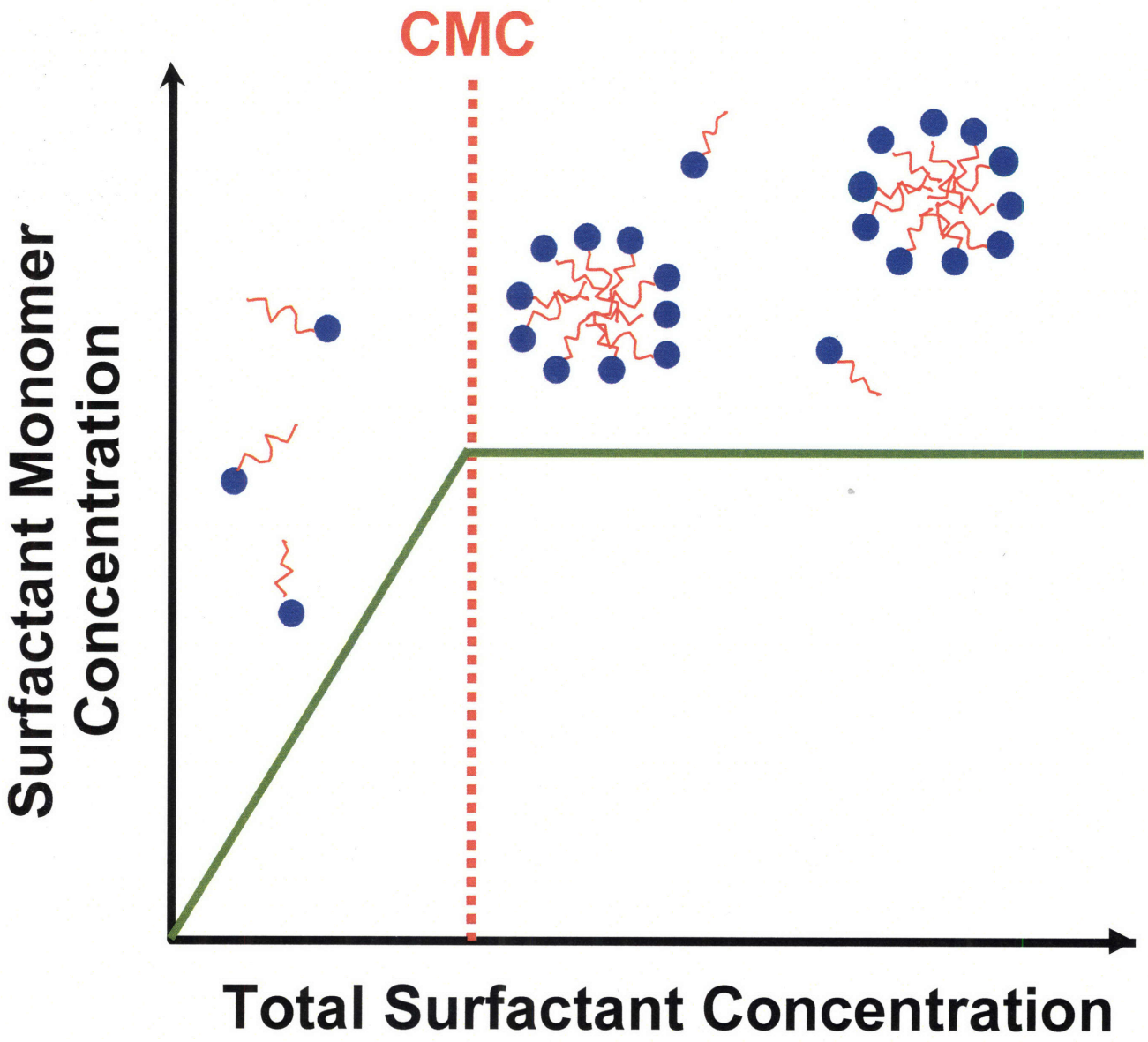

Figure 1-2. The concentration of surfactant monomers as a function of the total surfactant concentration, both below and above the Critical Micelle Concentration (CMC), in an aqueous surfactant solution.

The main driving force responsible for surfactant micellization in water is a phenomenon known as the hydrophobic effect (17). The hydrophobic effect is the result of the hydrophobic tails of the surfactants disrupting the structure of liquid water, forcing the water molecules to adopt a free-energetically unfavorable structured shell around these tails. Micelles are formed with the hydrophobic tails residing in the interior of the aggregates, referred to as the core of the micelle, with the hydrophilic heads residing at the micelle surfaces, as shown for an SDS micelle in *Figure 1-1*. This minimizes the contact between the surfactant hydrophobic tails and water, thereby releasing the water molecules that were in the structured shell around the hydrophobic tails, which in turn increases the entropy (or equivalently, decreases the free energy) of the surfactant solution (17). Competing with this increase in entropy due to the hydrophobic effect, the free-energy considerations that inhibit micellization include the entropic loss of localizing several surfactant molecules and any bound counterions (in the case of ionic surfactants like SDS and SCI) in the micelle, the interfacial free energy between the hydrophobic micelle core and water, and the repulsions of electrostatic and steric origin between the surfactant heads and any bound counterions (in the case of ionic surfactants like SDS and SCI) residing at the micelle core-water interface (17-24).

1.3. Humectant Physico-Chemical Characteristics

Humectants used as moisturizers are chemicals which attract water, mimicking the role of the dermal glycosaminoglycans and other hydrophilic components of the SC, such as Glycerol and amino acids (11). Any polyhydroxy small molecular weight organic compound has humectant properties, for example, Sorbitol, Propylene Glycol, and Glycerol (13). Humectants can diffuse into the SC from an aqueous solution contacting the skin, and once absorbed within

the SC, attract water and increase hydration. Humectants draw water largely from the dermis to the viable epidermis and the stratum corneum and rarely from the environment, when conditions of relative humidity exceed 70%. Since the ability of the skin to hold moisture varies with the relative humidity, humectants enable the skin to maintain a higher than normal equilibrium moisture content. Rhein et al. have determined the effect of Glycerol on a model lipid system (12). Their studies showed that Glycerol maintained the liquid crystalline state of the lipids at a relative humidity of 6%. In the absence of Glycerol, the model lipids showed substantial crystallization and exhibited multiple phases. Therefore, humectants such as Glycerol can preserve normal hydration of the skin under dry environmental conditions by maintaining the liquid crystalline structure of the lipid bilayers of the SC.

1.4. The Skin Barrier

Human skin is the largest organ in the body, measuring 1.85 m^2 in the average man and 1.6 m^2 in the average woman, and constitutes about 16% of the total body weight (1). The skin is the primary interface between the body and the surrounding environment, and as such, is the most important organ of protection. Its protective functions include: (i) water loss prevention, (ii) maintenance of body temperature, (iii) absorption of harmful UV radiation, (iv) prevention of carcinogens, for example, chemicals like PAH (poly cyclic aromatic hydrocarbons), from penetrating into the body, (v) mediation of inflammation through cutaneous metabolism, and (vi) protection against microbial insults by antimicrobial systems like lipids and iron-binding proteins (1, 2, 4, 5). These skin protective functions are carried out by the keratinizing epithelium tissue, which constitutes the skin barrier between the body and the surrounding environment (4, 5).

1.4.1. The Constituents of the Skin Barrier

Human skin consists of three stratified layers, as shown in *Figure 1-3.* The top most layer of the skin is called the stratum corneum (SC). The SC is a horny layer made up of non-nucleated, dead cells called corneocytes, which are embedded in a matrix of highly-ordered lipid lamellae. These lipid lamellae consist of lipid bilayers alternating with hydrophilic layers. The repeat distance between two lipid bilayers is 65 Å, with the two layers of lipid headgroups separated by about 10-20 Å (29) which is the size of a typical aqueous porous channel (see Section 1.4.2). The thickness of the SC ranges between 10-20 μm, and typically consists of 15 interlocking layers of corneocytes (30). These corneocytes are mainly flat and hexagonal in shape, are made up of tough keratin filaments, and are surrounded by a thick, proteinaceous envelope called the corneocyte envelope. The interlocking of the flat corneocytes with the lipid lamellae gives rise to the ordered *brick-and-mortar* structure of the SC (see *Figure 1-4.*) and makes it a very effective permeability barrier (1, 4, 28, 30, 31).

The layer immediately below the SC is the Viable Epidermis, referred to hereafter as the VE. The VE is a cellular and avascular layer having a thickness of 100-150 μm and consisting of living, nucleated cells called keratinocytes (31). These keratinocytes, upon terminal differentiation, lose their nuclei to form the corneocytes in the SC. The VE constitutes a hydrophilic environment and is not a major permeability barrier. The keratinizing epithelium, composed of the SC and the VE, is a perpetually renewing tissue, whose principal function is to create the SC (1, 4, 28, 31, 69).

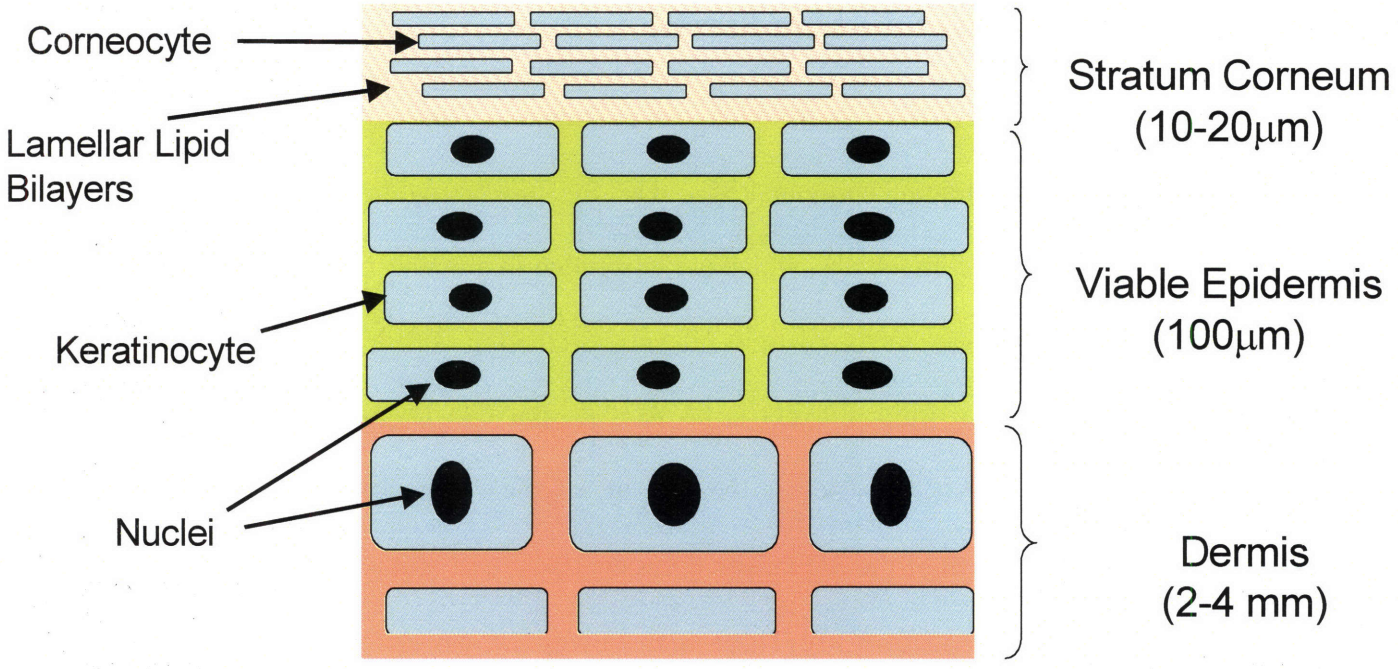

Figure 1-3. Schematic diagram of the skin, showing the three layers of the skin barrier. The stratum corneum (SC), which has a brick-and-mortar structure, is the primary constituent of this barrier.

The dermis constitutes the lower most layer of the skin and has a thickness of 2-4 mm (31). The biological function of the dermis is to mechanically support the epidermis and the cutaneous appendages, including sweat glands, sebaceous glands, and hair, as well as to supply nutrients to the basal layer of living cells in the epidermis. Because of its porous and highly-hydrated structure, the dermis is not a significant permeability barrier (especially to hydrophilic molecules) (1, 4, 28, 30, 31, 69). The dermis is well networked by blood capillaries, providing a transport path from the skin to the blood stream. For this reason, it is generally accepted that a chemical will enter the blood stream if it can permeate through the SC and the VE, and reach the dermis (4, 28, 30, 31). As a result, when the transepidermal skin permeability of a solute is

measured experimentally *in vitro*, often only the SC and the VE are used as the model skin membrane.

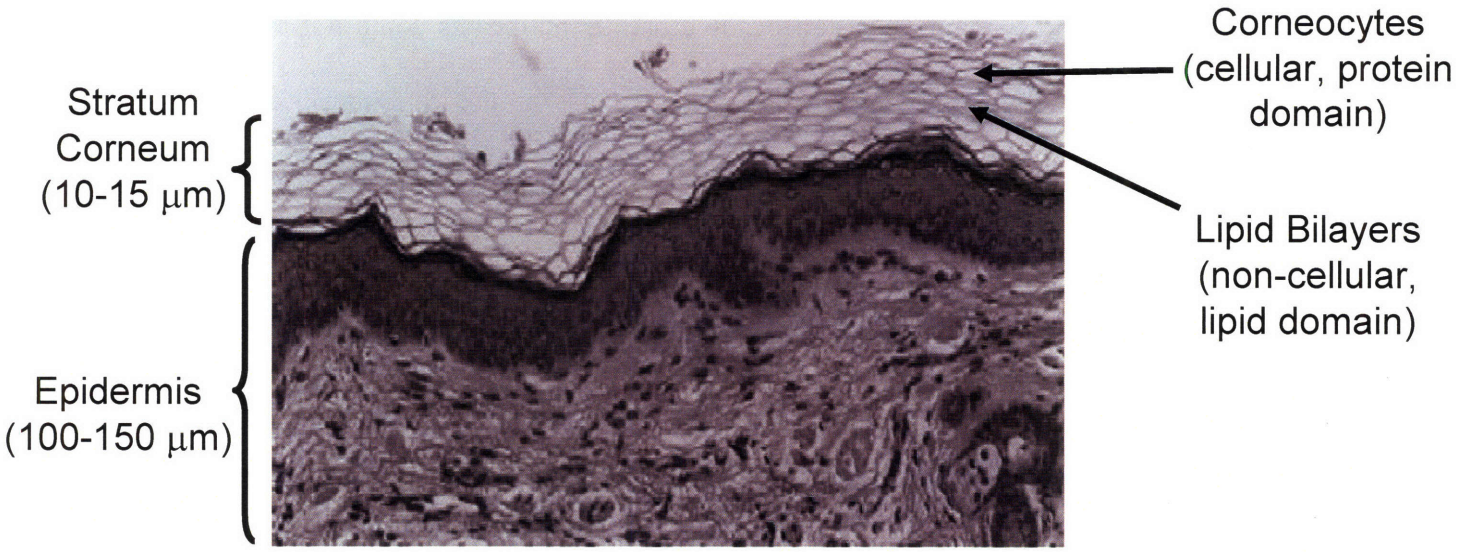

Figure 1-4. Electron micrograph showing the brick-and-mortar structure of the stratum corneum (SC), and of the viable epidermis, of formalin-fixed hairless, guinea pig skin (32). Note that the lipid bilayers in the SC have been stained black, while the corneocytes appear white.

1.4.2. Transdermal Aqueous Porous Pathways in the Stratum Corneum

The highly-ordered structure of the lipid bilayers confers on the SC an impermeable character. Yu et al. (37, 38) have shown recently, using a novel application of Two-Photon Fluorescence Microscopy (see Section 1.7.1), that the corneocytes, under passive skin permeation conditions, essentially act as sinks with respect to the transport of permeants across the SC. As a result, permeant molecules, under passive skin permeation conditions, do not traverse the SC through an intra-corneocyte diffusional pathway. Instead, these permeants traverse the SC by diffusing across the lipid lamellae (27). Although diffusion through lipid

lamellae can explain the permeation of hydrophobic molecules across the SC, it cannot explain the permeation of small, excessively hydrophilic, or of larger hydrophilic molecules, across the SC, as observed in some studies (39-41). Indeed, if no aqueous/hydrophilic porous pathways existed in the SC lipid domain, then aqueous/hydrophilic permeants could not traverse the SC solely through lipoidal/hydrophobic pathways that may exist in the lipid bilayer domains in the SC. The observation that hydrophilic molecules are able to permeate across the SC, even under passive skin permeation conditions, has led researchers to consider the existence of tortuous, aqueous porous pathways through the intercellular lipid lamellae in the SC. Although no direct experimental evidence has been provided to support the existence of these transdermal aqueous porous pathways, diffusion through such pores is viewed as a plausible explanation for the observed transdermal transport of hydrophilic solutes under passive skin permeation conditions (39-42).

Menon and Elias (42) have attempted to establish a morphological basis for the existence of a pore pathway in the mammalian SC. These authors have applied hydrophilic and hydrophobic tracers in vivo to murine skin under passive skin permeation conditions, and also under enhanced skin permeation conditions, including chemical enhancers, a lipid synthesis inhibitor, sonophoresis, and iontophoresis, and following that, they employed Ruthenium Tetroxide Staining and Microwave Post Fixation methods to visualize the penetration pathways. Their results showed that both the hydrophobic and the hydrophilic tracers localized to discrete lacunar domains embedded within the extracellular lipid lamellar domains. These authors have also observed that while these lacunar domains remained discontinuous under passive skin permeation conditions, permeation enhancement resulted in these domains gaining structural continuity. Hence, lacunar domains have been considered by these authors as providing a

physical basis for the existence of aqueous pores and polar pathways through the lipoidal domain in the SC.

Under passive skin permeation conditions, the lacunae between two layers of lipid headgroups in a lipid bilayer within the lipid lamellae domain of the SC may get filled up with water, and create an aqueous channel (29). Subsequently, the lipid bilayers may align vertically, causing these aqueous channels between their headgroups to align and form a tortuous, continuous aqueous porous pathway through the lipid lamellae domain in the SC (see *Figure 1-5*). Skin hydration, and application of other skin permeation enhancers, including chemical enhancers (for example, harsh surfactants, such as, SDS), may cause these lipid headgroups in a lipid bilayer to move further apart, thereby leading to an increase in the diameter of these aqueous porous pathways, as shown schematically in *Figures 1-6(a) and 1-6(b)*. This mechanism of disorder in the regular structure of the bilayer lipid lamellae leading to an increase in the separation distance between the bilayer lipid headgroups, and consequently, to an increase in the diameter of the aqueous channels that may exist between these lipid headgroups, may help explain how some skin permeation enhancers induce an increase in the permeation rate of hydrophilic solutes through the SC in the skin. On the other hand, humectants such as Glycerol can mitigate the extent of disorder in the bilayer lipid lamellar structure, thereby reducing the diameter of the aqueous channels as well as the permeation rate of hydrophilic solutes through these channels in the SC (see Chapter 3).

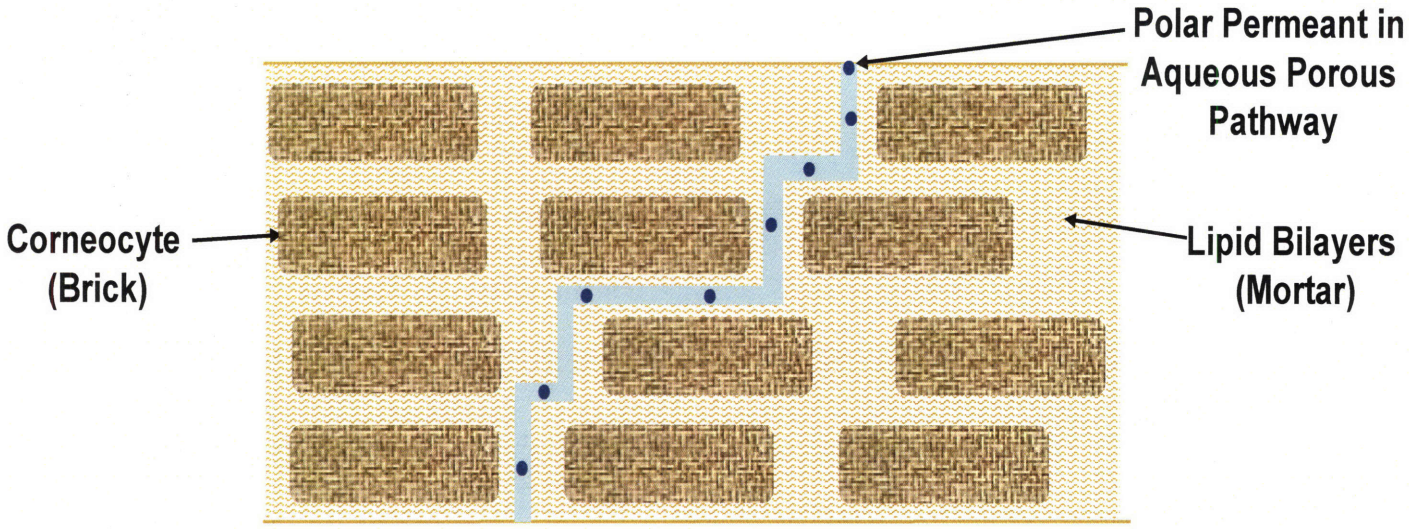

Figure 1-5. Schematic diagram that visualizes a transdermal aqueous porous pathway which exists between the lipid bilayers surrounding the corneocytes of the SC. The blue dots represent polar permeants that can penetrate across the SC through this pathway.

A third view, held by many researchers as the basis for the existence of transdermal aqueous porous pathways, is that imperfections in the SC lipid bilayers may result in pores in the SC that may connect to form tortuous, porous pathways responsible for the transport of hydrophilic solutes through the SC in the skin. These imperfections are believed to result in: (i) separation of grain boundaries, (ii) fault dislocations, (iii) lattice vacancies, and/or (iv) voids due to missing lipids or steric constraints placed by corneocytes on lamellar lipid domains (41). Many researchers have used Atomic Force Microscopy (AFM) and X-Ray diffraction of supported phospholipid bilayers to study structural defects in these lipid lamellar systems. Based on X-Ray diffraction, defects have been discovered in lipid bilayers under excess water conditions. Raphael et al. (43) have postulated that the temporary localized disordering of lipids may be the cause of lipid bilayer defects. Through AFM images of supported lipid bilayers,

Malghani et al. (44) have reported the existence of lipid bilayer defects. These studies support the view that bilayer imperfections may lead to tortuous, aqueous porous pathways in the SC in the skin.

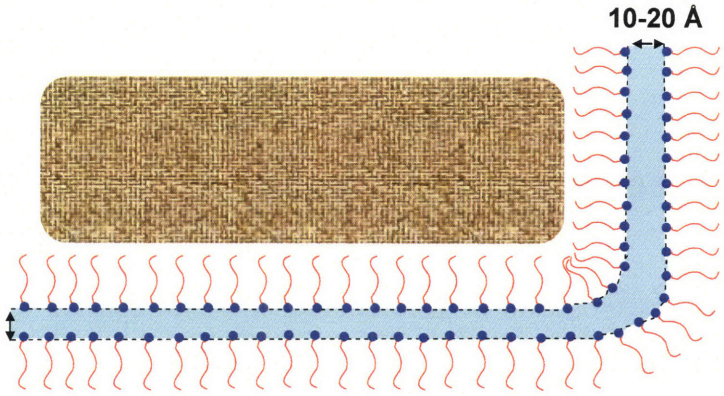

Figure 1-6 (a). Aqueous porous pathway around a corneocyte, which results from the separation between two layers of lipid headgroups under passive permeation conditions.

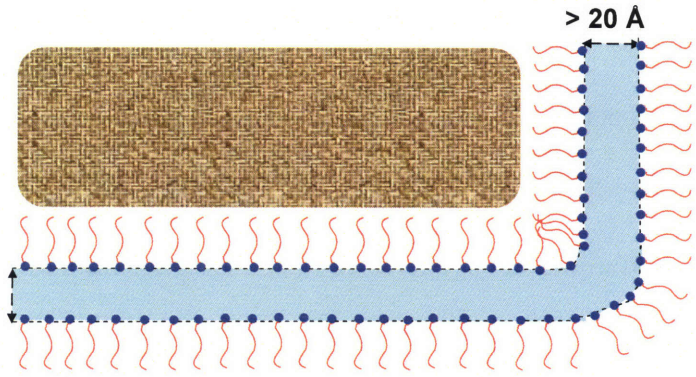

Figure 1-6 (b). Aqueous porous pathway around a corneocyte, which results from the separation between two layers of lipid headgroups under permeation enhancement conditions.

The transdermal aqueous porous pathways can be viewed as tortuous, cylindrical pores through the intercellular lipid lamellar domain in the SC, with the permeant molecules modeled

as hard spheres in motion through these pores (see *Figure 1-5*). The main aqueous pore pathway parameters of interest in this thesis are: (i) the aqueous pore radius, (ii) the porosity, which is defined as the fraction of cross-sectional SC area occupied by the aqueous pores, and (iii) the tortuosity, which is defined as the ratio of the tortuous length of the aqueous pore to the thickness of the SC (25, 39-41).

1.5. Effect of Surfactants on the Skin Barrier

The skin barrier is exposed to numerous, frequent, and repeated insults by surfactants present in skin cleansers and in skin care formulations. These chemicals, due to their surface activity, can clean the skin surface by removing dirt, but in so doing, are also known to penetrate into the SC and induce skin barrier perturbation (48-50, 61, 62, 71, 72, 78-81). Surfactant-induced skin barrier perturbation can lead to a loss of the skin barrier protective functions, which, in turn, can lead to various pathophysiological consequences, as illustrated in *Figure 1-7.*

. The anionic surfactant, SDS (see *Figure 1-1*), encountered in skin cleansing formulations, is a harsh skin agent (see below for a definition of a harsh skin agent), and is known to perturb the skin barrier, to denature keratins, and to compromise the skin barrier resistance (48, 61, 78, 80). Therefore, chemicals which are toxic to the skin, and which under normal circumstances would be prevented from penetrating into the skin by the skin barrier, are able to penetrate into skin whose barrier has been compromised by SDS. Accordingly, this compromised skin barrier resistance can lead to the associated problem of skin irritation. Skin irritation, in turn, may result in: (i) abnormal skin growth, for example, in parakeratosis – the retention of nuclei by the corneocytes, (ii) skin redness or erythema, and (iii) highly chapped and scaly skin (48). On the other hand, some mild skin agents (see below for a definition of a mild skin agent), such as the

nonionic surfactant $C_{12}E_6$, do not elicit a strong irritation response, yet induce skin dryness (48). Furthermore, there are still milder agents, for example, the anionic surfactant Sodium Cocoyl Isethionate (SCI), which do not induce either a strong irritation response or a significant extent of skin dryness (see Chapter 3) (61, 62, 79).

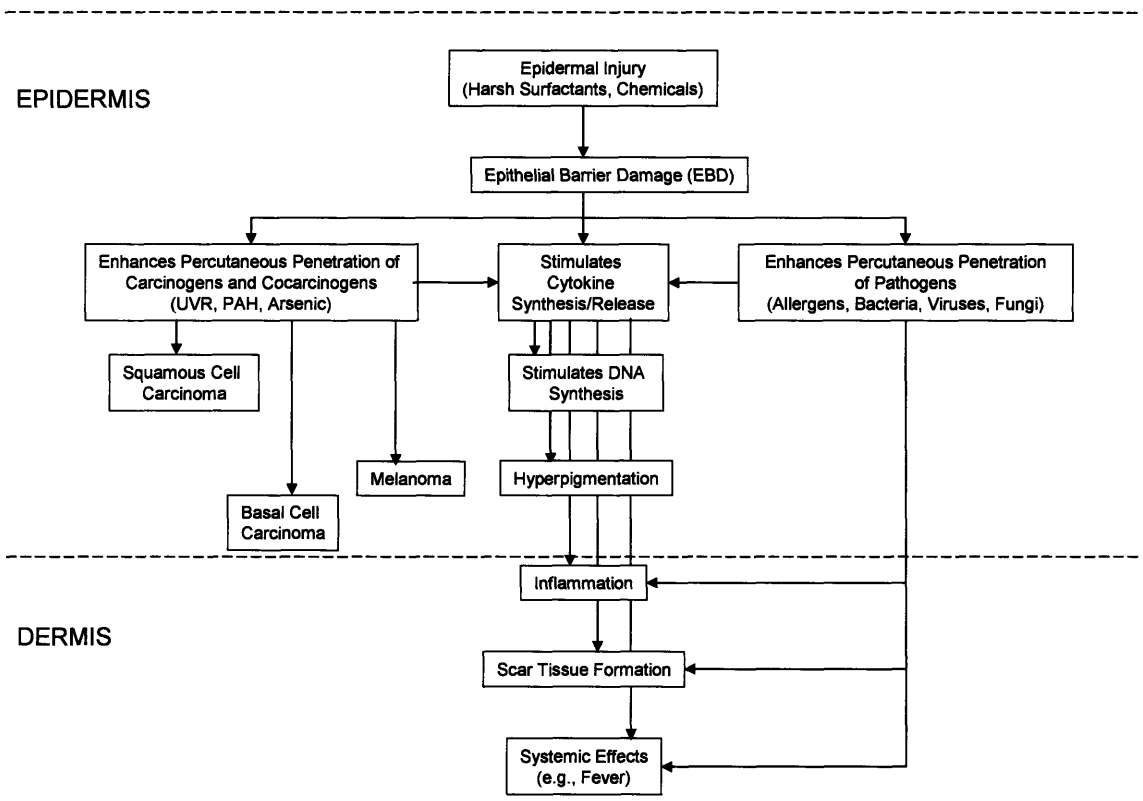

Figure 1-7. Schematic illustration of various pathophysiological downstream manifestations of skin epithelial barrier damage induced by surfactants. The epidermis depicted here is composed of the stratum corneum and the viable epidermis, which together, constitute the keratinizing epithelial tissue (49).

The SDS-induced dermatitis model is widely used in experimental dermatology as a model for skin irritation. Moore et al. (48, 71) have investigated the skin barrier damaging

properties of SDS above the CMC. Their studies have shown that SDS-induced skin barrier damage continues above the CMC. They have attributed this effect to the size of the SDS micelles by hypothesizing that the SDS micelles are small enough to penetrate into the SC through the aqueous pores (see Section 1.4.2). Moreover, they have also demonstrated that once these SDS micelles are complexed with poly (ethylene oxide) chains, they are sterically hindered from accessing these aqueous pores and, hence, can no longer induce SC barrier damage. Their studies have unambiguously shown that in addition to the SDS monomers, SDS micelles can also lead to SC barrier damage provided that they are small enough to penetrate into the SC through the aqueous pores. However, their studies did not demonstrate how these SDS monomers and SDS micelles, once inside the SC, induce barrier damage. Specifically, it is still unknown if the SDS monomers and the SDS micelles, once inside the SC, interact with the keratins and the corneocytes, and/or if they also partition into the lipid bilayers, thereby disordering the lipid bilayers in the SC (see Chapter 5 for a TPM visualization study that sheds light on some of these issues).

The skin irritation response may be modulated by two distinct mechanisms: (i) the direct interaction of a penetrating skin agent with the keratinocytes in the epidermis, and (ii) SC barrier disruption induced by the skin agent. Berardesca et al. (72) have hypothesized that SDS-induced dermatitis proceeds via mechanism (i), that is, by disruption in the secondary and tertiary structures of keratin in the keratinocytes by SDS, rather than by a delipidization of the SC lipid bilayers. Wood et al. (73) have found that SC barrier disruption induced by acetone or by tape stripping can stimulate cytokine production and promote skin inflammation. Their studies have shown that mechanism (ii), described above, can activate biochemical signals leading to irritant dermatitis. It is reasonable to assume that in most cases of skin irritation induced by surfactants

encountered in skin care products and detergents, mechanisms (i) and (ii) both play a role, with their relative importance being determined by: (a) the self-assembling characteristics of the surfactant, (b) the hydrophobicity/hydrophilicity of the surfactant, (c) the skin membrane characteristics, including changes in the aqueous pore radius and in the porosity-to-tortuosity ratio upon exposure to the surfactant solution, and (d) the skin penetration characteristics and the transdermal permeability of the surfactant.

Mild skin agents will be referred to, throughout this thesis, as those inducing little or no skin irritation response/erythema upon exposure to the skin (and, consequently, little or no SC barrier disruption through lipid extraction and interaction with keratin in the keratinocytes and in the corneocytes). The nonionic surfactant, $C_{12}E_6$, has been shown: (1) not to induce significant scaling and skin-roughness upon skin exposure (79), and (2) to be clinically mild to the skin without eliciting an erythema response, although it may induce skin dryness (48, 80, 81). Harsh skin agents will be referred to as those inducing a significant irritation response/erythema upon exposure to the skin (and, consequently, significant barrier damage and/or interaction with keratin in the keratinocytes and the corneocytes). In particular, SDS has been selected as a model harsh skin agent for the experiments to be conducted as part of this thesis (48-51, 61, 71, 72, 78-81). Through the work conducted as part of this thesis, I have investigated, at a fundamental level, the causes of skin barrier perturbation, that may lead to skin dryness and erythema, through a consideration of: (i) the molecular and self-assembling characteristics of a harsh and a mild surfactant, (ii) changes in the skin membrane characteristics (specifically, of the aqueous porous pathway characteristics) upon exposure to these agents, (iii) the transdermal permeability characteristics of these agents, and (iv) the partitioning of these agents within the SC following their penetration into the SC. Utilizing this fundamental understanding, I have also investigated

effective practical strategies to mitigate skin barrier perturbation induced by these surfactants, and therefore, to prevent skin dryness and irritation symptoms, such as irritant contact dermatitis (see Chapter 2).

1.6. Effect of Humectants on the Skin Barrier

The cosmetic industry is interested in the optimal delivery of certain active ingredients to the skin. Active ingredients, for example, humectants like Glycerol, when delivered to the skin in the appropriate amount can result in: (i) enhancement in the moisture retentive ability of the skin, (ii) healing of erythema, (iii) general skin lightening and toning, (iv) SC barrier repair, and (v) healing of acne (6-15, 74-77). Specifically, cosmetic scientists and researchers have focused on Glycerol to mitigate/recover the skin barrier damage induced by surfactants because: (1) Glycerol is a major determinant of SC water retention, and of the mechanical and the biosynthetic functions of the skin (74), (2) SDS-induced erythema and acanthosis (the benign thickening of the horny layer in the skin) in guinea pig skin is fully reversed by Glycerol treatment (75), (3) Loden et al.(76) have observed patients with atopic dermatitis to exhibit significantly less adverse skin reactions such as smarting (a sharp local superficial sensation) upon treatment with a 20% glycerin cream compared to a urea-saline cream, and (4) Glycerol can be regarded as a skin barrier stabilizing and moisturizing compound because it creates a stimulus for skin barrier repair and improves SC hydration after SC barrier damage induced by tape stripping and repeated washing with SDS (6).

The importance of Glycerol (or glycerin) in skin care products is well established, and Glycerol is widely used in cosmetic and pharmaceutical formulations. To explain its benefits, studies have focused on its humectant and smoothing effects (7), and on its protective functions

in emulsion systems against skin irritation (8). Researchers have shown that Glycerol diffuses into the SC, increases skin hydration, and relieves clinical signs of dryness (9-13). However, the mechanisms by which Glycerol mitigates SC barrier damage and relieves skin irritation and dryness are currently not well understood. One of the viewpoints held by researchers today is that Glycerol may influence the crystalline arrangement of the intercellular lipid bilayers. The bulk of the bilamellar lipid sheets are proposed to be in crystalline/gel domains bordered by lipids in a fluid crystalline state. In skin exhibiting SC barrier damage, the proportion of lipids in the solid state may be elevated, and subsequent skin exposure to Glycerol may help maintain these lipids in a liquid crystalline state at low relative humidity, thereby enhancing SC barrier function and decreasing SC water permeability (14). A second prevalent viewpoint is that Glycerol may increase the rate of corneocyte loss from the upper layers of the SC, through a keratolytical effect due to enhanced desmosome degradation, thereby reducing *scaliness* of dry skin and maintaining SC barrier (13, 15). A third, more recent viewpoint proposed by Fluhr et al. (6) is based on the hygroscopic property of Glycerol. Glycerol, by virtue of its high transdermal diffusivity, can penetrate into the SC, and, by virtue of its hygroscopic property, is able to bind water and reduce water evaporation. Therefore, Glycerol, by absorbing water, may modulate water fluxes in the SC, which, in turn, may lead to a stimulus for SC barrier repair.

As discussed in Section 1.4.1, the brick-and-mortar structure of the SC, with its periodic interlocking of corneocytes and lipid lamellae, presents the strongest barrier to the delivery of Glycerol to the skin. Diffusion through the multilamellar lipid domains cannot explain Glycerol transport to the deeper layers of the skin, including the dermis, because the lipid domains are hydrophobic while Glycerol is strongly hydrophilic. Hence, it is useful to invoke the existence of transdermal aqueous porous pathways (see Section 1.4.2) to explain the skin penetration of such

agents. One of the central goals of this thesis is the analysis of surfactant-skin penetration in the presence of Glycerol in the aqueous contacting solution, and how such an analysis may help explain mitigation of surfactant-induced skin barrier perturbation in the presence of Glycerol.

1.7. Thesis Overview

Having defined the overall goal of this thesis along with the thesis objectives, I proceed next to consider the experimental and theoretical procedures that I have pursued, as part of this research effort, to achieve these objectives. This section concludes with a brief discussion of the subsequent thesis chapters, including a discussion of the implications of the central results in each thesis chapter.

1.7.1. Experimental Framework

Bioengineering Assays to Quantitatively Determine the Macroscopic Extent of Skin Barrier Perturbation

Skin electrical current has been shown to be a useful quantitative indicator of the macroscopic extent of skin barrier perturbation induced by aqueous contacting solutions (25, 26, 41, 46-48, 53, 54, 84). An in vitro skin electrical current assay, based on the measurement of electrical current across pig full-thickness skin (p-FTS) that was exposed to aqueous contacting solutions of surfactants and humectants in diffusion cells was used to determine the macroscopic extent of skin barrier perturbation (see Chapter 2). The basis for these measurements is as follows: the higher the measured current for identical voltage signals, the lower is the skin barrier resistance, and hence, the greater is the extent of skin barrier perturbation (see Chapter 2).

Similar to skin electrical currents, permeability of the skin barrier to some permeants, for example, hydrophilic permeants, such as, Mannitol, can serve as a quantitative indicator of the integrity of the skin barrier (25, 26, 41, 46-48, 53, 54). Mannitol is: (1) a low molecular weight monosaccharide (MW=182 Da) (25, 39), and (2) a highly hydrophilic (log $K_{O/W}$ = -3.1) chemical (25, 39), which is not metabolized by the body, and hence, if desired, can also be used for in vivo skin permeation studies (25, 39). Being small in size and highly hydrophilic, Mannitol can access similar aqueous pores as do ions in order to transport across the skin barrier. This, in turn, makes Mannitol a suitable permeant to study in the context of the hindered-transport porous pathway model of the SC (25, 39, 40, 41, 63). In fact, these experiments quantitatively determine the cumulative amount of permeant (in our case, Mannitol) that has crossed p-FTS in a given time, and thereby, characterize the extent of skin barrier perturbation (see Chapter 2). These in vitro skin permeability assays use ^{14}C radiolabeled Mannitol and detect scintillation counts (number of radioactive disintegrations per unit time) by a scintillation counter, to quantify the radioactive permeant concentration in the receiver solution once the permeant has crossed the p-FTS membrane. These measurements can yield important information about transport characteristics of the skin barrier, and how these characteristics may be modified upon exposure to aqueous contacting solutions of surfactants and humectants.

Previous research in this area has shown that surfactants, such as SDS, can induce skin barrier perturbation upon penetrating into the skin barrier. Hence, if one can quantify the amount of SDS that may penetrate into the skin barrier upon exposing p-FTS to an aqueous contacting solution containing SDS, one can estimate the extent of skin barrier perturbation and barrier integrity. Such a surfactant skin penetration assay determines the extent of skin barrier perturbation through direct measurement of the amount of surfactant, in our case SDS, that can

penetrate into the skin barrier from an aqueous contacting solution (48, 71, 78, 83). Specifically, I have used ^{14}C radiolabeled SDS that can penetrate into p-FTS upon exposing p-FTS in diffusion cells to aqueous contacting solutions containing SDS (see Chapter 2 for a description of the diffusion cell setup used for this purpose). The viable epidermis (VE) along with the stratum corneum (SC) was heat-stripped following exposure to the aqueous SDS contacting solution. The heat-stripped VE+SC was then dissolved using a tissue solubilizer, and the amount of ^{14}C radiolabeled SDS bound to the VE+SC was determined using scintillation counts by a scintillation counter as before (see Chapter 2).

In addition to the in vitro skin electrical current, Mannitol skin permeability, and skin radioactivity assays discussed above, in vivo measurements were also pursued as part of this thesis. Specifically, Chapter 4 reports in vivo patch measurements carried out on volar forearm of human volunteers exposed to test solutions of surfactants, humectants, and their mixtures. Evaluation of the extent of erythema and skin dryness was carried out by: (i) expert grader assessments, as well as by (ii) chromameter assessments (85). Transepidermal water loss (TEWL) measurements, which quantify the extent of skin barrier perturbation in vivo, were obtained through evaporimeter measurements (86). Skin conductance measurements using a Skicon conductance meter were carried out to determine the extent of modification of skin surface hydration upon exposure to the surfactant and humectant solutions contained in the patches (87). Further details, including the protocol followed, along with a statistical analysis of these measurements in the context of the in vitro skin assays, will be reported in Chapter 4.

Visualization of Skin Barrier Morphology Using Two-Photon Fluorescence Microscopy

Traditional biopsies of tissues, such as human skin and p-FTS, can provide tissue morphological information with sub-cellular details, and is one of the principal tissue pathological analysis methods. However, this method has some inherent limitations: (1) the method involves tissue excision, fixation, and imaging to obtain useful morphological information, and as such, is of an invasive nature, and (2) much of the cellular biochemical information is inevitably lost during the surgical and fixation procedures (33). In addition, most of these imaging methods can only achieve two-dimensional images that do not capture three-dimensional structures like blood capillaries and sebaceous glands in complex tissues, such as, the keratinizing epithelium in human skin. Confocal laser scanning microscopy, that can address some of these limitations, is limited by: (a) a low penetration depth of scanning due to light scattering effects, and (b) an accrued tissue sample photo-bleaching and photo-damage due to repeated laser scanning (34, 35). Electron microscopy, such as, Scanning Electron Microscopy, has the ability to image with sub-micrometer detail, but this method does not delineate specific structural morphology using cell-specific markers, such as, fluorescently-labeled antibodies (35).

Two-Photon Fluorescence Microscopy (TPM), an important invention in biological imaging (36), has overcome these diagnostic limitations. TPM is a non-invasive, three-dimensional imaging technology based on two-photon induced nonlinear excitation of fluorophores (see Chapter 5). It has the capability for deep-tissue imaging (up to several hundred micrometers) and reduced photo-damage, even for opaque and highly scattering tissues, such as, human skin (33-38). In the past, studies have demonstrated the viability of using TPM as a new, exciting tool to study skin barrier morphology (37, 38). Because the inherent skin chromophores,

such as, NADH and flavoproteins, fluoresce in the green spectrum, while the Rhodamine-based fluorescent probes, such as Sulforhodamine B (SRB), fluoresce in the red spectrum, an appropriate filter set can be used to collect the skin autofluorescence signal in the green channel and the probe fluorescence signal in the red channel (see Chapter 5). With this in mind, using dual-channel TPM, the inherent skin barrier morphology detection in the green channel has been shown to provide a fingerprint relative to the fluorescent probe spatial distribution, as detected in the red channel, in the same piece of skin (see Chapter 5). Hence, not only does such an imaging procedure provide a novel approach to visualize the skin barrier, but it also provides an exciting way to visualize the spatial distribution of model fluorescent probes, such as Sulforhodamine B (SRB), in the skin barrier. In Chapter 5, dual-channel TPM was used to visualize the morphology of the skin barrier upon exposure to aqueous contacting solutions of surfactants and humectants, followed by exposure to aqueous SRB contacting solutions. In addition, Chapter 5 provides experimental details, including a schematic of the TPM apparatus.

1.7.2. Theoretical Framework

Although surfactant-induced skin barrier perturbation is a well-accepted phenomenon of biological and medical significance, no satisfactory quantitative models presently exist that can characterize and subsequently predict the extent of skin barrier perturbation and associated damage that may result from exposure to surfactants. Hence, most of the research accomplished in pharmaceutical and cosmetic laboratories, and biological laboratories in universities, across this country relies heavily on trial-and-error screening studies. In addition, lack of *predictive* models results in a significant amount of costly and time-consuming in vivo testing operations on human subjects as well as on animals, which can be potentially minimized through the development of integrated models which have the capability of determining, as well as of

predicting, the extent of skin barrier perturbation induced upon exposure to a surfactant solution of a certain concentration.

Humectants, such as Glycerol, have been shown to mitigate surfactant-induced skin barrier perturbation (see Section 1.6). It is not only an important fundamental problem, but it is also one of great practical significance to develop models that can quantify, as well as predict, the extent of skin barrier perturbation induced by surfactants, in the absence as well as in the presence of humectants. Such a prediction may shed light on the mechanisms through which humectants, such as Glycerol, can mitigate surfactant-induced skin barrier perturbation. The identification of such mechanisms can also provide useful guidelines to formulating pharmaceutical and cosmetic products that are mild to the skin barrier and that do not induce erythema or skin dryness.

These novel, integrated models have been developed utilizing a fundamental understanding of surfactant solution physical chemistry, in the absence and in the presence of humectants, along with transport characteristics of the skin barrier (25, 39-41, 63-68). For this purpose, hindered-transport aqueous porous pathway models that employ a distribution of pore sizes to quantify the extent of skin barrier perturbation have been developed and validated in Chapter 6 of this thesis.

1.7.3. Outline of the Thesis Chapters

The remainder of this thesis is divided into the following chapters. Chapter 2 describes the results of an in vitro investigation that determines how SDS affects the skin barrier properties in the presence of Glycerol. In this chapter, I have proposed a plausible hypothesis for how Glycerol may mitigate SDS-induced skin barrier perturbation that is based on the relative sizes of

the SDS micelles and the skin aqueous pores. Chapter 3 develops an experimental/theoretical framework for analyzing the skin barrier perturbation potential of SCI, a mild surfactant, including explaining its well-known skin mildness characteristics in vivo. Chapter 4 presents the development of an in vitro ranking metric to rank surfactants (SDS and $C_{12}E_6$), the control (PBS), and humectants (Glycerol and Propylene Glycol) based on their ability to perturb the skin barrier. The in vitro ranking metric developed in Chapter 4 was compared with in vivo *patch* measurements that were carried out to clinically determine the extent of erythema and visual dryness induced by aqueous solutions of the control, the surfactant, and the humectant solutions considered above. In Chapter 5, dual-channel TPM was used to visualize the morphology of the skin barrier upon contact with aqueous solutions of: (i) SDS, (ii) SCI, (iii) Glycerol, (iv) SDS+Glycerol, and (v) PBS (the control). The TPM visualization studies provided direct visual evidence that SDS could interact with the keratins of the corneocytes in the SC and induce corneocyte damage, which resulted in the creation of localized transport regions, LTRs. Upon adding Glycerol to a SDS aqueous contacting solution, the ability of SDS to penetrate into the SC and to induce corneocyte damage was significantly minimized. An analysis of the amount of fluorescent probe that penetrated into the SC as a function of the depth of the SC upon contacting p-FTS separately with the five aqueous contacting solutions considered showed that SDS enhanced the probe partition coefficient the most, and that the extent of SC barrier perturbation induced by these chemicals follows the order: (iii) < (v) < (ii) < (iv) < (i), which is consistent with the results of the ranking study presented in Chapter 4. In Chapter 6, a pore size distribution model was developed to gain more fundamental insight, beyond that attained through the *average* pore radius analysis presented in Chapter 2, into the nature of the pores induced by SDS and by SDS+Glycerol aqueous contacting solutions. The pore size distribution model results

revealed that adding Glycerol to the SDS aqueous contacting solution induces a shift in the pore size distribution – from one having larger pores to one having smaller pores. Finally, Chapter 7 summarizes the important results of this thesis, and discusses future research directions in the area of skin barrier perturbation induced by surfactants in the presence of humectants.

1.8. References

1. CA.Allen, The skin; a clinicopathological treatise, New York, Grune & Stratton (1967).
2. R.M.Adams, Occupational skin disease, in *Fitzpatrick's dermatology in general medicine. New York:McGraw-Hill, Health Professions Division, c1999.*
3. S.Dehkharghani, J.Bible, J.G.Chen, S.R.Feldman, and A.B.Fleischer, The economic burden of skin disease in the United States, *Journal of the American Academy of Dermatology*, 48(4):p. 592-599 (2003).
4. P.M.Elias and K.R.Feingold, Skin as an organ of protection, in Fitzpatrick's dermatology in general medicine. New York:McGraw-Hill, Health Professions Division, c1999.
5. C.K.Smith Pease, I.R.White, and D.A.Basketter, Skin as a route of exposure to protein allergens. *Clinical and Experimental Dermatology*, 27:p. 296-300 (2002).
6. J.W.Fluhr, M.Gloor, L.Lehmann, S. Lazzerini, F.Distante, and E.Berardesca, Glycerol accelerates recovery of barrier function in vivo, *Acta Derm Venereol*, 79:p. 418-421 (1999).
7. J.Bettinger, M. Gloor, A.Vollert, P.Kleesz, J.Fluhr, and W.Gehring, Comparison of different non-invasive test methods with respect to the different moisturizers on skin, *Skin Res. Technol.*, 5:p. 21-27 (1999).
8. A.M.Grunewald, J.Lorenz, M.Gloor, W.Gehring, and P.Kleesz, Lipophilic irritants. Protective values of urea and glycerol containing oil in water emulsions, *Dermatosen*, 44:p. 81-86 (1996).
9. M.D.Batt and E.Fairhurst, Hydration of the stratum corneum, *Int. J. Cosmet. Sci.*, 8:p. 253-256 (1986).
10. M.Loden, Urea-containing moisturizers influence barrier properties of normal skin, *Arch. Dermatol. Res.*, 288:p. 103-107 (1996).

11. E.J.Fendler, "Physico-chemical considerations", in *Dry skin and moisturizers: chemistry and function,* M.Loden and H.I.Maibach, Eds. (CRC Press, Boca Raton, 2000), p. 175-182.

12. L.D.Rhein, F.A.Simion, C.Froebe, J.Mattai, and R.H.Cagan, Development of a stratum corneum lipid model to study the cutaneous moisture barrier properties, *Colloid Surf,* 48:p.1-11 (1990).

13. D.S.Orth and Y.Appa, "Glycerine: a natural ingredient for moisturizing skin", in *Dry skin and moisturizers: chemistry and function,* M.Loden and H.I.Maibach, Eds. (CRC Press, Boca Raton, 2000), p. 213-228.

14. C.L.Froebe, F.A.Simion, H.Ohlmeyer, L.D.Rhein, J.Mattai, R.H.Cagan, and S.E.Friberg, Prevention of stratum corneum lipid phase transitions in vitro by glycerol – An alternative mechanism for skin moisturization, *J. Soc. Cosmet. Chem.*, 41:p. 51-65 (1990).

15. A.Rawlings, C.Harding, A.Watkinson, J.Banks, C.Ackermann, and R.Sabin, The effect of glycerol and humidity on desmosome degradation in stratum corneum, *Arch. Dermatol. Res.*, 287:p. 457-464 (1995).

16. K.L.Mittal, Solution chemistry of surfactants. Vol. 1 and 2. 1979, New York: Plenum Press.

17. C.Tanford, The hydrophobic effect. 1980, New York: Wiley.

18. A.Shiloach, and D.Blankschtein, Predicting micellar solution properties of binary surfactant mixtures, *Langmuir*, 14(7): p. 1618-1636 (1998).

19. A.Shiloach and D.Blankschtein, Measurement and prediction of ionic/nonionic mixed micelle formation and growth, *Langmuir*, 14:p. 7166-7182 (1998).

20. S.Puvvada and D.Blankschtein, Molecular-thermodynamic approach to predict micellization, phase behavior and phase separation of micellar solutions. I. Application to nonionic surfactants, *Journal of Chemical Physics*, 92: p. 3710-3724 (1990).

21. Y.J.Nikas and D.Blankschtein, Complexation of nonionic polymers and surfactants in dilute aqueous solutions, *Langmuir*, 10: p. 3512-3528 (1994).

22. V.Srinivasan and D.Blankschtein, Effect of counterion binding on micellar solution behavior: 1. Molecular-thermodynamic theory of micellization of ionic surfactants, *Langmuir*, 19: p. 9932-9945 (2003).

23. V.Srinivasan and D.Blankschtein, Effect of counterion binding on micellar solution behavior: 2. Prediction of micellar solution properties of ionic surfactant-electrolyte systems, *Langmuir*, 19: p. 9946-9961 (2003).

24. A.Goldsipe and D.Blankschtein, Modeling Counterion Binding in Ionic-Nonionic and Ionic-Zwitterionic Binary Surfactant Mixtures, *Langmuir*, 21: p. 9850-9865 (2005).

25. H.Tang, S.Mitragotri, D.Blankschtein, and R.Langer, Theoretical Description of Transdermal Transport of Hydrophilic Permeants: Application to Low-Frequency Sonophoresis, *Journal of Pharmaceutical Sciences*, 90(5):p. 545-568 (2001).

26. S. Mitragotri, D.Blankschtein, and R.Langer, Transdermal drug delivery using low frequency sonophoresis, *Pharmaceutical Research,* 13:p. 411-420 (1996).

27. M.E.Johnson, "Biophysical aspects of transdermal drug delivery and chemical enhancement", Ph.D thesis, Department of Chemical Engineering, Massachusetts Institute of Technology, Cambridge, MA, USA: p. 201-204 (1996).

28. R.Scheuplein, and I.Blank, Permeability of the skin. *Physical Review,* 51:p. 702-747 (1971).

29. J.A.Bouwstra, M.A.de Vries, G.S.Gooris, W.Bras, J.Brussee, and M.Ponec, Thermodynamic and structural aspects of the skin barrier, *Journal of Controlled Release*, 15:p. 209-220 (1991).

30. P.W.Wertz and D.E.Downing, Stratum Corneum: Biological and biochemical considerations, in J.Hadgraft, and R.H.Guy (Eds.). *Transdermal Drug Delivery: Developmental Issues and Research Initiatives, Marcel Dekker, Inc.* (1989).

31. E.J.Wood and P.T.Bladon, The human skin, Edward Arnold (1985).

32. H.L.Hood, M.E K.Kraeling, M.G.Robl, and R.L.Bronaugh, The effects of an alpha hydroxy acid (glycolic acid) on hairless guinea pig skin permeability, *Food and Chemical Toxicology*, 37:p. 1105-1111 (1999).

33. P.T.C.So, H.Kim, and I.E.Kochevar, Two-photon deep tissue ex vivo imaging of mouse dermal and subcutaneous structures, *Optics Express*, 3(9):p. 339-350 (1998).

34. P.T.C.So, C.Y.Dong, B.R.Masters, and K.M.Berland, Two-Photon Excitation Fuorescence Microscopy, *Annu. Rev. Biomed. Eng.*, 02:p. 399-429 (2000).

35. J.C.Malone, A.F.Hood, T.Conley, J.Nurnberger, L.A.Baldridge, J.L.Clendenon, K.W.Dunn, and C.L.Phillips, Three-dimensional imaging of human skin and mucosa by two-photon laser scanning microscopy, *Journal of Cutaneous Pathology*, 29:p. 453-458 (2002).

36. W.Denk, J.H.Strickler, and W.W.Webb, Two-photon laser scanning fluorescence microscopy. *Science*, 248:p. 73-76 (1990).

37. B.Yu, C.Y.Dong, P.T.So, D.Blankschtein, and R.Langer, In vitro visualization and quantification of oleic acid induced changes in transdermal transport using two-photon fluorescence microscopy, *Journal of Investigative Dermatology,* 117:p. 16-25 (2001).

38. B.Yu, "Elucidation of chemically-induced transdermal transport processes", Ph.D. thesis, Department of Chemical Engineering, Massachusetts Institute of Technology, Cambridge, MA, USA (2002).

39. K.D.Peck, A.H. Ghanem, and W.I.Higuchi, Hindered diffusion of polar molecules through and effective pore radii estimates of intact and ethanol treated human epidermal membrane, *Pharmaceutical Research*, 11(9):p. 1306-1314 (1994).

40. K.D.Peck, A.H.Ghanem, and W.I.Higuchi, The effect of temperature upon the permeation of polar and ionic solutes through human epidermal membrane, *Journal of Pharmaceutical Sciences*, 84(8):p. 975-982 (1995).

41. A.Tezel, A.Sens, and S.Mitragotri, Description of Transdermal transport of hydrophilic solutes during low-frequency sonophoresis based on a modified porous pathway model, *Journal of Pharmaceutical Sciences,* 92(2):p. 381-393 (2003).

42. G.K.Menon and P.M.Elias, Morphologic basis for a pore-pathway in mammalian stratum corneum, *Skin Pharmacology*, 10:p. 235-246 (1997).

43. R.M.Raphael, R.E.Waugh, S.Svetina, and B.Zeks, Fractional occurrence of defects in membranes and mechanically driven interleaflet phospholipids transport, *Physical Review B*, 64(5), art. no. 05913, part 1.

44. M.S.Malghani, J.Yang, and J.Wu, Generation and growth of bilayer defects induced by ultrasound, *Journal of the Accoustic Society of America*, 103:p. 1682-1685 (1998).

45. R.R.Burnette and B.Ongpipattanakul, Characterization of the permselective properties of excised human skin during iontophoresis, *Journal of Pharmaceutical Sciences*, 76:p. 765-773 (1987).

46. S.M.Sims, W.I.Higuchi, and V.Srinivasan, Skin alteration and convective solvent flow effects during iontophoresis: I. Neutral solute transport across human skin, *International Journal of Pharmaceutics*, 69:p. 109-121 (1991).

47. S.K.Li, A.H.Ghanem, and W.I.Higuchi, Pore charge distribution considerations in human epidermal membrane electroosmosis, *Journal of Pharmaceutical Sciences*, 88(10):p. 1044-1049(1999).

48. P.Moore, "A fundamental investigation of surfactant-induced skin irritation", Ph.D. thesis, Department of Chemical Engineering, Massachusetts Institute of Technology, Cambridge, MA, USA (2002).

49. This figure has been modified from Figure 12-4 and Figure 12-5 in P.M.Elias and K.R.Feingold, Skin as an Organ of Protection, in *Fitzpatrick's dermatology in general medicine, New York:McGraw-Hill, Health Professions Division, c1999.*

50. A.Di Nardo, K.Sugino, P.Wertz, J.Ademola, and H.I.Maibach, Sodium lauryl sulfate (SLS) induced irritant contact dermatitis: a correlation study between ceramides and in vivo parameters of irritation, *Contact Dermatitis*, 35:p. 86-91 (1996).

51. R.L.Bronaugh and H.I.Maibach, In vitro models for human percutaneous absorption, In H.I.Maibach et al. (Eds.). *Models in Dermatology, Karger, Bassel*, Vol.2, p.178-188, (1985).

52. R.L.Bronaugh, R.F.Stewart, E.R.Congdon, A.L.Giles. Jr, Methods for in vitro pecutaneous absorption studies. I. Comparison with in vivo results. *Toxicol. Appli. Pharmacol*, 62:p. 474-480 (1982).

53. H.Tang, "Experimental and theoretical investigation of the effects of low-frequency sonophoresis on transdermal drug transport", Ph.D. thesis, Department of Chemical Engineering, Massachusetts Institute of Technology, Cambridge, MA, USA (1997).

54. S.K.Li, A.H.Ghanem, K.D.Peck, and W.I.Higuchi, Characterization of the transport pathways induced during low to moderate voltage iontophoresis in human epidermal membrane, *Journal of Pharmaceutical Science*, 87: p. 40-48 (1998).

55. R.R.Warner, Y.L.Boissy, N.A.Lilly, M.J.Spears, K.McKillop, J.L.Marshall, and K.J.Stone, Water disrupts stratum corneum lipid lamellae: Damage is similar to surfactants, *Journal of Investigative Dermatology*, 113:p. 960-966 (1999).

56. S.K.Li, W.Suh, H.H.Parikh, A.Ghanem, S.C.Mehta, K.D.Peck, and W.I.Higuchi, Lag time data for characterizing the pore pathway of intact and chemically pretreated human epidermal membrane, *International Journal of Pharmaceutics*, 170:p. 93-108 (1998).

57. B.R.Masters, P.T.C.So, and E.Gratton, Optical biopsy of in vivo human skin: Multi-photon excitation microscopy. *Lasers Med Sci*, 13:p. 196-203 (1998).

58. K.H.Kim, C.Buehler, and P.T.C.So, High-speed, two-photon scanning microscope, *Applied Optics*, 38(28):p. 6004-6009 (1999).

59. B.R.Masters, P.T.C.So, and E.Gratton, Multiphoton excitation fluorescence microscopy and spectroscopy of in vivo human skin, *Biphysical Journal*, 72:p. 2405-2412 (1997).

60. R.Na, I.Stender, L.Ma, and H.C.Wulf, autofluorescence spectrum of skin: component bands and body site variations, *Skin Res. Technol.*, 6: p. 112-117 (2000).

61. K.P.Ananthapadmanabhan, K.K.Yu, C.L.Meyers, and M.P.Aronson, Binding of surfactants to stratum corneum, *Journal of the Society of Cosmetic Chemists*, 47:p. 185-200 (1996).

62. K.P.Ananthapadmanabhan, D.J.Moore, K.Subramanyan, M.Misra, and F.Meyer, Cleansing without compromise: The impact of cleansers on the skin barrier and the technology of mild cleansing, *Dermatologic Therapy*, 17:p. 16-25 (2004).

63. W.M.Deen, Hindered transport of large molecules in liquid-filled pores, *AIChE Journal*, 33(9):p. 1409-1425 (1987).

64. J.L.Anderson and J.A.Quinn, Restricted transport in small pores, a model for steric exclusion and hindered particle motion, *Biophysical Journal*, 14:p. 130 (1974).

65. F.G.Smith and W.M.Deen, Electrostatic effects on the partitioning of spherical colloids between dilute bulk solution and cylindrical pores, *Journal of Colloid and Interface Science*, 91(2):p. 571-590 (1983).

66. M.E.Johnson, D.Blankschtein, and R.Langer, Evaluation of solute permeation through the stratum corneum: lateral bilayer diffusion as the primary transport mechanism, *Journal of Pharmaceutical Sciences*, 86(10):p. 1162-1172 (1997).

67. D.M.Malone and J.L.Anderson, Hindered diffusion of particles through small pores. *Chemical Engineering Science*, 33:p. 1429-1440 (1978).

68. B.D.Mitchell and W.M.Deen, Theoretical effects of macromolecule concentration and charge on membrane rejection coefficients, *Journal of Membrane Science*, 19:p. 75 (1984).

69. H.Schaefer, and T.E.Redelmeier, *Skin Barrier*, Basel: Karger, 1996.

70. S.Mitragotri, M.E.Johnson, D.Blankschtein, and R.Langer, A theoretical analysis of partitioning, diffusion, and permeation across lipid bilayers, *Biophysical Journal*, 77:p. 1268-1283 (1999).

71. P.Moore, S.Puvvada, and D.Blankschtein, Challenging the surfactant monomer skin penetration model: Penetration of sodium dodecyl sulfate micelles into the epidermis, *Journal of Cosmetic Science*, 54:p. 29-46 (2003).

72. E.Beraradesca and F.Distante, Mechanisms of skin irritation, *Current problems in dermatology*, 23:p. 1-8 (1995).

73. L.C.Wood, S.M.Jackson, P.M.Elias, C.Grunfeld, and K.R.Feingold, Cutaneous barrier perturbation stimulates cytokine production in the epidermis of mice, *J Clin Invest*, 90:p. 482-487 (1992).

74. H.Mariko and A.S.Verkman, Glycerol replacement corrects defective skin hydration, elasticity, and barrier function in aquaporin-3-deficient mice, *Proceedings of the National Academy of Sciences of the United States of America*, 100(12):p.7360-7365 (2003).

75. A.E.Sagiv, A.Ingber, and S.Dikstein, A novel in vivo model in guinea pigs for dry skin syndrome, *Skin Research and Technology*, 6:p. 37-42 (2000).

76. M.Loden, A.C.Andersson, C.Anderson, I.M.Bergbrant, T.Frodin, H.Ohman, M.Sandstrom, T.Sarnhult, E.Voog, B.Stenberg, E.Pawlik, A.Haggqvist, A.Svensson, and M.Lindburg, A double-blind study comparing the effect of glycerin and urea on dry, eczematous skin in atopic patients, *Acta Derm Venereol*, 82:p. 45-47 (2002).

77. B.Forslind, A domain mosaic model of the skin barrier, *Acta Derm Venereol*, 74:p. 1-6 (1994).

78. L.D.Rhein, In vitro interactions: Biochemical and biophysical effects of surfactants on skin. In: *Surfactants in Cosmetics* (M.M.Rieger and L.D.Rhein, eds), p. 397-426. Surfactant Science Series, Marcel Dekker, Inc., Vol. 68 (1997).

79. G.Imokawa, Surfactant mildness. In: *Surfactants in Cosmetics* (M.M.Rieger and L.D.Rhein, eds), p. 427-471. Surfactant Science Series, Marcel Dekker, Inc., Vol. 68 (1997).

80. J.A.Faucher and E.D.Goddard, Interaction of keratinous substrates with sodium lauryl sulfate II. Permeation through stratum corneum, *Journal of the Society for Cosmetic Chemists*, 29:p. 339-352 (1978).

81. H.Korting, T.Herzinger, A.Hartinger, and M.Kerscher, Discrimination of the irritancy potential of surfactans in vitro by two cytotoxicity assays using normal human keratinocytes, HaCaT cells and 3T3 mouse fibroblast: Correlation with in vivo data from a soap chamber assay, *Journal of Dermatological Science*, 7:p. 119-129 (1994).

82. A.Tezel, A.Sens, and S.Mitragotri, Incorporation of lipophilic pathways into the porous pathway model for describing skin permeabilization during low frequency sonophoresis, *Journal of Controlled Release*, 83:p.183-188 (2002).

83. P.Moore, A.Shiloach, S.Puvvada, and D.Blankschtein, Penetration of mixed micelles into the epidermis: Effect of mixing sodium dodecyl sulfate with dodecyl hexa (ethylene oxide), *Journal of Cosmetic Science*, 54:p. 143-159 (2003).

84. Y.N.Kalia and R.H.Guy, The electrical characteristics of human skin in vivo, *Pharmaceutical Research*, 12:p. 1605-1613 (1995).

85. S.W.Babulak, L.D.Rhein, D.D.Scala, A.F.Simion, and G.L.Grove, Quantitation of erythema in a soap chamber test using the minolta chroma (reflectance) meter: Comparison of instrumental results with visual assessments, *J. Soc. Cosmet. Chem.* 37:p. 475-479 (1986).

86. G.L.Grove, M.J.Grove, C.Zerweck and E.Pierce: Computerized evaporimetry using the DermaLab TEWL probe, *Skin Res. & Tech*, 5:p. 9-13 (1999).

87. M.Obata, and H.Tagami, A rapid in vitro test to assess skin moisturizers, *J. Soc. Cosmet. Chem.*, 41:p. 235-241 (1990).

Chapter 2

2. The Role of Sodium Dodecyl Sulfate Micelles in Inducing Skin Barrier Perturbation in the Presence of Glycerol

2.1. Introduction and Significance

Human skin consists of three stratified layers, the stratum corneum, the viable epidermis, and the dermis (1). The stratum corneum (SC), which is the top most layer of the skin, possesses an ordered brick-and-mortar structure, which consists of the flat corneocytes (the cellular bricks), interlocked with the lipid lamellae (the intercellular mortar) (2-5). Compared to the porous structure of the viable epidermis and the porous-and-hydrated structure of the dermis, the rigid and ordered structure of the stratum corneum makes it a very effective permeability barrier that is primarily responsible for the skin barrier function (2-4). The lipid lamellae of the SC consist of lipid bilayers alternating with aqueous, hydrophilic layers (1-4). Under passive skin permeation conditions, permeants traverse the SC through diffusion across the lipid lamellae. Although diffusion through the "oily" lipid lamellae can explain the permeation of *hydrophobic* molecules

across the SC, it cannot explain the permeation of *hydrophilic* molecules across the SC, as observed in many earlier studies (6-9).

Indeed, if no aqueous/hydrophilic transport pathways existed within the SC oily lipid domain, then aqueous/hydrophilic permeants, for example Mannitol (6-9), could not traverse the SC solely through the lipoidal/hydrophobic pathways that exist in the lipid bilayer domains in the SC. The observation that hydrophilic solutes are able to permeate across the SC, even under passive skin permeation conditions, has led researchers to propose the existence of tortuous, aqueous porous pathways through the intercellular lipid lamellae in the SC. In fact, Menon and Elias have established a morphological basis for the existence of a pore pathway in the mammalian SC (10). Menon and Elias applied hydrophilic and hydrophobic tracers in vivo to murine skin under passive skin permeation conditions, and also under enhanced skin permeation conditions, including chemical enhancers, a lipid synthesis inhibitor, sonophoresis, and iontophoresis, and following that, utilized Ruthenium Tetroxide Staining and Microwave Post Fixation methods to visualize the resulting penetration pathways (10). Their results revealed that both the hydrophobic and the hydrophilic tracers localized to discrete *lacunar domains* embedded within the extracellular lipid lamellar domains (10). Menon and Elias also observed that under skin permeation enhancement conditions, the lacunar domains exhibited an increasing extent of structural continuity when compared to passive skin permeation conditions (10). Hence, structurally continuous lacunar domains have been considered by Menon and Elias as providing a physical basis for the existence of aqueous pores and polar pathways through the intercellular lipoidal mortar in the SC (10). These aqueous pores in the SC provide the primary skin barrier penetration and transport pathways for hydrophilic chemicals, which would otherwise not be

able to penetrate into the skin barrier through the lipoidal, hydrophobic pathways that exist in the SC (6-11).

In general, surfactants commonly encountered in skin-care formulations are known to reduce the barrier properties of the skin (11-15). It is well-accepted that surfactants have to first penetrate into the skin barrier before they can reduce the skin barrier properties. Therefore, if a formulator can minimize surfactant-skin penetration, this should also minimize the ability of the surfactant to reduce the skin barrier properties. Sodium Dodecyl Sulfate (SDS), an anionic surfactant and a model skin irritant, penetrates into and disrupts the skin barrier upon contacting it from an aqueous solution. The SDS monomers self-assemble to form micelles at concentrations above the Critical Micelle Concentration (CMC). Studies show, both in vitro and in vivo, that the SDS-induced skin barrier disruption is *dose-dependent*, and that it increases with an increase in the total SDS concentration above the CMC of SDS (11-13). This important observation contradicts the well-accepted *Monomer Penetration Model (MPM)*, which attempts to explain surfactant-skin penetration by considering solely the role of the surfactant monomers which can penetrate the skin barrier through the aqueous pores in the SC (11-23). The MPM does not consider the possibility that surfactant micelles may also contribute to surfactant-skin penetration, and consequently, to surfactant-skin barrier disruption, since it considers the micelles to be too large to penetrate through the aqueous pores that exist in the SC. In her comprehensive review of surfactant-skin interactions, Rhein stated that the observed dose dependence of surfactant-induced skin irritation beyond the CMC cannot be explained solely by the contribution of the monomeric surfactant (14). Indeed, Agner and Serup had earlier observed that the severity of the transepidermal water loss (TEWL) induced by SDS increased as the SDS concentration increased beyond the CMC of SDS (8.7 mM) (13). In separate studies,

Ananthapadmanabhan et al. (15) and Faucher et al. (16) observed that as the SDS concentration increased beyond the CMC, the extent of SDS-skin penetration also increased.

Through in vitro SDS-skin penetration studies, Moore et al. (11) provided substantial evidence which indicates that the amount of SDS that can penetrate into the skin barrier is dose-dependent, and furthermore, that the SDS surfactant in micellar form also contributes to SDS-skin penetration. In addition, Moore et al. demonstrated conclusively that the contribution of the SDS micelles to SDS-skin penetration dominates that of the SDS monomers at concentrations above the CMC, which are typically encountered in skin-care formulations (11).

In this chapter, I have further investigated, from a mechanistic perspective, *how* SDS micelles may contribute to SDS-skin penetration, thereby leading to the previously observed dose-dependence of SDS-induced skin barrier perturbation (11-23). Specifically, I will provide new evidence, through in vitro transdermal permeability and skin electrical current measurements, in the context of a hindered-transport porous pathway model of the SC (6-9, 42), that the aqueous pores in the SC *increase both in size and in porosity-to-tortuosity ratio* when skin is exposed to an aqueous SDS contacting solution, such that the average pore radius is larger than the SDS micelle radius. As a result, SDS micelles, contrary to the view put forward by the MPM, are not sterically hindered from penetrating into the skin barrier through these pores.

Inspired by the proposed mechanistic understanding of how SDS micelles may contribute to SDS-induced skin barrier perturbation, I have also investigated in vitro whether the addition of Glycerol, a well-known humectant and skin beneficial agent, to the aqueous SDS contacting solution can minimize the observed contribution of the SDS micelles to SDS-skin penetration. Although not within the scope of this chapter, if shown to be valid in vivo, such a strategy can also significantly reduce the amount of SDS that can penetrate into the skin barrier and induce

skin barrier perturbation in vivo. The in vitro results presented in this chapter are compared with in vivo results in Chapter 4.

My approach considers exposing skin in vitro to aqueous mixtures of Glycerol and SDS. The importance of Glycerol (or glycerin) in skin care products is well established, and Glycerol is widely used in cosmetic and pharmaceutical formulations (24-31). To explain its in vivo benefits, studies have focused on its humectant and smoothing effects (25) and on its protective functions in emulsion systems against skin irritation (26). Researchers have shown that Glycerol diffuses into the SC, increases skin hydration, and relieves clinical signs of dryness (27-29). One of the views regarding the effect of Glycerol on the skin held by researchers today is that Glycerol may influence the crystalline arrangement of the intercellular lipid bilayers. The bulk of the bilamellar lipid sheets are proposed to be in crystalline/gel domains bordered by lipids in a fluid crystalline state. In skin exhibiting SC barrier damage, the proportion of lipids in the solid state may be elevated, and subsequent skin exposure to Glycerol may help maintain these lipids in a liquid crystalline state at low relative humidity, thereby enhancing SC barrier function and decreasing SC water permeability (30). A second prevalent view is that Glycerol may increase the rate of corneocyte loss from the upper layers of the SC, through a keratolytical effect due to enhanced desmosome degradation, thereby reducing scaliness of dry skin and maintaining SC barrier (31). A third, more recent view advanced by Fluhr et al. is based on the hygroscopic property of Glycerol (24). Glycerol, by virtue of its high transdermal diffusivity, can penetrate into the SC, and, by virtue of its hygroscopic property, is able to bind water and thus reduce water evaporation. Therefore, Glycerol, by absorbing water, may modulate water fluxes in the SC, which, in turn, may lead to a stimulus for SC barrier repair.

However, it is still not well understood how Glycerol may mitigate surfactant-induced SC barrier perturbation induced by a formulation containing aqueous mixtures of Glycerol and a surfactant, such as SDS. Most of the studies discussed above (24-31) considered the application of Glycerol to forearm skin in vivo, either: (1) as dilute aqueous solutions containing 5-15 wt% Glycerol, or (2) as cosmetic formulations, such as barrier creams, containing a similar range of Glycerol concentrations. With this in mind, using such an aqueous mixture of SDS and 10 wt% Glycerol, I will demonstrate in vitro that the addition of Glycerol eliminates almost completely the contribution of the SDS micelles to SDS-skin penetration. Using dynamic light scattering (DLS) measurements, I will show that the addition of 10 wt% Glycerol to an aqueous SDS contacting solution does not increase the size of the SDS micelles, which if increased, could explain the observed reduced ability of SDS (present in the larger SDS micelles) to penetrate into the skin and induce less skin barrier perturbation in the presence of Glycerol. Furthermore, using surface tension measurements, I will show that the addition of 10 wt% Glycerol to an aqueous SDS contacting solution does not decrease the CMC, and hence, does not reduce the concentration of the SDS monomers contacting the skin, which if reduced, could explain the observed reduced ability of SDS (present in monomeric form) to penetrate into the skin and induce less skin barrier perturbation in the presence of Glycerol. Finally, using in vitro Mannitol skin permeability and skin electrical current measurements, in the context of a hindered-transport porous pathway model of the SC (6-9, 42), I will show that a plausible explanation of my findings is that the addition of 10 wt% Glycerol to an aqueous SDS contacting solution reduces the size and the porosity-to-tortuosity ratio of the aqueous pores in the SC relative to the SDS micelle size, such that the SDS micelles present in the contacting solution are sterically hindered

from penetrating into the SC. This, in turn, leads to significantly less SDS-induced skin barrier perturbation upon the addition of 10 wt% Glycerol.

2.2. Experimental

2.2.1. Materials

Sodium Dodecyl Sulfate (SDS) was purchased from Sigma Chemicals (St. Louis, MO). Analytical-grade Glycerol was purchased from VWR Chemicals (Cambridge, MA). ^{14}C-radiolabeled SDS and ^{3}H-radiolabeled Mannitol were purchased from American Radiolabeled Chemicals (St. Louis, MO). All these chemicals were used as received. Water was filtered using a Millipore Academic water filter (Bedford, MA). Phosphate buffered saline (PBS) was prepared using PBS tablets from Sigma Chemicals (St. Louis, MO) and Millipore filtered water, such that a phosphate concentration of 0.01 M along with a NaCl concentration of 0.137 M were obtained at a pH of 7.2.

2.2.2. Preparation of the Skin Samples

Female Yorkshire pigs (40-45kg) were purchased from local farms, and the skin (back) was harvested within one hour after sacrificing the animal. The subcutaneous fat was trimmed off using a razor blade, and the full-thickness pig skin was cut into small pieces (2cm × 2cm) and stored in a –80 °C freezer for up to 2 months. The surfactant penetration experiments were performed using pig full-thickness skin, referred to hereafter as p-FTS.

2.2.3. In Vitro Transdermal Permeability Measurements

Vertical Franz diffusion cells (Permegear Inc., Riegelsville, PA) were utilized in the in vitro transdermal permeability measurements (see *Figure 2-1*). All the experiments were performed at room temperature (25°C). Prior to each experiment, a p-FTS sample was mounted in the diffusion cell with the SC facing the donor compartment. Both the donor and the receiver compartments were filled with PBS, and the p-FTS sample was left to hydrate for 1 hour before the beginning of the experiment to allow the skin initial barrier property to reach steady state. At this point, the skin electrical current across the p-FTS sample was measured (see below), and only p-FTS samples with an initial skin current < 3 μA were utilized in the permeation studies (a well-accepted criterion for selecting suitable in vitro skin samples (6, 7)). The PBS in the donor compartment was then replaced with either 1.5 ml of an SDS aqueous solution or 1.5 ml of an SDS+10 wt% Glycerol aqueous solution. The solution in the donor compartment, referred to hereafter as the contacting solution, contacted the p-FTS sample for 5 hours. Note that a 5-hour exposure of the skin was chosen because this is a sufficiently long time to allow significant SDS-skin penetration, yet a short enough time to prevent the saturation of the skin with SDS. Subsequently, the contacting solution was removed and the donor compartment along with the p-FTS sample were rinsed 4 times with 2 ml of PBS to remove any trace chemical left on the skin surface and in the donor compartment. The receiver compartment was stirred with a magnetic stirrer at a speed of 400 rpm throughout the experiment to eliminate permeant bulk concentration gradients.

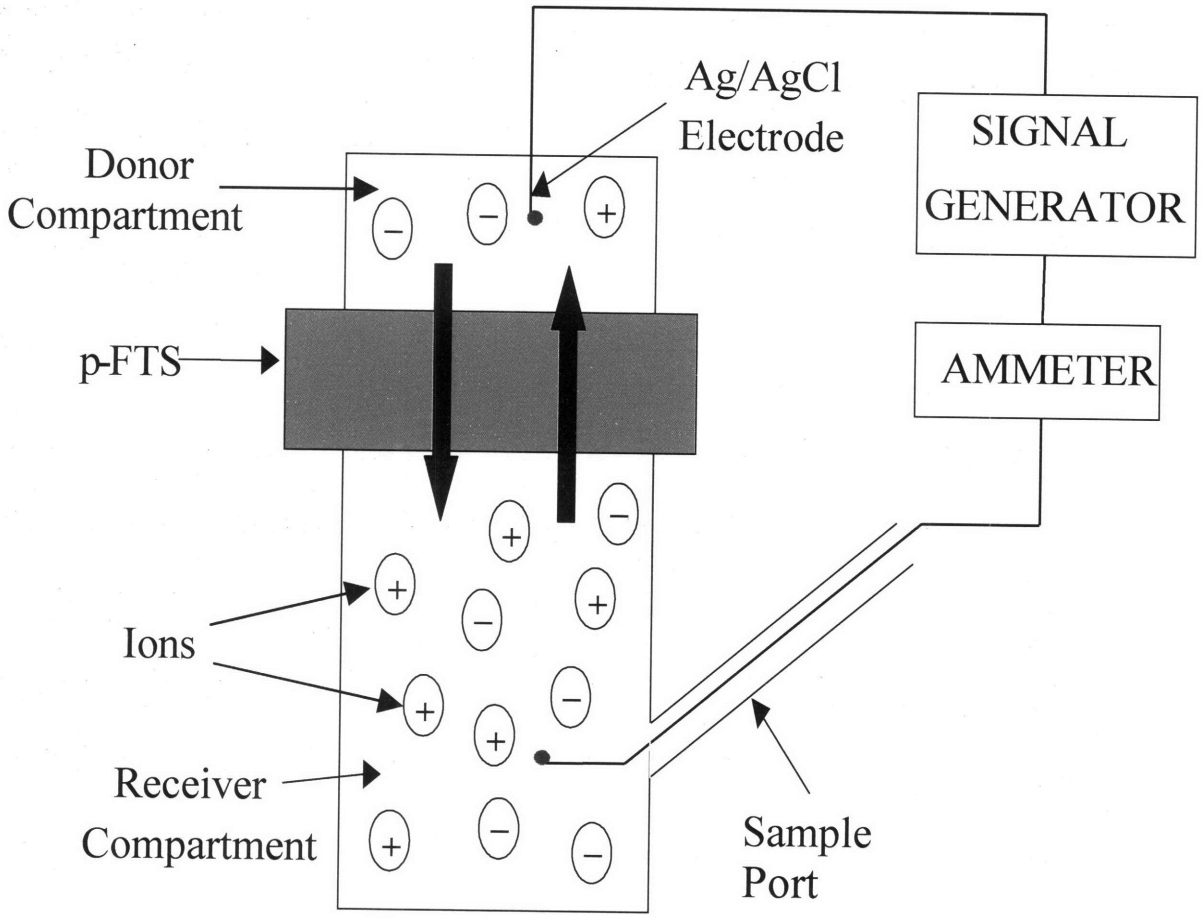

Figure 2-1. Vertical Franz diffusion cell experimental setup to measure Mannitol skin permeability, skin electrical current, and/or skin radioactivity in vitro.

Following the SDS and the SDS+10 wt% Glycerol aqueous contacting solutions treatments of the skin, the p-FTS samples in the diffusion cells were exposed to a contacting solution of ^{3}H-radiolabeled Mannitol in PBS (1–10 μCi/ml) for 24 hours. Mannitol is: (1) a low molecular weight monosaccharide (MW=182 Da) (6, 7), and (2) a highly hydrophilic (log $K_{O/W}$ = -3.1) chemical (7), which is not metabolized by the body, and hence, if desired, can also be used for in vivo skin permeation studies (6, 7). Being small in size and highly hydrophilic,

Mannitol can access similar aqueous pores as do ions in order to transport across the skin barrier. This, in turn, makes Mannitol a suitable permeant to study in the context of the hindered-transport porous pathway model of the SC (6-9). Pretreatment of p-FTS with (1) SDS or (2) SDS+10 wt% Glycerol aqueous contacting solutions in this manner, followed by passive Mannitol skin permeation, allowed for a controlled comparison of the skin barrier perturbation potential of solutions (1) and (2) at fixed exposure times of 5 hours. Throughout these experiments, solution samples were withdrawn from both the receiver (r) and the donor (d) compartments every two hours, and the concentrations of the radiolabeled permeant (Mannitol) in the two compartments (C_r and C_d, respectively) were measured using a liquid scintillation counter (Packard, Sheldon, CT). When the transport of Mannitol attained steady state, the Mannitol skin permeability, P, was calculated as follows (6, 7):

$$P = \frac{1}{AC_d}\left(\frac{d\left(C_r V_r\right)}{dt}\right) \tag{1}$$

where V_r is the volume of the receiver compartment, A = (1.77 cm^2) is the area of the SC exposed to the Mannitol solution in the donor compartment, and t is the exposure time.

Equation (1) is based on the following two assumptions: (i) the concentration of the permeant in the donor compartment is high, and does not deplete with time, and (ii) the concentration of the permeant in the donor compartment is always much higher than that in the receiver compartment. In the experiments reported here, assumptions (i) and (ii) were both satisfied because less than 2% of Mannitol in the contacting solution permeated across the p-FTS samples.

2.2.4. In Vitro Skin Electrical Current and Skin Electrical Resistivity Measurements

During each skin permeation experiment, two Ag/AgCl electrodes (E242, In Vivo Metrics, Healdsburg, CA) were placed in the donor and in the receiver compartments to measure the electrical current and the electrical resistivity across the p-FTS sample (see *Figure 2-1*). A 100 mV AC voltage (RMS) at 10 Hz was generated by a signal generator (Hewlett-Packard, Atlanta, GA), and was applied across the two electrodes for 5 s. The electrical current across the skin was measured using an Ammeter (Hewlett-Packard, Atlanta, GA). This ammeter was used to measure low AC currents and was accurate in the 0.1 μA range. The electrical resistance of the p-FTS sample was then calculated from Ohm's law (7). Because the measured skin electrical resistance is the sum of the actual skin electrical resistance and the background PBS electrical resistance, the latter was subtracted from the measured skin electrical resistance to obtain the actual skin electrical resistance. The skin electrical resistivity was then obtained by multiplying the actual skin electrical resistance by the skin area (A=1.77 cm^2). The skin electrical resistivity, being an intrinsic electrical property of the skin membrane, is a preferred measure in this analysis over the skin electrical resistance which is an extensive electrical property of the skin membrane (33). Therefore, by using the skin electrical resistivity, it will be easier to compare differences in the electrical properties of the skin barrier upon exposure of the skin to the SDS and to the SDS+10 wt% Glycerol aqueous contacting solutions. Skin electrical current and resistivity measurements were carried out before and during the permeation experiments at each predetermined sampling point. For each p-FTS sample, an average skin electrical resistivity was determined over the same time period for which the steady-state skin permeability, P, was calculated using Eq.(1). This average skin electrical resistivity, R, was then analyzed along with

the corresponding skin permeability, P, in the context of the theoretical framework presented below in the Theoretical Section.

2.2.5. In Vitro Skin Radioactivity Measurements

The p-FTS samples were mounted in vertical Franz diffusion cells, as was done in the case of the skin transdermal permeability measurements described above. Following a similar protocol, p-FTS samples were now exposed to aqueous contacting solutions containing 1.5 ml of SDS or 1.5 ml of SDS+10 wt% Glycerol. Each of these contacting solutions also contained about 1 μCi/ml of ^{14}C-SDS.

Diffusion of SDS into the skin took place for 5 hours, as before, and subsequently, the aqueous contacting solutions were removed and the donor compartment along with the p-FTS sample were rinsed 4 times with 2 ml of PBS to remove any trace chemical left on the skin surface and in the donor compartment. The p-FTS samples were then heat-stripped following a well-known procedure (11). Briefly, a p-FTS sample was placed in a water bath at 60°C for two minutes, and subsequently, the epidermis (the SC and the viable epidermis) that was exposed to the contacting solution was peeled off from the dermis. The exposed epidermis was then dried for two days in a fume hood and weighed. The dried epidermis was dissolved overnight in 1.5 ml of Soluene-350 (Packard, Meriden, CT). After the epidermis dissolved, 10 ml of Hionic Fluor scintillation cocktail (Packard) was added to the Soluene-350, and the concentration of radiolabeled SDS was determined using the Packard scintillation counter. Note that we did verify that the concentration of radiolabeled SDS in the contacting solution did not change appreciably during the 5-hour exposure to the skin. The concentration of radiolabeled SDS in the contacting solution was determined by using approximately 100 μl of the contacting solution and assaying for the radioactivity of ^{14}C-SDS using the scintillation cocktail assay described above.

Knowing the concentration of SDS in the contacting solution, C_{SDS}, the radioactivity of the contacting solution, $C_{rad,donor}$, the dry weight of the epidermis, m, and the radioactivity of the epidermis, $C_{rad,skin}$, I was able to determine the concentration of SDS in the dried epidermis, $C_{SDS,skin}$, using the following equation (11):

$$C_{SDS,skin} = \frac{C_{rad,skin} \cdot C_{SDS}}{C_{rad,donor} \cdot m} \tag{2}$$

2.2.6. Dynamic Light Scattering Measurements

The aqueous SDS and SDS+10wt% Glycerol solutions were prepared in Millipore filtered water with 100 mM of added NaCl. Note that 100 mM NaCl was added to screen potential electrostatic repulsions between the negatively-charged SDS micelles while performing the Dynamic Light Scattering (DLS) measurements (11, 34, 36-39). After mixing, the solutions were filtered through a 0.02 μm Anotop 10 syringe filter (Whatman International, Maidstone, England) directly into a cylindrical-scattering cell to remove any dust from the solution, and then sealed until use. Dynamic Light Scattering (34) was performed at 25°C and a 90° scattering angle on a Brookhaven BI-200SM system (Brookhaven, Holtsville, NY) using a 2017 Stabilite argon-ion laser (Spectra Physics) at 488 nm. The autocorrelation function was analyzed using the CONTIN program provided by the BIC Dynamic Light Scattering software (Brookhaven, Holtsville, NY), which determines the effective hydrodynamic radius, $\overline{R}_h$, of the scattering entities using the Stokes-Einstein relation (35):

$$\overline{R}_h = \frac{k_B T}{6\pi\eta\overline{D}} \tag{3}$$

where k_B is the Boltzmann constant, T is the absolute temperature, η is the viscosity of the aqueous salt solution, and $\overline{D}$ is the mean diffusion coefficient of the scattering entities.

In order to measure the size of the SDS micelles in the aqueous SDS and in the SDS+10 wt% Glycerol solutions, while eliminating the effects of interparticle interactions, the effective hydrodynamic radii were determined at several different SDS concentrations, and then extrapolated to a zero micelle concentration, which corresponds to the CMC of SDS, 8.7 mM (11, 34, 36-39). Note that the viscosity of a 10 wt% Glycerol aqueous solution is similar to that of water, and hence, viscosity effects did not play a significant role in these measurements.

2.2.7. Surface Tension Measurements

We utilized surface tension measurements to determine the critical micelle concentration, CMC, of the SDS and of the SDS+10 wt% Glycerol aqueous micellar solutions. It is well-known that as the surfactant concentration, X, is increased, both the hydrophobicity of the surfactant tails and the high water-air surface free energy promote the adsorption of the surfactant molecules onto the surface (40). The increase in the surface pressure due to surfactant surface adsorption leads to a lowering of the surface tension, σ. Beyond a certain threshold surfactant concentration, the CMC, it becomes more favorable, from a free energy point of view, for the surfactant molecules added to the solution to form micelles, rather than to continue to adsorb at the surface. This is reflected in a negligible change in surface tension, σ, with increasing surfactant concentration, X, beyond the CMC. The "break" in the σ versus X curve, therefore, approximates the concentration at which micellization first takes place (40). In order to determine this "break", the equilibrium surface tensions of SDS in water and of SDS in water+10 wt% Glycerol were measured as a function of the logarithm of the SDS solution concentration using a Kruss K-11 tensiometer (Charlotte, NC) with a platinum plate. Additional experimental details can be found in reference (41). The experimental uncertainty in the surface tension

measurements was approximately 0.05 dyn/cm. The temperature was held constant at 25.0±0.1°C by a thermostatically-controlled jacket around the sample.

A plot of σ as a function of the logarithm of the surfactant concentration, X, was generated using the procedure outlined above for the SDS and for the SDS+10 wt% Glycerol aqueous micellar solutions. Linear regression was utilized to determine the best fit line on either side of the break in the curve, and the value of the SDS concentration at the intersection of these two best-fit lines was taken as the experimental CMC value.

2.3. Theoretical

2.3.1. Determination of the Radius and the Porosity-to-Tortuosity Ratio of the Skin Aqueous Pores Using Hindered-Transport Theory

Tang et al. (7) have recently demonstrated the existence of a linear-log relationship between the Mannitol skin permeability, P, and the average skin electrical resistivity, R. Specifically, within statistical error, the following relation holds (7):

$$\log P = \log C - \log R \tag{4}$$

where $C = (k_B T/2z^2 F c_{ion} e_0)^* (D_p^{\infty} H(\lambda_p)/ D_{ion}^{\infty} H(\lambda_{ion}))$ is a constant that depends on the average skin aqueous pore radius, r_{pore}, through $H(\lambda_p)$ and $H(\lambda_{ion})$, as follows (7, 8, 63): [3]

$$H(\lambda_i) = \phi_i\left(1 - 2.1044\lambda_i + 2.089\lambda_i^3 - 0.948\lambda_i^5\right), \text{ for } \lambda_i \leq 0.4 \tag{5}$$

[3] It is noteworthy that the skin aqueous pores have a distribution of pore radii (41). In this chapter, we imply the *average* pore radius to be the *mean* of this distribution of pore radii, and denote this as the *radius* of the aqueous pores.

where i = p (permeant, in our case, Mannitol) or ion, r_{pore} = pore radius, $\lambda_i = r_i/r_{pore}$, and ϕ_i (the partition coefficient of i) = $(1-\lambda_i)^2$. Note that Eq.(5) considers only steric, hard-sphere particle (p or ion)-pore wall interactions, and does not account for longer-range interactions, such as, electrostatic and van der Waals interactions (7). Although the ions (and the permeant molecules) in the contacting solutions may be charged, Tang et al. have shown that Eq.(5) is valid provided that the Debye-Hückel screening length – the length scale associated with the screening of electrostatic interactions between the ions (or between the charged permeants) and the negatively-charged skin aqueous pore walls – is much smaller than the average skin aqueous pore radius, r_{pore} (7). Tang et al. also showed that for the PBS control contacting solution containing Na^+ and Cl^- ions, and also for the Mannitol aqueous solution, the Debye-Hückel screening length ≤ 7 Å, which is much smaller than the typical average skin aqueous pore radii, that is, than the sizes of the aqueous pores, of approximately 15-25 Å (7). The quantities, D_p^{∞} and D_{ion}^{∞} , appearing in C refer to the permeant and to the ion infinite-dilution diffusion coefficients, respectively (note that these quantities correspond typically to the bulk diffusion coefficients of the permeant and of the ion in the dilute donor contacting solutions used in the in vitro transdermal permeability and electrical resistivity measurements).

According to the hindered-transport theory (42), the hindrance factor for permeant or ion transport, $H(\lambda_i)$, is a function of both the permeant/ion type and of the skin membrane characteristics. The four intrinsic membrane characteristics of the skin barrier are: (1) the porosity, ε, which is the fraction of the skin area occupied by the aqueous pores, (2) the tortuosity, τ, which is the ratio of the permeant diffusion path length within the skin barrier to the skin barrier thickness, (3) the average pore radius, r_{pore}, and (4) the skin barrier thickness, ΔX.

Based on these four membrane characteristics, one can express the permeability, P, of a hydrophilic permeant, such as, Mannitol, through the skin aqueous pores as follows (6, 7, 42):

$$P = \frac{\left(\frac{\varepsilon}{\tau}\right) D_p^{\infty} H(\lambda_p)}{\Delta X} \tag{6}$$

Therefore, from Eqs. (4)-(6), once one can determine P and R upon exposure of p-FTS to contacting aqueous solutions of SDS and SDS+10 wt% Glycerol, one can also determine the radius of the aqueous pores as the average skin pore radius, r_{pore}, and the ratio of porosity-to-tortuosity, defined as ε/τ, if all the other parameters, such as ΔX, are known (see the appendix, where we illustrate how to deduce r_{pore} and ε/τ when p-FTS is contacted with SDS aqueous solutions). The porosity-to-tortuosity ratio, ε/τ, is proportional to the number of tortuous aqueous pores per unit cross sectional area of the SC, that is, to the pore number density (see Chapter 4). In the context of the hindered-transport aqueous porous pathway model of the SC, an increase in the porosity, ε, and/or a decrease in the tortuosity, τ, which increases the porosity-to-tortuosity ratio, ε/τ, of the aqueous pores can be interpreted as an increase in the number of tortuous aqueous pores per unit cross sectional area of the SC (see Chapter 4).[4]

A harsh surfactant like SDS can induce skin barrier perturbation by modifying the SC aqueous porous pathways as follows: (1) increasing the size of the existing aqueous pores in the SC, and/or (2) increasing the number density of the existing aqueous pores in the SC, or both. It then follows, in the context of the hindered-transport aqueous porous pathway model, that mechanism (1) involves increasing r_{pore}, while mechanism (2) involves increasing ε/τ (6–9, 42). In *Table 2-1*, I report r_{pore} values resulting from the exposure of p-FTS to

[4] This statement is true provided that the increase in the porosity-to-tortuosity ratio, ε/τ, of the aqueous pores is not due to a significant increase in the average aqueous pore radius, r_{pore} (see Chapter 4).

contacting solutions of: (a) SDS in water, (b) SDS+10 wt% Glycerol in water, (c) PBS control, and (d) 10 wt% Glycerol in water. Note that in *Table 2-1*, I have reported the ε/τ values resulting from the exposure of p-FTS to the contacting solutions (a)-(d) normalized by the ε/τ value resulting from the exposure of p-FTS to contacting solution (c), which I have denoted as $(\varepsilon/\tau)_{normal}$. It then follows that when $(\varepsilon/\tau)_{normal} > 1$, it indicates that the contacting solution creates more aqueous pores in the SC relative to those created by the PBS control, while when $(\varepsilon/\tau)_{normal} < 1$, it indicates that the contacting solution creates fewer aqueous pores relative to those created by the PBS control.

2.4. Results and Discussion

2.4.1. Effect of Glycerol on SDS-Induced Skin Barrier Perturbation

In order to quantify the effect of the SDS concentration in the skin aqueous contacting solution on the skin barrier in the absence and in the presence of Glycerol, I utilized the in vitro transdermal permeability and the skin electrical current measurements discussed above. The physical basis for these measurements is as follows: a large skin electrical current or transdermal permeability, which results from a high transfer rate of permeant molecules (Mannitol in our case) or of ions, respectively, across the skin, is indicative of a large extent of skin barrier perturbation in vitro (1-7). Therefore, if upon exposure of the skin to an aqueous contacting solution of SDS or of SDS+10 wt% Glycerol, one observes a high skin electrical current (corresponding to a low average skin electrical resistivity) or permeability, one may conclude that the contacting solution has induced skin barrier perturbation, thereby compromising the skin barrier.

With the above expectation in mind, I conducted skin electrical current measurements for aqueous contacting solutions of SDS ranging in SDS concentrations from 1 mM to 200 mM.[5] The results of these measurements are shown as striped bars in *Figure 2-2*. As can be seen, the extent of skin barrier perturbation, quantified in terms of the skin electrical current, continues to increase with an increase in the SDS concentration in the contacting solution above the CMC of SDS (8.7 mM).[6] According to the monomer penetration model (MPM) adopted by many researchers in the past, only the surfactant monomers are able to penetrate into the skin barrier and induce skin barrier perturbation, while the micelles, due to their larger size relative to that of the monomers, are not able to do so. Hence, according to the MPM, the skin barrier perturbation induced by a surfactant contacting solution should not increase significantly upon increasing the total surfactant concentration above the CMC.[7] However, the skin electrical current results clearly show that an increase in the SDS concentration in the contacting solution above the CMC induces a significant increase in the skin electrical current (see *Figure 2-2*). This observation is consistent with the results reported by other researchers in previous studies (11-19). For example, Moore et al. (11) found that SDS micelles contribute to SDS-skin penetration. Therefore, it is natural that SDS micelles should also contribute to skin barrier perturbation, as I have demonstrated experimentally through these skin electrical current measurements. Indeed,

[5] Note that 1 wt% SDS = 35mM, and that the CMC of SDS = 8.7mM = 0.25wt%.

[6] Recall that the CMC is the *threshold* total surfactant concentration above which the concentration of the surfactant monomers remains approximately constant, while that of the surfactant micelles increases upon increasing the total surfactant concentration. This is because, above the CMC, any new surfactant molecules added to the solution self-assemble to form micelles, a process that is thermodynamically more favorable than to remain as free monomers in the surfactant solution.

[7] This statement implies that a surfactant monomer, or a micelle, has to first penetrate into the skin barrier in order to induce skin barrier perturbation. Consequently, if one can minimize, or prevent altogether, penetration of surfactant into the skin, one should be able to minimize skin barrier perturbation induced by the surfactant monomers or by the micelles.

these measurements indicate unequivocally that SDS micelles contribute to skin barrier perturbation, as reflected in the observed increase in the skin electrical current above the CMC.[8]

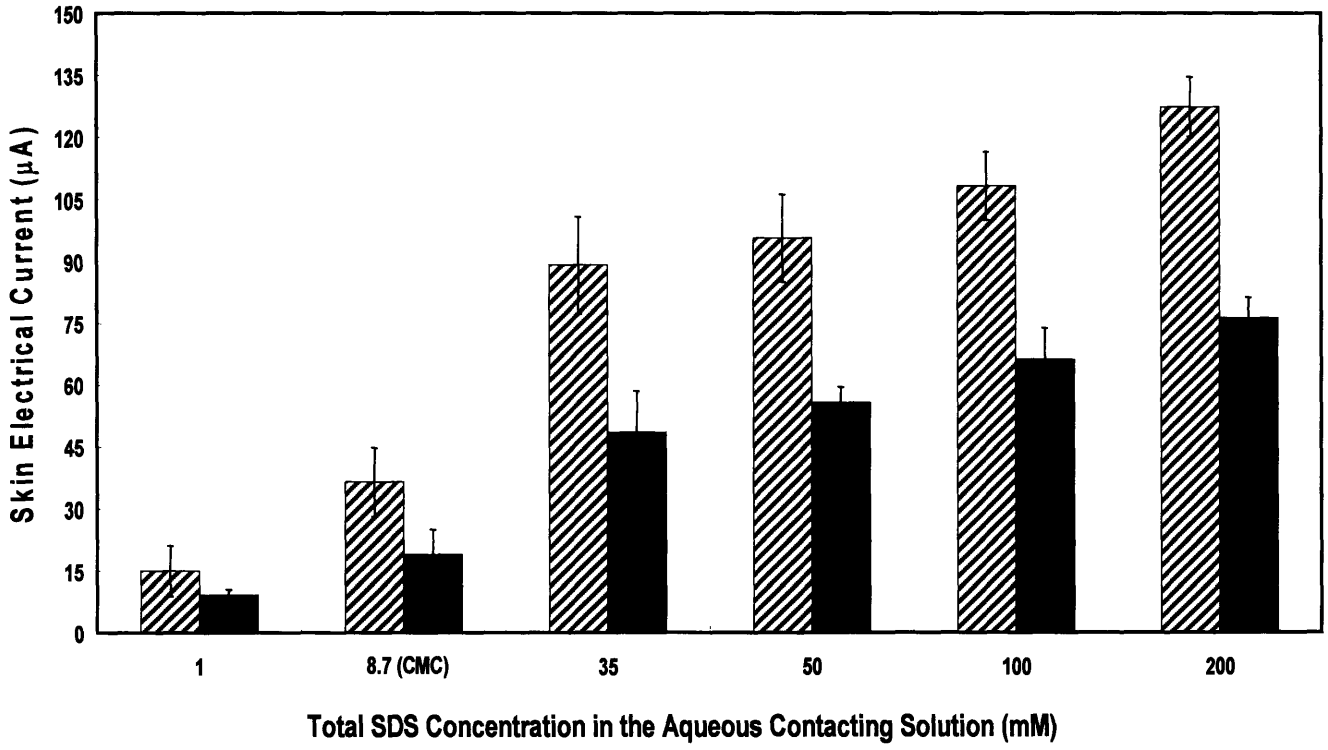

Figure 2-2. Comparison of the in vitro skin electrical currents induced by SDS aqueous contacting solutions (striped bars) and by SDS+10 wt% Glycerol aqueous contacting solutions (filled bars). The error bars represent standard errors based on 6-10 p-FTS samples.

[8] It is noteworthy that the skin electrical current induced by PBS (phosphate buffered saline), which served as the control for these experiments, was 11±4 μA, which is comparable to that induced by a 1 mM SDS solution (see *Figure 2-2*).

Next, I measured skin electrical currents upon exposing p-FTS to aqueous contacting solutions of SDS (1-200 mM) + 10 wt% Glycerol. The results of these measurements are shown as filled bars in *Figure 2-2* (see above).

Figure 2-2 clearly shows that the filled bars (corresponding to the skin electrical currents induced by the SDS+10 wt% Glycerol aqueous contacting solutions) are much shorter than the striped bars (corresponding to the skin electrical currents induced by the SDS aqueous contacting solutions). This important finding clearly shows that the addition of 10 wt% Glycerol to an SDS aqueous contacting solution significantly reduces SDS-induced skin barrier perturbation, as quantified by the skin electrical currents.

Finally, I measured in vitro Mannitol skin permeabilities upon exposing p-FTS samples to aqueous contacting solutions of SDS(1-200 mM) and of SDS(1-200 mM)+10 wt% Glycerol. The results of these measurements are shown in *Figure 2-3*. In *Figure 2-3*, the diamonds correspond to the permeability values resulting from exposure to the SDS aqueous contacting solutions, and the triangles correspond to the permeability values resulting from exposure to the SDS+10 wt% Glycerol aqueous contacting solutions. These measurements seem to indicate that: (1) the SDS micelles, in general, do contribute to skin barrier perturbation, as reflected in the increasing P values with increasing SDS concentration above the CMC of SDS (8.7 mM), and (2) the addition of Glycerol minimizes SDS micelle-induced skin barrier perturbation, as reflected in the triangles lying below the diamonds in *Figure 2-3*.

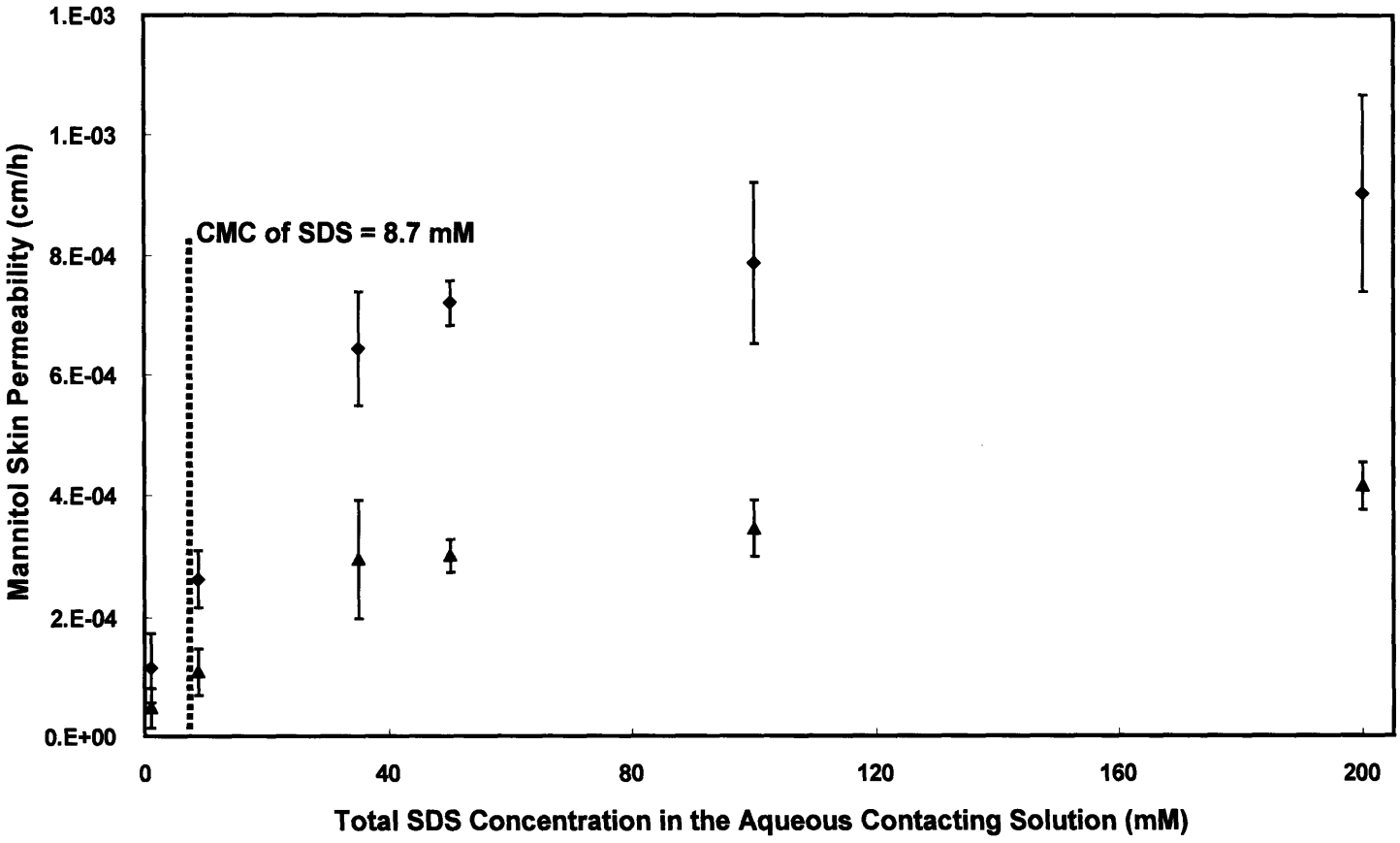

Figure 2-3. Comparison of the in vitro Mannitol skin permeability induced by SDS aqueous contacting solutions (diamonds) and by SDS+10 wt% Glycerol aqueous contacting solutions (triangles). The dotted vertical line at an SDS concentration of 8.7 mM denotes the CMC of SDS. The error bars represent standard errors based on 6-10 p-FTS samples.

2.4.2. Effect of Glycerol on SDS-Skin Penetration

I developed the skin radioactivity assay discussed above to directly quantify the amount of SDS that can penetrate into the skin barrier from an SDS aqueous contacting solution in the absence and in the presence of 10 wt% Glycerol (see Section 2.2.5). Use of this assay allows one to directly measure the contribution of the SDS micelles, in the absence and in the presence of 10 wt% Glycerol, to SDS-skin penetration. The results of our measurements are shown in *Figure 2-4*.

The concentrations of SDS in the skin barrier (in wt%) resulting from the exposure of p-FTS to aqueous contacting solutions of SDS (1-200 mM) correspond to the diamonds in *Figure 2-4*. One can clearly see that upon increasing the total SDS concentration in the contacting solution above the CMC (8.7 mM), the concentration of SDS in the skin barrier increases significantly. In *Figure 2-4*, the contribution of the SDS monomers to SDS skin penetration above the CMC remains approximately constant above 8.7 mM (the CMC value), and corresponds to the horizontal solid line. On the other hand, the total SDS contribution to SDS skin penetration increases above the CMC, and corresponds to the dashed line, drawn as a guide to the eye. Clearly, the difference between the dashed and the solid lines at any given total SDS concentration corresponds to the contribution of the SDS micelles to SDS skin penetration. Note that below the CMC, only the SDS monomers are available for penetration into the skin. Consequently, the diamonds and the triangles overlap below the CMC (see *Figure 2-4*). These results are in excellent agreement with the SDS-skin penetration results reported by Moore et al. (11). Indeed, these authors showed earlier that: (i) there is a significant SDS micellar contribution to SDS skin penetration, and (ii) the SDS micellar contribution increases with an increase in the total SDS concentration above the CMC.

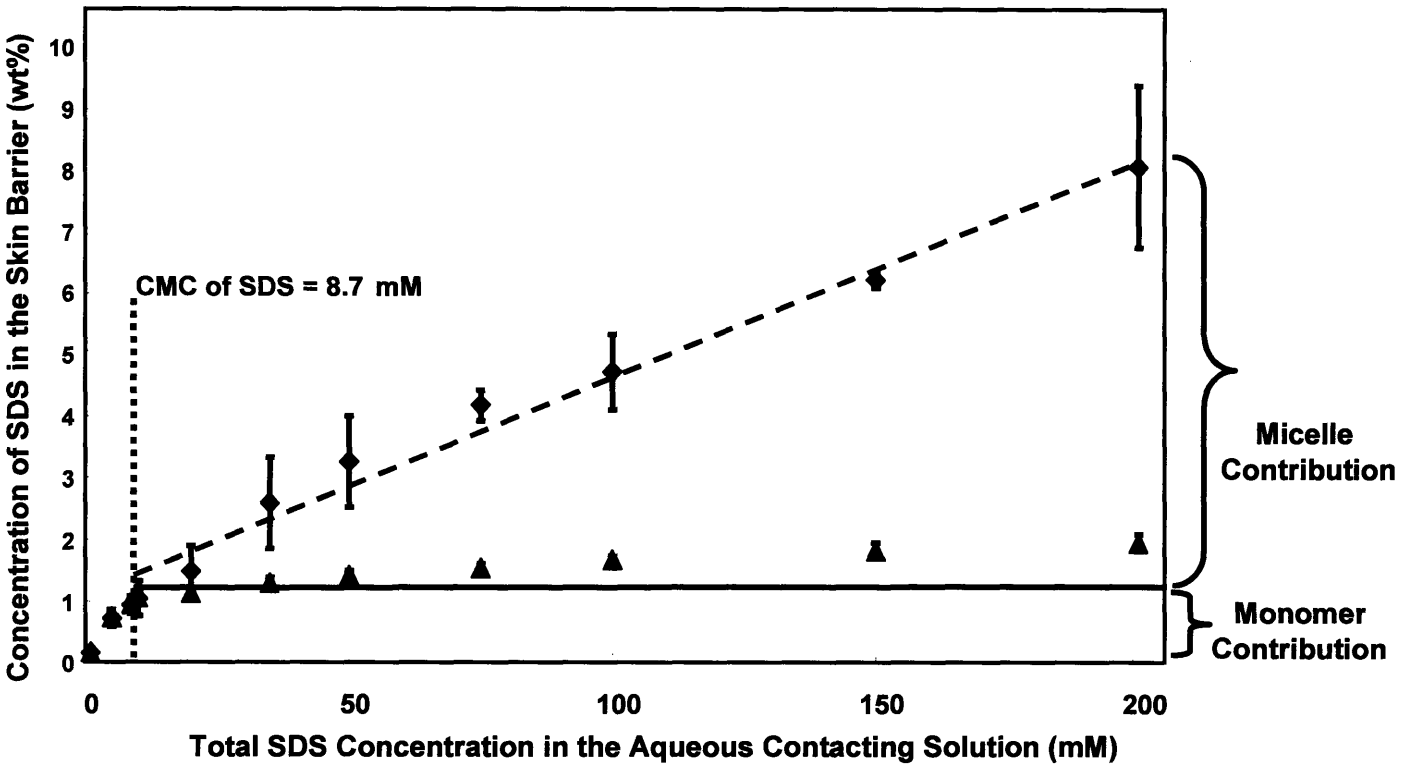

Figure 2-4. Comparison of SDS-skin penetration in vitro induced by aqueous contacting solutions of SDS (diamonds) and of SDS+10 wt% Glycerol (triangles). The dotted vertical line at an SDS concentration of 8.7 mM denotes the CMC of SDS. The dashed line passing through the diamonds is drawn as a guide to the eye. The error bars represent a standard error based on 6-10 p-FTS samples.

However, in this chapter, I have demonstrated in vitro, for the first time, that the significant SDS micellar contribution to SDS-skin penetration also leads to a large extent of SDS skin barrier perturbation, as quantified by the observed increases in the skin electrical currents and in the Mannitol skin permeabilities (see *Figures 2-2 and 2-3*, respectively). These in vitro results suggest, from a practical, formulation design point of view, that any strategy designed to minimize skin barrier perturbation induced by surfactants like SDS, in addition to minimizing the penetration of the surfactant monomers into the skin, as was done in the past, may also benefit from minimizing the penetration of the surfactant micelles into the skin. In this chapter, I have investigated in vitro such a simple and useful practical strategy by using mixtures of SDS and Glycerol, which we discuss next.

Specifically, I conducted skin radioactivity assays using ^{14}C-SDS in the presence of 10 wt% added Glycerol in aqueous solution to measure the amount of SDS that may penetrate into the skin barrier in the presence of Glycerol (corresponding to the triangles in *Figure 2-4*). It is interesting to observe that the triangles and the diamonds overlap below the CMC in *Figure 2-4*. At an SDS concentration below the CMC of SDS (8.7 mM), the SDS aqueous contacting solution essentially consists of SDS monomers contacting the skin. Therefore, upon adding 10 wt% Glycerol to the SDS aqueous contacting solution, one can observe that the SDS monomers are not hindered from penetrating into the skin. However, the addition of 10 wt% Glycerol to the SDS aqueous contacting solution at concentrations above the CMC significantly impacts SDS-skin penetration. Indeed, as can be seen, the presence of 10 wt% Glycerol in the SDS contacting solution eliminates almost completely the amount of SDS that can penetrate into the skin barrier from the high SDS concentration contacting solutions. The significant difference between the diamonds (or the dashed line) and the triangles (which lie very close to the SDS monomer

contribution corresponding to the solid line) clearly shows that SDS micelles, which would have contributed to skin penetration in the absence of 10 w% Glycerol, cannot do so in the presence of 10 wt% Glycerol in the contacting solution. These in vitro results suggest that the addition of 10 wt% Glycerol to the SDS contacting solutions may also represent a simple, yet very useful, practical strategy to mitigate SDS-induced skin barrier perturbation in vivo by preventing the SDS micelles from penetrating into the skin barrier.

In Section 2.4.3, I put forward several hypotheses to explain, from a mechanistic viewpoint, why Glycerol, without affecting the skin penetration ability of the SDS monomers, is able to significantly reduce the ability of the SDS micelles to contribute to SDS-skin penetration in vitro.

2.4.3. Possible Hypotheses to Explain the Effect of Glycerol on the Observed In Vitro Dose-Independence of SDS-Skin Penetration

Using micelle stability arguments put forward by Patist et al. (43), Moore et al. have shown that the kinetics of micelle dissolution cannot be invoked to explain the observed dose-dependence of SDS-skin penetration (11). Moore et al. have also compared the time constant for the breakup of SDS micelles to replenish the decreased SDS monomer supply to the SC as the SDS molecules penetrate into the skin with the time constant for SDS diffusion across the skin. This comparison has unambiguously shown that the rate-determining step for SDS-skin penetration is governed by the diffusion, or the penetration, through the SC and not by the micelle kinetics (11). Furthermore, Moore et al. have shown that micelle disintegration upon impinging on the SC and subsequent absorption by the skin barrier also does not seem to be a plausible mechanism to explain the observed dose-dependence of SDS-skin penetration (11, 44, 45). With all of the above in mind, according to Moore et al., a consistent hypothesis to explain

the observed dose-dependence of SDS-skin penetration considers the ability of SDS micelles to penetrate into the SC, based on a size limitation (11). Without directly measuring the skin aqueous pore radius, r_{pore} , and the porosity-to-tortuosity ratio, ε/τ, Moore et al. hypothesized [9] that a free SDS micelle, being smaller than the aqueous pore, is able to penetrate into the SC, while a PEO-bound SDS micelle, being larger then the aqueous pore, is not able to do so (11). My hypothesis to explain the observed dose-dependence of SDS-skin penetration in the *absence* of Glycerol is similar to that of Moore et al. (11), the difference being that I have further substantiated this hypothesis by directly determining the average skin aqueous pore radius, r_{pore} , and the pore number density, ε/τ, of the skin aqueous pores induced by SDS.

Considering the skin penetration of *both* the SDS monomers and the SDS micelles, I have investigated in vitro the following three hypotheses to explain the ability of Glycerol to minimize the contribution of SDS micelles to SDS-skin penetration: (1) the addition of 10 wt% Glycerol to the SDS aqueous contacting solution reduces the concentration of the SDS monomers contacting the skin, and/or (2) the addition of 10 wt% Glycerol to the SDS aqueous contacting solution increases the SDS micelle size relative to that of the skin aqueous pores, such that the larger SDS micelles can no longer penetrate through these aqueous pores into the SC, and/or (3) the addition of 10 wt% Glycerol to the SDS aqueous contacting solution reduces the radius, r_{pore} , and the porosity-to-tortuosity ratio, ε/τ, of the skin aqueous pores, such that the SDS micelles, which are on average larger than the skin aqueous pores, can no longer penetrate into the SC and contribute to SDS-skin penetration. According to Hypothesis 3, in addition to the decrease in the radius of

[9] Note that Moore et al. (11), to their credit, compared micelle sizes for free SDS micelles and PEO-bound SDS micelles, using DLS measurements similar to those reported here, and found that the PEO-bound SDS micelle had a larger hydrodynamic radius than the free SDS micelle. This observation, along with the observation that the PEO-bound SDS micelle, unlike the free SDS micelle, did not contribute to SDS-skin penetration, formed the basis for their hypothesis that SDS micelles can penetrate into the SC, based on a size limitation. However, Moore et al. did not measure the effect of SDS on the radius and on the porosity-to-tortuosity ratio of the skin aqueous pores directly, as is done here.

the aqueous pores, the decrease in the porosity-to-tortuosity ratio should further limit the ability of the SDS micelles to penetrate into the SC through these aqueous pores.

I have investigated Hypothesis (1) by conducting surface tension measurements (see Section 2.2.7) to deduce the CMC of SDS in aqueous solution in the absence and in the presence of 10 wt% Glycerol. Hypothesis (2) was investigated through DLS measurements to determine the SDS micelle hydrodynamic radius in aqueous solution in the absence and in the presence of 10 wt% Glycerol (see Section 2.4.5). Finally, I investigated Hypothesis (3) by determining the radius and the porosity-to-tortuosity ratio of the skin aqueous pores induced by aqueous SDS contacting solutions in the absence and in the presence of 10 wt% Glycerol through the average skin electrical resistivity and Mannitol skin permeability measurements, in the context of the hindered-transport porous aqueous pathway model (see Sections 2.2.3, 2.2.4, and 2.3.1). I discuss the results of studies (1)-(3) above in the following three sections.

2.4.4. Results from the Surface Tension Measurements to Determine the CMC

Recall that the CMC of a SDS aqueous contacting solution is the *threshold* total SDS concentration above which the concentration of the SDS monomers remains approximately constant, while that of the SDS micelles continues to increase upon increasing the total SDS concentration. Therefore, if the addition of 10 wt% Glycerol to the SDS aqueous contacting solution results in a lowering of the CMC, one may conclude that the number of SDS monomers contacting the skin decreases in the presence of Glycerol, which may explain why Glycerol reduces SDS-skin penetration. However, my surface tension results indicate that the CMC of SDS in the presence of 10 wt% Glycerol is *9.2 mM*, which is slightly larger than the CMC of SDS in the absence of Glycerol *(8.7 mM)*. Our CMC value in the presence of Glycerol is in excellent agreement with previously reported CMC values of SDS in water/glycerol binary

mixtures (46). Therefore, based on the CMC values of SDS in water and in a 10 wt% Glycerol aqueous solution, one may conclude that Hypothesis 1 is not valid, and therefore, cannot explain the observed ability of Glycerol to reduce SDS-skin penetration.

2.4.5. Results from the Dynamic Light Scattering (DLS) Measurements to Determine the Size of the SDS Micelles

Using DLS, I determined the sizes of the SDS micelles in aqueous solutions, in the absence and in the presence of 10 wt% Glycerol. *Figure 2-5* shows the results of the DLS measurements in terms of the SDS micelle hydrodynamic radii in: (a) water and (b) 10 wt% Glycerol aqueous solutions. The SDS micelle hydrodynamic radii were determined by extrapolation to a zero micelle concentration, which corresponds to the CMCs of SDS solutions corresponding to (a), 8.7 mM (see the diamonds in *Figure 2-5*), and to (b), 9.2 mM (see the triangles in *Figure 2-5*). Using a linear regression analysis, I determined that the hydrodynamic radius of the free SDS micelles corresponding to (a) is *19.5±1Å*, while that corresponding to (b) is *18.5±1Å*. The SDS micelle hydrodynamic radii corresponding to (a) reported here are in excellent agreement with the values reported previously by Moore et al. (11) and by Almgren et al. (47). Therefore, these results indicate that the SDS micelle size is slightly *smaller, not larger*, in the SDS aqueous solution with 10 wt% added Glycerol, and hence, cannot explain how Glycerol minimizes the SDS micellar contribution to SDS-skin penetration. In other words, Hypothesis 2 is not valid either.

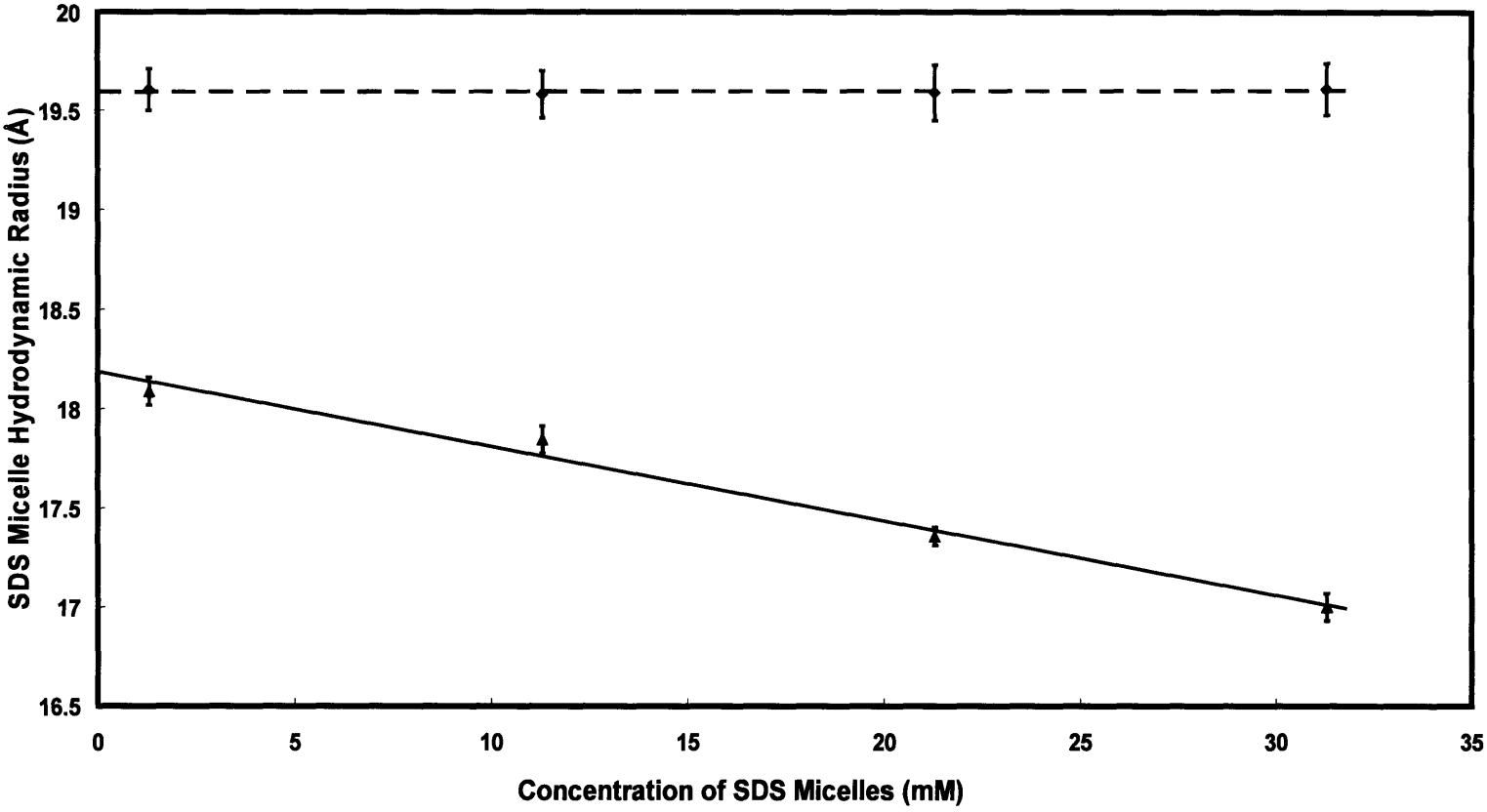

Figure 2-5. Measured effective radii of SDS micelles in aqueous solutions in the absence (diamonds) and in the presence (triangles) of 10 wt% Glycerol plotted versus the SDS concentration minus the CMC, which corresponds to the concentration of the SDS micelles, using DLS measurements at 25°C. The SDS micelle radii were determined using a CONTIN analysis. The error bars reflect standard errors based on 6 samples at each SDS concentration.

2.4.6. Results from an Analysis of the Hindered-Transport Aqueous Porous Pathway Model to Determine the Radius and the Porosity-to-Tortuosity Ratio of the Skin Aqueous Pores

I quantified the extent of skin barrier perturbation using the average aqueous pore radius and the porosity-to-tortuosity ratio, as quantitative descriptors of the SC morphological changes upon exposure to: (a) an aqueous solution of SDS (1-200 mM) and (b) an aqueous solution of SDS (1-200 mM)+10wt% Glycerol. Specifically, an increase in the radius and/or in the porosity-to-tortuosity ratio of the aqueous pores corresponds to an increased perturbation in the skin barrier (1, 6, 7, 10, 42). The radius and the porosity-to-tortuosity ratio of the skin aqueous pores resulting from the exposure to contacting solutions (a) and (b) above were determined using the hindered-transport model of the skin aqueous porous pathways, along with the in vitro Mannitol transdermal permeability and the average skin electrical resistivity measurements. For completeness, I also conducted similar measurements on p-FTS which was exposed to: (c) the PBS control, and to (d) 10 wt% Glycerol aqueous contacting solutions.

In *Figure 2-6*, I have plotted the log of the Mannitol skin permeability, P (cm/h), against the log of the average skin electrical resistivity, R (kohm-cm^2), over the same exposure time, exhibited by p-FTS samples exposed to solutions (a), the diamonds, and (b), the triangles, above. Each diamond/triangle represents a log P value of one p-FTS sample at steady state and the corresponding log R (the log of the average skin electrical resistivity value). The slopes of the best-fit curves resulting from linear regressions, the dashed line for (a) and the solid line for (b), are not statistically different from the theoretically predicted slope value of -1, thereby indicating consistency with the hindered-transport aqueous porous pathway model analysis for p-FTS samples exposed to contacting solutions (a) and (b) above (6, 7). Also, note that the dashed line

has a larger intercept value than that corresponding to the solid line, which reflects a larger average pore radius, r_{pore}, for p-FTS samples exposed to (a) than to (b).

Having determined r_{pore}, the porosity-to-tortuosity ratio, ε/τ, was determined using Eq.(6), in which all the parameters, except ε/τ are known in advance (recall that ΔX=15μm) (6, 7). Using the model described above, I found that the average pore radius does not depend on the SC thickness, ΔX, while the porosity-to-tortuosity ratio is directly proportional to ΔX. The aqueous porosity-to-tortuosity ratio, ε/τ, values resulting from exposure of the p-FTS samples to contacting solutions (a)-(d) above were normalized by the ε/τ value resulting from exposure of the p-FTS samples to the PBS control solution, solution (c), which served as the baseline, and have been denoted as $(\varepsilon/\tau)_{normal}$ (see the Appendix, where I illustrate how to obtain r_{pore} and $(\varepsilon/\tau)_{normal}$ for p-FTS samples exposed to (a)).

The deduced values of r_{pore} and $(\varepsilon/\tau)_{normal}$ corresponding to solutions (a)-(d) above are reported in *Table 2-1*. As can be seen, the average pore radius, r_{pore} , corresponding to (a) is *33±5Å,* while that corresponding to (b) is *20±5Å*, which is similar to the average pore radius corresponding to (c), *20±3Å*. In addition, the normalized porosity-to-tortuosity ratio, $(\varepsilon/\tau)_{normal}$, corresponding to (a), *7±1*, is about twice that corresponding to (b), *3±1*. Interestingly, one can also see that a 10 wt% Glycerol aqueous solution (contacting solution d) reduces r_{pore} and $(\varepsilon/\tau)_{normal}$ by about 50% relative to the PBS control.

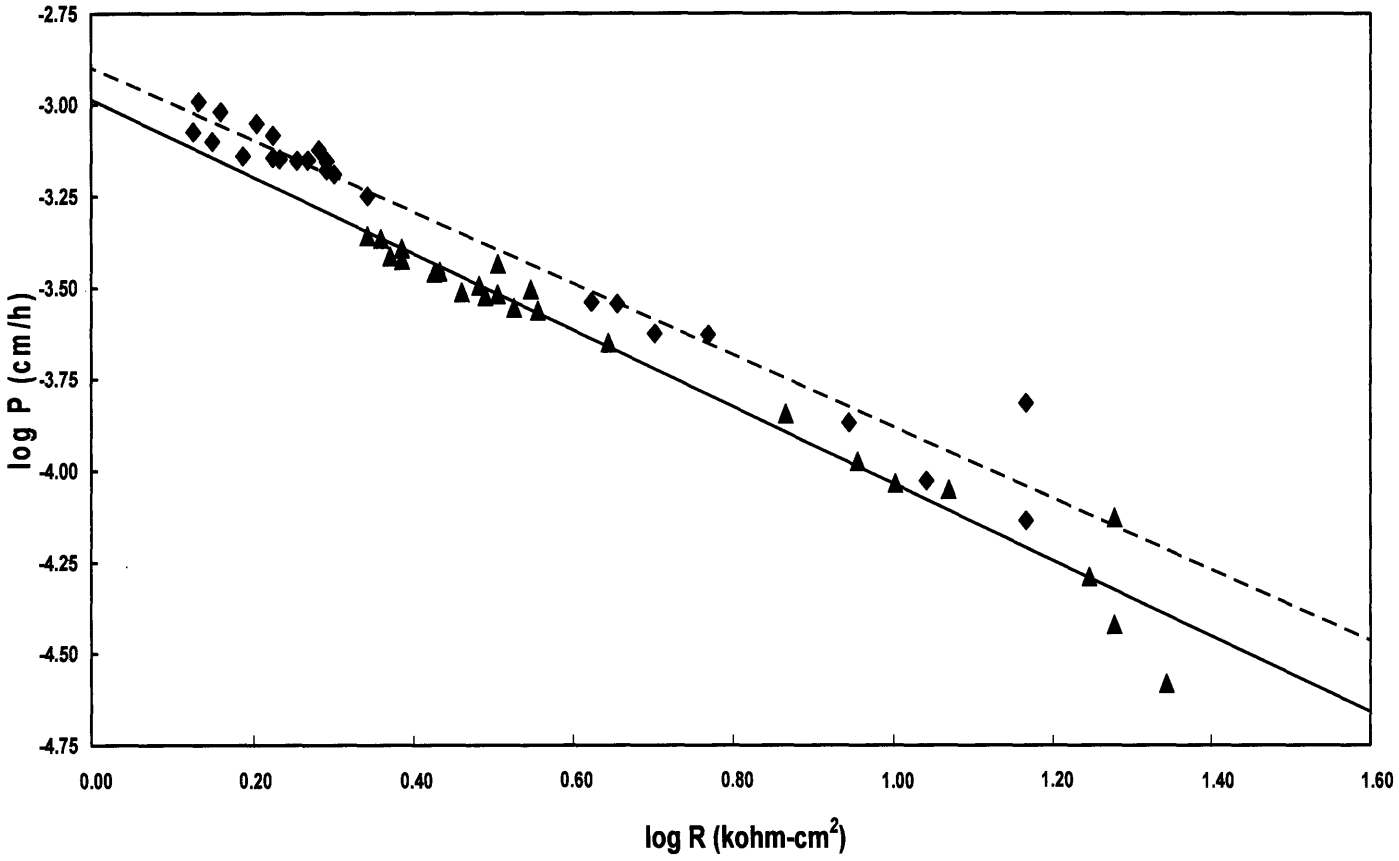

Figure 2-6. Experimental correlation between the in vitro Mannitol transdermal permeability, P (cm/h), and the in vitro skin electrical resistivity, R (kohm-cm^2), exhibited by p-FTS samples exposed to an aqueous solution of SDS (1-200 mM), the diamonds, and to an aqueous solution of SDS (1-200 mM)+10 wt% Glycerol, the triangles. Each data point corresponds to a log P value of one p-FTS sample at steady state and the associated log R, the log of the average skin electrical resistivity value over the same time period. The slopes of the best-fit curves resulting from a linear regression are: (1) -0.98±0.06 for SDS (1-200 mM), with R^2=0.9636, shown as the dashed line, and (2) -1.05±0.06 for SDS (1-200 mM)+10 wt% Glycerol, with R^2=0.9653, shown as the solid line. Note that these slope values are not statistically different from the theoretically predicted value of -1.

The results in *Table 2-1* indicate that a SDS aqueous contacting solution containing micelles, in the presence of 10 wt% Glycerol, induces a lower extent of skin barrier perturbation, as reflected in the lower average pore radius and normalized porosity-to-tortuosity ratio, when compared to an SDS aqueous contacting solution, in the absence of Glycerol. In fact, in the absence of Glycerol, a SDS micelle of *19.5±1Å* hydrodynamic radius experiences no steric hindrance in penetrating through aqueous pores in the SC that have an average pore radius of *33±5Å* (see *Table 2-1*). However, in the presence of 10 wt% Glycerol, a SDS micelle of *18.5±1Å* hydrodynamic radius experiences significant steric hindrance in penetrating through smaller aqueous pores in the SC that have an average pore radius of *20±5Å* (see *Table 2-1*).

Table 2-1. Skin aqueous pore characteristics induced by various aqueous contacting solutions: (a) SDS, (b) SDS+10 wt% Glycerol, (c) PBS Control, and (d) 10 wt% Glycerol. Note that we have reported ε/τ values resulting from the exposure of p-FTS to the contacting solutions (a)-(d) normalized by the ε/τ value resulting from the exposure of p-FTS to contacting solution (c), which we have denoted as $(\varepsilon/\tau)_{normal}$.

Type of Aqueous Contacting Solution	*Average Pore Radius, r_{pore} (Å)*	*Normalized Porosity-to-Tortuosity Ratio, $(\varepsilon/\tau)_{normal}$*
(a) SDS	33±5	7±1
(b) SDS + 10 wt% Glycerol	20±5	3±1
(c) PBS Control	20±3	1
(d) 10 wt% Glycerol	11±4	0.5±0.1

Moreover, the presence of 10 wt% added Glycerol in the SDS aqueous contacting solution reduces the $(\varepsilon/\tau)_{normal}$ value from 7±1 to 3±1, which is more than a 50% reduction in the normalized porosity-to-tortuosity ratio. Hence, adding 10 wt% Glycerol to an aqueous SDS micellar contacting solution minimizes the micellar contribution to SDS-skin penetration in vitro by minimizing both the average pore radius and the porosity-to-tortuosity ratio of the skin aqueous pores.

The results of this study indicate that the data is consistent with Hypothesis 3: *Glycerol reduces both the radius of the aqueous pores in the SC relative to that of the SDS micelles, as well as the porosity-to-tortuosity ratio*, which if not reduced, would allow SDS micelles to contribute to SDS-skin penetration in vitro.

2.4.7. Possible Structural Modes of Interaction of Glycerol and SDS with the Skin Barrier

These results indicate that the addition of 10 wt% Glycerol to an aqueous contacting solution of SDS mitigates skin barrier perturbation in vitro by reducing the skin aqueous pore radius and the aqueous porosity-to-tortuosity ratio. I propose two scenarios to rationalize these results. According to the first scenario, it is well-accepted that because of its strong hygroscopic property and ability to modulate water fluxes in the SC, Glycerol can diffuse into the SC and bind water within the SC (24, 28, 29). In fact, researchers have observed a significant positive correlation in vivo between the skin-moisturizing ability of Glycerol, as determined through skin conductance measurements, and the corresponding amount of Glycerol found in the skin barrier (52). As a result, water-binding by Glycerol in the SC reduces the mobility of water within the SC. The limited mobility of water within the SC may result in lacunar domains, as observed by Menon and Elias (10), losing structural continuity, partially or completely, within the

extracellular lipid bilayers of the SC. I suggest that a *partial* loss in the structural continuity of lacunar domains is responsible for a *reduction in the radius* of the corresponding aqueous pores, while a *complete* loss in continuity of lacunar domains is responsible for the *elimination or closing* of the corresponding aqueous pores, that is, for a reduction in the overall number density (or equivalently, the porosity-to-tortuosity ratio) (see Chapter 4) of the aqueous pores in the SC. *Figure 2-7* illustrates schematically a combination of lacunae that are continuous under normal skin hydration conditions, resulting in an aqueous pore, but may become discontinuous upon exposure of the skin to Glycerol, thereby resulting in a size reduction, or a closing, of the aqueous pore. A second scenario describing how Glycerol may result in partial, or complete, loss of the structural continuity of lacunar domains considers the ability of Glycerol to maintain the intercellular lipid mortar in a liquid crystalline state, as opposed to a solid crystalline state (30). Froebe et al. have shown that addition of 10 wt% Glycerol to a mixture of SC lipids in vitro inhibited the transition from liquid to solid crystals, which could maintain the intercellular lipid mortar in the SC and potentially minimize the size, as well as the continuity, of the lacunar domains within the SC (30). Most likely, both scenarios may play a role in inducing partial, and/or complete, loss of structural continuity of the lacunar domains, thereby resulting in a reduction in the radius, and/or in the number density, and thereby the porosity-to-tortuosity ratio, of the aqueous pores in the SC. On the other hand, in vitro as well as in vivo studies document that surfactants like SDS have an opposite effect on the SC lipids and on the corneocyte keratins. SDS has been shown to induce direct alteration to the structure of the intercellular lipid mortar (48, 49), as well as to disrupt the keratin structure of the corneocytes in the SC (16, 50, 51). Both of these effects can induce the formation of additional lacunar domains, as well as enhance the structural continuity of existing lacunar domains.

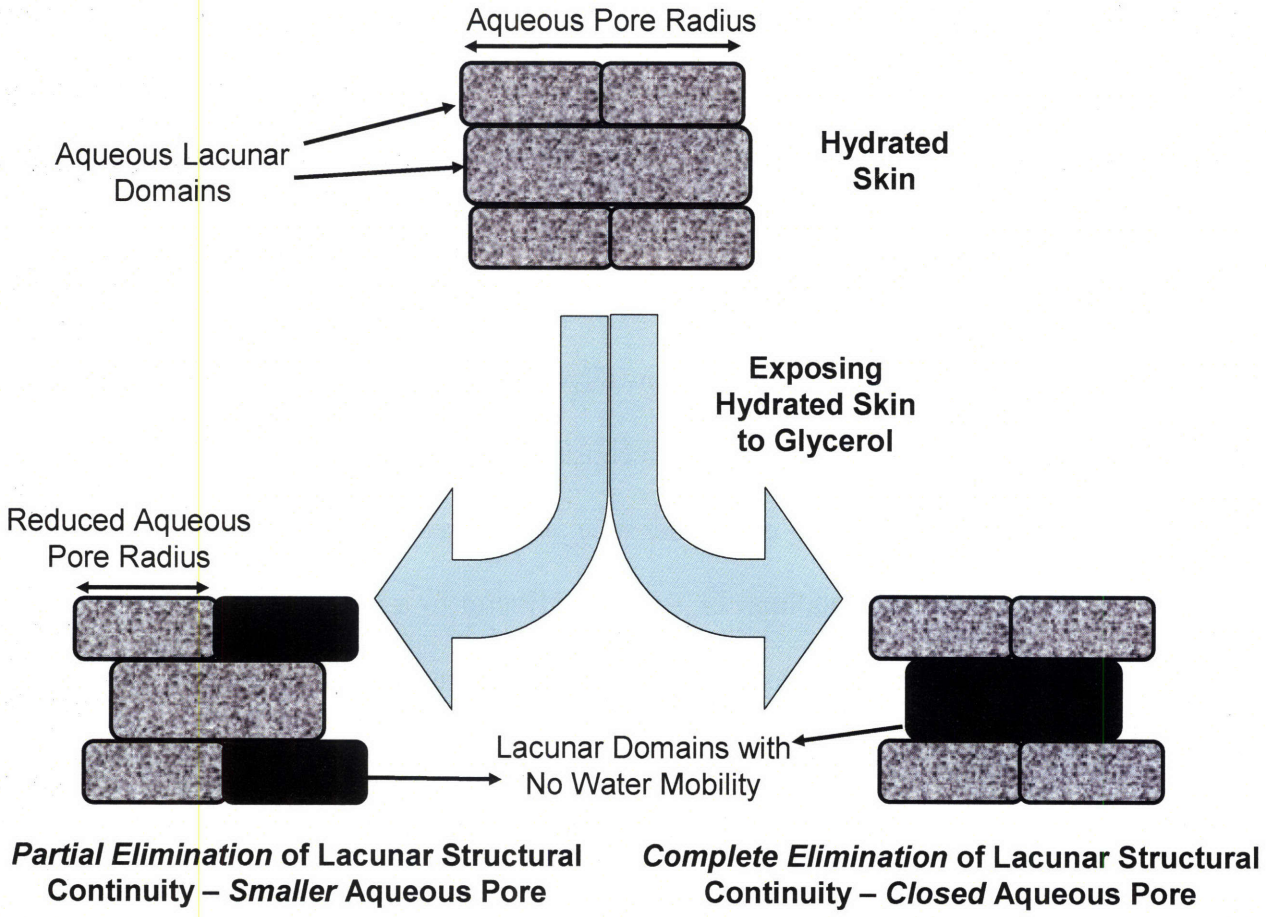

Figure 2-7. Schematic illustration of possible structural modes of interaction of aqueous lacunar domains in the hydrated skin barrier with Glycerol. Aqueous lacunar domains, shown in grey, gain structural continuity in hydrated skin to form an aqueous pore. However, when Glycerol is added to the hydrated skin barrier, lacunar domains shown in black lose structural continuity due to Glycerol binding water and minimizing water mobility, either partially, resulting in a smaller aqueous pore, or completely, resulting in a closed aqueous pore.

This is how SDS may induce an increase in the radius, and/or in the porosity-to-tortuosity ratio, of the aqueous pores in the SC. A mixture of SDS and Glycerol in an aqueous contacting solution will result in: (1) Glycerol reducing, while (2) SDS increasing the radius and the porosity-to-tortuosity ratio of the aqueous pores in the SC. These considerations may help rationalize how adding 10 wt% Glycerol to a SDS aqueous contacting solution can reduce the radius and the porosity-to-tortuosity ratio of the aqueous pores induced by SDS in the SC.

2.5. Conclusions

According to a well-accepted view in the cosmetics literature, surfactant micelles cannot penetrate into the skin due to size limitations, and as a result, surfactant-induced skin barrier perturbation should be determined solely by the concentration of the surfactant monomers (11-23). Moore et al. (11) have recently shown that this is not the case for a model skin irritant, the surfactant SDS. Instead, they hypothesized that SDS micelles can penetrate into the skin barrier and induce skin barrier perturbation. In this chapter, for the first time, using Mannitol transdermal permeability and average skin electrical resistivity measurements in the context of a hindered-transport aqueous porous pathway model, I have demonstrated in vitro that SDS induces an increase in the average radius of the skin aqueous pores, from $20\pm3\text{Å}$ to $33\pm5\text{Å}$, such that the SDS micelles of size $19.5\pm1\text{Å}$ can penetrate into the SC through these aqueous pores. In addition, SDS induces a 7-fold increase in the porosity-to-tortuosity ratio of these aqueous pores, thereby significantly enhancing the SDS micellar contribution to SDS-skin penetration and to skin barrier perturbation in vitro.

Using in vitro skin radioactivity measurements, I demonstrated that adding 10 wt% Glycerol to an aqueous SDS micellar contacting solution significantly reduces: (i) the total extent

of SDS-skin penetration, and (ii) the SDS micelle contribution to SDS-skin penetration. This is due to the fact that Glycerol eliminates almost completely the contribution of the SDS micelles to SDS-skin penetration. Through Dynamic Light Scattering measurements, I have verified that Glycerol does not increase the size of the SDS micelles, which if increased, could have minimized the SDS micellar contribution to SDS-skin penetration. In addition, through surface tension measurements that were used to determine the CMC values of SDS in water and in a 10 wt% Glycerol aqueous solution, I have shown that Glycerol does not reduce the concentration of the SDS monomers contacting the skin, which if reduced, could have minimized the SDS monomeric contribution to SDS-skin penetration. Using in vitro transdermal permeability and average skin electrical resistivity measurements upon exposure of the skin to aqueous contacting solutions of SDS and of SDS+10 wt% added Glycerol, in the context of a hindered-transport aqueous porous pathway model, I have conclusively demonstrated that the addition of 10 wt% Glycerol prevents SDS micelles from penetrating into the skin barrier by: (1) reducing the radius of the skin aqueous pores induced by the SDS aqueous contacting solution, from *33±5Å to 20±5Å*, such that a SDS micelle of radius *18.5±1Å* in an aqueous SDS micellar solution with 10 wt% added Glycerol experiences steric hindrance and cannot penetrate into the SC, and (2) reducing the porosity-to-tortuosity ratio of the skin aqueous pores by more than 50%, thereby further reducing the ability of the SDS micelles to penetrate into the SC and induce skin barrier perturbation.

In the next chapter, Chapter 3, I investigate the well-known skin mildness of the anionic surfactant, Sodium Cococyl Isethionate (SCI), used in syndet (synthetic detergent) bars, by examining the size of the SCI micelles relative to that of the skin aqueous pores.

2.6. Appendix

2.6.1. Determination of the Radius and the Porosity-to-Tortuosity Ratio of the Skin Aqueous Pores Resulting from Exposure of p-FTS to SDS Aqueous Contacting Solutions

Average skin electrical resistivities, R, and Mannitol skin permeabilities, P, were measured upon exposure of p-FTS to SDS aqueous contacting solutions, as discussed in the text, and the resulting log P vs. log R plot is shown in *Figure 2-6* (see diamonds and the dashed line).

It is noteworthy that the slope of the best-fit straight line (the dashed line) through the diamonds in *Figure 2-6* is 0.98±0.06, which is statistically similar to the theoretical value of -1 (see Eq.(4)). The R^2 value is 0.96, which is close to 1. Hence, these results lend further support to the validity of the hindered-transport skin aqueous porous pathway model developed by Tang et al. (7). The intercept value in *Figure 2-6* is -2.90±0.03.

The infinite-dilution diffusion coefficient of Mannitol, D_p^{∞}, is 0.672×10^{-5} cm^2/s at 25°C (6, 7). The hydrodynamic radius of Mannitol, r_p, is 4.44Å (6, 7). Because skin electrical currents were measured in PBS that contained Na^+ and Cl^- as the dominant ions, the Na^+ ions were used to model the current carrying ions present in the solution. The infinite-dilution diffusion coefficient of the Na^+ ions, D_{ion}^{∞}, is 1.33×10^{-5} cm^2/s at 25°C (7). The hydrodynamic radius of the Na^+ ion, r_{ion}, is 2.2Å (7). In addition, I have used the following parameter values in C (see Eq.(4) in the Theoretical section): $k_B=1.38\times10^{-23}$ J/K (Boltzmann constant), T=298 K, $F=9.6485\times10^4$ C/mol (Faraday constant), z = 1 (in the PBS solution, since NaCl is the dominant electrolyte), c_{ion}=0.137 M, and $e_0=1.6\times10^{-19}$ C. Using these parameter values, along with the experimentally

determined value of C, I was able to determine the value of the ratio: $H(\lambda_p)/H(\lambda_{ion})$ (see the expression for C in Section 2.3.1). Next, using: (i) Eq.(5), (ii) the hydrodynamic radii values of Mannitol and Na^+, that is, 4.44 and 2.2Å, and (iii) the value of the ratio $H(\lambda_p)/H(\lambda_{ion})$, I was able to numerically solve for the average pore radius, r_{pore}. The average pore radius, r_{pore}, was found to be 33±5Å, which I have taken as the radius of the skin aqueous pores. Note that $H(\lambda_p)$ and $H(\lambda_{ion})$ are each less than 0.4, which is necessary for Eq.(5) to be valid (6, 7, 42). Having determined the aqueous pore radius, r_{pore} , the porosity-to-tortuosity ratio, ε/τ, was determined using Eq.(6), in which all the parameters, except for ε/τ, are known in advance (since ΔX=15μm) (6, 7).

The porosity-to-tortuosity ratio, ε/τ, for p-FTS exposed to the PBS control aqueous solution was determined using a calculation similar to the one for p-FTS exposed to the SDS aqueous contacting solutions presented in this appendix. Finally, the porosity-to-tortuosity ratio, ε/τ, resulting from the exposure of p-FTS to the SDS aqueous contacting solutions was normalized by the ε/τ value resulting from the exposure of p-FTS to the PBS control aqueous solution. I calculated this normalized value, $(\varepsilon/\tau)_{normal}$, to be 7±1 (see *Table 2-1*).

2.7. References

1. R.Scheuplein and I.Blank, Permeability of the skin, *Physiol. Rev.*, 51:p. 702-747 (1971).
2. P.M.Elias, Lipids and the epidermal permeability barrier, *Arch. Dermatol. Res.*, 270:p. 95-117 (1981).
3. P.W.Wertz and D.E.Downing, "Stratum corneum: biological and biochemical considerations", in *Transdermal Drug Delivery: Developmental issues and research initiatives*. J.Hadgraft and R.H.Guy, Eds. (Marcel Dekker, Inc. 1989), pp. 1-22.
4. R.L.Bronaugh and H.I.Maibach, "In vitro models for human percutaneous absorption", in *Models in Dermatology*. H.I.Maibach et al., Eds. (Karger, Bassel, 1985), Vol. 2, pp. 178-188.
5. M.Heisig, R.Lieckfeldt, G.Wittum, G.Mazurkevich, and G.Lee, Non steady-state descriptions of drug permeation through stratum corneum.1. The biphasic brick-and-mortar model, *Pharm. Res.*, 13:p. 421-426 (1996).
6. K.D.Peck, A.H. Ghanem, and W.I.Higuchi, Hindered diffusion of polar molecules through and effective pore radii estimates of intact and ethanol treated human epidermal membrane, *Pharm. Res.*, 11:p. 1306-1314 (1994).
7. H.Tang, S.Mitragotri, D.Blankschtein, and R.Langer, Theoretical description of transdermal transport of hydrophilic permeants: Application to low-frequency sonophoresis, *J. Pharm. Sci.*, 90:p. 545-568 (2001).
8. K.D.Peck, A.H.Ghanem, and W.I.Higuchi, The effect of temperature upon the permeation of polar and ionic solutes through human epidermal membrane, *J. Pharm. Sci.*, 84:p. 975-982 (1995).

9. A.Tezel, A.Sens, and S.Mitragotri, Description of transdermal transport of hydrophilic solutes during low-frequency sonophoresis based on a modified porous pathway model, *J. Pharm. Sci.*, 92:p. 381-393 (2003).

10. G.K.Menon, and P.M.Elias, Morphologic basis for a pore-pathway in mammalian stratum corneum, *Skin Pharmacol.*, 10:p. 235-246 (1997).

11. P.Moore, S.Puvvada, and D.Blankschtein, Challenging the surfactant monomer skin penetration model: Penetration of sodium dodecyl sulfate micelles into the epidermis, *J. Cosmet. Sci.*, 54:p. 29-46 (2003).

12. L.D.Rhein, F.A.Simion, R.L.Hill, R.H.Cagan, J.Mattai, and H.I.Maibach, Human cutaneous response to a mixed surfactant system: Role of solution phenomenon in controlling surfactant irritation, *Dermatologica*, 180:p. 18-23 (1990).

13. T. Agner and J. Serup, Sodium lauryl sulphate for irritant patch testing - A dose-response study using bioengineering methods for determination of skin irritation, *J. Invest. Dermatol.*, 95:p. 543-547 (1990).

14. L.D. Rhein, "In vitro interactions: Biochemical and biophysical effects of surfactants on skin", in *Surfactants in Cosmetics*, M.M. Rieger and L.D. Rhein, Eds. (Marcel Dekker Inc, New York, 1997), pp. 397-426.

15. K.P.Ananthapadmanabhan, C.L.Meyers, and M.P.Aronson, Binding of surfactants to stratum corneum, *J. Soc. Cosmet. Chem.*, 47:p. 185-200 (1996).

16. J.A.Faucher and E.D.Goddard, Interaction of keratinous substrates with sodium lauryl sulfate: I. Sorption, *J. Soc. Cosmet. Chem.*, 29:p. 323-337 (1978).

17. J.A.Faucher and E.D.Goddard, Interaction of keratinous substrates with sodium lauryl sulfate: II. Permeation through stratum corneum, *J. Soc. Cosmet. Chem.*, 29:p. 339-352 (1978).

18. C.H.Lee and H.I.Maibach, Study of cumulative irritant contact dermatitis in man utilizing open application on subclinically irritated skin, *Contact Dermatitis*, 30:p. 271-275 (1994).

19. L.D.Rhein, C.R.Robbins, K.Fernee, and R.Cantore, Surfactant structure effects on swelling of isolated human stratum corneum, *J. Soc. Cosmet. Chem.*, 37:p. 125-139 (1986).

20. J.Vilaplana, J.M.Mascaro, C.Trullas, J.Coll, C.Romaguera, C.Zemba, and C.Pelejero, Human irritant response to different qualities and concentrations of cocoamidopropylbetaines: a possible model of paradoxical irritant response, *Contact Dermatitis*, 26:p. 289-294 (1992).

21. K.P.Wilhelm, M.Samblebe, and C.P.Siegers, Quantitative in vitro assessment of N-alkyl sulphate-induced cytotoxicity in human keratinocytes (HaCaT). Comparison with in vivo human irritation tests, *Br. J. Dermatol.*, 130:p. 18-23 (1994).

22. K.P.Wilhelm, A.B.Cua, H.H.Wolff, and H.I.Maibach, Surfactant-induced stratum corneum hydration in vivo: Prediction of the irritation potential of anionic surfactants, *J. Invest. Dermatol.*, 101:p. 310-315 (1993).

23. K.P.Wilhelm, G.Freitag, and H.H. Wolff, Surfactant-induced skin irritation and skin repair, *J. Am. Acad. Dermatol.*, 30:p. 944-949 (1994).

24. J.W.Fluhr, M.Gloor, L.Lehmann, S. Lazzerini, F.Distante, and E.Berardesca, Glycerol accelerates recovery of barrier function in vivo, *Acta Derm Venereol*, 79:p. 418-421 (1999).

25. J.Bettinger, M. Gloor, A.Vollert, P.Kleesz, J.Fluhr, and W.Gehring, Comparison of different non-invasive test methods with respect to the different moisturizers on skin, *Skin Res. Technol.*, 5:p. 21-27 (1999).

26. A.M.Grunewald, J.Lorenz, M.Gloor, W.Gehring, and P.Kleesz, Lipophilic irritants. Protective values of urea and glycerol containing oil in water emulsions, *Dermatosen*, 44:p. 81-86 (1996).

27. M.D.Batt and E.Fairhurst, Hydration of the stratum corneum, *Int. J. Cosmet. Sci.*, 8:p. 253-256 (1986).

28. M.Loden, Urea-containing moisturizers influence barrier properties of normal skin, *Arch. Dermatol. Res.*, 288:p. 103-107 (1996).

29. D.S.Orth and Y.Appa, "Glycerine: a natural ingredient for moisturizing skin", in *Dry skin and moisturizers: chemistry and function,* M.Loden and H.I.Maibach, Eds. (CRC Press, Boca Raton, 2000), pp. 213-228.

30. C.L.Froebe, F.A.Simion, H.Ohlmeyer, L.D.Rhein, J.Mattai, R.H.Cagan, and S.E.Friberg, Prevention of stratum corneum lipid phase transitions in vitro by glycerol – An alternative mechanism for skin moisturization, *J. Soc. Cosmet. Chem.*, 41:p. 51-65 (1990).

31. A.Rawlings, C.Harding, A.Watkinson, J.Banks, C.Ackermann, and R.Sabin, The effect of glycerol and humidity on desmosome degradation in stratum corneum. *Arch. Dermatol. Res.*, 287:p. 457-464 (1995).

32. G.B.Kasting, L.A.Bowman, DC electrical properties of frozen, excised human skin, *Pharm. Res.*, 7:p. 134-143 (1990).

33. J.Kushner, D.Blankschtein, and R.Langer, Experimental demonstration of the existence of highly permeable localized transport regions in low-frequency sonophoresis, *J. Pharm. Sci.*, 93:p. 2733-2745 (2004).

34. L.Magid, "Light scattering in micellar systems" in *Dynamic Light Scattering: The Method and Some Applications*, W. Brown, Ed. (Oxford University Press, Oxford, 1993), pp. 554-593.

35. A.Einstein, *Investigation on the Theory of Brownian Movement*, New York: Dover, 58, (1956).

36. W.Brown, J.Fundin, and M.G. Miguel, Poly(ethylene oxide)-sodium dodecyl sulfate interactions studied using static and dynamic light scattering, *Macromolecules*, 25:p. 7192-7198 (1992).

37. P.J.Missel, N.A.Mazer, G.B.Benedek, and M.C. Carey, Influence of chain length of the sphere-to-rod transition in alkyl sulfate micelles, *J. Phys. Chem.*, 87:p. 1264-1277 (1983).

38. A.Rohde and E.Sackman, Quasieleatic light-scattering studies of micellar sodium dodecyl sulfate solutions at the low concentration limit, *J. Colloid Interface Sci.*, 70:p. 494-505 (1979).

39. P.L.Dubin, J.H.Grubner, J.Xia, and H. Zhang, The effect of cations on the interaction between dodecylsulfate micelles and poly(ethyleneoxide), *J. Colloid Interface Sci.*, 148:p. 35-41 (1992).

40. T.R.Carale, Q.T.Pham, and D.Blankschtein, Salt effects on intramicellar interactions and micellization of nonionic surfactants in aqueous solutions, *Langmuir*, 10:p. 109-121 (1994).

41. M.Mulqueen and D.Blankschtein, Theoretical and experimental investigation of the equilibrium oil-water interfacial tensions of solutions containing surfactant mixtures, *Langmuir*, 18:p. 365-376 (2002).

42. W.M.Deen, Hindered transport of large molecules in liquid-filled pores, *AIChE J.*, 33:p. 1409-1425 (1987).

43. A.Patist, B.K.Jha, S.G.Oh, and D.O.Shah, Importance of micellar relaxation time on detergent properties, *J. Surf. Det.*, 2:p. 317-324 (1999).

44. D.Dhara and D.O.Shah, Stability of sodium dodecyl sulfate micelles in the presence of a range of water-soluble polymers: A pressure-jump study, *J. Phys. Chem. B*, 105:p. 7133-7138 (2001).

45. D.M.Bloor and E.W.Jones, Kinetic and equilibrium studies associated with the binding of surface-active agents to macromolecules, *Chem. Soc. Farad. Trans.* 2, 78:p. 657-669 (1981).

46. D.J.Lee and W.H.Huang, Enthalpy-entropy compensation in micellization of sodium dodecyl sulphate in water/methanol, water/ethylene glycol and water/glycerol binary mixtures, *Colloid Polym Sci*, 24:p. 160-165 (1996).

47. M.Almgren and S.Swarup, Size of sodium dodecyl sulfate micelles in the presence of additives. 2. Aromatic and saturated hydrocarbons, *J. Phys. Chem.*, 86:p. 4212-4216 (1982).

48. J.L.Leveque, J.De Regal, D.Saint-Leger, and D.Billy, How does sodium lauryl sulfate alter the skin barrier function in man? A multiparametric approach, *Skin Pharmacol.*, 6:p. 111-115 (1993).

49. Y.Kawasaki, D.Quan, K,Sakamota, and H.I.Maibach, Electron resonance studies on the influence of anionic surfactants on human skin, *Dermatology*, 194:p. 238-242 (1997).

50. E.Barany, M.Lindburg, and M.Loden, Biophysical characterization of skin damage and recovery after exposure to different surfactants, *Contact Dermatitis*, 40:p. 98-103 (1999).

51. M.Loden, The simultaneous penetration of water and sodium lauryl sulfate through isolated human skin, *J. Soc. Cosmet. Chem.*, 41:p. 227-233 (1990).

52. T.Okamoto, H.Inoue, S.Anzai, and H.Nakajima, Skin-moisturizing effect of polyols and their absorption into human stratum corneum, Preprint of the Annual Scientific Meeting, *Society of Cosmetic Chemists* (1997).

Chapter 3

3. Why is Sodium Cocoyl Isethionate (SCI) Mild to the Skin Barrier? An In Vitro Investigation Based on the Relative Sizes of the SCI Micelles and the Skin Aqueous Pores

3.1. Introduction

Sodium Cocoyl Isethionate (SCI) is an important surfactant ingredient in personal washing bars, and is known to be *milder*, or less irritating, to the skin than *harsher* skin agents, such as other anionic surfactants like Sodium Dodecyl Sulfate (SDS) and soap (sodium salts of fatty acids such as stearic and palmitic acids) (1-8). In vivo and in vitro studies have shown that SCI does not significantly reduce the barrier properties of the skin (1-23, 39, 41). Several factors have been proposed to explain the mildness of SCI relative to the harshness of other skin agents used in skin cleansers, including: (i) a lower critical micelle concentration (CMC) value for SCI resulting in a lower SCI monomer activity with the skin barrier (1-3, 15), (ii) reduced penetration of SCI into the skin barrier (1-5), and (iii) decreased binding of SCI to proteins and lipids in the stratum corneum (SC), which is the primary constituent of the skin barrier, resulting in a lower skin irritation response (3-9).

The interactions of SCI with the SC proteins have been studied extensively (1, 3, 15, 42). These studies have shown that one of the factors responsible for skin mildness/harshness of a surfactant solution is the charge density of the surfactant polar head group. For example, it has been shown that SCI has a lower charge density than SDS, and therefore, binds less strongly to the SC proteins (1, 42). The CMC of the SCI aqueous solution was considered as another important factor. Specifically, Ananthapadmanabhan et al. (1) observed that SCI has a lower CMC than SDS and binds to proteins in the SC only about one-fifth as much as SDS under similar solution conditions and exposure times. The interaction of SCI with SC lipids has also been investigated to shed light on the mechanisms of SCI-induced skin barrier perturbation. Specifically, nonionic surfactants such as alkyl polyglucosides, which do not interact strongly with SC proteins, have been shown to dissolve stearic acid and cholesterol to a much greater extent than mild anionic surfactants like SCI (42). Because SCI does not selectively remove fatty acids and cholesterol from the lipid bilayers in the SC, it does not induce significant biological damage through the modification of lipid biosynthetic functions due to changes in the relative levels of various lipids in the SC (17-20).

It is well-accepted that surfactants have to first penetrate into the skin barrier before they can reduce the skin barrier properties. Therefore, if a formulator can minimize surfactant-skin penetration, this should also minimize the ability of the surfactant to reduce the skin barrier properties. Previous research has investigated the process of SDS skin penetration from an aqueous contacting solution by itself (11), as well as when mixed with: (i) a polymer – Poly Ethylene Oxide (PEO) (11), (ii) a nonionic surfactant – Dodecyl Hexa (Ethylene Oxide) $C_{12}E_6$ (12), and (iii) a humectant – Glycerol (13). It is well-known that the SDS monomers self-assemble in aqueous solution to form micelles at SDS concentrations which are greater than the

CMC of SDS. Due to the hydrophilic nature of the resulting SDS micelles, they are expected to penetrate into the SC through aqueous pores that exist in the SC (11, 13). These aqueous pores in the SC are located in the *lacunae* and other aqueous regions surrounded by polar lipids in the lipoidal *mortar* between the corneocyte *bricks* that comprise the *brick-and-mortar* structure of the SC (24, 25). It has been shown recently that the SDS micelles are smaller in radius than the average radii of these aqueous pores, and therefore, contribute to SDS skin penetration and induce skin barrier perturbation (11-13). Strong evidence that the SDS micelles do indeed contribute to SDS skin penetration is also provided by the observed dose dependence of SDS skin penetration and barrier perturbation, which was found to increase as the total SDS concentration was increased beyond the CMC of SDS (8-13). In cases (i) and (ii) above, where PEO and $C_{12}E_6$ were added separately to aqueous SDS contacting solutions, the SDS micelle radius increased relative to the aqueous pore radius, such that the larger SDS micelles became sterically hindered from penetrating into the SC through the aqueous pores (11, 12). On the other hand, in case (iii), when Glycerol was added to an aqueous SDS contacting solution, I found that the average aqueous pore radius decreased relative to the SDS micelle radius, such that the SDS micelles became sterically hindered from penetrating into the SC through the smaller aqueous pores (13).

In this chapter, I hypothesize that the well-documented skin mildness of SCI is due to the inability of the SCI micelles to contribute to skin penetration and induce skin barrier perturbation. To test this hypothesis, I have determined the average radius and the porosity-to-tortuosity ratio, of the aqueous pores in the SC when an aqueous solution of SCI contacts the skin. To this end, I have conducted in vitro Mannitol skin permeability and skin electrical current measurements in the context of a hindered-transport aqueous porous pathway model of the SC. I

have also carried out dynamic light scattering (DLS) measurements to determine the radius of the SCI micelles present in the aqueous solution contacting the skin. Such a combined in vitro investigation can explain the well-documented in vivo and in vitro skin mildness of SCI (1-3, 42) by showing that the radius of an SCI micelle is significantly larger than that of the skin aqueous pores. As a result, SCI in micellar form is unable to penetrate into the SC through these aqueous pores. Finally, I have also measured the penetration of SCI into the skin using in vitro ^{14}C-radiolabeled SCI skin radioactivity assays. Because only the SCI monomers can contribute to SCI skin penetration, due to the inability of the SCI micelles to do so based on the size limitation discussed above, I will show that the SCI skin penetration is dose independent, an important finding which further validates this hypothesis.

3.2. Experimental

3.2.1. Materials

Sodium Cocoyl Isethionate (SCI) from BASF was provided to me by UNILEVER (Edgewater, NJ). ^{14}C-radiolabeled SCI and ^{3}H-radiolabeled Mannitol were purchased from American Radiolabeled Chemicals (St. Louis, MO). Sodium Chloride (NaCl) was purchased from Sigma Chemicals (St. Louis, MO). All these chemicals were used as received. Water was filtered using a Millipore Academic water filter (Bedford, MA). Phosphate Buffered Saline (PBS) was prepared using PBS tablets from Sigma Chemicals (St. Louis, MO) and Millipore filtered water, such that a phosphate concentration of 0.01 M along with a NaCl concentration of 0.137 M were obtained at a pH of 7.2.

3.2.2. Preparation of the Skin Samples

Female Yorkshire pigs (40-45kg) were purchased from local farms, and the skin (back) was harvested within one hour after sacrificing the animal. The subcutaneous fat was trimmed off using a razor blade, and the full-thickness pig skin was cut into small pieces (2cm × 2cm) and stored in a –80 °C freezer for up to 2 months. The surfactant penetration experiments were conducted using pig full-thickness skin, referred to hereafter as p-FTS.

3.2.3. In Vitro Transdermal Permeability Measurements

Vertical Franz diffusion cells (Permegear Inc., Riegelsville, PA) were utilized in the in vitro transdermal permeability measurements (11, 12, 31). Prior to each experiment, a p-FTS sample was mounted in the diffusion cell with the SC facing the donor compartment. Both the donor and the receiver compartments were filled with PBS, and the p-FTS sample was left to hydrate for 1 hour before the beginning of the experiment to allow the skin initial barrier property to reach steady state. At this point, the skin electrical current across the p-FTS sample was measured, and only p-FTS samples with an initial skin current < 3 μA were utilized in the permeation studies (11, 12, 28, 31). The PBS in the donor compartment was then replaced with 1.5 ml of an SCI aqueous solution. The diffusion cell was then transferred to a temperature-controlled oven, with the temperature set at 35°C to prevent SCI precipitation from the contacting solution in the donor compartment of the diffusion cell (42). The donor compartment of the diffusion cell was covered by para-film to prevent water evaporation at this temperature. The SCI aqueous contacting solution in the donor compartment contacted the p-FTS sample for 5 hours (11, 12). Subsequently, the contacting solution was removed and the donor compartment along with the p-FTS sample were rinsed 4 times with 2 ml of PBS to remove any trace chemical

left on the skin surface and in the donor compartment. The receiver compartment was stirred with a magnetic stirrer at a speed of 400 rpm throughout the experiment to eliminate permeant bulk concentration gradients.

Following the SCI aqueous contacting solution treatments of the skin, the p-FTS samples in the diffusion cells were exposed to a contacting solution of ^{3}H-radiolabeled Mannitol in PBS (1–10 μCi/ml) for 24 hours (24, 27, 31). Throughout these experiments, solution samples were withdrawn from both the receiver (r) and the donor (d) compartments every two hours, and the concentrations of the permeant (Mannitol) in the two compartments (C_r and C_d, respectively) were measured using a liquid scintillation counter (Packard, Sheldon, CT). When the transport of Mannitol attained steady state, the Mannitol skin permeability, P, was calculated as follows (24, 27, 31):

$$P = \frac{1}{AC_d}\left(\frac{d\left(C_r V_r\right)}{dt}\right) \tag{2}$$

where V_r is the volume of the receiver compartment, A is the area of the SC exposed to the Mannitol solution in the donor compartment, and t is the exposure time.

3.2.4. In Vitro Skin Electrical Current and Skin Electrical Resistivity Measurements

During each skin permeation experiment, two Ag/AgCl electrodes (E242, In Vivo Metrics, Healdsburg, CA) were placed in the donor and in the receiver compartments to measure the electrical current and the electrical resistivity across the p-FTS sample (31). A 100 mV AC voltage (RMS) at 10 Hz was generated by a signal generator (Hewlett-Packard, Atlanta, GA), and was applied across the two electrodes for 5 s. The electrical current across the skin was measured using an Ammeter (Hewlett-Packard, Atlanta, GA). This ammeter was used to

measure low AC currents and was accurate in the 0.1 μA range. The electrical resistance of the p-FTS sample was then calculated from Ohm's law (31). Because the measured skin electrical resistance is the sum of the actual skin electrical resistance and the background PBS electrical resistance, the latter was subtracted from the measured skin electrical resistance to obtain the actual skin electrical resistance. The skin electrical resistivity was then obtained by multiplying the actual skin electrical resistance by the skin area (A=1.77 cm^2). Additional details about this procedure are provided in (13). Skin electrical current and resistivity measurements were carried out before and during the permeation experiments at each predetermined sampling point. For each p-FTS sample, an average skin electrical resistivity was determined over the same time period for which the steady-state skin permeability, P, was calculated using Eq.(1). This average skin electrical resistivity, R, was then analyzed along with the corresponding skin permeability, P, in the context of the hindered-transport aqueous porous pathway model of the SC (26, 27, 31).

3.2.5. In Vitro Skin Radioactivity Measurements

The p-FTS samples were mounted in vertical Franz diffusion cells, as was done in the case of the skin transdermal permeability measurements described above. Following a similar protocol, p-FTS samples were now exposed to aqueous contacting solutions containing 1.5 ml of SCI (see Chapter 2). Each of these contacting solutions also contained about 1 μCi/ml of ^{14}C-SCI. Diffusion of SCI into the skin took place for 5 hours, as before, and subsequently, the concentration of SCI in the skin barrier was determined using a previously published skin radioactivity assay protocol (11-13).

3.2.6. Dynamic Light Scattering Measurements

The aqueous SCI solutions were prepared in Millipore filtered water with 100 mM of added NaCl. Note that 100 mM NaCl was added to screen potential electrostatic repulsions between the negatively-charged SCI micelles while performing the Dynamic Light Scattering (DLS) measurements (11, 13, 35-37). After mixing, the solutions were filtered through a 0.02 μm Anotop 10 syringe filter (Whatman International, Maidstone, England) directly into a cylindrical-scattering cell to remove any dust from the solution, and then sealed until use. Dynamic Light Scattering was performed at 35°C and a 90° scattering angle on a Brookhaven BI-200SM system (Brookhaven, Holtsville, NY) using a 2017 Stabilite argon-ion laser (Spectra Physics) at 513.5 nm. The autocorrelation function was analyzed using the CONTIN program provided by the BIC Dynamic Light Scattering software (Brookhaven, Holtsville, NY), which determines the effective hydrodynamic radius, $\overline{R}_h$, of the scattering entities using the Stokes-Einstein relation (35):

$$\overline{R}_h = \frac{k_B T}{6\pi\eta\overline{D}} \tag{2}$$

where k_B is the Boltzmann constant, T is the absolute temperature, η is the viscosity of the aqueous salt solution, and $\overline{D}$ is the mean diffusion coefficient of the scattering entities. For simplicity, we refer to $\overline{R}_h$ as the micelle radius. Additional details can be found in references (11-13).

3.3. Theoretical

3.3.1. Determination of the Average Radius and the Porosity-to-Tortuosity Ratio of the Skin Aqueous Pores in Skin Exposed to the Aqueous SCI Contacting Solutions

Tang et al. (31) developed a hindered-transport aqueous porous pathway model of the SC that can be used to determine the average radius and the porosity-to-tortuosity ratio of the aqueous pores in the SC following exposure of the skin to aqueous solutions containing chemical enhancers, such as surfactants, or following exposure of the skin to physical enhancers, such as ultrasound. I have recently utilized this model to determine the average radius and the porosity-to-tortuosity ratio of the aqueous pores in skin (p-FTS) that was contacted by an aqueous solution of SDS (see Chapter 2 and (13)). Similarly, I have utilized this model here to determine the average radius and the porosity-to-tortuosity ratio of the aqueous pores in skin (p-FTS) that was contacted by an aqueous solution of SCI. A comparison of the values of the average radii and the porosity-to-tortuosity ratio resulting from skin exposure to: (i) the SCI contacting solution (referred to hereafter as solution (a)), (ii) the SDS contacting solution (referred to hereafter as solution (b)), and (iii) the PBS control (referred to hereafter as solution (c)) is presented in *Table 3-1*. Note that the average radii and the porosity-to-tortuosity ratio corresponding to solutions (b) and (c) are reproduced from reference (13) (also see Chapter 2). In ref. (13), I discussed in detail the application of the hindered-transport aqueous porous pathway model to determine the average radius and the porosity-to-tortuosity ratio of the aqueous pores upon skin exposure to surfactant aqueous contacting solutions. With this in mind, here, I will only summarize briefly the main assumptions and key equations of this model.

The fundamental underlying assumption of the porous pathway model is that hydrophilic permeants, such as Mannitol, as well as current-carrying ions, traverse the SC through the same tortuous, cylindrical aqueous pores. Other model assumptions include: (i) the permeants/ions behave as hard spheres that experience solely steric, hard-sphere particle (permeant or ion)-pore wall interactions, and (ii) the anions and the cations in the electrolyte solution have the same valence, z, and similar diffusion coefficients. Although the ions (and the permeant molecules) in the contacting solutions may be charged, Tang et al. showed that assumption (i) is valid provided that the Debye-Hückel screening length – the length scale associated with the screening of electrostatic interactions between the ions (or between the charged permeants) and the negatively-charged skin aqueous pore walls – is much smaller than the average skin aqueous pore radius, r_{pore} (31). Tang et al. also showed that for the PBS control contacting solution containing Na^+ and Cl^- ions, and also for the Mannitol aqueous contacting solution, the Debye-Hückel screening length $\leq$ 7 Å, which is much smaller than the typical average skin aqueous pore radii (approximately 15-25 Å) (31). Furthermore, because the Na^+ and the Cl^- ions are the two dominant current-carrying ions in the PBS electrolyte solution, which have the same valence and similar diffusion coefficients, assumption (ii) is also satisfied. When assumptions (i) and (ii) are satisfied, the hindered-transport aqueous porous pathway model indicates the existence of a linear-log relationship between the Mannitol skin permeability, P, and the average skin electrical resistivity, R. Specifically, within statistical error, the following relation holds (31):

$$\log P = \log C - \log R \qquad (3)$$

where $C = [k_B T/2z^2 F c_{ion} e_0] * [D_p^{\infty} H(\lambda_p)/ D_{ion}^{\infty} H(\lambda_{ion})]$ is a constant that depends on the average skin aqueous pore radius, r_{pore}, through $H(\lambda_p)$ and $H(\lambda_{ion})$, as follows (24, 27, 31):

$$H(\lambda_i) = \phi_i\left(1 - 2.1044\lambda_i + 2.089\lambda_i^3 - 0.948\lambda_i^5\right), \text{ for } \lambda_i \leq 0.4 \quad (4)$$

where i = p (permeant, in our case, Mannitol) or ion, r_i is the radius of solute i, $\lambda_i = r_i/r_{pore}$, $H(\lambda_i)$ is the hindrance factor for permeant or ion transport, and ϕ_i (the partition coefficient of solute i) = $(1-\lambda_i)^2$. The quantities, D_p^{∞} and D_{ion}^{∞}, appearing in C refer to the permeant and to the ion infinite-dilution diffusion coefficients, respectively (note that these quantities correspond typically to the bulk diffusion coefficients of the permeant and the ion in the dilute donor contacting solutions used in the in vitro transdermal permeability and electrical resistivity measurements). In addition, in C, k_B is the Boltzmann constant (1.38×10^{-23} J/K), T is the absolute temperature (298 K), F is the Faraday constant (9.6485×10^4 C/mol), c_{ion} is 0.137 M, and e_0 is 1.6×10^{-19} C.

According to the hindered-transport theory (26), one can express the permeability, P, of a hydrophilic permeant, such as, Mannitol, through the skin aqueous pores as follows:

$$P = \frac{\left(\frac{\varepsilon}{\tau}\right) D_p^{\infty} H(\lambda_p)}{\Delta X} \quad (5)$$

where ε is the porosity, which is the fraction of the skin area occupied by the aqueous pores, τ is the tortuosity, which is the ratio of the permeant diffusion path length within the skin barrier (the SC) to the thickness of the skin barrier (the SC), ΔX. Therefore, using Eqs.(3)-(5), once P and R are determined experimentally upon exposure of p-FTS to contacting aqueous solutions of SCI, one can also determine the average skin aqueous pore radius, r_{pore}, and the ratio of porosity-to-tortuosity, defined as ε/τ, if all the other parameters, such as ΔX, are known (see ref. (13) for an illustration of how to deduce r_{pore} and ε/τ when p-FTS is contacted with an aqueous SDS solution). The porosity-to-tortuosity ratio, ε/τ, can be related to the pore number density, which corresponds to the number of tortuous aqueous pores per unit cross-sectional area of the SC (see

Chapter 4). In the context of the hindered-transport aqueous porous pathway model of the SC, an increase in the porosity, ε, and/or a decrease in the tortuosity, τ, which results in an increase in the porosity-to-tortuosity ratio, ε/τ, of the aqueous pores can be interpreted as indicating an increase in the pore number density of the SC (see Chapters 2 and 4, and (13, 24, 27, 31)).

3.4. Results and Discussion

3.4.1. Determination of the Average Radius and the Porosity-to-Tortuosity Ratio of the Skin Aqueous Pores

I quantified the extent of skin barrier perturbation using the skin average aqueous pore radius and the porosity-to-tortuosity ratio as quantitative descriptors of the morphological changes in the SC that occur upon skin exposure to aqueous SCI contacting solutions (0.2-200 mM).[10] Specifically, the average radius and the porosity-to-tortuosity ratio of the skin aqueous pores were determined using the hindered-transport model of the skin aqueous porous pathways, along with the in vitro Mannitol transdermal permeability and the average skin electrical resistivity measurements. To gain additional insight, I have also compared the results corresponding to the aqueous SCI contacting solution (solution (a)) with those corresponding to the aqueous SDS contacting solution (solution (b)) and to the PBS control (solution (c)) [see *Table 3-1*] (13).

The results of the skin electrical current and the Mannitol transdermal permeability measurements are shown in *Figures 3-1* and *3-2*, respectively. Note that a large (or small) skin electrical current or transdermal permeability, which results from a high (or low) transfer rate of permeant molecules (Mannitol in our case) or of ions, respectively, across the skin, is indicative

[10] Note that for SCI, 1 mM=0.03 wt%.

of a large (or small) extent of skin barrier perturbation in vitro (3, 13, 27-33). In *Figures 3-1* and *3-2*, one can clearly see that the values of the skin electrical current and of the Mannitol transdermal permeability both increase sharply as the SCI concentration increases from 0.2 to 1 mM (the CMC of SCI), but do not continue to increase significantly with an increase in the SCI concentration in the contacting solution beyond the CMC (1 mM). According to the monomer penetration model (MPM) adopted by many researchers in the past (1-15), only the surfactant monomers are able to penetrate into the skin barrier and induce skin barrier perturbation, while the micelles, due to their larger size relative to that of the monomers, are not able to do so. Hence, according to the MPM, the skin barrier perturbation induced by a surfactant contacting solution should not increase significantly upon increasing the total surfactant concentration beyond the CMC. Therefore, these in vitro measurements clearly show that the skin barrier perturbation induced by SCI is *dose independent and follows the MPM.*

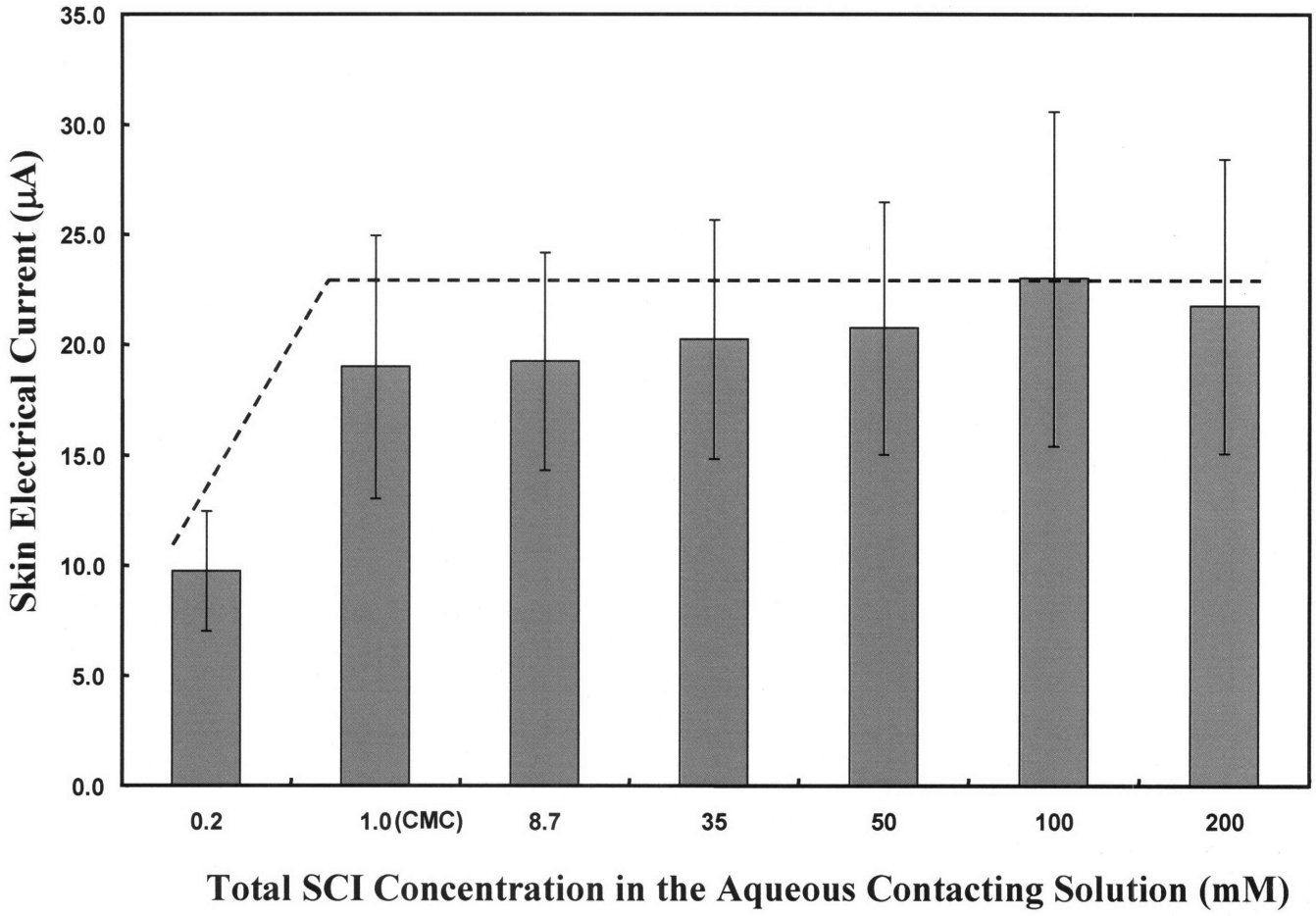

Figure 3-1. Skin electrical currents induced in vitro by SCI aqueous contacting solutions (0.2 to 200 mM). The dashed line passing above the filled bars is drawn as a guide to the eye. There is a sharp increase in the skin electrical current upon an increase in the SCI concentration from 0.2 to 1.0 mM (the CMC of SCI). However, an additional increase in the SCI concentration beyond the CMC of 1.0 mM does not result in an increase in the in vitro skin electrical current. The error bars represent standard errors based on 6 p-FTS samples.

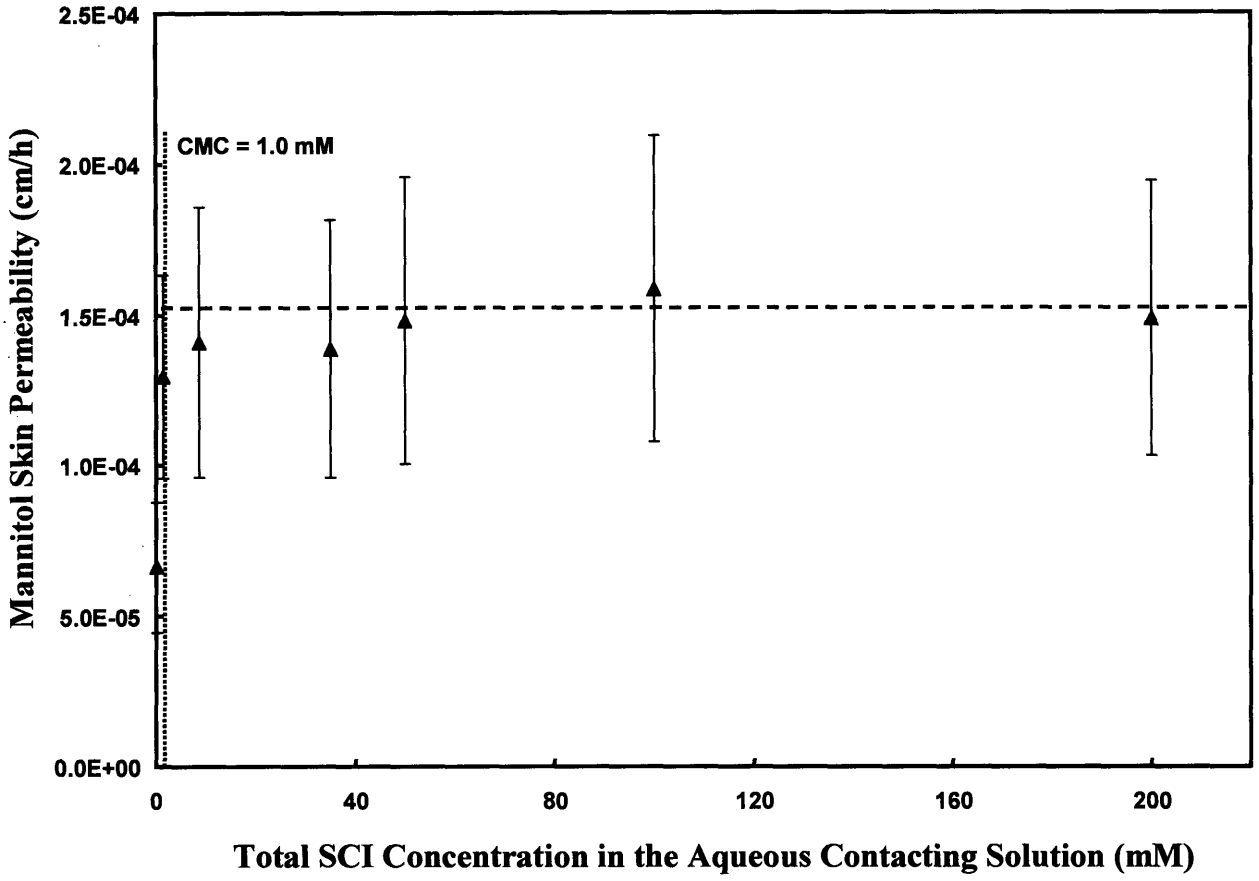

Figure 3-2. Mannitol skin permeability induced in vitro by SCI aqueous contacting solutions (triangles). The dotted vertical line at an SCI concentration of 1.0 mM denotes the CMC of SCI. The dashed line passing close to the triangles is drawn as a guide to the eye. There is a sharp increase in the Mannitol skin permeability upon an increase in the SCI concentration from 0.2 to 1.0 mM. However, an additional increase in the SCI concentration beyond the CMC of 1.0 mM does not result in an increase in the Mannitol skin permeability. The error bars represent standard errors based on 6 p-FTS samples.

In *Figure 3-3*, I have plotted the experimental correlation between the Mannitol transdermal permeability, P (cm/h), and the average skin electrical resistivity, R (kohm-cm^2), over the same exposure time, exhibited by p-FTS samples exposed to the aqueous SCI contacting solutions (0.2-200 mM). Each triangle represents a log P value of one p-FTS sample at steady state and the corresponding log R value (the log of the average skin electrical resistivity value). The slope of the best-fit curve resulting from a linear regression (R^2=0.91) is not statistically different from the theoretically predicted slope value of -1, thereby indicating the validity of utilizing the hindered-transport aqueous porous pathway model in the SCI case (13, 27, 31). The average aqueous pore radius, r_{pore}, was determined from the intercept value of the dashed line with the log P axis (see *Figure 3-3*) (13, 27, 31). Having determined r_{pore}, the porosity-to-tortuosity ratio was determined using Eq.(5), in which all the parameters, except ε/τ, the porosity-to-tortuosity ratio, are known [recall that ΔX=15μm] (13, 31). Using the model described above, I found that the average pore radius does not depend on the SC thickness, ΔX, while the porosity-to-tortuosity ratio is directly proportional to ΔX. The porosity-to-tortuosity ratio, ε/τ, resulting from exposure of the p-FTS samples to aqueous SCI contacting solutions were normalized by the ε/τ value resulting from exposure of the p-FTS samples to the PBS control solution, which served as the baseline, and have been denoted as $(\varepsilon/\tau)_{normal}$. Note that the r_{pore} and the ε/τ values for the aqueous SDS contacting solution (1-200 mM) (solution (b)) and for the PBS control solution (solution (c)) are reproduced from reference (13) (also see Chapter 2).

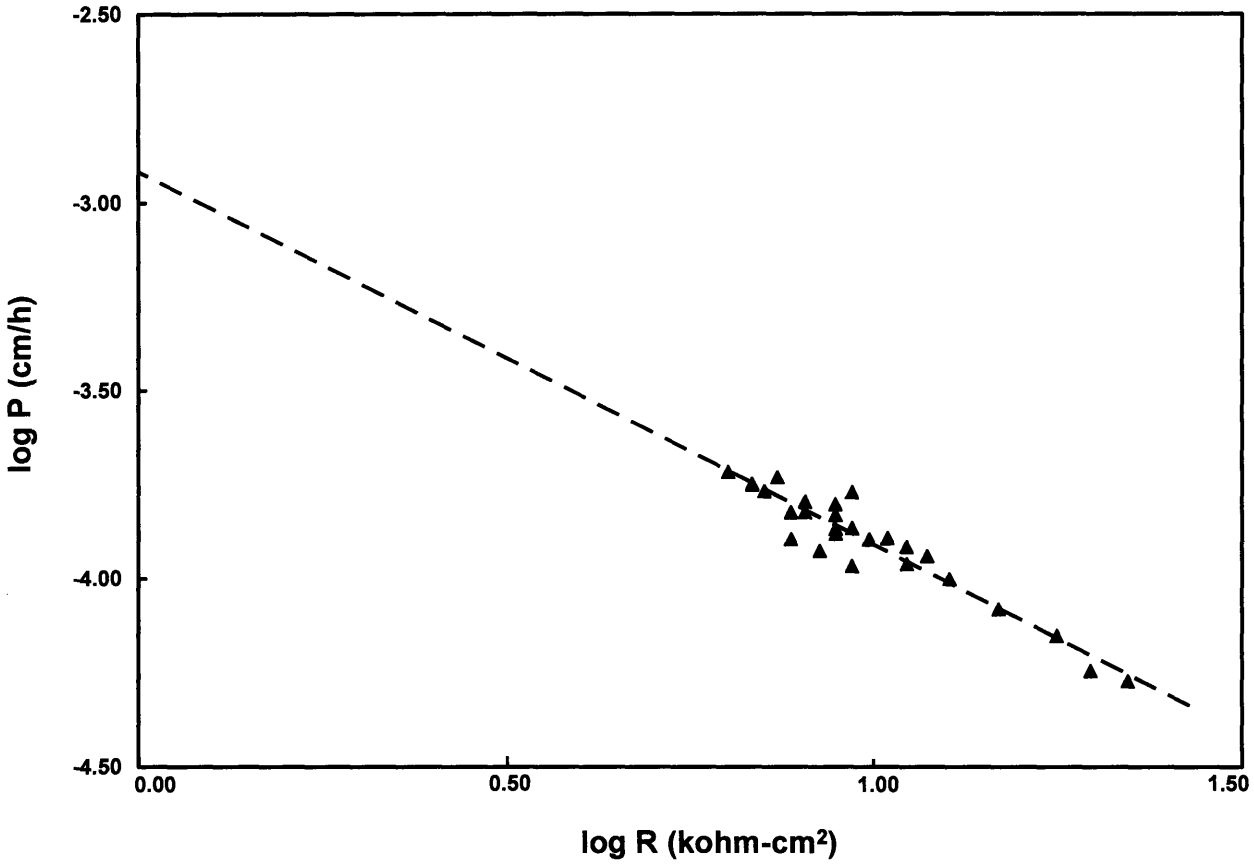

Figure 3-3. Experimental correlation between the Mannitol skin permeability, P (cm/h), and the average skin electrical resistivity, R (kohm-cm^2), exhibited by p-FTS samples exposed to aqueous contacting solutions of SCI (0.2-200 mM), the triangles. Each data point corresponds to a log P value of one p-FTS sample at steady state and the associated log R, the log of the average skin electrical resistivity value over the same time period. The slope of the best-fit curve resulting from a linear regression is -0.98±0.06 with R^2=0.91, shown as the dashed line. Note that the slope value is not statistically different from the theoretically predicted value of -1.

The deduced values of r_{pore} and $(\varepsilon/\tau)_{normal}$ corresponding to solutions (a)-(c) above are reported in *Table 3-1*. Specifically, the deduced average aqueous pore radius, r_{pore}, corresponding to solution (a) is *29±5Å*, which is smaller than the deduced r_{pore} value corresponding to solution (b) (*33±5Å*). The normalized porosity-to-tortuosity ratio, $(\varepsilon/\tau)_{normal}$, corresponding to solution (a), *2±1*, is less than half that corresponding to solution (b), *7±1*. Therefore, not only does the *mild* SCI surfactant induce smaller aqueous pores, but it also results in a lower porosity-to-tortuosity ratio of these aqueous pores when compared to the *harsh* SDS surfactant.

Table 3-1. Skin aqueous pore characteristics resulting from skin exposure to: (i) the SCI aqueous contacting solution considered here (solution (a)), and (ii) the SDS aqueous contacting solution (solution (b)), and the PBS control aqueous contacting solution (solution (c)), along with the corresponding surfactant solution characteristics, including the micelle radii and the CMCs. Note that the results for solutions (a) and (b) are reproduced from reference (13). The hindered-transport aqueous porous pathway model was used, along with the in vitro Mannitol transdermal permeability and average skin electrical resistivity measurements, to determine the average pore radius, r_{pore} , and the porosity-to-tortuosity ratio, ε/τ, resulting from skin exposure to solutions (a), (b), and (c). Note that I have reported ε/τ values resulting from the exposure of p-FTS to contacting solutions (a)-(c) normalized by the ε/τ value resulting from the exposure of p-FTS to contacting solution (c), which I have denoted as $(\varepsilon/\tau)_{normal}$. The SCI micelle radius was determined using dynamic light scattering (DLS) measurements at 35°C. The CMC of SCI at 35°C was provided by the BASF Company.

Type of Aqueous Contacting Solution	*Average Aqueous Pore Radius, r_{pore} (Å)*	*Normalized Porosity-to-Tortuosity Ratio, $(\varepsilon/\tau)_{normal}$*	*Micelle Radius, (Å)*	*Critical Micelle Concentration, CMC (mM)*
(a) SCI	29±5	2±1	33.5 ±1	1.0
(b) SDS	33±5	7±1	19.5 ±1	8.7
(c) PBS Control	20±3	1	N/A	N/A

3.4.2. Determination of the SCI Micelle Size Using Dynamic Light Scattering (DLS)

Using DLS, I determined the size (radius) of the SCI micelles in aqueous solutions, as shown in *Figure 3-4* (for details, see references (11-13)). The SCI micelle radius was determined by extrapolation to a zero SCI micelle concentration. Using a linear regression analysis, we found that the SCI micelle radius is *33.5±1Å*.

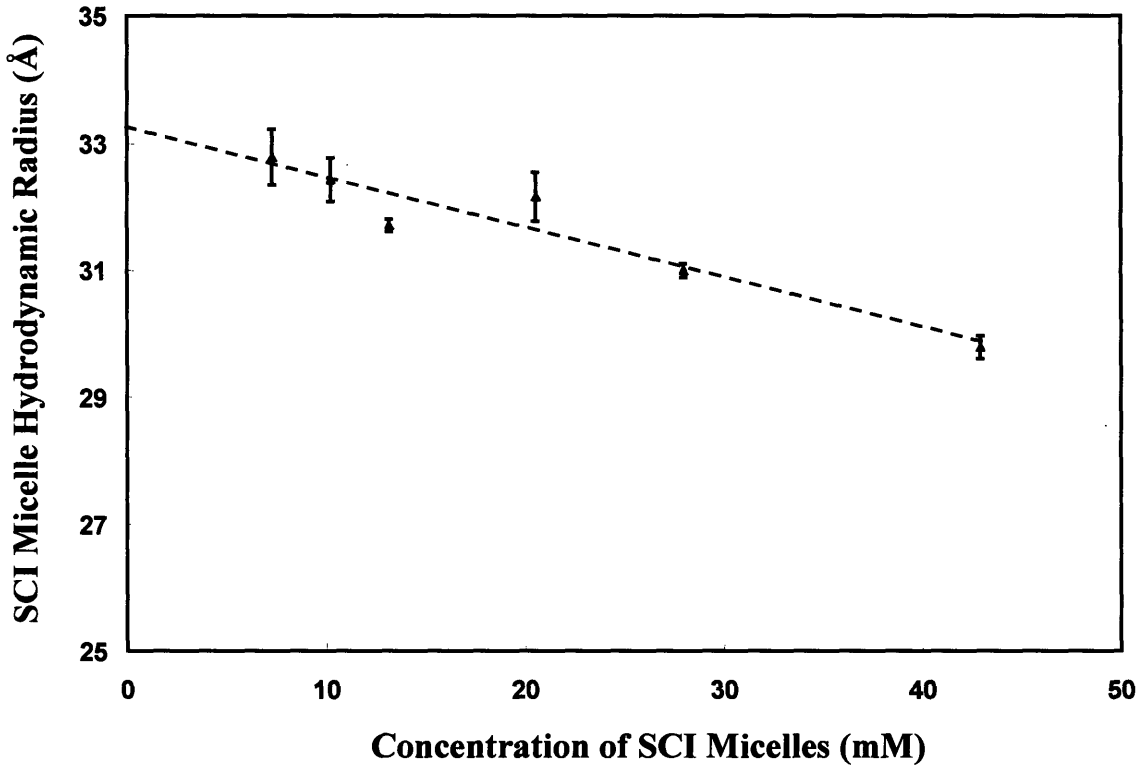

Figure 3-4. Measured radii of the SCI micelles in aqueous solutions (triangles) plotted versus the SCI concentration minus the CMC, corresponding to the concentration of the SCI micelles, using DLS measurements at 35°C. The SCI micelle radii were determined using a CONTIN analysis. The error bars represent standard errors based on 6 samples at each SCI concentration.

3.4.3. Plausible Explanation for the Skin Mildness of SCI

SCI is a mild skin agent that is not known to significantly induce skin barrier perturbation in vivo. In order to provide a plausible explanation for the observed skin mildness of SCI, it will be instructive to examine the micelle size and the CMC of SCI, along with the SCI-induced average skin aqueous pore radius and the porosity-to-tortuosity ratio. As discussed above, the average aqueous pore radius, r_{pore} , induced by an aqueous SCI contacting solution is *29±5Å,* while the radius of the SCI micelle is *33.5±1Å* (see *Table 3-1*). Therefore, the larger SCI micelle experiences significant steric hindrance in penetrating through aqueous pores that have, on average, a smaller radius.[11] On the other hand, a SDS micelle having a radius of *19.5±1Å* experiences no steric hindrance in penetrating through aqueous pores in the SC that have an average pore radius of *33±5Å* (see *Table 3-1* and reference (13)). In addition, the normalized porosity-to-tortuosity ratio, $(\varepsilon/\tau)_{normal}$, corresponding to the aqueous SCI contacting solution *2±1*, is less than half that corresponding to the SDS aqueous contacting solution, *7±1*.

With the above findings in mind, my explanation for the observed dose independence of SCI skin penetration and associated skin barrier perturbation is based on a comparison of the radius of a SCI micelle with the average radius of the skin aqueous pores induced by the aqueous SCI contacting solutions. Specifically, the SCI micelle radius is larger than the average aqueous pore radius, and therefore, the SCI micelles are sterically hindered from penetrating into the SC through these skin aqueous pores.

---

[11] In fact, the skin aqueous pores have a distribution of pore radii (13, 41). The *average* pore radius is the *mean* of this distribution of pore radii. In Chapter 6, the size distribution of skin aqueous pores upon exposure to SDS (1 wt%) and to SDS (1 wt%) + Glycerol (10 wt%) have been modeled using single-parameter exponential and truncated normal distribution functions.

As a result, SCI in micellar form does not contribute to skin penetration and associated skin barrier perturbation.[12] Note that in providing this plausible explanation regarding the skin mildness of SCI, I have implicitly assumed that a surfactant monomer, or a micelle, has to first penetrate into the skin barrier in order to induce skin barrier perturbation, an assumption which has been validated by in vivo studies (1-10, 14-16). Because the concentration of the SCI monomers is approximately constant above the CMC (1 mM) while that of the SCI micelles increases, a natural manifestation of our explanation of the skin mildness of SCI should be a dose independence of the SCI skin penetration (see Section 3.4.4), which should reflect primarily the penetration of SCI in monomeric form, rather than in micellar form, into the skin barrier. I have determined that the SCI skin penetration is indeed dose independent through a ^{14}C-radiolabeled SCI skin assay, and discuss this important finding in the Section 3.4.4.

3.4.4. Verification of the Explanation for the Skin Mildness of SCI Using the SCI Skin Radioactivity Assay

I developed the skin radioactivity assay discussed in Section 3.2.5 to directly quantify the amount of ^{14}C-SCI that can penetrate into the skin barrier from an SCI aqueous contacting solution. Use of this assay allows one to directly measure the contribution of the SCI micelles to SCI skin penetration. The concentrations of SCI in the skin barrier (in wt%) resulting from the exposure of p-FTS to aqueous contacting solutions of SCI (0.2-200 mM) correspond to the triangles in *Figure 3-5*. In *Figure 3-5*, one can clearly see that the SCI concentration in the skin

[12] The CMC of SCI is 1 mM which is much lower than the CMC of SDS (8.7 mM), which is a well-known harsh skin agent. Therefore, at a surfactant concentration above the CMC, SCI has a much smaller concentration of monomers that come in contact with the skin than SDS. Hence, not only does SCI form larger micelles (relative to SDS) that cannot penetrate into the SC, but it also has a lower concentration of monomers contacting the skin (relative to SDS) that can penetrate into the SC and induce skin barrier perturbation.

barrier increases significantly as the SCI concentration in the aqueous contacting solution is increased from 0.2 mM to about 5 mM, which is close to the CMC of SCI (1 mM).

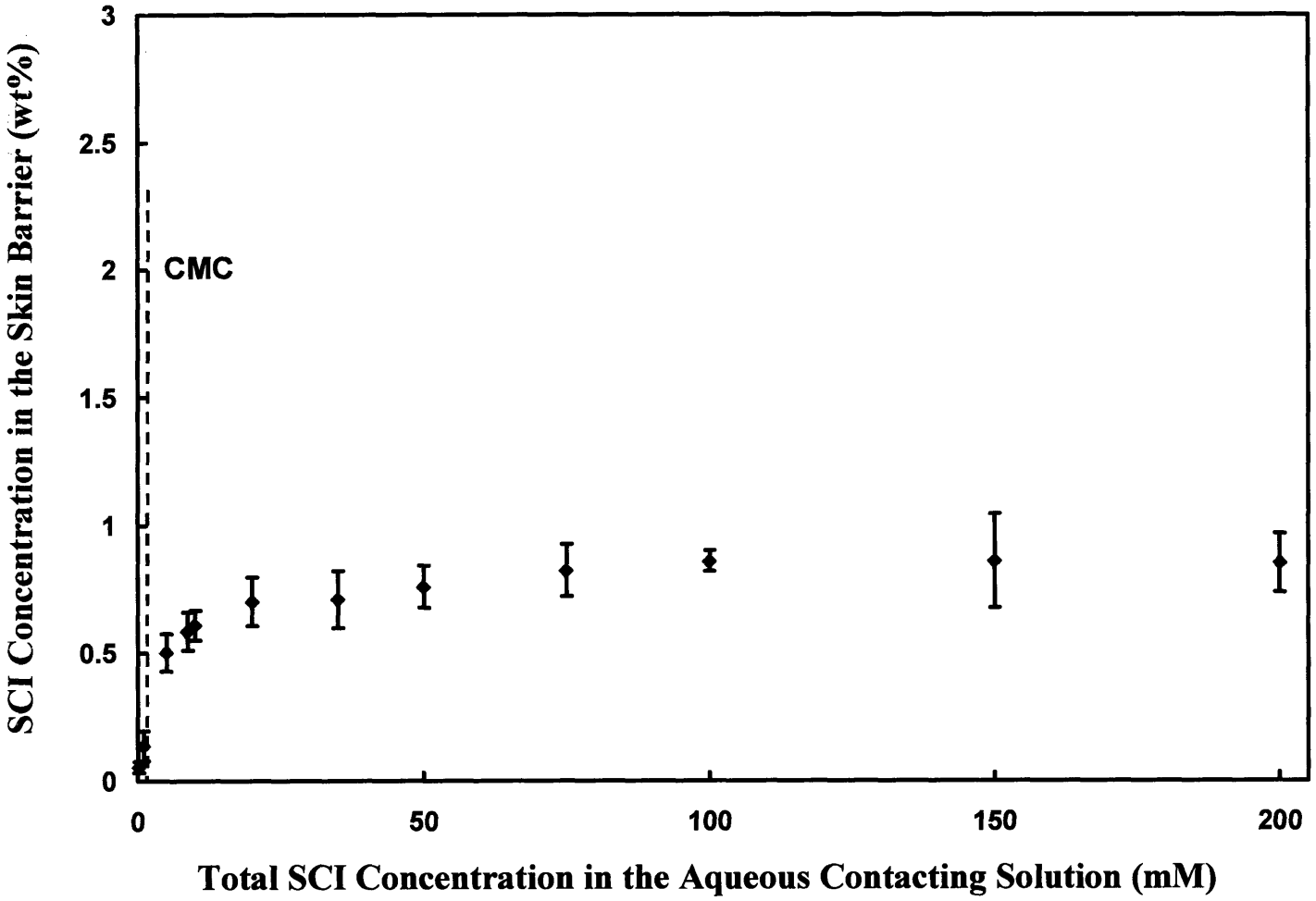

Figure 3-5. Skin penetration of SCI in vitro induced by aqueous contacting solutions of SCI (triangles). The dotted vertical line at an SCI concentration of 1.0 mM denotes the CMC of SCI. The error bars represent standard errors based on 6 p-FTS samples.

However, upon increasing the total SCI concentration in the contacting solution to higher values, 50-200 mM, the concentration of SCI in the skin barrier does not increase significantly. I quantified the relative contributions of the SCI monomers and the SCI micelles to SCI skin penetration by using a multiple linear regression (MLR) analysis of the experimental data presented in *Figure 3-5*. The following relation is applicable and forms the basis of the MLR analysis (please see reference (11) for additional details):

$$C_{skin} = \alpha \cdot C_{mon} + \beta \cdot C_{mic} \tag{6}$$

where C_{skin} is the concentration of SCI in the skin barrier (mmol/g), C_{mon} is the concentration of the SCI monomers in the aqueous contacting solution, and C_{mic} is the concentration of the SCI micelles in the aqueous contacting solution. The value of C_{mon} was set to 1 mM (the CMC of SCI) while the value of C_{mic} was obtained using a mass balance ($C_{SCI,total} - C_{mon}$), where $C_{SCI,total}$ is the total concentration of SCI in the aqueous contacting solution . The regression coefficients, α and β, in Eq.(6), which quantify the contributions of a SCI monomer and a SCI micelle, respectively, to SCI skin penetration, were determined using the MLR analysis. Specifically, I found that: $\alpha = 1.6\times10^{-2}\pm8.4\times10^{-4}$ and $\beta = 6.8\times10^{-5}\pm9.8\times10^{-6}$ (R^2=0.93). Since α is more than two orders-of-magnitude larger than β (α/β=238), this result clearly demonstrates that a SCI monomer, when compared to a SCI micelle, is the predominant species contributing to SCI skin penetration. This, in turn, results in the observed dose independence of SCI skin penetration. Interestingly, a similar MLR analysis performed by Moore et al. (11) for SDS skin penetration showed that the value of the SDS monomer-to-micelle contribution ratio, our α/β, is 3.25, which is much smaller than the SCI monomer-to-micelle contribution ratio of 238.[13] Therefore, this quantitative comparison indicates that unlike a SDS micelle, a SCI micelle does not penetrate

[13] I conduct a similar analysis in Chapter 6 and find that the value of α/β for SDS skin penetration is 4.163, which is close to 3.25 determined by Moore et al. (11).

significantly into the skin, and hence, leads to a dose independent skin penetration in the SCI case. The amount of SCI that penetrates into the skin barrier in vitro from aqueous contacting solutions was found to be approximately ten-fold lower than that of SDS (11, 13), which provides further evidence that the SCI micelles, unlike the SDS micelles (11, 13), do not contribute significantly to skin penetration.

In summary, the results in *Figure 3-5*, as well as the MLR analysis, clearly show that SCI in micellar form does not contribute significantly to SCI skin penetration, which in turn, leads to the observed *dose independence* of SCI skin penetration. This observation is consistent with my explanation of the skin mildness of SCI proposed above.[14] The SCI skin radioactivity results reported here are also consistent with recent studies (1, 42). For example, Ananthapadmanabhan et al. found that SCI binds to human SC to a lower extent than SDS, and also that SCI binding, unlike SDS binding, does not increase above the CMC of SCI (1).

3.5. Conclusions

Using Mannitol transdermal permeability and skin electrical resistivity measurements in the context of a hindered-transport aqueous porous pathway model of the SC, I determined that the average aqueous pore radius resulting from skin exposure to an aqueous SCI contacting solution is *29±5Å*. Using dynamic light scattering measurements, I found that the SCI micelle radius is *33±1Å*. These results provide a plausible explanation for the well-documented skin mildness of SCI. Indeed, since the SCI micelles are larger in size than the average skin aqueous

[14] In fact, Moore et al. have shown that micelle kinetics as well as micelle disintegration upon impinging on the SC and subsequent absorption by the SC do not affect surfactant-skin penetration (11).

pores, they are sterically hindered from penetrating into the SC through the smaller skin aqueous pores.

A natural manifestation of my explanation for the skin mildness of SCI is that the SCI skin penetration should also be dose independent. Using ^{14}C-radiolabeled SCI and in vitro skin radioactivity measurements, I demonstrated that SCI penetrates into the SC in a dose independent manner. Furthermore, through in vitro skin electrical current and Mannitol transdermal permeability measurements, I demonstrated that SCI induces skin barrier perturbation in a dose independent manner. On the other hand, I have observed in previous studies that the harsh skin agent SDS, which is also an anionic surfactant like SCI, penetrates into the SC and induces skin barrier perturbation in a dose dependent manner because the SDS micelle, being smaller in size than the average skin aqueous pores, can penetrate into the SC through these pores (11, 13). Furthermore, the amount of SCI that penetrates into the skin barrier in vitro from an aqueous contacting solution was found to be significantly lower than that of SDS (11, 13), which may be related to earlier in vitro and in vivo observations that SCI is *mild*, while SDS is *harsh*, to the skin barrier (1, 10-17, 23, 42). Finally, an aqueous SCI contacting solution results in a 60% lower porosity-to-tortuosity ratio in vitro than an aqueous SDS contacting solution, which is also consistent with the fact that SCI is known to be *mild* to the skin barrier and is also known to induce low skin barrier perturbation in vivo.

In the next chapter, Chapter 4, I develop an in vitro ranking metric capable of ranking aqueous surfactant/humectant systems based on their perturbation of the skin aqueous pores, and validate the results through in vivo skin barrier measurements.

3.6. References

1. K.P.Ananthapadmanabhan, K.K.Yu, C.L.Meyers, and M.P.Aronson, Binding of surfactants to stratum corneum, *J. Soc. Cosmet. Chem.*, 47:p. 185-200 (1996).
2. D.D.Strube, S.W.Koontz, R.I.Murahata, and R.F.Theiler, The flex wash test: A test method for evaluating the mildness of personal washing products, *J. Soc. Cosmet. Chem.*, 40:p. 297-306 (1989).
3. G.Imokawa, Surfactant mildness, in *Surfactants in Cosmetics*, M.M. Rieger and L.D. Rhein, Eds. (Marcel Dekker Inc, New York, 1997), pp. 427-471.
4. R.Scheuplein, and I.Blank, Permeability of the skin, *Physiol. Rev.*, 51:p. 702-747 (1971).
5. W.Abraham, "Surfactant effects on skin barrier", in *Surfactants in Cosmetics*, M.M.Rieger and L.D.Rhein, Eds. (Marcel Dekker Inc, New York, 1997), pp. 437-487.
6. J.A.Faucher and E.D.Goddard, Interaction of keratinous substrates with sodium lauryl sulfate: I. Sorption, *J. Soc. Cosmet. Chem.*, 29:p. 323-337 (1978).
7. J.A.Faucher and E.D.Goddard, Interaction of keratinous substrates with sodium lauryl sulfate: II. Permeation through stratum corneum, *J. Soc. Cosmet. Chem.*, 29:p. 339-353 (1978).
8. L.D.Rhein and F.A.Simion, "Surfactant interactions with Skin", in *Interfacial Phenomena in Biological Systems*, Surfactant Science Series, Marcel Dekker, New York, 39, pp. 33-49 (1991).
9. K.P.Wilhelm, G.Frietag, and H.H.Wolff, Surfactant induced skin irritation and skin repair. *J. Am. Acad. Dermatol.*, 30:p. 944-949 (1994).

10. T.Agner and J.Serup, Sodium lauryl sulfate for irritant patch testing – A dose-response study using bioengineering methods for determination of skin irritation, *J. Soc. Cosmet. Chem.*, 95:p. 543-547 (1990).

11. P.Moore, S.Puvvada, and D.Blankschtein, Challenging the surfactant monomer skin penetration model: Penetration of sodium dodecyl sulfate micelles into the epidermis, *J. Cosmet. Sci.*, 54:p. 29-46 (2003), and references cited therein.

12. P.Moore, A.Shiloach, S.Puvvada, and D.Blankschtein, Penetration of mixed micelles into the epidermis: Effect of mixing sodium dodecyl sulfate with dodecyl hexa(ethylene oxide), *J. Cosmet. Sci.,* 54:p. 143-159 (2003), and references cited therein.

13. S.Ghosh and D.Blankschtein, The role of sodium dodecyl sulfate (SDS) micelles in inducing skin barrier perturbation in the presence of glycerol, accepted for publication in *J. Cosmet. Sci.(2007)*, and references cited therein.

14. L.D.Rhein, F.A.Simion, R.L.Hill, R.H.Cagan, J.Mattai, and H.I.Maibach, Human cutaneous response to a mixed surfactant system: Role of solution phenomenon in controlling surfactant irritation, *Dermatologica*, 180:p., 18-23 (1990).

15. L.D. Rhein, In vitro interactions: Biochemical and biophysical effects of surfactants on skin, in *Surfactants in Cosmetics*, M.M. Rieger and L.D. Rhein, Eds. (Marcel Dekker Inc, New York, 1997), pp. 397-426.

16. C.H.Lee and H.I.Maibach, Study of cumulative irritant contact dermatitis in man utilizing open application on subclinically irritated skin, *Contact Dermatitis*, 30:p. 271-275 (1994).

17. L.D.Rhein, C.R.Robbins, K.Fernee, and R.Cantore, Surfactant structure effects on swelling of isolated human stratum corneum, *J. Soc. Cosmet. Chem.*, 37:p. 125-139 (1986).

18. A.de la Maza, L.Coderch, O.Lopez, J.Baucells, and J.L.Parra, Permeability changes caused by surfactants in liposomes that model the stratum corneum lipid composition, *J. Am. Oil. Chem. Soc.*, 74:p. 1-8 (1997).

19. C.L.Froebe, F.A.Simion, L.D.Rhein, R.H.Cagan, and A.Kligman, Stratum corneum lipid removal by surfactants: relation to in vivo irritation, *Dermatologica*, 181:p. 277-283 (1990).

20. D.T.Downing, W.Abraham, K.K.Wegner, K.W.Willman, and J.L.Marshall, Partition of sodium dodecyl sulfate into stratum corneum lipid liposomes, *Arch. Dermatol. Res.*, 285:p. 151-157 (1993).

21. J.Vilaplana, J.M.Mascaro, C.Trullas, J.Coll, C.Romaguera, C.Zemba, and C.Pelejero, Human irritant response to different qualities and concentrations of cocoamidopropylbetaines: a possible model of paradoxical irritant response, *Contact Dermatitis*, 26:p. 289-294 (1992).

22. K.P.Wilhelm, M.Samblebe, and C.P.Siegers, Quantitative in vitro assessment of N-alkyl sulphate-induced cytotoxicity in human keratinocytes (HaCaT). Comparison with in vivo human irritation tests, *Br. J. Dermatol*, 130:p. 18-23 (1994).

23. K.P.Wilhelm, A.B.Cua, H.H.Wolff, and H.I.Maibach, Surfactant-induced stratum corneum hydration in vivo: Prediction of the irritation potential of anionic surfactants, *J. Invest. Dermatol.*, 101:p. 310-315 (1993).

24. G.K.Menon and P.M.Elias, Morphologic basis for a pore-pathway in mammalian stratum corneum, *Skin Pharmacol.*, 10:p. 235-246 (1997).

25. P.M.Elias, Lipids and the epidermal permeability barrier, *Arch. Dermatol. Res.*, 270:p. 95-117 (1981).

26. W.M.Deen, Hindered transport of large molecules in liquid-filled pores, *AIChE J.*, 11:p. 1306-1314 (1987).

27. K.D.Peck, A.H. Ghanem, and W.I.Higuchi, Hindered diffusion of polar molecules through and effective pore radii estimates of intact and ethanol treated human epidermal membrane, *Pharm. Res.*, 11:p. 1306-1314 (1994).

28. K.D.Peck, J.Hsu, S.K.Li, A. Ghanem, and W.I.Higuchi, Flux enhancement effects of ionic surfactants upon passive and electroosmotic transdermal transport, *J. Pharm. Sci.*, 87:p. 11-1169 (1998).

29. K.D.Peck, V.Srinivasan, S.K.Li, W.I.Higuchi, and A.Ghanem, Quantitative description of the effect of molecular size upon electroosmotic flux enhancement during iontophoresis for a synthetic membrane and human epidermal membrane, *J. Pharm. Sci.*, 85:p. 781-788 (1996).

30. S.K.Li, W.Suh, H.H.Parikh, A.Ghanem, S.C.Mehta, K.D.Peck, and W.I.Higuchi, Lag time data for characterizing the pore pathway of intact and chemically pretreated human epidermal membrane. *Int. J. Pharm.*, 170:p. 93-108 (1998).

31. H.Tang, S.Mitragotri, D.Blankschtein and R.Langer, Theoretical description of transdermal transport of hydrophilic permeants: Application to low-frequency sonophoresis. *J. Pharm. Sci.*, 90: 545-568 (2001).

32. A.Tezel, A.Sens, and S.Mitragotri, Description of transdermal transport of hydrophilic solutes during low-frequency sonophoresis based on a modified porous pathway model, *J. Pharm. Sci.*, 92:p. 381-393 (2003).

33. S.K.Li, A.H.Ghanem, K.D.Peck, and W.I.Higuchi, Characterization of the transport pathways induced during low to moderate voltage iontophoresis in human epidermal membrane, *J. Pharm. Sci.*, 87:p. 40-48 (1998).

34. J.Kushner, D.Blankschtein, and R.Langer, Experimental demonstration of the existence of highly permeable localized transport regions in low-frequency sonophoresis, *J. Pharm. Sci.*, 93:p. 2733-2745 (2004).

35. A.Einstein, *Investigation on the Theory of Brownian Movement*, New York: Dover, 58, (1956).

36. L.Magid, "Light scattering in micellar systems" in *Dynamic Light Scattering: The Method and Some Applications*, W. Brown, Ed. (Oxford University Press, Oxford, 1993), pp. 554-593.

37. A.Rohde and E.Sackman, Quasieleatic light-scattering studies of micellar sodium dodecyl sulfate solutions at the low concentration limit, *J. Colloid Interface Sci.*, 70:p. 494-505 (1979).

38. R.R.Warner, Y.L.Boissy, N.A.Lilly, M.J.Spears, K.McKillop, J.L.Marshall, and K.J.Stone, Water disrupts stratum corneum lipid lamellae: Damage is similar to surfactants. *J. Invest. Dermatol.*, 113:p. 960-966 (1999).

39. J.L.Zatz and B.Lee, "Skin Penetration enhancement by surfactants", in *Surfactants in Cosmetics*, M.M.Rieger and L.D.Rhein, Eds. (Marcel Dekker Inc, New York, 1997), pp. 501-517.

40. Y.J.Nikas and D.Blankschtein, Complexation of non-ionic polymers and surfactants in dilute aqueous solutions. *Langmuir*, 10:p. 3512-3528 (1994).

41. M.Loden, The simultaneous penetration of water and sodium lauryl sulfate through isolated human skin, *J. Soc. Cosmet. Chem.*, 41:p. 227-233 (1990).

42. K.P.Ananthapadmanabhan, D.J.Moore, K.Subramanyan, M.Misra, and F.Meyer, Cleansing without compromise: The impact of cleansers on the skin barrier and the technology of mild cleansing, *Dermatologic Therapy*, 17:p. 16-25 (2004).

Chapter 4

4. Ranking of Aqueous Surfactant-Humectant Systems Based on an Analysis of *In Vitro* and *In Vivo* Skin Barrier Perturbation Measurements

4.1. Introduction

In Chapters 2 and 3, macroscopic in vitro skin barrier measurements, including average skin electrical resistivity (R) and Mannitol skin (transdermal) permeability (P), were used in the context of a hindered-transport theory, to calculate the average pore radius (r_{pore}) and the porosity-to-tortuosity ratio (ε/τ) of the skin aqueous pores (1-6). Specifically, it was possible to quantify the extent of *in vitro* skin barrier perturbation that an aqueous surfactant/humectant system induces by examining the modifications of r_{pore} and ε/τ relative to an in vitro PBS (Phosphate Buffered Saline) control. The harsh surfactant Sodium Dodecyl Sulfate (SDS) was shown to induce significant skin barrier perturbation in vitro relative to the PBS control, while the humectant Glycerol was shown to preserve the skin barrier in vitro and to mitigate skin barrier perturbation (see Chapter 2 and (7-11, 16-19, 25-30)). It is of practical value to be able to extend these findings to other aqueous surfactant/humectant systems. For example, if a

correlation is observed between the extent of skin barrier perturbation *in vivo* and the modification to the skin aqueous pores that an aqueous surfactant/humectant system induces *in vitro* relative to a control, then this would allow one to *rank* these chemicals based on their ability to perturb the skin aqueous pores *in vitro*.

With the above in mind, a *ranking metric* that combines the characteristics of the skin aqueous pores will be developed (see Section 4.2.6), which can potentially: (i) reduce, or eliminate altogether, several costly and time-consuming operations, such as, human and animal testing and trial-and-error screening, and (ii) simultaneously screen and rank many surfactants and humectants for use in skin-care formulations, thereby significantly speeding up the effort and time required to bring new skin-care formulations to the market. In addition, a suitable ranking metric that uses the skin electrical currents induced in vitro relative to an in vitro PBS control can be combined with corresponding Mannitol skin permeability measurements, in the context of a hindered-transport aqueous porous pathway model. Specifically, the hindered-transport model will allow for the quantification of the modifications of: (i) the average pore radius, and (ii) the pore number density, induced by aqueous surfactant/humectant systems relative to the in vitro PBS control, thereby shedding light on the mechanism of in vitro skin barrier perturbation induced by the aqueous surfactant/humectant system considered (see Section 4.2.6). Knowledge of the mechanism of in vitro skin barrier perturbation induced by aqueous surfactant/humectant systems can be valuable in designing skin-care formulations containing these chemicals that are *mild* to the skin and that minimize, or eliminate altogether, skin barrier perturbation (17-19, 23, 24, 28, 32).

This chapter is devoted to the development of an in vitro ranking metric, using skin electrical current measurements relative to an in vitro PBS control, that is capable of ranking

aqueous surfactant/humectant systems based on their ability to perturb the skin aqueous pores in vitro. In addition, Mannitol skin permeability measurements were conducted that allowed: (i) further in vitro validation of the conclusions reached from the ranking metric study, and (ii) combination, with the skin electrical current measurements conducted as part of the ranking study, in the context of the hindered-transport aqueous porous pathway model, to determine the average pore radius and the pore number density values induced by the aqueous surfactant/humectant systems in vitro. For this purpose, the anionic surfactant SDS and the nonionic surfactant $C_{12}E_6$ (Dodecyl Hexa (Ethylene Oxide)), and the humectants, Propylene Glycol (PG) and Glycerol (G), were selected (see Section 4.2). The enhancements in the average pore radii and pore number densities induced by these two surfactants and two humectants relative to the in vitro PBS control were analyzed to gain mechanistic insight into their skin barrier perturbation/mitigation characteristics.

SDS is known to induce skin erythema (8-11, 17), while $C_{12}E_6$ is known to induce skin dryness when exposed to human skin in vivo (16, 18 19). On the other hand, PG and G are both humectants which are known to preserve the skin barrier, and to maintain the water content of the skin when applied to human skin in vivo (27-31). The in vitro ranking of the two surfactants and the two humectants relative to the in vitro PBS control was compared with various in vivo skin barrier measurements (see below), and the correlation between the in vitro ranking metric analysis and the in vivo skin barrier measurements was investigated (see Sections 4.4.2 and 4.4.3).

The well-accepted in vivo soap chamber test [15] was utilized to carry out the following measurements: (1) Transepidermal water loss (TEWL) to determine the moisture vapor flux over the skin as measured by an evaporimeter, which serves as an excellent quantitative indicator of skin barrier perturbation in vivo (see Section 4.3.1), (2) Visual skin dryness scores determined by an expert grader to clinically assess the extent of skin dryness (see Section 4.3.2), and (3) Skin erythema (redness) determined by the colorimetry scale of a chromameter to assess the extent of clinical irritation symptom (see Section 4.3.3). The results of these measurements are summarized, and compared with the in vitro measurements, in Section 4.4.3. In Section 4.4.4, the results of a comparative study between the in vitro skin barrier mitigation characteristics induced upon adding 10 wt% Glycerol to SDS aqueous contacting solutions, reported in Chapter 2, and the in vivo measurements conducted upon adding 10 wt% Glycerol to a 1 wt% SDS aqueous contacting solution are presented. Finally, the main conclusions of the studies reported in this chapter are presented Section 4.5.

4.2. *In Vitro* Skin Barrier Studies

4.2.1. Materials

Sodium Dodecyl Sulfate (SDS) was purchased from Sigma Chemicals (St. Louis, MO). Analytical-grade Glycerol (G) and Propylene Glycol (PG) were purchased from VWR Chemicals (Cambridge, MA). ^{3}H-radiolabeled Mannitol was purchased from American Radiolabeled Chemicals (St. Louis, MO). Dodecyl Hexa (Ethylene Oxide), $C_{12}E_6$, was purchased from Nikko Chemicals (Tokyo, Japan). All these chemicals were used as received. Water was

[15] The in vivo soap chamber test was conducted by CyberDERM Clinical Studies in Broomall, PA, in collaboration with Neutrogena Corporation, Los Angeles, CA, using a well-accepted and previously published protocol (12, 13, 20-23). See Section 4.3 for additional details.

filtered using a Millipore Academic water filter (Bedford, MA). Phosphate buffered saline (PBS) was prepared using PBS tablets from Sigma Chemicals (St. Louis, MO) and Millipore filtered water, such that a phosphate concentration of 0.01 M along with a NaCl concentration of 0.137 M were obtained at a pH of 7.2.

4.2.2. Preparation of the Solutions

For the in vitro skin barrier studies, the following aqueous solutions were prepared: (i) an anionic surfactant solution – SDS (1 wt%), (ii) a nonionic surfactant solution – $C_{12}E_6$ (1 wt%), (iii) a control solution – Phosphate Buffered Saline (PBS), (iv) a humectant solution – Propylene Glycol (PG) (10 wt%), and (v) a humectant solution – Glycerol (G) (10 wt%).

4.2.3. Preparation of the Skin Samples

Female Yorkshire pigs (40-45kg) were purchased from local farms, and the skin (back) was harvested within one hour after sacrificing the animal. The subcutaneous fat was trimmed off using a razor blade, and the full-thickness pig skin was cut into small pieces (2cm × 2cm) and stored in a –80 °C freezer for up to 2 months. The in vitro experiments involve contacting pig full-thickness skin (p-FTS) with aqueous surfactant-humectant and PBS control solutions (i)-(v) (see Section 4.2.2).

4.2.4. Mannitol Transdermal Permeability Measurements

Vertical Franz diffusion cells (Permegear Inc., Riegelsville, PA) were used for the Mannitol skin permeability measurements (see Chapter 2). All the experiments were performed at room temperature (25°C). The p-FTS samples were mounted in the diffusion cells with the SC facing the donor compartments. Both the donor and the receiver compartments were filled with

PBS, and the p-FTS samples were left to hydrate for 1 hour before the beginning of the experiment to allow the skin initial barrier property to reach steady state (see Chapter 2). At this point, the skin electrical current across the p-FTS sample was measured, and only p-FTS samples with an initial skin current < 3 μA were utilized in the Mannitol skin permeability studies (see Chapter 2). PBS in the donor compartments was then replaced separately with 1.5 ml of aqueous contacting solutions (i)-(v) (see Section 4.2.2), and left in contact with the SC of the p-FTS samples for 5 hours (see Chapter 2). Subsequently, aqueous contacting solutions (i)-(v) were removed and the donor compartments along with the p-FTS samples were rinsed 4 times with 2 ml of PBS to remove any trace chemical left on the skin surface and in the donor compartments. Subsequently, the p-FTS samples in the diffusion cells were exposed to aqueous contacting solutions of ^{3}H-radiolabeled Mannitol in PBS (1–10 μCi/ml) for 24 hours. For additional experimental details, including a discussion of the liquid scintillation counting method used to determine the Mannitol skin permeability, see Chapter 2.

4.2.5. Skin Electrical Current and Resistivity Measurements

During each Mannitol skin permeability experiment, two Ag/AgCl electrodes (E242, In Vivo Metrics, Healdsburg, CA) were placed in the donor and in the receiver compartments to measure the electrical current and the electrical resistivity across the p-FTS samples (see Chapter 2). A 100 mV AC voltage (RMS) at 10 Hz was generated by a signal generator (Hewlett-Packard, Atlanta, GA), and was applied across the two electrodes for 5 s. The electrical current across the skin was measured using an Ammeter (Hewlett-Packard, Atlanta, GA). The electrical resistance of the p-FTS sample was then calculated from Ohm's law (see Chapters 2 and 3). The skin electrical resistivity was obtained by multiplying the actual skin electrical resistance by the skin area (A=1.77 cm^{2}) (see Chapter 2 for additional details). Skin electrical current and

resistivity measurements were carried out before and during the permeation experiments at each predetermined sampling point. For each p-FTS sample, an average skin electrical resistivity was determined over the same time period for which the steady-state Mannitol skin permeability, P, was calculated (see Chapter 2).

4.2.6. Development of an In Vitro Test to Rank Aqueous Surfactant/Humectant Systems

The central objective for developing an in vitro ranking metric is to *rank* aqueous surfactant-humectant contacting solutions (i), (ii), (iv), and (v), relative to the in vitro PBS control (iii), based on the *extent* of their perturbation to the skin aqueous pores. For this purpose, I chose skin electrical current induced by aqueous contacting solutions (i)-(v), relative to the in vitro PBS control (contacting solution iii), as the preferred in vitro ranking test. Specifically, I adopted the following in vitro ranking metric (*RM*):

$$RM = \frac{I_E}{I_C} \tag{1}$$

where E denotes the enhancer (that is, aqueous contacting solutions (i), (ii), (iv), and (v)), C denotes the control (that is, the in vitro PBS control (iii)), I_E denotes the skin electrical current induced by E, and I_C denotes the skin electrical current induced by C. Note that RM in Eq.(1) corresponds to the *enhancement in the skin electrical current.*

The in vitro skin electrical current measurements reported in Chapters 2 and 3 show that these measurements are: (i) extremely sensitive to small changes in the extent of skin barrier perturbation, (ii) highly reproducible, and (iii) simpler to implement, less time consuming, and safer than typical skin permeability measurements which make use of radioactive materials and

involve relatively complex assaying procedures. In addition to benefits (i)-(iii), I will show that the in vitro skin electrical current measurements correlate well with the in vivo skin barrier measurements reported in this chapter (see Section 4.4.3).

As shown in Chapter 2, skin electrical current measurements can also be related to average skin electrical resistivity, R, values, which, in turn, can be combined with Mannitol skin permeability, P, values, in the context of the hindered-transport aqueous porous pathway model (1-5). Specifically, by analyzing Log P as a function of Log R, two important characteristics of the skin aqueous pores can be obtained: (i) the average pore radius, r_{pore}, and (ii) the porosity-to-tortuosity ratio, ε/τ. In order to determine if aqueous contacting solutions (i)-(v) induce skin barrier perturbation by increasing the average pore radius and/or the pore number density (number of pores/unit area) of the aqueous pores in the SC (see Section 4.1), it is important to consider the relationship between r_{pore} and ε/τ. Specifically,

$$\frac{\varepsilon}{\tau} = \frac{(N_P)(\pi r_{pore}^2)}{a_{total}}\left(\frac{1}{\tau}\right) = \left(\frac{N_P}{a_{total}\tau}\right)\pi r_{pore}^2 = \pi\rho r_{pore}^2 \qquad (2)$$

where N_p is the number of aqueous pores contained within a SC cross-sectional area of a_{total}, and ρ is the number of tortuous pores/unit area = $(N_p/a_{total}\tau)$ = pore number density. Interestingly, Eq.(2) shows that ε/τ increases linearly with ρ and quadratically with r_{pore}. Because aqueous contacting solutions (i)-(v) may modify either r_{pore} and/or ρ, an analysis of the ranking metric to obtain mechanistic insight on the extent of perturbation of the skin aqueous pores should incorporate changes in both r_{pore} and ρ. Once r_{pore} and ε/τ are determined using the theoretical analysis involving the Log P and Log R values (see Chapter 2), Eq.(2) can be used to obtain ρ.

The skin permeability (P) of a hydrophilic permeant, such as Mannitol, can be modeled by considering transport of the hydrophilic permeant through the skin aqueous pores (see Chapter 2 and (1-4)). Specifically, this results in the well-known relationship between P and the aqueous pore characteristics, given by (1-6):

$$P = \left(\frac{\varepsilon}{\tau}\right)\left(\frac{D_p^{\infty}}{L}\right)H(\lambda_p) \tag{3}$$

where D_p^{∞} is the permeant (p) infinite-dilution diffusion coefficient, L is the thickness of the SC, and $H(\lambda_p)$ is the hindrance factor experienced by permeant p as it partitions into the SC from the aqueous contacting solution and diffuses across the SC. The hindrance factor, $H(\lambda_p)$, is a nonlinear function of λ_p, where λ_p is the ratio of the permeant radius, r_p, and the average pore radius, r_{pore}, that is, $\lambda_p = r_p/r_{pore}$ (5, 6). By combining Eqs.(2) and (3), it follows that P is a function of both ρ and r_{pore} for a specific hydrophilic permeant, such as Mannitol. Specifically,

$$P = \left(\pi\rho r_{pore}^2\right)\left(\frac{D_p^{\infty}}{L}\right)H(\lambda_p) \tag{4}$$

Because P is inversely proportional to $[RH(\lambda_i)/H(\lambda_p)]$,[16] and R is inversely proportional to the skin electrical current, I, P is directly proportional to $[IH(\lambda_p)/H(\lambda_i)]$ (see Chapter 2 and (1-4), as well as Eq.(5) below). Therefore, the ranking metric adopted here, which corresponds to the enhancement in the skin electrical current, can also be expressed as an enhancement in the Mannitol skin permeability, within the context of the hindered-transport aqueous porous pathway model (1-5). Specifically,

[16] Note that analogous to λ_p, $\lambda_i = r_i/r_{pore}$, where i represents the current-carrying ion (1).

$$RM = \frac{I_E}{I_C} = \frac{\left(P\frac{H(\lambda_i)}{H(\lambda_p)}\right)_E}{\left(P\frac{H(\lambda_i)}{H(\lambda_p)}\right)_C} = \frac{\left(\frac{\varepsilon}{\tau}H(\lambda_i)\right)_E}{\left(\frac{\varepsilon}{\tau}H(\lambda_i)\right)_C} = \frac{\left(\rho r_{pore}^2 H(\lambda_i)\right)_E}{\left(\rho r_{pore}^2 H(\lambda_i)\right)_C} \quad (5)$$

where I have used Eq.(3), and the fact that $(D_p^\infty/L)_E = (D_p^\infty/L)_C$.[17]

It is instructive to consider the following characteristics of the in vitro ranking metric, RM: (1) RM is numerically equal to unity for the in vitro PBS control (iii), and (2) increasing values of RM indicate an increase in the extent of perturbation to the skin aqueous pores, and hence, an increase in the extent of skin barrier perturbation. In addition, it is also worth noting the following implications regarding the ranking metric when analyzed in the context of the hindered-transport aqueous porous pathway model:[18] (i) it scales linearly with the skin permeability (P) of a hydrophilic permeant,[19] (ii) it is a linear function of ρ and a nonlinear function of r_{pore}, and (iii) because it depends on both ρ and r_{pore}, it can shed light on the mechanism of skin barrier perturbation; specifically, one can determine if an aqueous contacting solution induces a high ranking metric value by increasing r_{pore}, ρ, or both. The results of the in vitro ranking metric study are presented in Section 4.4.1, and are compared with in vivo skin barrier measurements in Section 4.4.3.

---

[17] Because D_p^∞/L does not depend on the nature of the aqueous contacting solution, and depends solely on the choice of the permeant (Mannitol in the present case) and the skin model used (p-FTS in the present case), it follows that $(D_p^\infty/L)_E = (D_p^\infty/L)_C$.

[18] It is important to note that RM, which is defined as the enhancement in the skin electrical current induced by E relative to C (see Eq.(1)), is *independent* of the hindered-transport aqueous porous pathway model. However, the hindered-transport aqueous porous pathway model can be used to further analyze the RM to determine r_{pore} and ρ.

[19] Because the skin electrical resistivity (R) scales linearly with P (see Chapter 2 and (25)) and P scales linearly with the ranking metric, the ranking metric also scales linearly with R.

4.3. *In Vivo* Skin Barrier Studies

The in vivo skin barrier studies were carried out by CyberDERM Clinical Studies in Broomall, PA, in collaboration with Neutrogena Corporation, Los Angeles, CA. The objective of this study was to conduct quantitative in vivo skin barrier perturbation measurements upon contacting volar forearm skin test sites of human volunteers with aqueous solutions (i), (ii), (iv), and (v) (see Section 4.2.2). The control for these in vivo measurements was a skin test site that was not occluded and that was not exposed to aqueous contacting solutions (i)-(v), and therefore, had no in vivo reaction induced by aqueous contacting solutions (i)-(v). This control will be referred to hereafter as the *in vivo control* to differentiate it from the in vitro PBS control (iii). Note that this in vivo control was adopted because studies have shown that natural hydration of the skin in vivo can be mimicked in vitro by contacting skin with a PBS solution that has a pH = 7-7.4 (the in vitro control, see Section 4.2.2), which is similar to the in vivo pH of the hydrated SC (8-12). The *in vivo* skin barrier perturbation studies were carried out using a modified soap chamber test (7, 12, 13). The modified soap chamber test involved application of patches containing aqueous contacting solutions (i), (ii), (iv), and (v) to skin test sites on the volar forearms of 96 female volunteers (4 groups of 24). The volunteers were interviewed to verify that they had no known allergies to soaps or fragrances, and that they were not using any medications that could have interfered with the results of the study. In addition, the transepidermal water loss rate (TEWL), discussed in Section 4.3.1, for these volunteers was less than 10 g/m^2hr at the beginning of the study.[20] Following the appropriate selection of the volunteers, the extent of in vivo skin barrier perturbation on a volar forearm skin test site was

[20] Note that the equivalent *in vitro* selection criterion used was a skin current < 3 μA at the beginning of the study (see Section 4.2.5 and Chapter 2).

evaluated using various in vivo measurements (see Sections 4.3.1-4.3.3) on Day 1 (prior to treatment). Subsequently, the patch containing one of aqueous contacting solutions (i), (ii), (iv), and (v) was applied to the skin test site for 5 hours. After approximately 18-20 hours (on Day 2), the skin test site was re-evaluated, according to the in vivo measurements discussed in Sections 4.3.1-4.3.3. Some of the skin test sites were not exposed to the patches, and were left non-occluded to serve as the in vivo control. The in vivo measurements will be reported as deviations from the baseline measurements (see Section 4.4.2), which include initial measurements prior to exposure of a test site to a contacting test formulation.

4.3.1. Measurement of Transepidermal Water Loss Using an Evaporimeter

Transepidermal water loss (TEWL) measurements provide a noninvasive instrumental assessment of the skin barrier function in vivo. Specifically, skin barrier perturbation may lead to a disruption of the intercellular lipid bilayers in the SC, thereby resulting in elevated water loss rates. Such elevated water loss rates can, in turn, lead to the skin becoming dry and chapped, thereby enhancing skin dryness (15-19).

The TEWL measurements were made using an evaporimeter (Broomall, PA) with probes manufactured by Cortex Technology (Hadsund, Denmark) and available in the US through CyberDERM, Inc. (Broomall, PA). This instrument is based on the vapor pressure gradient estimation method as designed by Nilsson and initially utilized by the Servo Med Evaporimeter (20). The probes contain two sensors that measure the temperature and relative humidity at two fixed points along the axis normal to the skin surface. This arrangement is such that the device can electronically derive a value that corresponds to evaporative water loss from the skin surface expressed in g/m^2hr. Additional details on the TEWL measurements using an evaporimeter can be found in (21 and 22).

The TEWL measurements were conducted following a 15-30 minute acclimation period in a controlled environment with the relative humidity maintained at less than 50% and the temperature maintained at $21\pm1^{\circ}C$. At baseline (that is, with no exposure to a contacting test formulation), TEWL measurements were conducted for each of the skin test sites. Any individuals with TEWL values outside the normal range (>10 g/m^2hr) were excluded at this time. The test formulations were then applied to the test sites under occlusive soap chambers. On Day 2 (approximately 18-20 hours after patch removal), TEWL measurements were conducted for each of the skin test sites as described above.

4.3.2. Evaluation of Visual Skin Dryness by an Expert Grader

The visual skin dryness on the volar forearm test sites of each candidate were evaluated by an expert grader using the grading scale described in Table 4-1. Intermediate grades were allowed so that finer distinctions could be made. To conduct the study in an objective manner with no biases, the expert grader was not made aware of the contents of the patches containing aqueous contacting solutions (i), (ii), (iv), and (v). One should note that the range [0-2] contained all the visual skin dryness scores (see *Table 4-1* and Section 4.4.2). Although these scores correspond to the *mild* range, the expert grader was nevertheless able to effectively discriminate between the observed low levels of visual skin dryness.

Table 4-1. Expert grader score system used to determine the visual skin dryness as part of the in vivo soap chamber skin barrier measurements.

Grade	Description
0	None
2	Slight flaking/uplifting of flakes (patchy and/or powdered appearance)
4	Moderate flaking/uplifting flakes (uniform) and/or slight scaling
6	Severe flaking/scaling, uplifting of scales and/or slight fissuring
8	Severe scaling/uplifting scales; with severe fissuring/cracking

4.3.3. Measurement of Skin Erythema Using a Chromameter

Skin erythema was measured instrumentally by a Minolta CR-200 Chromameter that is based on a standardized reflectance technique using a tristimulus system. The tristimulus system makes use of color reading values on three independent axes: (i) L* axis, reflecting the tone of lightness/darkness, with positive values indicating lightness and negative values indicating darkness, (ii) a* red/green axis, reflecting the extent of redness/greenness, with positive values indicating a reddish tinge and negative values indicating a greenish tinge, and (iii) b* blue/yellow axis, reflecting the extent of blueness/yellowness, with positive values indicating a bluish tinge and negative values indicating a yellowish tinge. Specifically, the color reading values were translated into the L*a*b* coordinates whose spacing correlates closely with color changes perceived by the human eye. For the evaluation of skin erythema using a chromameter, only values along the a* red/green axis that can capture the extent of redness (erythema) of the skin were considered. Sets of three a* readings from each of the volar forearm test sites were taken on Day 1 (prior to exposure, which served as the baseline), as well as on Day 2 (approximately 18-20 hours after patch removal), and the average a* value was calculated for each site at each time point. A positive a* value along the red/green axis, relative to the baseline measurements, indicates that the patch containing the aqueous contacting solution has induced skin redness (erythema) (13). Additional details can be found in (13 and 14).

4.4. Results and Discussion

4.4.1. Results of the In Vitro Skin Barrier Measurements in the Context of a Ranking Metric

The average skin electrical currents induced by aqueous contacting solutions (i)-(v) are reported in *Figure 4-1*. It is important to note that the measurement of skin electrical currents *in vivo* is different from the measurement of skin electrical currents *in vitro*. The *in vivo* skin electrical current (or conductance) measurement is carried out on dry skin, with a low value indicating less hydrated skin that displays a greater extent of skin barrier perturbation (15). On the other hand, the *in vitro* skin electrical current measurement is performed on skin in contact with a PBS solution (see Section 4.2.5 and Chapter 2). Consequently, a high skin electrical current in vitro indicates that the skin barrier has been compromised because ions can traverse the barrier more freely (see Chapter 2 and (15, 24)).

The skin electrical currents induced by aqueous surfactant solutions (i) (1 wt% SDS) and (ii) (1 wt% $C_{12}E_6$) are significantly higher than those induced by the in vitro PBS control solution (iii) and by the aqueous humectant solutions (iv) (10 wt% PG) and (v) (10 wt% G). Clearly, and perhaps as expected, these results indicate that surfactants induce the greatest extent of perturbation to the skin aqueous pores through which ions can cross the skin barrier, thereby resulting in the largest observed skin electrical current values.[21] In addition, aqueous contacting solution (v) (10 wt% G) induces a lower skin electrical current than aqueous contacting solution

[21] Note that 1 wt% SDS induces a larger skin electrical current in vitro, and consequently, a greater extent of perturbation to the skin aqueous pores in vitro than that induced by 1 wt% $C_{12}E_6$ in vitro. This finding is consistent with SDS inducing a greater extent of erythema than $C_{12}E_6$, although $C_{12}E_6$ does induce skin dryness (see Section 4.4.2 and (16-19)).

(iv) (10 wt% PG).[22] This is consistent with the observation that G is able to diffuse into the SC, increasing skin hydration and relieving clinical signs of erythema and skin-dryness, more readily than PG and the in vitro PBS control (iii) (see Chapter 2 and (25-30)).

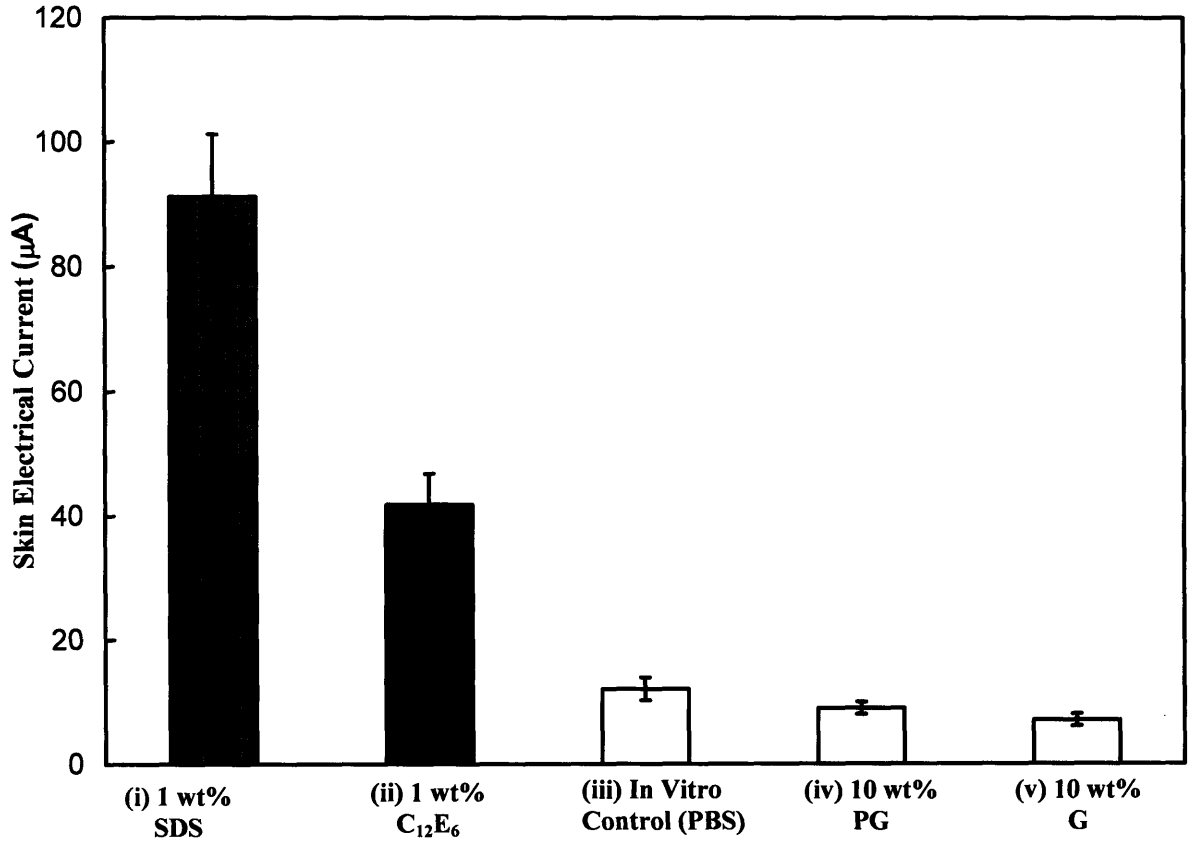

Figure 4-1. Skin electrical currents induced by aqueous solutions (i)-(v) upon contacting p-FTS in vitro in diffusion cells. The error bars represent standard errors based on 6 p-FTS samples.

More specifically, the following effects of Glycerol on the skin barrier have been reported in the literature: (i) Glycerol affects the crystalline arrangement of the intercellular lipid

[22] A student-t test with a significance ($p<0.05$) indicates that each of the bars in *Figure 4-1* is statistically different from the other bars.

bilayers, thereby enhancing SC barrier function and decreasing SC water permeability (29), (ii) Glycerol increases the rate of corneocyte loss from the upper layers of the SC, through a keratolytical effect on desmosome degradation, thereby reducing scaliness of dry skin and maintaining SC barrier (28), and (iii) Glycerol can penetrate into the SC, and, due to its high hygroscopic property, is able to bind water and thus reduce water evaporation (25).

The Mannitol skin permeability values induced by aqueous contacting solutions (i)-(v) are reported in *Figure 4-2*. As can be seen, aqueous contacting solution (i) (1 wt% SDS) induces the largest Mannitol skin permeability in vitro. Because the 1 wt% aqueous SDS contacting solution (i) induces the largest perturbation to the skin aqueous pores relative to the other aqueous contacting solutions ((ii)-(v)), the Mannitol skin permeability values are the largest for SDS. This result is consistent with those of the skin electrical current measurements (see above). In addition, the 1 wt% $C_{12}E_6$ aqueous contacting solution (ii) induces a significantly larger Mannitol skin permeability relative to the in vitro control (iii) and also relative to the aqueous humectant solutions (iv) and (v). This result is consistent with those of the in vivo skin barrier measurements which show that a 1 wt% $C_{12}E_6$ aqueous contacting solution induces a larger extent of erythema and skin dryness than a 10 wt% PG and a 10 wt% G aqueous contacting solution (see Section 4.4.2). It is important to note that aqueous contacting solution (v) (10 wt% G) induces the smallest extent of perturbation to the skin aqueous pores relative to the other aqueous contacting solutions (i)-(iv), as reflected in both the in vitro skin electrical current and the Mannitol skin permeability measurements (see *Figures 4-1* and *4-2*). This finding is consistent with the in vivo skin barrier measurements which show that Glycerol is indeed the mildest to the skin barrier (see Section 4.3).[23]

[23] A student-t test with a significance ($p<0.05$) indicates that each of the bars in *Figure 4-2* is statistically different from the other bars.

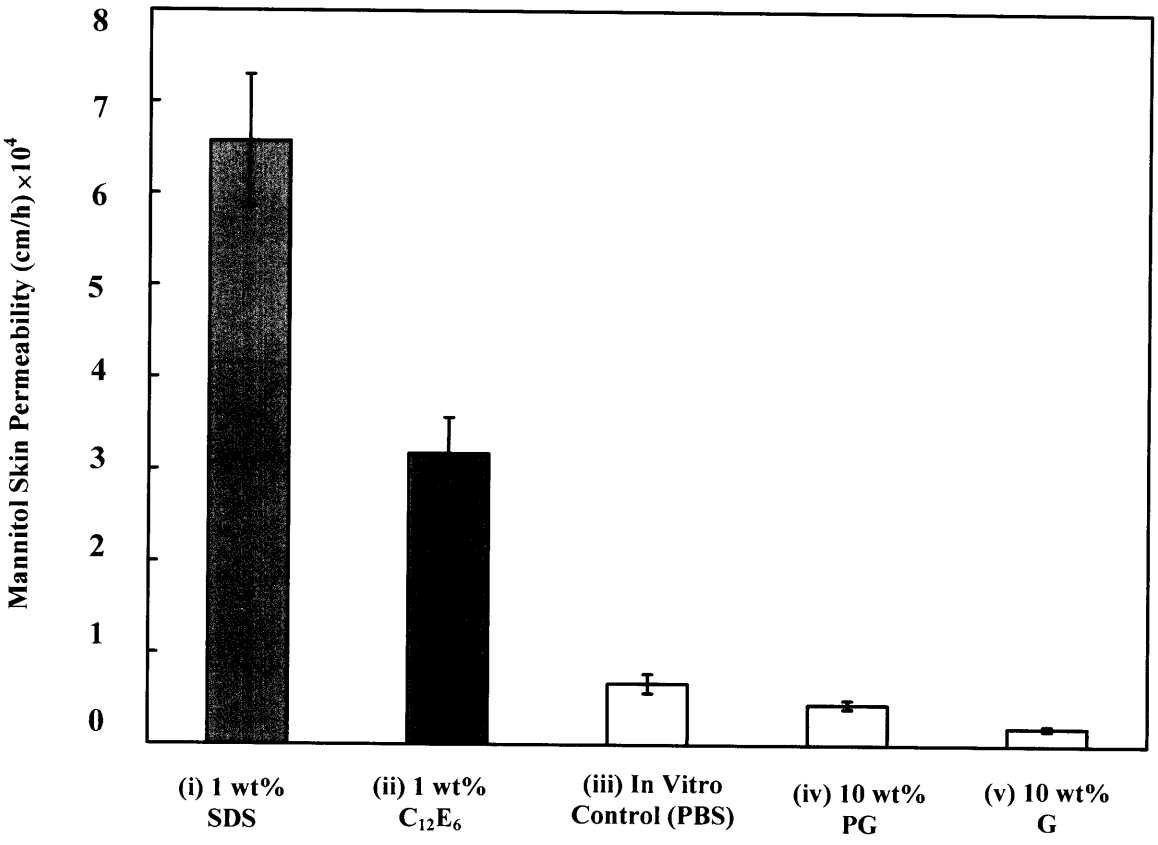

Figure 4-2. Mannitol skin permeability induced by aqueous solutions (i)-(v) upon contacting p-FTS in vitro in diffusion cells. The error bars represent standard errors based on 6 p-FTS samples.

The results of the in vitro ranking metric, RM, corresponding to the enhancement in the skin electrical current values relative to the in vitro control (iii), are reported in *Table 4-2*. The skin electrical current values were converted to skin electrical resistivity values according to the procedure described in Section 4.2.5, and detailed in Chapter 2. The Mannitol skin permeability values, P, and the skin electrical resistivity values, R, were then analyzed in the context of the theoretical model presented in Section 4.2.6 to obtain the average pore radius (r_{pore}) and the pore number density (ρ), which are reported in *Table 4-2*.

Table 4-2. Ranking Metric (RM) values, permeability enhancements, average pore radii, and pore number density enhancements induced by aqueous solutions (i)-(v) upon contacting p-FTS in vitro in diffusion cells. Note that the error bars represent standard errors based on 6 p-FTS samples. Note that 'E' indicates enhancer (aqueous contacting solutions (i), (ii), (iv), and (v)) and 'C' indicates the in vitro PBS control (iii).

Type of Aqueous Contacting Solution	*Ranking Metric RM (= I_E / I_C)*	*Permeability Enhancement (= P_E / P_C)*	*Average Pore Radius, r_{pore} (Å)*	*Pore Number Density Enhancement (= ρ_E / ρ_C)*
(i) 1 wt% SDS	7.6±1.0	9.8±2.0	33±5	2.6±1.0
(ii) 1 wt% $C_{12}E_6$	3.5±1.0	4.7±1.0	38±3	0.7±0.5
(iii) PBS Control	1.0	1.0	20±3	1.0
(iv) 10 wt% PG	0.8±0.2	0.7±0.2	18±2	0.9±0.3
(v) 10 wt% G	0.6±0.1	0.3±0.1	11±4	1.7±0.8

Recall that Eq.(1) indicates that if the RM value corresponding to an aqueous contacting solution is less than one, then that aqueous contacting solution induces a lower extent of skin barrier perturbation relative to the in vitro PBS control (iii). Conversely, if the RM value corresponding to an aqueous contacting solution is greater than one, then that aqueous contacting solution induces a larger extent of skin barrier perturbation relative to the in vitro PBS control (iii). An examination of *Table 4-2* reveals that aqueous humectant contacting solutions (iv) and (v) induce a lower extent of skin barrier perturbation because their RM values are both less than one, while aqueous surfactant contacting solutions (i) and (ii) induce a larger extent of skin barrier perturbation because their RM values are both greater than one. In addition, *Table 4-2* reveals the following order of ranking for aqueous contacting solutions (i)-(v) (from the *harshest* to the *mildest*): (i) (1 wt% SDS) > (ii) (1 wt% $C_{12}E_6$) > (iii) (in vitro PBS control) > (iv) (10 wt% PG) > (v) (10 wt% G).

It is important to note that the ranking of the permeability enhancement, P_E/P_C (see the third column in *Table 4-2*) follows the order of ranking obtained using the in vitro ranking metric (RM), which corresponds to the skin electrical current enhancement, I_E/I_C. This result indicates a strong correlation between skin electrical current and Mannitol skin permeability measurements in vitro.

Table 4-2 also reveals that 1 wt% $C_{12}E_6$ (aqueous contacting solution (ii)) induces the largest average pore radius, r_{pore}, value when compared to aqueous contacting solutions (i)-(v). Nevertheless, 1 wt% $C_{12}E_6$ ranks below 1 wt% SDS in terms of skin barrier perturbation, as reflected in both the RM and P_E/P_C values in *Table 4-2*. This reflects the fact that 1 wt% SDS induces a much larger ρ_E/ρ_C value than that induced by 1 wt% $C_{12}E_6$, which more than offsets the larger r_{pore} value induced by 1 wt% $C_{12}E_6$. In addition, *Table 4-2* reveals that the ranking metric (RM) value corresponding to 1 wt% $C_{12}E_6$ (aqueous contacting solution (ii)) is significantly larger than the RM values corresponding to the in vitro PBS control (iii) and to the aqueous humectant contacting solutions (iv) and (v).

Transmission electron microscopy studies (16, 19) have provided evidence that nonionic surfactants like $C_{12}E_6$ can disorder, and at times, disrupt the ordered intercellular lipid bilayers in the SC. The disordering of the lipid bilayers of the SC can in turn result in a compromised skin barrier, and may also result in skin dryness (8-11, 16-20). Another interesting observation from *Table 4-2* is that 10 wt% PG (aqueous contacting solution (iv)) induces a smaller ρ_E/ρ_C value, yet a larger RM value compared to 10 wt% G (aqueous contacting solution (v)). This result reflects the fact that 10 wt% PG induces a significantly larger r_{pore} value relative to 10 wt% G, which more than offsets the smaller ρ_E/ρ_C value that it induces relative to 10 wt% G. There is

evidence provided by the in vivo measurements reported in Section 4.4.2, as well as by other researchers (25, 27, 28), that G, because of its superior hygroscopic character, can better modulate water fluxes in the SC relative to PG, and therefore, can preserve the skin barrier more effectively than PG. It is important to note that the key measure of in vitro skin barrier perturbation is RM, which ranks aqueous contacting solutions (i)-(v) appropriately. The other, model dependent variables, such as, r_{pore} and ρ_E/ρ_C, provide additional information, thereby shedding light on the nature of the aqueous pores induced in the SC upon contacting p-FTS in vitro with aqueous contacting solutions (i)-(v).

4.4.2. Results of the In Vivo Skin Barrier Measurements

Transepidermal water loss (TEWL) values, determined using an evaporimeter as described in Section 4.3.1, are reported in *Figure 4-3*. In this figure, the height of each bar corresponds to the average TEWL value, which is measured as a deviation from the baseline, as explained in Section 4.3.1. Recall that TEWL is a measure of how easily water passes through the skin. Therefore, skin whose barrier has been compromised should exhibit a higher TEWL value (8, 9).

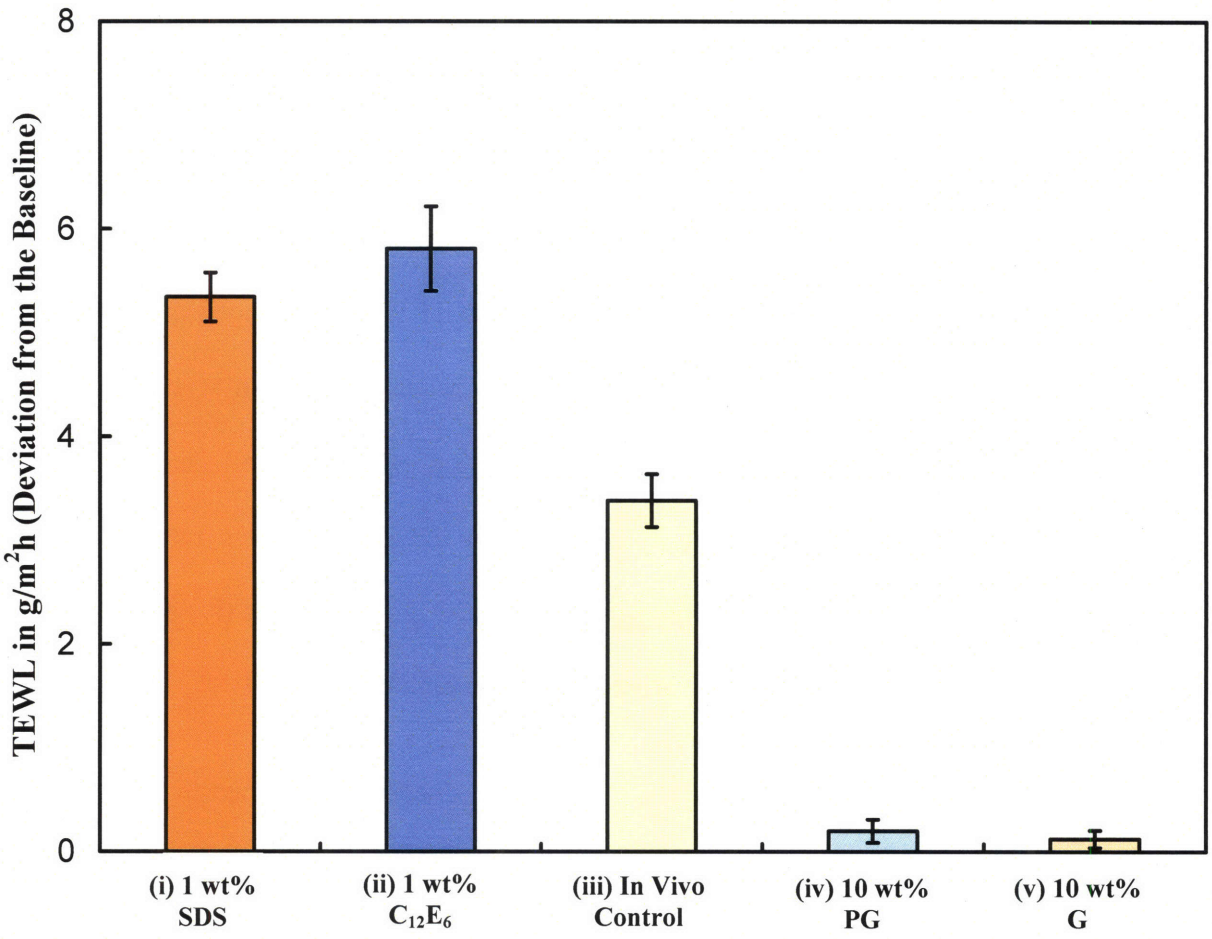

Figure 4-3. Transepidermal Water Loss (TEWL) values, with the error bars corresponding to standard errors, that were measured using an evaporimeter upon contacting human skin in vivo with aqueous contacting solutions (i), (ii), (iv), (v), and for the in vivo control (iii).

The orange and blue bars in *Figure 4-3,* which correspond to the two aqueous surfactant contacting solutions ((i) and (ii)), are significantly higher than those corresponding to the in vivo control (iii), and to the two aqueous humectant contacting solutions ((iv) and (v)) (student-t test, $p<0.05$). These results indicate that aqueous surfactant contacting solutions (i) and (ii) induce a significantly larger extent of skin barrier perturbation, as determined by TEWL, relative to the in vivo control (iii), and to the two aqueous humectant contacting solutions (iv) and (v). In addition, a student t-test conducted at a significance of ($p<0.05$) indicates: (1) no significant difference

between the TEWL values corresponding to the two humectant aqueous contacting solutions (iv) and (v), (2) no significant difference between the TEWL values corresponding to the two surfactant aqueous contacting solutions (i) and (ii), and (3) a statistically significant difference between the TEWL values corresponding to the two surfactant aqueous contacting solutions (i) and (ii) relative to the in vivo control (iii), and between the TEWL values corresponding to the two humectant aqueous contacting solutions (iv) and (v) relative to the in vivo control (iii). These results indicate that aqueous humectant contacting solutions (iv) and (v) induce statistically lower skin barrier perturbation, as quantified by the TEWL values, relative to the in vivo control (iii). On the other hand, aqueous contacting surfactant solutions (iv) and (v) induce statistically higher skin barrier perturbation relative to the in vivo control (iii).

Visual skin dryness scores, determined by an expert grader as described in Section 4.3.2, are reported in *Figure 4-4*. In this figure, the height of each bar corresponds to the average visual skin dryness score, which is measured as a deviation from the baseline, as discussed in Section 4.3.2. The orange and blue bars in *Figure 4-4*, which correspond to the two aqueous surfactant contacting solutions ((i) and (ii)), are significantly higher than those corresponding to the in vivo control (iii) [24] and to the two aqueous humectant contacting solutions (iv) and (v).

These results indicate that aqueous surfactant contacting solutions (i) and (ii) induce a significantly larger extent of skin dryness relative to the in vivo control (iii), and to the two aqueous humectant contacting solutions (iv) and (v), as determined by an expert grader. A student-t test did not indicate any significant difference ($p>0.05$) between the visual skin dryness

[24] Note that the control for the in vivo skin barrier measurements is a skin test site exhibiting natural skin hydration, that is not occluded and is not exposed to aqueous contacting solutions (i), (ii), (iv), and (v), while the control for the in vitro skin barrier measurements is a p-FTS sample that is exposed to PBS. The reason why the in vitro PBS control can be compared to the in vivo non-exposed, non-occluded control was discussed in Section 4.3.

scores corresponding to the in vivo control (iii), and to the two aqueous humectant contacting solutions (iv) and (v).

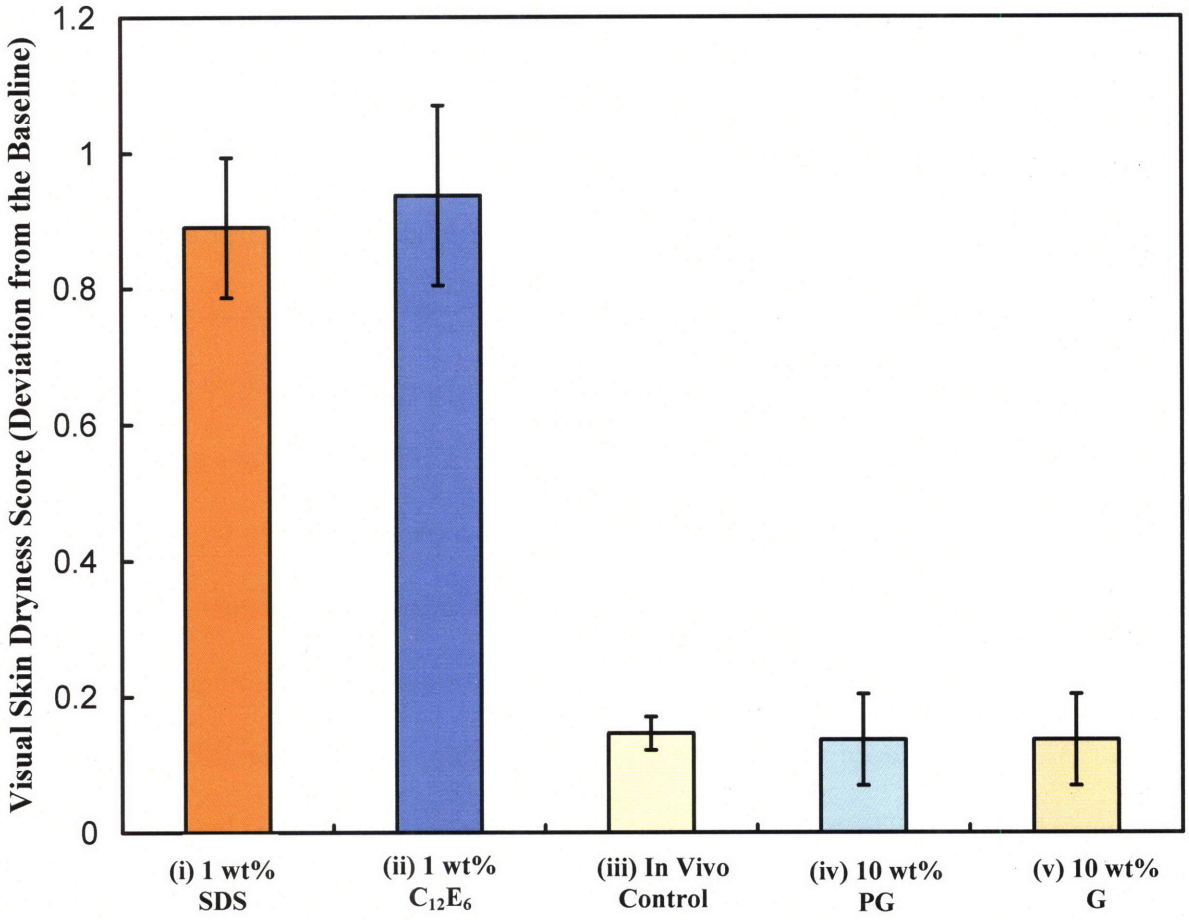

Figure 4-4. Visual skin dryness scores, with the error bars corresponding to standard errors, which were determined by an expert grader upon contacting human skin in vivo with aqueous contacting solutions (i), (ii), (iv), (v), and for the in vivo control (iii).

This result indicates that the expert grader could not discriminate skin dryness visually between the two aqueous humectant solutions (iv) and (v) relative to the in vivo control. In addition, no significant differences were noted ($p>0.05$, student-t test) between the visual skin dryness scores corresponding to the two aqueous surfactant solutions (i) and (ii). One should

note that in comparing results from the TEWL measurements and the visual skin dryness scores, the TEWL measurements more closely resemble the in vitro skin barrier perturbation measurements (skin electrical current and Mannitol skin permeability) (see *Figures 4-1, 4-2, 4-3, and 4-4*) (12-15).

In addition, an instrumental measurement like TEWL allows for finer discrimination between the effects of aqueous humectant solutions (iv) and (v), and the in vivo control, relative to the visual skin dryness scores determined by an expert grader. Indeed, the expert grader was unable to discriminate between the effects of aqueous humectant solutions (iv) and (v), and the in vivo control (iii) (see *Figure 4-4*). Both the TEWL measurements and the visual skin dryness scores indicate that the aqueous surfactant solution containing 1 wt% $C_{12}E_6$ induces significant skin dryness relative to the in vivo control and to the aqueous humectant solutions (iv) and (v). This finding is consistent with in vivo studies that have shown that although nonionic surfactants like $C_{12}E_6$ do not induce significant erythema (skin redness), relative to SDS, they can be drying to the skin (16-19). This reflects the fact that nonionic surfactants like $C_{12}E_6$ can interact with the intercellular lipid bilayers of the SC, disorder them, thereby increasing water loss from the skin, which in turn, results in skin dryness.

Skin erythema scores, determined using a chromameter as described in Section 4.3.3, are reported in *Figure 4-5*. In this figure, the height of each bar corresponds to the average skin erythema score, which is measured as a deviation from the baseline (see Section 4.3.3). Note that the orange bar in *Figure 4-5*, which corresponds to aqueous surfactant contacting solution (i) containing 1 wt% SDS, is above the chromameter reading of zero, which indicates that SDS is indeed *harsh* to the skin and induces skin erythema (redness) relative to the baseline measurement (8-11, 16-19, 24, 32). On the other hand, the blue bar in *Figure 4-5*, which

corresponds to aqueous surfactant contacting solution (ii) containing 1 wt% $C_{12}E_6$, is not statistically different ($p>0.05$) from a chromameter reading of zero, which indicates that $C_{12}E_6$, is indeed *mild* to the skin and does not induce skin erythema (redness) relative to the baseline measurement (16-19).[25]

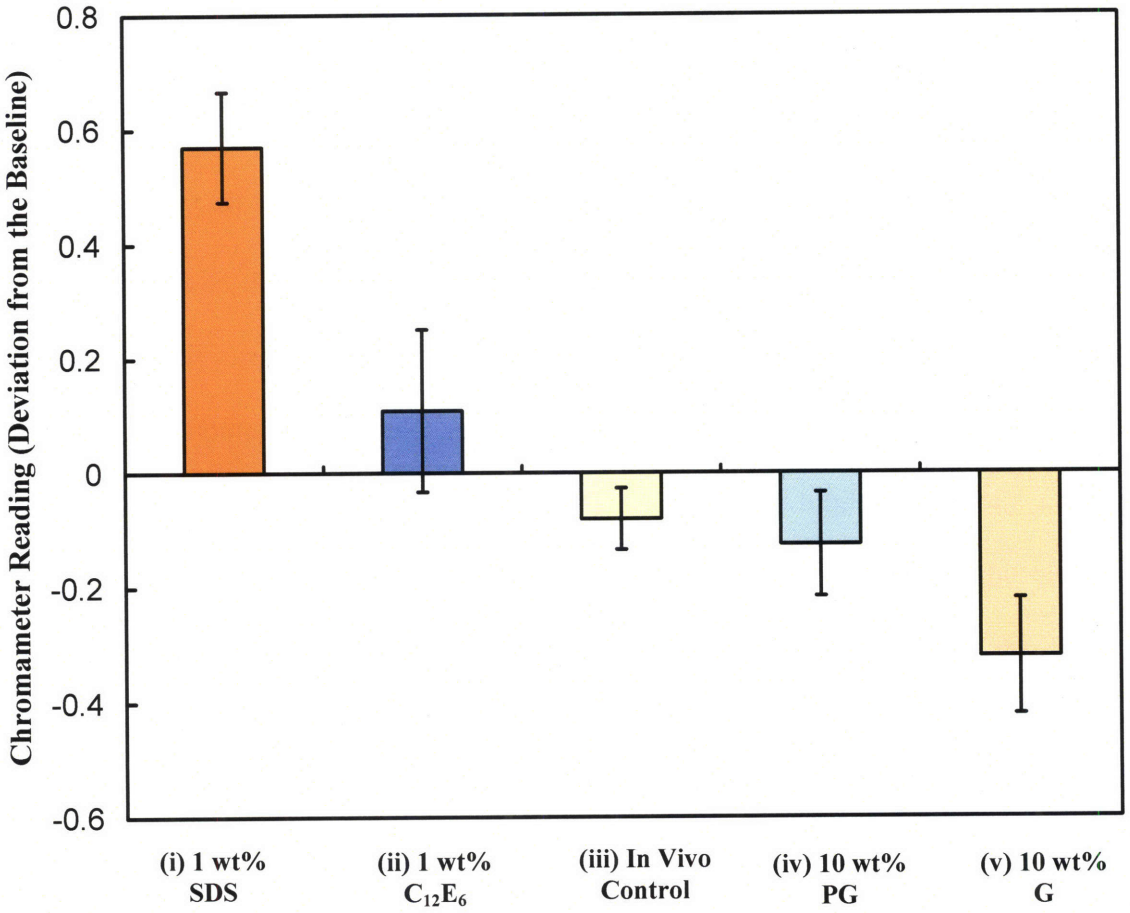

Figure 4-5. Skin erythema scores, with the error bars corresponding to standard errors, that were measured using a Minolta chromameter upon contacting human skin in vivo with aqueous contacting solutions (i), (ii), (iv), (v), and for the in vivo control (iii).

[25] It is important to note that a *mild* surfactant is defined in the skin-care literature as one which does not induce erythema (skin redness) (16-19). On the other hand, a *harsh* surfactant is defined as one which induces erythema (8-11, 16-19). It is also important to keep in mind that a *mild* surfactant such as $C_{12}E_6$ induces skin barrier perturbation because it induces skin dryness by disordering intercellular lipid bilayers in the SC (see the in vivo TEWL measurements in *Figure 4-3* and the visual skin dryness scores in *Figure 4-4*).

In fact, a student-t test did indicate a significant difference ($p<0.05$) between the skin erythema (redness) chromameter reading corresponding to aqueous contacting solution (i) (1 wt% SDS) and that corresponding to aqueous contacting solution (ii) (1 wt% $C_{12}E_6$). One should stress that the TEWL measurements and the visual skin dryness scores determine the extent of intercellular lipid bilayer perturbation in the SC, while the chromameter measurements of erythema (skin redness) determine the extent of denaturing of the keratins in the corneocyte/keratinocyte domains of the SC and the VE (viable epidermis), which leads to an increase in the cutaneous blood flow and associated skin redness (8-11, 14-17, 19-24, 32). Therefore, the results in *Figure 4-5* indicate that SDS induces a larger extent of erythema (skin redness) relative to $C_{12}E_6$, because SDS can interact strongly with the keratins of the corneocytes and the keratinocytes, relative to $C_{12}E_6$. As a result, because SDS can interact with both the keratins and the intercellular lipid bilayers in the SC, while $C_{12}E_6$ can interact only with the intercellular lipid bilayers in the SC, SDS can induce a larger extent of skin barrier perturbation relative to $C_{12}E_6$ (8-11, 16-20, 24). The in vitro skin barrier measurements discussed in Section 4.4.1 corroborate this finding.

In *Figure 4-5*, the bars corresponding to the in vivo control (iii) and to the two aqueous humectant contacting solutions (iv) and (v) are below the chromameter reading of zero, which indicates that no skin erythema (redness) was observed in these three cases. In addition, no statistical difference ($p>0.05$) was observed between the chromameter reading values induced by the in vivo control (iii) and aqueous humectant contacting solution (iv) containing 10 wt% PG. However, a statistically significant difference ($p<0.05$) was observed between the chromameter reading values induced by the in vivo control (iii) and aqueous humectant contacting solution (v) containing 10 wt% G. These results indicate that Glycerol has a stronger beneficial impact on the

skin barrier relative to Propylene Glycol, which is consistent with the in vitro ranking metric results discussed in Section 4.4.1 (25-29, 31).

4.4.3. Relationship Between the In Vitro and In Vivo Skin Barrier Perturbations Induced by Aqueous Surfactant-Humectant Systems

The in vitro ranking metric (RM) analysis and the Mannitol skin permeability measurements indicate that the two surfactant aqueous contacting solutions ((i) and (ii)) induce a significantly larger extent of skin barrier perturbation relative to the in vitro PBS control (iii), and relative to the two humectant aqueous contacting solutions ((iv) and (v)). The in vivo TEWL measurements, the visual skin dryness scores, and the chromameter measurements of in vivo skin erythema (redness) are consistent with the in vitro results (see *Figures 4-3, 4-4, and 4-5*). The in vitro ranking metric analysis also predicts that aqueous contacting solution (i) containing 1 wt% SDS induces the largest extent of skin barrier perturbation in vitro. Conversely, aqueous contacting solution (v) containing 10 wt% G was predicted to induce the smallest extent of skin barrier perturbation in vitro. A similar result was obtained from the chromameter measurements of in vivo skin erythema (redness) (see *Figure 4-5*). Note that the TEWL values (see *Figure 4-3*) and the visual skin dryness scores (see *Figure 4-4*) corresponding to aqueous contacting solution (ii) (1 wt% $C_{12}E_6$) were found not to be statistically different ($p>0.05$) from those corresponding to aqueous contacting solution (i) (1 wt% SDS). In addition, the in vitro RM analysis and the Mannitol skin permeability measurements indicate that aqueous contacting solution (v) containing 10 wt% G induces a smaller extent of skin barrier perturbation, and therefore better preserves the skin barrier, relative to aqueous contacting solution (iv) containing 10 wt% PG (see Section 4.4.1 and *Table 4-2*). This result is consistent with the chromameter measurements of in vivo erythema (see *Figure 4-5*).

In view of the agreement between the in vitro ranking metric analysis and the in vivo skin barrier measurements summarized above, the methodology presented in this chapter to rank aqueous surfactant/humectant systems based on their ability to perturb the skin aqueous pores *in vitro* should be useful to a formulator of skin-care products who is interested in understanding skin barrier perturbation induced by aqueous surfactant/humectant systems *in vivo*. The in vitro ranking methodology presented here represents a novel approach to rank surfactants and humectants used in skin-care formulations, and may potentially reduce the need to conduct costly and time-consuming in vivo skin barrier measurements (see Section 4.5).

4.4.4. Comparison of the In Vitro and In Vivo Effects of Adding 10 wt% Glycerol to an Aqueous SDS Contacting Solution

In Chapter 2, I presented an in vitro analysis which makes use of skin electrical current and Mannitol skin permeability measurements to determine the effect of adding 10 wt% Glycerol to an aqueous SDS contacting solution. Specifically, skin electrical current and Mannitol skin permeability values were measured following exposure of p-FTS to an aqueous contacting solution containing SDS (1 wt%) + G (10 wt%). These values are reported again in *Table 4-3* for completeness. In terms of the ranking metric (RM) analysis presented here (see Section 4.2.6), a RM value of 4.1±1.0 corresponds to an aqueous contacting solution containing SDS (1 wt%) + G (10 wt%), a value that is obtained by taking the ratio of the skin electrical current values in *Table 4-3* corresponding to the aqueous contacting solution containing SDS (1 wt%)+G (10 wt%) (49±10 μA) relative to the in vitro PBS control (12±3 μA). On the other hand, *Table 4-3* also shows that the RM value corresponding to an aqueous contacting solution containing SDS (1 wt%) is (91±10)/(12±3) = 7.6±1.0, which is significantly higher than the RM value of 4.1±1.0 corresponding to an aqueous contacting solution containing SDS (1 wt%)+G (10 wt%).

Therefore, as already shown in Chapter 2, adding 10 wt% G to an aqueous contacting solution containing 1 wt% SDS significantly reduces in vitro skin barrier perturbation. The Mannitol skin permeability values reported in *Table 4-3* also indicate a decrease in skin barrier perturbation induced by an aqueous contacting solution containing 1 wt% SDS+10 wt% G ($P=30\pm10\times10^{-5}$ cm/hr), relative to an aqueous contacting solution containing 1 wt% SDS ($P=66\pm10\times10^{-5}$ cm/hr). The in vivo TEWL results in *Table 4-3* indicate that the TEWL value corresponding to an aqueous contacting solution containing SDS (1 wt%)+G (10 wt%) is statistically lower ($p<0.05$) than that corresponding to an aqueous contacting solution containing SDS (1 wt%).[26] In addition, the in vivo visual skin dryness scores in *Table 4-3* reveal that an aqueous contacting solution containing SDS (1 wt%)+G (10 wt%) induces statistically lower ($p<0.05$) visual skin dryness than that induced by an aqueous contacting solution containing SDS (1 wt%). Taken together, the in vivo TEWL and visual skin dryness results reported in *Table 4-3* imply that adding 10 wt% G to an aqueous SDS (1 wt%) contacting solution mitigates the ability of SDS to perturb the skin barrier. In Chapter 2, using dynamic light scattering measurements to determine the effective SDS micelle hydrodynamic radii in the presence and in the absence of 10 wt% G, I showed unambiguously that SDS micelles are too large to penetrate into the skin aqueous pores in vitro when 10 wt% G is added to the aqueous contacting solution containing SDS (1 wt%). As a result, SDS in micellar form is not able to contribute to SDS skin penetration and associated SDS-induced skin barrier perturbation. Therefore, the in vivo TEWL and visual skin dryness results reported in *Table 4-3* support the in vitro results reported in Chapter 2 by clearly showing

[26] It is important to note that the TEWL value corresponding to an aqueous contacting solution containing SDS (1 wt%)+G (10 wt%) is statistically not different ($p>0.05$) from that corresponding to the in vivo control (iii), while it is statistically lower ($p<0.05$) than that corresponding to an aqueous contacting solution containing SDS (1 wt%). This finding provides additional evidence for the ability of Glycerol to mitigate SDS-induced skin barrier perturbation.

a smaller extent of skin barrier perturbation in vivo induced by an aqueous contacting solution containing 1 wt% SDS in the presence of 10 wt% G, relative to that in the absence of 10 wt% G.

Table 4-3. In vitro and in vivo skin barrier measurements for aqueous contacting solutions containing SDS (1 wt%) and SDS (1 wt%)+Glycerol (10 wt%), including a comparison with the appropriate in vitro/in vivo controls. The table reports average values and standard errors.

		Aqueous Contacting Solutions		
	Skin Barrier Measurements	SDS (1 wt%)	SDS (1 wt%) + Glycerol (10 wt%)	Control (In Vitro/In Vivo)*
In Vitro	Skin Electrical Current (μA)	91±10	49±10	12±3
	Mannitol Skin Permeability (cm/hr)×10^5	66±10	30±10	7±3
	Average Pore Radius, r_{pore} (Å)	33±5	20±5	20±3
	Enhancement in $\rho = \rho_E / \rho_C$ **	2.6±1	2.9±1	1
In Vivo	TEWL (Barrier Damage)	5.30±0.20	4.00±0.40	3.40±0.30
	Visual Skin Dryness	0.89±0.11	0.60±0.13	0.15±0.02
	Chromameter (Erythema)	0.57±0.11	0.58±0.14	-0.08±0.05***

* The in vitro control corresponds to PBS in water (aqueous contacting solution (iii), see Section 4.2.2), and the in vivo control corresponds to a no reaction, non-occluded control (see Section 4.3).

** The enhancement in the aqueous pore number density, ρ, is reported relative to the in vitro control. In addition, recall that E denotes enhancer (that is, aqueous contacting solutions (i), (ii), (iv), and (v)) and C denotes the in vitro control (that is, aqueous contacting solution (iii)).

*** Note that the in vivo control showed erythema values close to zero, which is not unexpected (the small negative mean value of -0.08 results from the fact that some of the volunteers in the control group exhibited lower skin redness on Day 2, when compared to Day 1).

Although the TEWL and visual skin dryness values repeated in *Table 4-3* indicate that Glycerol can indeed mitigate SDS-induced skin barrier perturbation in vivo, a similar corroboration was not obtained using the chromameter measurements of skin erythema (redness). This is because the chromameter scores in *Table 4-3* indicate no statistical difference ($p>0.05$)

between the erythema (skin redness) scores corresponding to an aqueous contacting solution containing 1 wt% SDS in the absence of G (0.57±0.11), relative to that in the presence of 10 wt% G (0.58±0.14). It is possible that an aqueous contacting solution containing 1 wt% SDS + 10 wt% G may induce an initial cutaneous reaction that attracts increased blood flow to the dermis of the affected skin site, thereby leading to skin redness (erythema), even though the skin barrier may not be significantly perturbed (8-11, 14, 17, 24, 32). Therefore, the skin at the corresponding site may appear red from an increased blood flow to the dermis, without the skin barrier being compromised, which would lead to a higher erythema score. Accordingly, the in vivo erythema response associated with adding 10 wt% Glycerol to an aqueous SDS contacting solution on the skin barrier needs to be investigated further. For example, in vivo cutaneous biochemical reaction pathways triggering erythema, which may be triggered by SDS even in the presence of Glycerol, could be investigated (8, 9, 14, 32-36). It is also possible that: (1) a higher concentration of SDS than the 1 wt% used in the in vivo soap chamber, (2) a higher concentration of Glycerol than the 10 wt% used in the in vivo soap chamber, and/or (3) longer exposure times of the in vivo soap chamber, may be necessary to discriminate between the in vivo erythema induced by SDS in the presence of Glycerol relative to that induced by SDS in the absence of Glycerol.

4.5. Conclusions

Macroscopic in vitro skin barrier measurements, which quantify the extent of skin barrier perturbation induced by aqueous surfactant/humectant contacting solutions commonly encountered in skin-care formulations, can be effectively used to *rank* these contacting solutions. Such a ranking is based on the ability of the solutions to perturb the skin aqueous pores of the

stratum corneum (SC). An in vitro ranking metric was developed using the enhancement in the skin electrical current induced by an aqueous surfactant/humectant contacting solution, relative to an in vitro PBS control aqueous contacting solution, as the metric. In vitro Mannitol skin permeability measurements, when combined with skin electrical resistivity measurements, in the context of a hindered-transport aqueous porous pathway model, provided mechanistic insight on the results of the in vitro ranking metric analysis. Specifically, the pore number density (ρ) and the average pore radius (r_{pore}) of the skin aqueous pores induced by aqueous solutions of surfactants and humectants contacting p-FTS were determined. The in vitro skin electrical current/resistivity and Mannitol skin permeability measurements were carried out using the following aqueous solutions: (i) an anionic surfactant solution – SDS (1 wt%), (ii) a nonionic surfactant solution – $C_{12}E_6$ (1 wt%), (iii) an in vitro control solution – PBS, and (iv) a humectant solution – Propylene Glycol (PG) (10 wt%), and (v) a humectant solution – Glycerol (G) (10 wt%). Utilizing the in vitro ranking metric introduced in this chapter, I obtained the following ranking order, from the mildest to the harshest, for the surfactants and the humectants considered above, based on their ability to perturb the skin aqueous pores: (v) 10 wt% G < (iv) 10 wt% PG < (iii) PBS < (ii) 1 wt% $C_{12}E_6$ < (i) 1 wt% SDS.

To substantiate the findings above, in vivo soap chamber measurements were carried out on human subjects by CyberDERM Clinical Studies (Broomall, PA), in collaboration with Neutrogena Corporation (Los Angeles, CA). Specifically, the following in vivo skin barrier measurements were conducted: (1) Transepidermal water loss (TEWL) determined using an evaporimeter, (2) Visual skin dryness determined by an expert grader, and (3) Skin erythema measurements using a chromameter. The overall implications of the in vivo results is that aqueous surfactant contacting solutions (i) and (ii) induce a larger extent of skin dryness and

erythema relative to aqueous humectant contacting solutions (iv) and (v). In addition, the in vivo measurements (1)-(3) above indicate that a 1 wt% aqueous SDS contacting solution induces the largest extent of skin barrier perturbation, while a 10 wt% aqueous Glycerol contacting solution induces the smallest extent of skin barrier perturbation. Both of these in vivo findings are consistent with the results of the in vitro ranking metric analysis. Therefore, determining the in vitro perturbation to the skin aqueous pores induced by aqueous surfactant/humectant systems represents a viable practical strategy to *predict* their in vivo skin barrier perturbation potential.

Because of the correlation established between the in vitro ranking metric analysis and the in vivo skin barrier measurements, the in vitro ranking methodology formulated in this chapter, which quantifies the perturbation to the skin aqueous pores, can potentially be used to screen and rank many surfactants and humectants for use in skin-care formulations, without the need to conduct costly and time-consuming human and animal testing procedures. Such a practical strategy could significantly speed up the effort and time required to bring new skin-care formulations to the market.

In the next chapter, Chapter 5, I report the results of a novel two-photon microscopy (TPM) visualization study that is conducted to visually determine, as well as quantify, the extent of perturbation to the skin morphology induced by aqueous surfactant/humectant systems.

4.6. References

1. H.Tang, S.Mitragotri, D.Blankschtein, and R.Langer, Theoretical description of transdermal transport of hydrophilic permeants: Application to low-frequency sonophoresis, *Journal of Pharmaceutical Sciences*, 90:p. 545-568 (2001).
2. K.D.Peck, A.H. Ghanem, and W.I.Higuchi, Hindered diffusion of polar molecules through and effective pore radii estimates of intact and ethanol treated human epidermal membrane, *Pharmaceutical Research*, 11(9):p. 1306-1314 (1994).
3. K.D.Peck, A.H.Ghanem, and W.I.Higuchi, The effect of temperature upon the permeation of polar and ionic solutes through human epidermal membrane, *Journal of Pharmaceutical Sciences*, 84(8):p. 975-982 (1995).
4. A.Tezel, A.Sens, and S.Mitragotri, Description of transdermal transport of hydrophilic solutes during low-frequency sonophoresis based on a modified porous pathway model, *Journal of Pharmaceutical Sciences,* 92(2):p. 381-393 (2003).
5. W.M.Deen, Hindered transport of large molecules in liquid-filled pores, *AIChE Journal*, 33(9):p. 1409-1425 (1987).
6. J.L.Anderson, and J.A.Quinn, Restricted transport in small pores, a model for steric exclusion and hindered particle motion, *Biophysical Journal*, 14:p. 130 (1974).
7. F.A.Simion, L.D.Rhein, G.L.Grove, J.M.Wojtkowski, R.H.Cagan, and D.D. Scala, Sequential order of skin responses to surfactants during a soap chamber test, *Contact Dermatitis*, 25:p. 242-249 (1991).
8. T.Agner, and J.Serup, Sodium lauryl sulphate for irritant patch testing – A dose-response study using bioengineering methods for determination of skin irritation, *Journal of Investigative Dermatology*, 95:p. 543-547 (1990).

9. K.-P. Wilhelm, C. Surber, and H.I. Maibach, Quantification of sodium lauryl sulfate irritant dermatitis in man: Comparison of four techniques: skin color reflectance, transepidermal water loss, laser Doppler flow measurement and visual scores, *Archives of Dermatological Research*, 281: p. 293-295 (1989).

10. K.-P. Wilhelm, M. Samblebe, and C.-P. Siegers, Quantitative in vitro assessment of N-alkyl sulphate-induced cytotoxicity in human keratinocytes (HaCaT) – Comparison with in vivo human irritation tests, *British Journal of Dermatology*, 130:p. 18-23 (1994).

11. K.-P. Wilhelm, A.B. Cua, H.H. Wolff, and H.I. Maibach, Surfactant-induced stratum corneum hydration in vivo: Prediction of the irritation potential of anionic surfactants. *Journal of Investigative Dermatology*, 101:p. 310-315 (1993).

12. P.J.Frosch, and A.M.Kligman, The soap chamber test - A new method for assessing the irritancy of soaps, *J Am Acad Dermatol.*, 1(1):p. 35-41 (July, 1979).

13. S.W.Babulak, L.D.Rhein, D.D.Scala, A.F.Simion, and G.L.Grove, Quantitation of erythema in a soap chamber test using the minolta chroma (reflectance) meter: Comparison of instrumental results with visual assessments, *J. Soc. Cosmet. Chem.*, 37:p. 475-479 (1986).

14. Personal Communication by S. Hornby, Neutrogena Corporation, Los Angeles, CA.

15. H.Tagami, M.Ohi, K.Iwatsuki, Y.Kanamaru, M.Yamada, and B.Ichijo, Evaluation of the skin surface hydration in vivo by electrical measurement, *Journal of Investigative Dermatology*, 75: p. 500-507 (1980).

16. K.P.Anathapadmanabhan, C.L.Meyers, and M.P.Aronson, Binding of surfactants to stratum corneum, *J. Soc. Cosmet. Chem.*, 47:p. 185-200 (1996).

17. L.D.Rhein, In Vitro Interactions: Biochemical and biophysical effects of surfactants on skin. In: *Surfactants in Cosmetics,* M.M.Rieger and L.D.Rhein, Eds.(Surfactant Science Series, Marcel Dekker, Inc., Vol. 68), p. 397-426 (1997).

18. G.Imokawa, Surfactant mildness. In: *Surfactants in Cosmetics,* M.M.Rieger and L.D.Rhein, Eds. (Surfactant Science Series, Marcel Dekker, Inc., Vol. 68), p. 427-471 (1997).

19. K.P.Ananthapadmanabhan, D.J.Moore, K.Subramanyan, M.Misra, and F.Meyer, Cleansing without compromise: The impact of cleansers on the skin barrier and the technology of mild cleansing, *Dermatologic Therapy*, 17:p. 16-25 (2004).

20. J.Pinnagoda, R.A.Tupker, T.Anger, and J.Serup, Guidelines for transepidermal water loss (TEWL) measurement, *Contact Dermatitis*, 22:p. 164-178 (1990).

21. G.L.Grove, M.J.Grove, C.Zerweck and E.Pierce, Comparative metrology of the evaporimeter and the DermaLab® TEWL probe, *Skin Res. & Tech.*, 5:p. 1-8 (1999).

22. G.L.Grove, M.J.Grove, C.Zerweck and E.Pierce, Computerized evaporimetry using the DermaLab® TEWL probe, *Skin Res. & Tech.*, 5:p. 9-13 (1999).

23. M.Obata and H.Tagami, A rapid in vitro test to assess skin moisturizers, *J. Soc. Cosmet. Chem.*, 41:p. 235-241 (1990).

24. P.Moore, "A fundamental investigation of surfactant-induced skin irritation", Ph.D. thesis, Department of Chemical Engineering, Massachusetts Institute of Technology, Cambridge, MA, USA (2002).

25. J.W.Fluhr, M.Gloor, L.Lehmann, S. Lazzerini, F.Distante, and E.Berardesca, Glycerol accelerates recovery of barrier function in vivo, *Acta Derm Venereol*, 79:p. 418-421 (1999).

26. J.Bettinger, M. Gloor, A.Vollert, P.Kleesz, J.Fluhr, and W.Gehring, Comparison of different non-invasive test methods with respect to the different moisturizers on skin, *Skin Res. Technol.*, 5:p. 21-27 (1999).

27. M.D.Batt and E.Fairhurst, Hydration of the stratum corneum, *Int. J. Cosmet. Sci.*, 8:p. 253-256 (1986).

28. D.S.Orth and Y.Appa, Glycerine: a natural ingredient for moisturizing skin. In: *Dry skin and moisturizers: chemistry and function,* M.Loden and H.I.Maibach, Eds. (CRC Press, Boca Raton, 2000), pp. 213-228.

29. C.L.Froebe, F.A.Simion, H.Ohlmeyer, L.D.Rhein, J.Mattai, R.H.Cagan, and S.E.Friberg, Prevention of stratum corneum lipid phase transitions in vitro by glycerol – An alternative mechanism for skin moisturization, *J. Soc. Cosmet. Chem.*, 41:p. 51-65 (1990).

30. A.Rawlings, C.Harding, A.Watkinson, J.Banks, C.Ackermann, and R.Sabin, The effect of glycerol and humidity on desmosome degradation in stratum corneum, *Arch. Dermatol. Res.*, 287:p. 457-464 (1995).

31. M.Hannuksela, Glycols. In: *Dry skin and moisturizers: chemistry and function,* M.Loden and H.I.Maibach, Eds. (CRC Press, Boca Raton, 2000), p. 413-419.

32. W.Abraham, Surfactant effects on skin barrier. In: *Surfactants in Cosmetics,* M.M.Rieger and L.D.Rhein, Eds, (Surfactant Science Series, Marcel Dekker, Inc., Vol. 68), p. 471-487 (1997).

33. CA.Allen, The skin; a clinicopathological treatise, New York, Grune & Stratton (1967).

34. R.M.Adams, Occupational skin disease, in *Fitzpatrick's dermatology in general medicine. New York:McGraw-Hill, Health Professions Division, c1999.*

35. P.M.Elias and K.R.Feingold, Skin as an organ of protection, in Fitzpatrick's dermatology in general medicine. New York:McGraw-Hill, Health Professions Division, c1999.

36. C.K.Smith Pease, I.R.White, and D.A.Basketter, Skin as a route of exposure to protein allergens. *Clinical and Experimental Dermatology*, 27:p. 296-300 (2002).

Chapter 5

5. Visualization and Quantification of Skin Barrier Perturbation Induced by Surfactant-Humectant Systems Using Two-Photon Fluorescence Microscopy

5.1. Introduction and Motivation

In Chapter 1, I presented a brief overview of the application of Two-Photon Fluorescence Microscopy (TPM) as a novel imaging tool for human skin and pig full-thickness skin (p-FTS). Specifically, the advantages of using TPM to image skin and to obtain visual and quantitative morphological information were discussed relative to other available methods, including: (a) traditional skin tissue biopsy, and (b) skin imaging tools such as electron microscopy and confocal laser scanning microscopy (1-4). The key advantages that TPM has over methods (a) and (b) above include: (i) it is a non-invasive technique that does not require tissue excision and fixation, thereby avoiding loss of important cellular and morphological information, which is a concern using invasive methods such as (a), and (ii) it can image skin to a depth of several hundred micrometers with reduced photo-damage, which is not possible with imaging methods such as (b).

In the past, studies have demonstrated the viability of using TPM to visualize, as well as to quantify, human skin morphological characteristics. In particular, Yu et al. developed a TPM visualization technique to visualize, as well as to quantify, the effect of a chemical enhancer, Oleic Acid (OA), on human skin (5-8). Specifically, Yu et al. used TPM to visually determine three-dimensional spatial distributions of the hydrophilic and the hydrophobic fluorescent probes, Sulforhodamine B (SRB) and Rhodamine B Hexyl Ester (RBHE), respectively, in excised full-thickness human cadaver skin exposed to phosphate buffered saline (PBS), the control, and to OA, the chemical enhancer. Both SRB and RBHE were observed to reside primarily in the intercellular lipid bilayer region surrounding the corneocytes within the stratum corneum (SC). In addition, from the TPM skin images, Yu et al. calculated the changes in the concentration gradient and in the vehicle-to-skin partition coefficient of each probe in the skin samples exposed to OA and to PBS (5). These calculations were subsequently used, along with theoretically derived mathematical expressions of transdermal transport, to quantitatively characterize the OA-induced relative changes to the SC transport characteristics, including the SC diffusion coefficient and the SC diffusion length of the two fluorescent probes (5, 8). Furthermore, based on the results of these studies, Yu et al. were able to conclude that for the hydrophobic RBHE probe, the OA-induced enhancement in the skin epithelial barrier permeability was driven primarily by an increase in the vehicle-to-skin partition coefficient, leading to an increase in the steepness of the RBHE probe concentration gradient across the skin (5). The primary OA-induced changes in the transdermal transport properties of the hydrophilic SRB probe included increases in both the vehicle-to-skin partition coefficient and the skin diffusion coefficient (5). These findings, utilizing the TPM skin imaging methodology data analysis and transdermal transport modeling, demonstrate that, in addition to providing visual

scans that clearly delineate probe distributions in the SC, the subsequent quantification of these TPM skin images provides additional important insight into the mechanistic changes in transdermal transport underlying the visualized changes in probe distributions across the SC (5, 8).

In addition to the fluorescence originating from the hydrophobic/hydrophilic fluorescent probes that have penetrated into the skin, the skin has an inherent florescence, referred to as the *skin autofluorescence*, that originates from endogenous fluorophores in the skin, including reduced pyridine nucleotides, flavoproteins, collagen, and elastin (9, 10). Na et al. (10) showed that excitation wavelengths ranging from 340 to 380 nm, in the skin autofluorescence emission spectrum, have two major component bands centered at 450 nm (75% of the spectrum) and 520 nm (25% of the spectrum). Using an appropriate filter set in the TPM apparatus (see Section 5.2.6), these emission wavelengths can be collected by the green channel, while wavelengths of 578 nm and 586 nm which are the emission peaks of the fluorescent probes RBHE and SRB, respectively, can be collected by the red channel. Since there is minimal wavelength overlap between the red and the green channels, a quantification of probe spatial distributions relative to the brick-and-mortar SC structure in the same skin sample, at precisely the same skin spatial locations, can be achieved by this technique of dual-channel (the green channel and the red channel) TPM. *Hence, the skin inherent structural features, as delineated in the green channel, can provide a fingerprint relative to the probe spatial distribution, as delineated in the red channel.*

Yu et al. utilized this advanced dual-channel TPM method to determine mechanisms of OA-induced skin barrier perturbation. By an overlap of the fluorescence intensities of the red/probe and green/autofluorescence channels, they could deduce that the hydrophobic RBHE

probe was localized in the intercellular lipid bilayer region of the SC. In addition, they reported that OA induced the formation of RBHE microdomains within the SC. On the other hand, Yu et al. observed that OA induced the hydrophilic SRB probe to preferentially partition across the corneocyte envelopes and diffuse into the corneocytes within the SC. Hence, the dual-channel TPM skin images that were obtained by Yu et al. upon exposing human skin to OA and to SRB for 24 hours provided evidence for the existence of intra-corneocyte diffusion in addition to the commonly accepted lipid bilayer transdermal pathway (6).[27] Therefore, the OA enhancer mechanism was clearly shown to be a function of the fluorescent probe physicochemical properties.

Because the permeability and morphological characteristics of pig full-thickness skin (p-FTS) are similar to those of human skin, pig skin is an excellent model for human skin for both in vitro and in vivo skin permeability and imaging studies (12, 13). With this in mind, I have utilized TPM imaging of p-FTS samples to obtain visual and quantitative insight on the effect of aqueous surfactant-humectant systems on the skin barrier (see Section 5.2 for additional details). Through past research in the surfactant-induced skin barrier perturbation area, it is now well accepted that surfactants (both as monomers and as micelles) have to first penetrate into the SC in order to induce skin barrier perturbation (14-22). However, once surfactants have penetrated into the SC, it is not known whether they are located in the keratins in the corneocytes or in the intercellular lipids in the lamellar bilayers comprising the SC. Several researchers have hypothesized that surfactants interact with the corneocyte keratins (12, 19, 22) and also with the lamellar lipid bilayers (18, 23). An imaging method that can visualize the location of a

[27] Recently, Kushner et al. have also carried out dual-channel TPM visualization studies of human skin exposed to ultrasound and to the harsh surfactant, Sodium Dodecyl Sulfate (SDS) (11). These studies also provided evidence for intra-corneocyte probe diffusion induced by ultrasound and SDS (11).

fluorescent probe in the SC that has been exposed to an aqueous surfactant solution may help shed light on this issue. For example, if the surfactant penetrates into the corneocytes and denatures the corneocyte keratins, then this will result in increased corneocyte permeability to the fluorescent probe. Therefore, the fluorescent probe will be located in the corneocyte domains of the SC, and accordingly, will be detected in the TPM skin images. Alternatively, if the surfactant penetrates into the intercellular lipid bilayers of the SC and disorders the lipid bilayer domains of the SC, then the fluorescent probe will also penetrate into the lipid bilayers and can be detected in the TPM skin images. By contacting skin with surfactant solutions in the presence and in the absence of humectants, in the context of these TPM skin visualizations studies, one can obtain fundamental insight into the modification of the skin barrier morphology induced by surfactants in the presence of humectants. Specifically, one may be able to determine conclusively if a specific surfactant interacts strongly with the keratins in the corneocytes and/or with the intercellular lipids. Furthermore, one may also determine conclusively how such surfactant-skin interactions are modified by a humectant like Glycerol when it is added to the aqueous surfactant solution contacting the skin.

The remainder of this chapter summarizes the results of an in vitro TPM visualization study of physical SC perturbations induced by aqueous contacting solutions of surfactants and humectants relative to an aqueous control solution (PBS). For this purpose, I have carried out TPM imaging studies of p-FTS exposed to aqueous contacting solutions containing: (i) SDS (an anionic surfactant which is a harsh skin agent, see Chapters 2 and 4), (ii) SDS+Glycerol (a surfactant/humectant mixture, see Chapters 2 and 4), (iii) SCI (an anionic surfactant which is a mild skin agent, see Chapter 3), (iv) PBS (the control), and (v) Glycerol (a humectant which is a skin beneficial agent, see Chapters 2 and 4). The TPM visualization studies were carried out

using the hydrophilic fluorescent probe, Sulforhodamine B (SRB), which penetrates into the skin through aqueous pores in the SC, and hence, can shed light on the modification of these aqueous pores induced by surfactants in the presence of humectants (5-8, 11, 29, 30, 33, 34). Specifically, SRB emits a fluorescent signal in the red channel, has an emission peak wavelength of 586 nm, an absorbance peak wavelength of 565 nm, and has a molecular weight of 559 Da (37). The p-FTS samples were exposed to aqueous contacting solutions (i)-(v) separately, and subsequently, were contacted with aqueous SRB solutions (see Section 5.2.2). Following these SRB exposures, the p-FTS samples were dried and visualized using the TPM apparatus (see Section 5.2.5). Using a filter set in the TPM apparatus, the emission wavelengths resulting from the presence of SRB in the skin (probe fluorescence) were collected by the red channel, while the emission wavelengths resulting from the inherent fluorophores present in the skin (skin autofluorescence) were collected by the green channel, thereby enabling dual-channel TPM skin imaging of p-FTS samples exposed to solutions (i)-(v) (see Section 5.2.6). The results of the TPM visualization study are presented in Section 5.4. Finally, Section 5.5 summarizes the main conclusions of this chapter.

5.2. Experimental

5.2.1. Materials

Sodium Dodecyl Sulfate (SDS) was purchased from Sigma Chemicals (St. Louis, MO). Analytical-grade Glycerol was purchased from VWR Chemicals (Cambridge, MA). Sulforhodamine B (SRB), a hydrophilic fluorescent probe, was obtained from Molecular Probes (Eugene, OR). Sodium Cocoyl Isethionate (SCI) from BASF was provided to us by UNILEVER (Edgewater, NJ). Water was filtered using a Millipore Academic water filter (Bedford, MA).

Phosphate Buffered Saline (PBS) was prepared using PBS tablets from Sigma Chemicals (St. Louis, MO) and Millipore filtered water, such that a phosphate concentration of 0.01M along with a NaCl concentration of 0.137M were obtained at a pH of 7.2. All these chemicals were used as received.

5.2.2. Preparation of the Solutions

For the visualization of SRB in p-FTS, a solution of 0.05 mg/ml of SRB in PBS was prepared. The following aqueous solutions of surfactants, a humectant, and surfactant+humectant that contacted p-FTS were prepared: (i) a harsh surfactant solution – SDS (1 wt%), (ii) a harsh surfactant+humectant solution – SDS (1 wt%) + Glycerol (10 wt%), (iii) a mild surfactant solution – SCI (1 wt%), [28] (iv) a control solution – PBS, and (v) a humectant solution – Glycerol (10 wt%). Aqueous solutions (i)-(v) were used to be consistent with the in vitro studies carried out in Chapters 2 and 3. Note that a mild surfactant+humectant solution – SCI (1 wt%)+Glycerol (10 wt%) , did not induce skin morphological modifications different from those induced by solutions (iv) and (v), and therefore, was not considered here.

5.2.3. Preparation of the Skin Samples

Female Yorkshire pigs (40-45kg) were purchased from local farms, and the skin (back) was harvested within one hour after sacrificing the animal. The subcutaneous fat was trimmed off using a razor blade, and the full-thickness pig skin was cut into small pieces (2cm × 2cm) and stored in a –80 °C freezer for up to 2 months. The TPM skin visualization experiments were performed using p-FTS.

---

[28] Note that p-FTS samples were contacted with aqueous SCI solutions at 35°C. This is because SCI (1 wt%) is soluble in water at 35°C, and not at room temperature (25°C) (see Chapter 3).

5.2.4. In Vitro Diffusion Cell Skin Exposure to Surfactant-Humectant Systems Followed by Exposure to SRB

Prior to use in the TPM skin visualization experiments, the p-FTS sample was thawed for half an hour. The p-FTS sample was then mounted in a vertical Franz diffusion cell obtained from Permegear (Bethlehem, PA) with the SC facing the donor compartment. Both the donor and the receiver compartments were filled with PBS, and the p-FTS sample was left to hydrate for 1 hour to allow the skin initial barrier property to reach steady state. At this point, the skin electrical current across the p-FTS sample was measured, and only p-FTS samples with an initial skin current < 3 μA were utilized in the permeation studies (see Chapter 2 for additional details). The PBS in the donor compartment of the diffusion cell was then replaced with 1.5 ml of aqueous contacting solution (i), (ii), (iii), or (v). The aqueous solution in each donor compartment was then allowed to contact the p-FTS sample for 5 hours. Following this skin treatment with each aqueous contacting solution, the aqueous contacting solution was removed and the donor compartment along with the p-FTS sample were rinsed 4 times with 2 ml of PBS to remove any trace chemical left on the skin surface and in the donor compartment. Subsequently, each p-FTS sample was exposed to an aqueous SRB fluorescent probe solution in the diffusion cell for an additional 24 hours.

Each p-FTS sample was then removed from the diffusion cell, rinsed 4 times with 2 ml of PBS as before, and blotted with a Kimwipe (Kimberly Clark, Roswell, GA) to ensure the removal of any excess SRB present on the skin surface. The circular area of the skin exposed to SRB was cut out with a surgical carbon steel razor blade (VWR Scientific, Media, PA), and subsequently sealed in a 2.5 mm imaging chamber (Coverwell, Grace Bio-Laboratories, Bend, OR) with a coverslip (VWR Scientific, Media, PA) that contacted the SC side of the p-FTS

Discriminator. The number of photons collected at each pixel, for the red and green channel images, is counted and recorded digitally by the computer (9, 25).

Aqueous contacting solutions (i)-(v) (see Section 5.2.2) were exposed separately to 7 p-FTS samples, and six 100 μm x 100 μm skin sites were imaged for each p-FTS sample. Each p-FTS sample was imaged to a depth of 40 μm. Specifically, for each skin site imaged, forty one 100 μm x 100 μm images were obtained, the first one at the skin surface (z=0) and the last one 40 μm below the skin surface (z=40), each separated by a depth of 1 μm from the other.

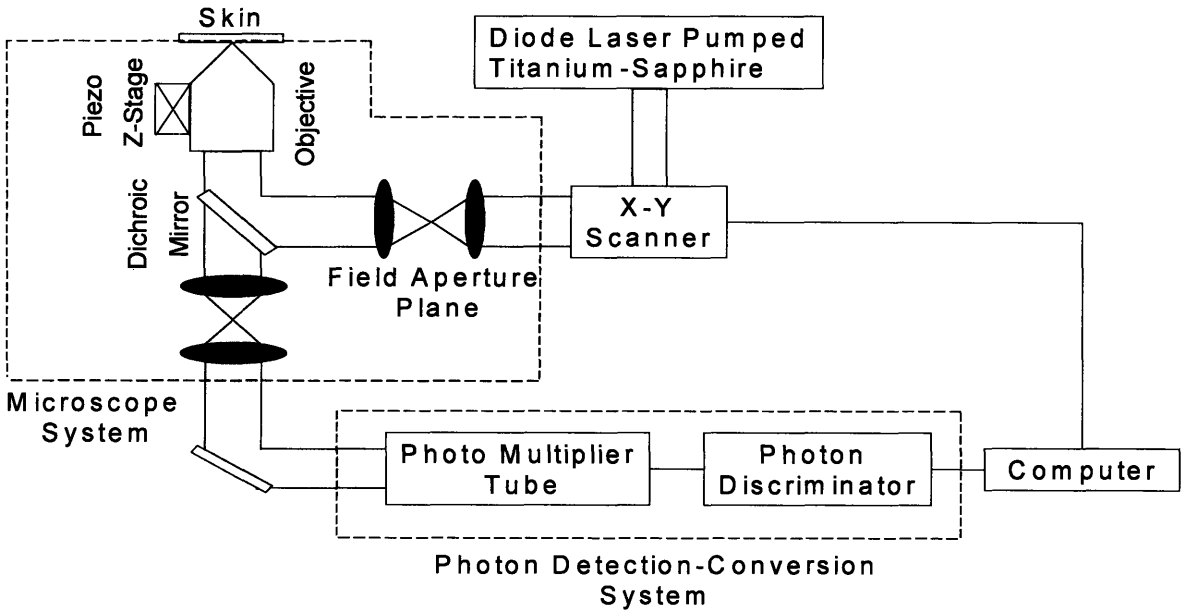

Figure 5-1. Schematic illustration of the apparatus used for the Two-Photon Fluorescence microscopy (TPM) skin imaging experiments (5, 25).

It was observed that most of the SRB probe was present in the p-FTS samples within a depth of 20 μm below the skin surface. Consequently, the TPM skin images obtained within the first 20 μm below the skin surface were analyzed (5-8, 11), and images obtained at layers corresponding to z=3 (3 μm below the skin surface) and z=20 (20 μm below the skin surface) are

Discriminator. The number of photons collected at each pixel, for the red and green channel images, is counted and recorded digitally by the computer (9, 25).

Aqueous contacting solutions (i)-(v) (see Section 5.2.2) were exposed separately to 7 p-FTS samples, and six 100 μm x 100 μm skin sites were imaged for each p-FTS sample. Each p-FTS sample was imaged to a depth of 40 μm. Specifically, for each skin site imaged, forty one 100 μm x 100 μm images were obtained, the first one at the skin surface (z=0) and the last one 40 μm below the skin surface (z=40), each separated by a depth of 1 μm from the other.

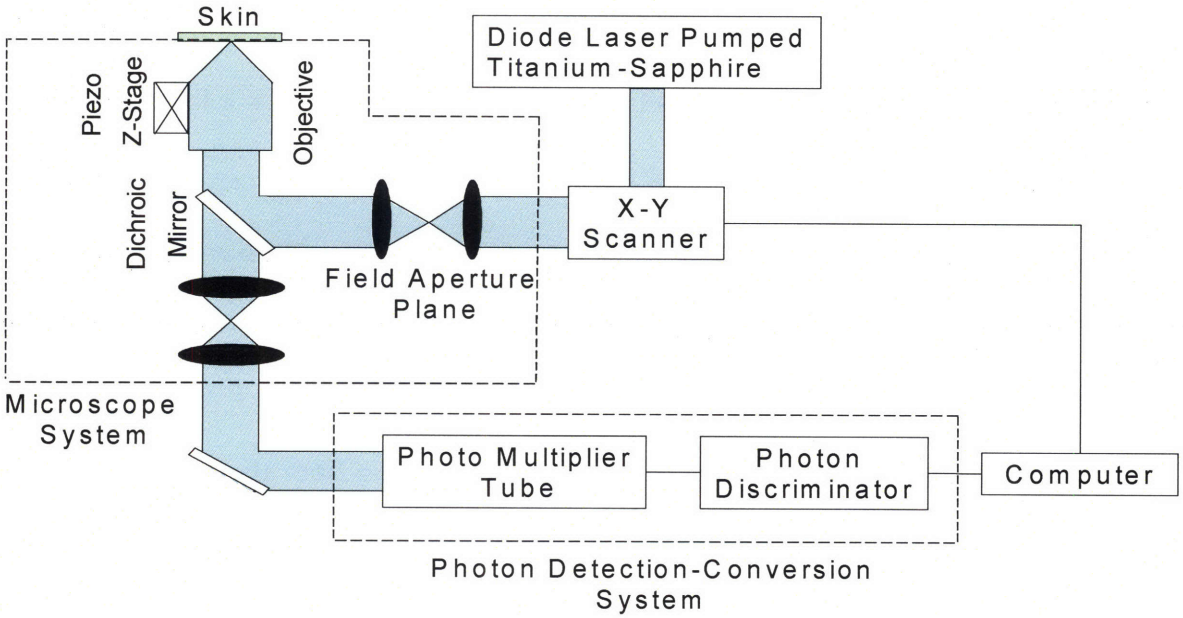

Figure 5-1. Schematic illustration of the apparatus used for the Two-Photon Fluorescence microscopy (TPM) skin imaging experiments (5, 25).

It was observed that most of the SRB probe was present in the p-FTS samples within a depth of 20 μm below the skin surface. Consequently, the TPM skin images obtained within the first 20 μm below the skin surface were analyzed (5-8, 11), and images obtained at layers corresponding to z=3 (3 μm below the skin surface) and z=20 (20 μm below the skin surface) are

presented in Section 5.4. One should note that 3μm below the skin surface is within the SC, while 20 μm below the skin surface is within the viable epidermis (VE) (see Chapter 1). Therefore, the effects of aqueous contacting solutions (i)-(v) were visualized on the structure of *both* the SC and the VE (see Section 5.4.1).

5.2.6. Determination of SC Morphological Changes Induced by Surfactant-Humectant Systems Using a Deconstruction Analysis of the Dual-Channel TPM Images

The investigation of the effect of aqueous SDS and aqueous SDS+Glycerol contacting solutions presented in Chapter 2 indicates that the addition of 10 wt% Glycerol to an SDS aqueous solution contacting the skin reduces the ability of the SDS micelles to penetrate into the epidermis, thereby significantly reducing the amount of SDS in the epidermis. Presumably, this reduction in the amount of SDS that can penetrate into the epidermis should also reduce SDS interactions with the keratins in the epidermis. Specifically, this should result in a reduction in the ability of SDS to rupture the corneocyte envelopes, and expose and disrupt secondary and tertiary structures of keratin in the corneocytes in the SC. On the other hand, mild surfactants such as SCI are known to perturb the ordered intercellular lipid bilayers in the SC, thereby inducing skin dryness. In fact, researchers have hypothesized that the skin barrier perturbation response may be modulated by both of these two distinct mechanisms, that are: (i) the direct interaction of a penetrating skin agent with the keratins in the corneocytes in the SC, and (ii) bilayer disruption and delipidization of the SC lipid bilayers. Furthermore, either or both of these mechanisms can potentially trigger cytokine production, thereby triggering biochemical signals and promoting skin inflammation. Therefore, in order to mitigate skin barrier

perturbation induced by surfactant-humectant systems, it is important to be able to minimize the deleterious effects of mechanisms (i) and (ii) above on the skin barrier. Clearly, the first step in this direction involves being able to identify if mechanism (i), or (ii), or both, induce significant skin barrier perturbation. The dual-channel TPM skin images obtained following exposure of the skin to surfactant-humectant systems, when analyzed using the image deconstruction analysis described below, can identify the relative roles of mechanisms (i) and (ii) in inducing skin barrier perturbation.

To elucidate the effect of aqueous contacting solutions (i)-(v) (see Section 5.2.2) on the corneocyte keratins and on the intercellular lipid bilayers of the SC, a two-dimensional slice, 5 pixels (width) [y=1 to 5] x 256 pixels (length) [x =1 to 256], [29] of the red channel (SRB) and the green channel (skin auto-fluorescence) TPM skin images was selected for analysis of the location of SRB relative to the inherent skin barrier morphology. Note that the arbitrarily selected line width of 5 pixels accounts for intensity variations along the width of the slice, while limiting the inclusion of intensities that may result from different SC morphological features in the average value (6). The slice of 5 pixels (width) x 256 pixels (length) was deconstructed into its pixel intensity values to determine the intercellular region width, defined by the fluorescence intensity peak widths. At each position along the length of this slice, the intensities of the corresponding 5 pixels along the width were averaged and then normalized. Because the skin autofluorescence and the SRB fluorescence signals span two different intensity ranges, the fluorescence intensity normalization enables a comparison of the relative changes in the spatial intensity distributions between these two fluorescence intensity signals in the context of the same

[29] Note that in the TPM skin images, 256 pixels corresponds to 100 μm in dimension; therefore, a 100 μm x 100 μm image is actually a collection of 256 x256 = 65536 pixels.

normalized scale, where values of zero reflect the absence of a fluorescence intensity signal and values of 1 reflect maximum fluorescence intensity signals (6).

The green channel skin autofluorescence intensity spectrum, plotted as a function of the length of the slice (in pixels, 1-256), reveals: (i) the peak-to-peak separation which indicates the width of the corneocytes in the SC, and (ii) the peak width which indicates the intercellular spacing that is essentially comprised of the intercellular lipid bilayers and the corneocyte envelopes (see Chapter 1 and (5-8, 11)). The corresponding plot of the SRB fluorescence intensity spectrum for the red channel describes the SRB distribution relative to the inherent skin morphology, as defined by the green channel skin autofluorescence intensity spectrum. The peak widths and peak heights in the normalized average SRB intensity profile in p-FTS samples exposed to aqueous contacting solutions (i), (ii), (iii), and (v) were compared to the peak width and peak height of SRB in the p-FTS sample exposed to the aqueous PBS control contacting solution (iv). Through this comparison, it was possible to determine an enhancement, or a reduction, in the SRB penetration into the corneocytes induced by solutions (i), (ii), (iii), and (v) relative to the PBS control solution (iv). Specifically, an increase in the peak height and a decrease in the peak width indicate less SRB penetration into the corneocytes relative to the intercellular lipid bilayers. This serves as a qualitative indicator of mechanism (ii) above, that is, intercellular lipid bilayer disruption, because a disordering of the lipid bilayers induced by the surfactant-humectant system should result in an increase in the defects or voids in the bilayers, which in turn, should increase the size/number of aqueous pores (see Chapter 1 and (26-28)) through which SRB may penetrate into the lipid bilayers of the SC. Conversely, as the peak height decreases and the peak width increases, there is more SRB present inside the corneocytes relative to the intercellular lipid bilayers. This serves as a qualitative indicator of mechanism (i),

that is, keratin denaturation in the corneocytes, because a disruption of the corneocyte envelope and subsequent keratin denaturation induced by the surfactant-humectant system should result in an increase in SRB penetration into the corneocytes in the SC.

5.3. Theoretical

5.3.1. Determination of Enhancements in Aqueous Pore Characteristics Induced by Surfactant-Humectant Systems Using the SRB Intensity Profiles in the SC

The four intrinsic aqueous pore characteristics of the SC include: (1) the porosity, ε, (2) the tortuosity, τ, (3) the pore radius, r_{pore},[30] and (4) the SC thickness (ΔX) (see Chapter 1 and (29-33, 36)). The goal of the analysis presented here is to obtain quantitative values of the enhancements in the aqueous pore radius, r_{pore}, and in the porosity-to-tortuosity ratio, ε/τ, induced by aqueous contacting solutions (i), (ii), (iii), and (v) – denoted hereafter as the chemical enhancer *(E)*, relative to the aqueous PBS contacting solution (iv) – denoted hereafter as the control *(C)*. In addition to the visual insights that can be obtained from the TPM skin visualization studies (see Sections 5.2.5, 5.4.1, and 5.4.2), the analysis presented below can provide quantitative insight on the modification of the skin barrier induced by the enhancer relative to the control.

[30] Note that r_{pore} is, in fact, an *average* aqueous pore radius (see Section 5.4.3 and Table 5-1). In the case of a size distribution of aqueous pore radii, r_{pore} can be considered to be the *expectation* value of this distribution (see Chapter 6).

Based on the four characteristics of the skin barrier (1)-(4) (see above), one can express the permeability, P_i, of permeant i (where i corresponds to SRB in the TPM skin visualization studies presented here) across the SC through the skin aqueous pores as follows (29, 30, 33):

$$P_i = \frac{\varepsilon D_i^{pore}}{\tau \Delta X} \tag{1}$$

where D_i^{pore} is the diffusion coefficient of permeant i in the aqueous pore. Note that D_i^{pore} can be related to the infinite-dilution diffusion coefficient of permeant i in the bulk aqueous solution, D_i^{∞}, using the following relation (29-31):

$$D_i^{pore} = D_i^{\infty} H(\lambda_i) \tag{2}$$

where $H(\lambda_i)$ is the hindrance factor accounting for the hindered diffusion of permeant i, modeled as a hard sphere of radius, r_i, through the aqueous cylindrical pore, and λ_i is the ratio of the permeant i radius to the aqueous pore radius, that is, $\lambda_i = r_i / r_{pore}$.

Anderson and Quinn have defined $H(\lambda_i)$ for a spherical permeant i in a cylindrical pore as follows (32):

$$H(\lambda_i) = \phi_i \left(1 - 2.1044\lambda_i + 2.089\lambda_i^3 - 0.948\lambda_i^5\right), \text{ for } \lambda_i \leq 0.4 \tag{3}$$

where ϕ_i is the partition coefficient of permeant i, defined as $C_i^{pore} / C_i^{\infty}$, where C_i^{pore} is the concentration of permeant i in the pore, and C_i^{∞} is the concentration of permeant i in the bulk solution. Note that Eq.(3) considers only steric, hard-sphere permeant i-pore wall interactions, and does not account for long-range electrostatic or van der Waals interactions (31, 32).

Using Eq.(2) in Eq.(1), one can express the permeability, P_i, as follows:

$$P_i = \frac{\left(\frac{\varepsilon}{\tau}\right) D_i^{\infty} H(\lambda_i)}{\Delta X} \tag{4}$$

Upon exposing skin to a chemical enhancer, *E*, relative to a control, *C*, in the context of Eq.(4), the following relation between the enhancement in the permeability of permeant *i*, $(E_i)_P$, and the SC aqueous pore radii values corresponding to *E* and *C*, $r_{pore,E}$ and $r_{pore,C}$, reflected in $H(\lambda_i)_E$ and $H(\lambda_i)_C$, respectively, is obtained:

$$(E_i)_P \equiv \frac{(P_i)_E}{(P_i)_C} = \frac{\left(\frac{\varepsilon}{\tau}\right)_E}{\left(\frac{\varepsilon}{\tau}\right)_C} \left(\frac{D_{i,E}^{\infty}}{D_{i,C}^{\infty}}\right) \left[\frac{H(\lambda_i)_E}{H(\lambda_i)_C}\right] \left(\frac{\Delta X_C}{\Delta X_E}\right) \tag{5}$$

The permeability of permeant *i*, P_i, across the SC membrane can also be defined in terms of the flux of permeant *i* across the membrane (in the z direction) as follows (5, 34, 35):

$$P_i = \frac{J_i}{\Delta C_i} = \frac{-D_i^{pore}\left(\frac{dC_i}{dz}\right)}{C_i^d - C_i^r} \tag{6}$$

where the trans-membrane flux, J_i, is predicted by Fick's First Law of Diffusion, and ΔC_i denotes the concentration difference between the donor and the receiver chambers of the diffusion cell. Assuming an infinite donor-infinite receiver condition (see Chapter 2), that is, $C_i^d(t) - C_i^r(t) \approx C_i^d(t) \approx C_i^d(0) \equiv C_i^d$, one can simplify Eq.(6) as follows:

$$P_i = \frac{-D_i^{pore}\left(\frac{dC_i}{dz}\right)}{C_i^d} \tag{7}$$

Next, considering the same probe donor concentration, C_i^d, for the enhancer and the control, one can write the permeability enhancement, $(E_i)_P$, using Eq.(7) as follows:

$$(E_i)_P \equiv \frac{(P_i)_E}{(P_i)_C} = \frac{D_{i,E}^{pore}}{D_{i,C}^{pore}} \frac{(dC_i/dz)_E}{(dC_i/dz)_C} \tag{8}$$

where $D_{i,E}^{pore}$ is the probe (or permeant) *i* pore permeability in the chemical enhancer case, and $D_{i,C}^{pore}$ is the probe (or permeant) *i* pore permeability in the control case. One can then utilize Eq.(2) and express $D_{i,E}^{pore}$ and $D_{i,C}^{pore}$ in terms of $H(\lambda_i)_E$ and $H(\lambda_i)_C$ to obtain the following relation:

$$\frac{D_{i,E}^{pore}}{D_{i,C}^{pore}} = \frac{D_{i,E}^{\infty}}{D_{i,C}^{\infty}} \left(\frac{H(\lambda_i)_E}{H(\lambda_i)_C} \right) = \frac{H(\lambda_i)_E}{H(\lambda_i)_C} \tag{9}$$

where the *infinite dilution* diffusion coefficients of probe *i* were cancelled out because they are equal in the enhancer and in the control solutions, that is, $D_{i,E}^{\infty} = D_{i,C}^{\infty}$.

Next, noting that: (i) $D_{i,E}^{\infty} = D_{i,C}^{\infty}$, and (ii) $\Delta X_E \approx \Delta X_C$ (the SC intrinsic thickness is constant), one can rewrite Eq.(5) as follows:

$$(E_i)_P = \frac{\left(\frac{\varepsilon}{\tau}\right)_E}{\left(\frac{\varepsilon}{\tau}\right)_C} \frac{(D_i^{\infty})_E}{(D_i^{\infty})_C} \left[\frac{H(\lambda_i)_E}{H(\lambda_i)_C} \right] \left(\frac{\Delta X_E}{\Delta X_C} \right) = \frac{\left(\frac{\varepsilon}{\tau}\right)_E}{\left(\frac{\varepsilon}{\tau}\right)_C} \left[\frac{H(\lambda_i)_E}{H(\lambda_i)_C} \right] \tag{10}$$

Because the concentration of SRB (probe *i*) inside the skin, C_i, is proportional to its fluorescence intensity, I_i, (5-8, 11), the SRB concentration gradient in the skin is proportional to the SRB intensity gradient in the skin, which can be determined through the TPM skin visualization measurements (see Section 5.4.3 and 5, 11, 34). Therefore, one can now determine

the enhancement in the SRB concentration gradient inside the skin induced by a chemical enhancer, E, relative to a control, C, through the following relationship:

$$\frac{(dC_i/dz)_E}{(dC_i/dz)_C} = \frac{(dI_i/dz)_E}{(dI_i/dz)_C} \tag{11}$$

Furthermore, using Eq.(9) in Eq.(8) along with Eq.(11), one can express the permeability enhancement of probe i, $(E_i)_P$, as follows:

$$(E_i)_P = \frac{\left(\frac{dI_i}{dz}\right)_E}{\left(\frac{dI_i}{dz}\right)_C}\left[\frac{H(\lambda_i)_E}{H(\lambda_i)_C}\right] \tag{12}$$

Comparing Eq.(12) with Eq.(10), one finds that the enhancement in the porosity-to-tortuosity ratio, ε/τ, is equal to the enhancement in the SRB probe intensity gradient in the skin. Specifically,

$$\frac{\left(\frac{\varepsilon}{\tau}\right)_E}{\left(\frac{\varepsilon}{\tau}\right)_C} = \frac{\left(\frac{dI_i}{dz}\right)_E}{\left(\frac{dI_i}{dz}\right)_C} \tag{13}$$

The partition coefficient, ϕ_i, of permeant i partitioning into a skin aqueous pore from a bulk solution contacting the skin can be evaluated as follows (31, 32):

$$\phi_i = \frac{C_i^{pore}}{C_i^{\infty}} = 2\int_0^{1-\lambda_i} e^{[-E(r)/kT]} r dr \tag{14}$$

Equation (14) indicates that in the case of weak electrostatic and van der Waals interactions, that is, when $E(r) \approx 0$, the permeant-pore partition coefficient, ϕ_i, is equal to $(1-\lambda_i)^2$, which accounts solely for steric, hard-sphere interactions (31). Therefore, when steric interactions dominate, it

follows that the *overall* partition coefficient, Φ_i, of permeant *i* partitioning into *all the available aqueous pores on the surface of the SC* from a bulk solution contacting the skin is given by (31, 32):

$$\Phi_i = \varepsilon\phi_i = \varepsilon(1-\lambda_i)^2 \tag{15}$$

Note that the *overall* partition coefficient, Φ_i, of permeant *i*, is equal to the ratio of the concentration of permeant *i* at the SC surface, $C_i(z=0)$, and the bulk concentration of permeant *i* in the donor solution, C_i^d, that is, $\Phi_i = C_i(z=0)/C_i^d$. The enhancement in the partition coefficient (for steric, hard-sphere SRB probe-aqueous pore wall interactions, see Eq.(15)) can then be related to the ratio of the SRB probe skin surface intensity, for the chemical enhancer *(E)* and for the control *(C),* as follows:

$$(E_i)_\Phi = \frac{\varepsilon_E(1-\lambda_i)_E^2}{\varepsilon_C(1-\lambda_i)_C^2} = \frac{\left[\dfrac{C_i(z=0)}{C_i^d}\right]_E}{\left[\dfrac{C_i(z=0)}{C_i^d}\right]_C} = \frac{I_i(z=0)_E}{I_i(z=0)_C} \tag{16}$$

where we have made the following assumptions: (i) a similar probe *i* (in our case, SRB) donor concentration, C_d^i, for the chemical enhancer and for the control cases (5-8, 11), and (ii) the ratio of the SC surface concentration of probe *i* for the chemical enhancer and for the control cases is identical to the ratio of the corresponding skin surface (z=0) intensities of probe *i* (5-8, 11).

Joe Kushner, in his PhD thesis (11), showed that the effective diffusion path length for SRB does not change significantly relative to untreated skin, when skin samples are exposed to aqueous SDS contacting solutions. Given that: (a) aqueous contacting solution (i) which contains 1 wt% SDS is expected to have the strongest effect on the skin barrier relative to the other

aqueous contacting solutions (ii)-(v), and (b) aqueous contacting solution (i) does not significantly modify the SRB diffusion path length,[31] it is reasonable to assume that $\tau_E = \tau_C$. Therefore, using that $\tau_E = \tau_C$ in Eq.(13), one obtains:

$$\frac{\varepsilon_E}{\varepsilon_C} = \frac{\left(\frac{dI_i}{dz}\right)_E}{\left(\frac{dI_i}{dz}\right)_C} \tag{17}$$

where the ratio of the SRB intensity gradients in the skin induced by E and C, $[(dI_i/dz)_E/(dI_i/dz)_C]$, can be determined experimentally using TPM (see above). Next, using Eq.(17) for $\varepsilon_E/\varepsilon_C$ in Eq.(16), one obtains:

$$\frac{(1-\lambda_i)_E^2}{(1-\lambda_i)_C^2} = \frac{\left[\frac{I_i(z=0)_E}{I_i(z=0)_C}\right]}{\left[\frac{(dI_i/dz)_E}{(dI_i/dz)_C}\right]} \equiv A \tag{18}$$

where $I_i(z=0)_E$ and $I_i(z=0)_C$ are also obtained using TPM. Therefore, the quantity A in Eq.(18) is uniquely determined using the TPM skin visualization measurements. In addition, recalling that $\lambda_{i,E} = r_i/r_{pore,E}$ and $\lambda_{i,C} = r_i/r_{pore,C}$, Eq.(18) shows that:

$$\frac{\left(1-\frac{r_i}{r_{pore,E}}\right)}{\left(1-\frac{r_i}{r_{pore,C}}\right)} = A^{1/2} \tag{19}$$

[31] The SRB diffusion path length through the SC (11, 38) is equal to the product of the tortuosity of the aqueous pores (τ) × SC thickness (ΔX), because being hydrophilic, SRB traverses the SC through the aqueous pores and not through lipoidal pathways (5-8, 11, 26, 29). Since both the diffusion path length and the SC thickness are assumed to be constant, it follows that τ should be constant as well.

Since A can be determined uniquely using the TPM skin visualization measurements, and r_i , the SRB hydrodynamic radius, can be determined to be 5.6Å using the Stokes-Einstein equation (see Chapters 2 and 3), by solving Eq.(19), it becomes possible to obtain $r_{pore,E}$, and thereby, the enhancement in the pore radius induced by E relative to C, $E_{r_{pore}} = r_{pore,E} / r_{pore,C}$ (see Section 5.4) *if* $r_{pore,C}$ *can be determined.* In Chapters 2 and 3, I used a previously published, well-accepted aqueous porous pathway model that is based on the hindered-transport of a hydrophilic permeant (Mannitol) and ions through aqueous pores in the SC (29-33, 36), and showed that $r_{pore,C}$ = 20±3Å. Using this value of $r_{pore,C}$ = 20±3Å, along with the value of A determined using TPM, in Eq.(19) it is then possible to determine $r_{pore,E}$ as well as the enhancement in the pore radius, $E_{r_{pore}}$.

5.4. Results and Discussion

5.4.1. Comparison of the TPM Skin Images Close to the SC Surface (z = 3μm) with the TPM Skin Images Below the SC (z = 20μm)

In *Figures 5-2 and 5-3*, I show representative TPM skin images (100 μm × 100 μm) of SRB in p-FTS samples that were exposed to aqueous contacting solutions (i)-(v) (see Section 5.2.2) and visualized at a depth of z = 3 μm below the skin surface, and at a depth of z = 20 μm below the skin surface. The corneocytes are denoted by C (see *Figures 5-2(a), (c), and (e)* and *Figures 5-3(a) and (c))*, and the nuclei of the keratinocytes are denoted by N (see *Figures 5-2(b), (d), and (f)* and *Figures 5-3(b) and (d))*. One can clearly see that the TPM skin images corresponding to aqueous contacting solution (i) (1 wt% SDS), see *Figures 5-2 (a) and (b)*, are the brightest among all the reported TPM skin images (see *Figures 5-2 and 5-3* along with their

associated color scale bars). This is because the TPM skin images shown in *Figures 5-2 (a)* and *(b)* correspond to a p-FTS sample exhibiting a larger extent of skin barrier perturbation, and consequently, show a larger amount of the SRB fluorescent probe that has penetrated into the skin (both at z = 3 μm and at z = 20 μm), than all the other TPM skin images shown in *Figures 5-2* and *5-3*.

In Chapter 2, I have already shown that the addition of 10 wt% Glycerol to a SDS contacting solution above the CMC significantly inhibits SDS skin penetration by reducing the porosity-to-tortuosity ratio, ε/τ, and the average pore radius, r_{pore}, of the aqueous pores in the SC, such that the SDS micelles cannot penetrate into the skin barrier. Therefore, one would expect less SDS skin penetration and associated smaller extent of skin barrier perturbation, and consequently, lower amounts of SRB in the skin, due to the presence of Glycerol in the aqueous SDS contacting solution. The TPM skin images in *Figures 5-2(c) and (d)*, when compared to those in *Figures 5-2 (a)* and *(b)*, show that, indeed, a smaller extent of skin barrier perturbation due to the presence of Glycerol in an aqueous SDS contacting solution results in a smaller extent of SRB skin penetration. A smaller amount of SRB in the skin barrier, in turn, generates a weaker fluorescence signal. Consequently, the TPM skin images obtained upon exposing p-FTS samples to solution (ii) (1 wt% SDS+10 wt% Glycerol) (see *Figures 5-2 (c) and (d) with their associated color scale bars*) exhibit a dark red color, as opposed to the bright red color seen in the TPM skin images of p-FTS samples exposed to contacting solution (i) (1 wt% SDS), which reflects a larger amount of SRB in the skin barrier (see *Figures 5-2 (a) and (b) with their associated color scale bars*).

The corneocytes in the TPM skin image shown in *Figure 5-2 (a)* exhibit a color gradient which is not exhibited by the corneocytes in the TPM skin image shown in *Figure 5-2 (c)*, indicating that the presence of 10 wt% Glycerol in the SDS contacting solution minimizes SRB penetration into the corneocytes. This is because Glycerol minimizes SDS skin penetration, thereby minimizing the ability of SDS to interact with the keratins as well as with the lipids comprising the corneocyte envelopes which surround the corneocytes in the stratum corneum (SC). Consequently, the corneocyte envelopes, which would otherwise be damaged by SDS (12, 19, 22), are not compromised, and prevent SRB from penetrating into the corneocytes.

A related observation is the formation of LTRs (localized transport regions) in the TPM skin image shown in *Figure 5-2 (a)*, and the absence of LTRs in the TPM skin image shown in *Figure 5-2 (c)*. The LTRs are localized regions within the skin barrier characterized by a larger extent of skin barrier perturbation. Consequently, a permeant diffusing across the skin barrier would exhibit a high LTR permeability relative to the non-LTR permeability and to the overall skin barrier permeability (37, 38). Kushner et al. (37) and Pliquet et al. (38) have observed LTRs in the SC upon exposing skin to ultra sound+SDS and to high voltage electric pulses, respectively. It is noteworthy that the diameters of the LTRs reported by Pliquet et al. (38) are in the range of 40-80 μm, similar to the diameters of the LTRs observed in *Figure 5-2 (a)*. The LTRs observed by Kushner et al. (37) are larger in diameter (10-40 mm), because ultrasound+SDS acts as a more effective enhancer than the ones considered in this study or by Pliquet et al. (38).

It is also important to note that the LTRs are not sweat ducts or hair follicles, as observed in this study, by Kushner et al. (37), and by Pliquet et al. (38). Glycerol may minimize the formation of LTRs by minimizing SDS skin penetration and associated damage to the corneocyte

envelopes and to the corneocytes. Such LTRs do not form in the skin barrier exposed to aqueous contacting solution (iii) (1 wt% SCI), as shown in *Figures 5-2 (e) and (f)*. This is because SDS, being a harsher skin agent than SCI (see Chapters 2 and 3, and (19)), interacts strongly with the skin barrier. Because of the inherent heterogeneity of the skin barrier, the SDS-skin barrier interaction is heterogeneous in nature. One of the manifestations of this heterogeneous interaction is the formation of heterogeneous LTRs in the skin barrier. The milder surfactant, SCI, exhibits a weaker skin barrier interaction relative to SDS, particularly with the corneocyte envelopes and the corneocyte keratins (see Chapter 3 and (19)). Therefore, SCI does not induce the formation of LTRs in the skin barrier.

At z = 20 μm, the TPM skin image of the p-FTS sample exposed to solution (i) shows more SRB relative to the TPM skin images of the p-FTS samples exposed to solutions (ii)-(v) (see *Figure 5-2 (b)* with its associated color scale bar and compare it to *Figures 5-2 (d)* and *(f)*, and to *Figures 5-3 (b)* and *(d)*, with their associated color scale bars). Therefore, not only does SDS (1 wt%) induce a greater extent of skin barrier perturbation, but in addition, this perturbation extends *deeper* into the skin barrier relative to the skin barrier perturbation induced by aqueous contacting solutions (ii)-(v).

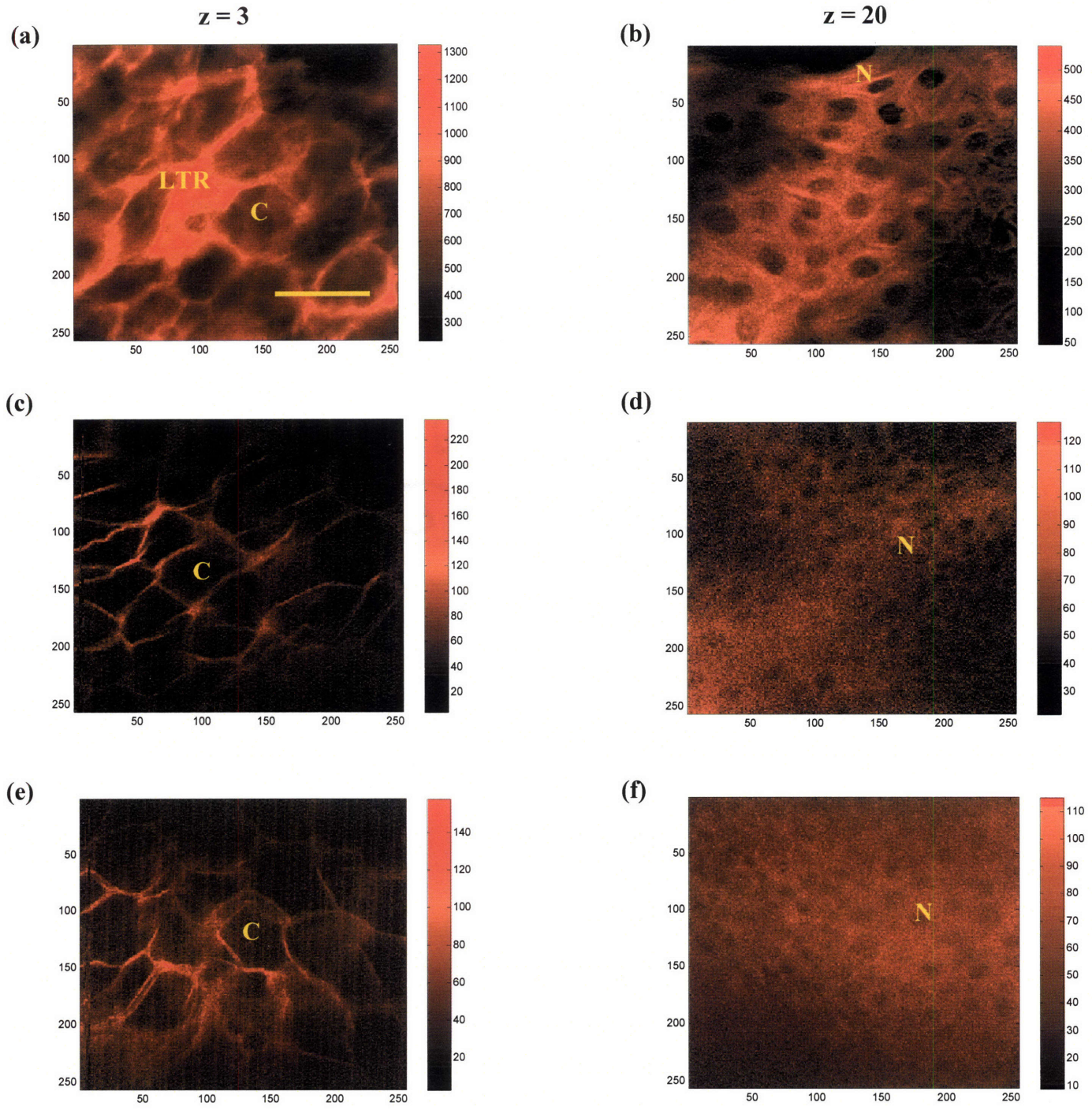

Figure 5-2. TPM images of SRB in p-FTS samples that were exposed to aqueous contacting solutions (i) (1 wt% SDS), (ii) (1 wt% SDS+10 wt% Glycerol), and (iii) (1 wt% SCI), and visualized at a depth of: (i) 3 μm below the skin surface (z=3), shown in (a), (c), and (e), respectively, and (ii) 20 μm below the skin surface (z=20), shown in (b), (d), and (f), respectively. The color scale bars indicate an increase in SRB concentration as the color progresses from a low value close to zero (black) to a high value (red). Key: C – corneocyte, N – nucleus of a keratinocyte, LTR – localized transport region, and yellow line in (a) – 25 μm.

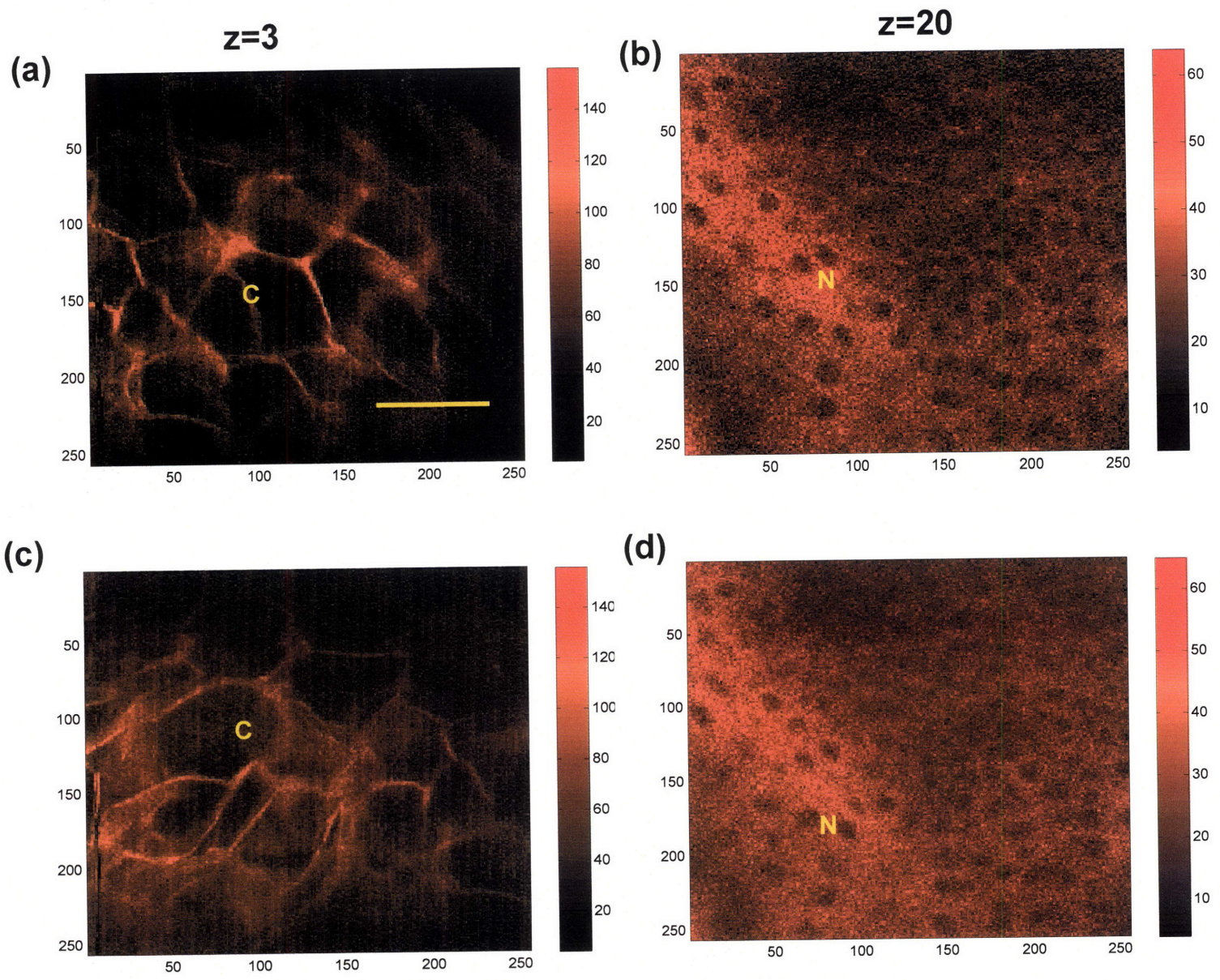

Figure 5-3. TPM images of SRB in p-FTS samples that were exposed to aqueous contacting solutions (iv) (PBS Control) and (v) (10 wt% Glycerol), and visualized at a depth of: (i) 3 μm below the skin surface (z=3), shown in (a) and (c), respectively, and (ii) 20 μm below the skin surface (z=20), shown in (b) and (d), respectively. The color scale bars indicate an increase in SRB concentration as the color progresses from a low value close to zero (black) to a high value (red). Key: C – corneocyte, N – nucleus of a keratinocyte, and yellow line in (a) – 25 μm.

5.4.2. Analysis of the Dual-Channel TPM Skin Images Close to the SC Surface ($z = 3\mu m$)

The dual-channel TPM skin images of p-FTS samples exposed to aqueous contacting solutions (i)-(v), at $z = 3\mu m$, are shown in *Figures 5-4, 5-5, and 5- 6*. In all these figures: (a) the SRB probe fluorescence (red channel) images are shown in the top panels (*Figures 5-4 (a) and (d), Figures 5-5 (a) and (d), and Figure 5-6 (a)*), (b) the skin autofluorescence (green channel) images are shown in the bottom panels (*Figures 5-4 (c) and (f), Figures 5-5 (c) and (f), and Figure 5-6 (c)*), and (c) the overlay of the normalized SRB probe fluorescence (the red line) and the skin autofluorescence (the green line) spectra are shown in the middle panels (*Figures 5-4 (b) and (e), Figures 5-5 (b) and (e), and Figure 5-6 (b)*).

Yu et al. have shown that the skin autofluorescence spatial intensity distribution is independent of the specific SRB skin penetration pathways (6). As a result, the SRB skin spatial distributions can be characterized relative to the green channel skin autofluorescence maps of the intrinsic skin morphology (6). In the green channel TPM skin images in *Figures 5-4, 5-5,* and *5-6,* the corneocytes correspond to the dark polyhedral regions surrounded by the green autofluorescence of the SC intercellular lipid bilayers. The SRB skin spatial distributions shown in these figures provide evidence that aqueous contacting solutions (ii)-(v) primarily interact with the intercellular lipid bilayers of the SC and induce SRB to be localized within the bilayer domains of the SC. On the other hand, aqueous contacting solution (i), containing 1 wt% SDS, interacts strongly with the lipid bilayers as well as with the corneocytes of the SC, thereby inducing SRB penetration into the corneocytes as well as into the lipid bilayers of the SC (compare *Figures 5-4 (a) and (c)*).

A quantification of the observations made above about the dual-channel TPM skin images is presented below. For this purpose, a linear image deconstruction analysis was used (see Section 5.2.6). The normalized red and green channel fluorescence intensities within a linear deconstruction path of 256 × 5 pixel skin area (see the yellow rectangles in the top and bottom panels in *Figures 5-4, 5-5, and 5-6*) were examined to quantify the SC morphological modifications induced by aqueous contacting solutions (i)-(v). As mentioned above, these plots are shown in the middle panels in *Figures 5-4, 5-5, and 5-6*. In *Figure 5-4 (b)*, the autofluorescence spectrum (green line) of the p-FTS sample exposed to solution (i) (1 wt% SDS) exhibits one major peak at x = 102 pixels, and three minor peaks at x = 10 pixels, x = 163 pixels, and x = 225 pixels. These four peaks correspond to the positions of the intercellular lipid bilayer regions shown in the yellow box marking the linear path evaluated in the corresponding green channel TPM skin image (see *Figure 5-4 (c)*).[32] The red channel TPM skin image shown in *Figure 5-4 (a)* also has these 4 peaks as observed in the green channel TPM skin image (see *Figure 5-4 (c)).* The SRB probe intensity spectrum peak widths (see the red line in *Figure 5-4 (b))* are larger than those corresponding to the skin autofluorescence peaks (see the green line in *Figure 5-4 (b))*. This difference between the SRB probe fluorescence and the skin autofluorescence intensity peak widths provides unambiguous evidence of SDS-induced SRB penetration into the corneocytes of the SC (see Section 5.2.5 and (5-8, 11, 34)). In addition, the minor peak heights corresponding to the red channel spectrum are larger than the minor peak heights corresponding to the green channel spectrum (see the red and green lines in *Figure 5-4 (b)*). This provides evidence that SDS promotes SRB penetration into the lipid bilayers, in addition to promoting penetration into the corneocytes. These results indicate that not only does

[32] Note that the distance between each of these peaks corresponds approximately to the length of a corneocyte (20-40 μm), thereby implying that the positions of these peaks denote the locations of the intercellular bilayer regions in the SC (5-8, 11).

SDS rupture the corneocyte envelopes and denatures the corneocyte keratins, but that it also disrupts the intercellular lipid bilayers, thereby inducing SRB penetration into the corneocytes (the bricks) and into the lipid bilayers (the mortar) in the SC.

In *Figure 5-4 (e)*, the autofluorescence spectrum (green line) of the p-FTS sample exposed to solution (ii) (1 wt% SDS+10 wt% Glycerol) exhibits two major peaks, at x = 50 pixels and x = 145 pixels, and three minor peaks at x = 1 pixels, x = 73 pixels, and x = 254 pixels. These five peaks again correspond to the positions of the intercellular lipid bilayer regions (see above). The SRB probe intensity spectrum peak heights (see the red line in *Figure 5-4 (e))* are almost identical to those corresponding to the skin autofluorescence peaks (see the green line in *Figure 5-4 (e)).* This indicates that contacting solution (ii) does not induce any significant SRB penetration into the lipid bilayers of the SC. The peak widths corresponding to the peaks at x = 1 pixels and x = 145 pixels are larger for the SRB probe fluorescence intensity spectrum (the red line in *Figure 5-4 (e))* relative to the skin autofluorescence intensity spectrum (the green line in *Figure 5-4 (e))*. This indicates penetration of the SRB probe into these regions, which are, in fact, the corneocyte regions of the SC. Therefore, these TPM results indicate that adding 10 wt% Glycerol to an aqueous 1 wt% SDS contacting solution mitigates SDS-induced intercellular lipid bilayer disruption, but does not eliminate SDS-induced SRB penetration into the corneocyte regions of the SC.

In *Figure 5-5 (b),* the autofluorescence spectrum (green line) of the p-FTS sample exposed to solution (iii) (1 wt% SCI) exhibits two major peaks, at x = 1 pixels and x = 107 pixels, and three minor peaks at x = 57 pixels, x = 158 pixels, and x = 210 pixels. These five peaks again correspond to the positions of the intercellular lipid bilayer regions (see above). The SRB probe intensity spectrum peak heights (see the red line in *Figure 5-5 (b))* are higher than

those corresponding to the skin autofluorescence peaks (see the green line in *Figure 5-5 (b)*). This indicates that contacting solution (iii) promotes SRB penetration into the intercellular lipid bilayers of the SC. However, upon comparing *Figures 5-5 (a), (b), (c)* with *Figures 5-4 (a), (b), (c)*, which correspond to 1 wt% SDS, it is clear that 1 wt% SCI induces a lower SRB penetration into the intercellular lipid bilayers relative to 1 wt% SDS. [33] This finding is consistent with transmission electron micrography (TEM) studies on the effect of SCI on the skin barrier reported by Ananthapadmanabhan et al. (19, 39). Specifically, these authors found that SCI does not induce skin-dryness relative to SDS, because SCI disorders the intercellular lipid bilayer structure in the SC to a lower extent than SDS (see Chapter 3, and (19, 39)). The SRB probe intensity spectrum peak widths (see the red line in *Figure 5-5 (b)*) are slightly larger than the skin autofluorescence intensity spectrum peak widths (see the green line in *Figure 5-5 (b)*). This difference between the SRB probe fluorescence and the skin autofluorescence intensity peak widths provides evidence of SCI-induced SRB penetration into the corneocytes, albeit to a lower extent than that induced by SDS (see above).[34]

In *Figure 5-5 (e),* the peaks corresponding to the skin autofluorescence intensity spectrum are lower in height than those corresponding to the SRB probe fluorescence intensity spectrum. This indicates that when p-FTS samples are exposed to the PBS control solution (contacting solution (iv)) followed by exposure to the SRB probe solution, SRB is located within the intercellular lipid bilayers. The peak widths corresponding to the red and green channels in

[33] Comparing *Figures 5-4 (d), (e), (f)* with *Figures 5-5 (a), (b), (c),* one can observe that contacting solution (iii) containing 1 wt% SCI promotes a lower extent of SRB penetration into the intercellular lipid bilayers relative to contacting solution (ii) containing 1 wt% SDS+10 wt% Glycerol.

[34] Indeed, SDS induces a larger difference in the SRB fluorescence and skin autofluorescence peak widths than SCI (compare *Figures 5-4 (b) and 5-5 (b)*). This is because SDS, being a harsh surfactant, interacts more strongly with the corneocyte envelopes and corneocyte keratins than SCI, which is a mild surfactant (see Chapters 2 and 3, and (19, 39)).

Figure 5-5 (e) are very similar, thereby showing that very little SRB probe is present in the corneocyte regions of the SC.

In *Figure 5-6 (b)*, the intensity spectrum peaks corresponding to the skin autofluorescence is almost identical to that corresponding to the SRB probe fluorescence intensity spectrum, including the peak positions, widths, and heights. This indicates that very little SRB probe is present in the intercellular lipid bilayer region of the SC. In addition, the widths of the peaks corresponding to the red channel (SRB probe fluorescence) intensity are similar to those corresponding to the green channel (skin autofluorescence) intensity. Therefore, very little SRB probe is present in the corneocyte region of the SC. Indeed, when p-FTS samples are exposed to solution (v) (10 wt% Glycerol), Glycerol reduces the average pore radii and the porosity-to-tortuosity ratio of the aqueous pores in the SC (see Chapter 2) through which hydrophilic permeants like SRB penetrate into the SC. As a result, p-FTS samples that were exposed to solution (v) containing 10 wt% Glycerol, and subsequently exposed to the SRB contacting solution, show very little SRB penetration into the SC. Therefore, SRB is not present in any significant amount either in the intercellular lipid bilayer region or in the corneocyte region of the SC.

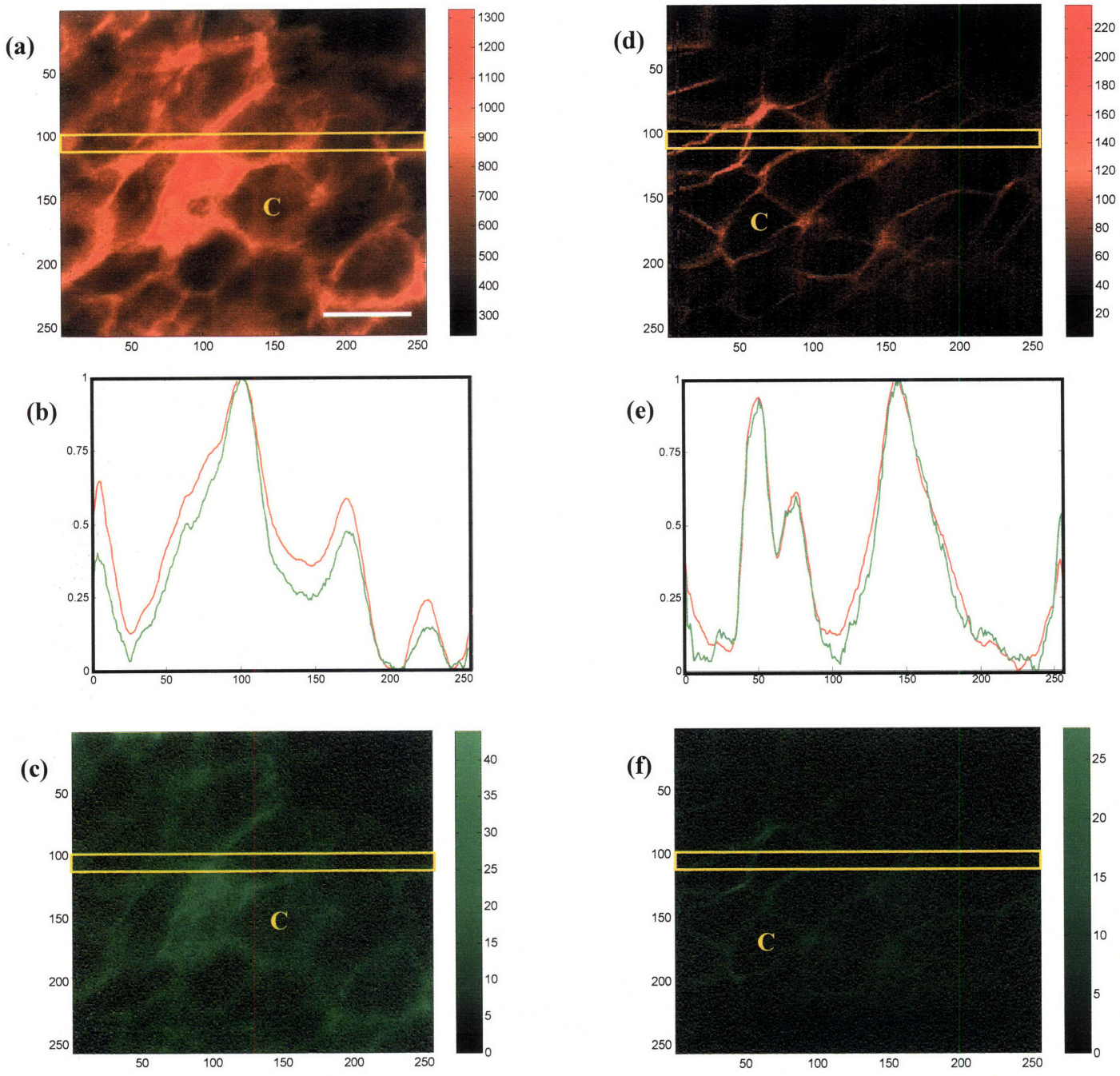

Figure 5-4. Dual-channel TPM skin images of p-FTS samples at z=3 μm that were exposed to solution (i, 1 wt% SDS): (a) – SRB fluorescence (red channel), (c) – skin autofluorescence (green channel), with the linear fluorescence intensity deconstruction regions marked by the yellow rectangles. The red and the green lines in (b) represent the normalized SRB fluorescence and skin autofluorescence spectra, respectively. Figures (d), (f), and (e) are the analogous figures for p-FTS samples that were exposed to solution (ii, 1 wt% SDS+10 wt% Glycerol). The color scale bars indicate an increase in SRB intensity for the red channel images (a) and (d), and an increase in skin autofluorescence intensity for the green channel images (c) and (f), as the color progresses from a low value close to zero (black) to a high value (red/green). Key: C – corneocyte, white line in (a) – 25 μm.

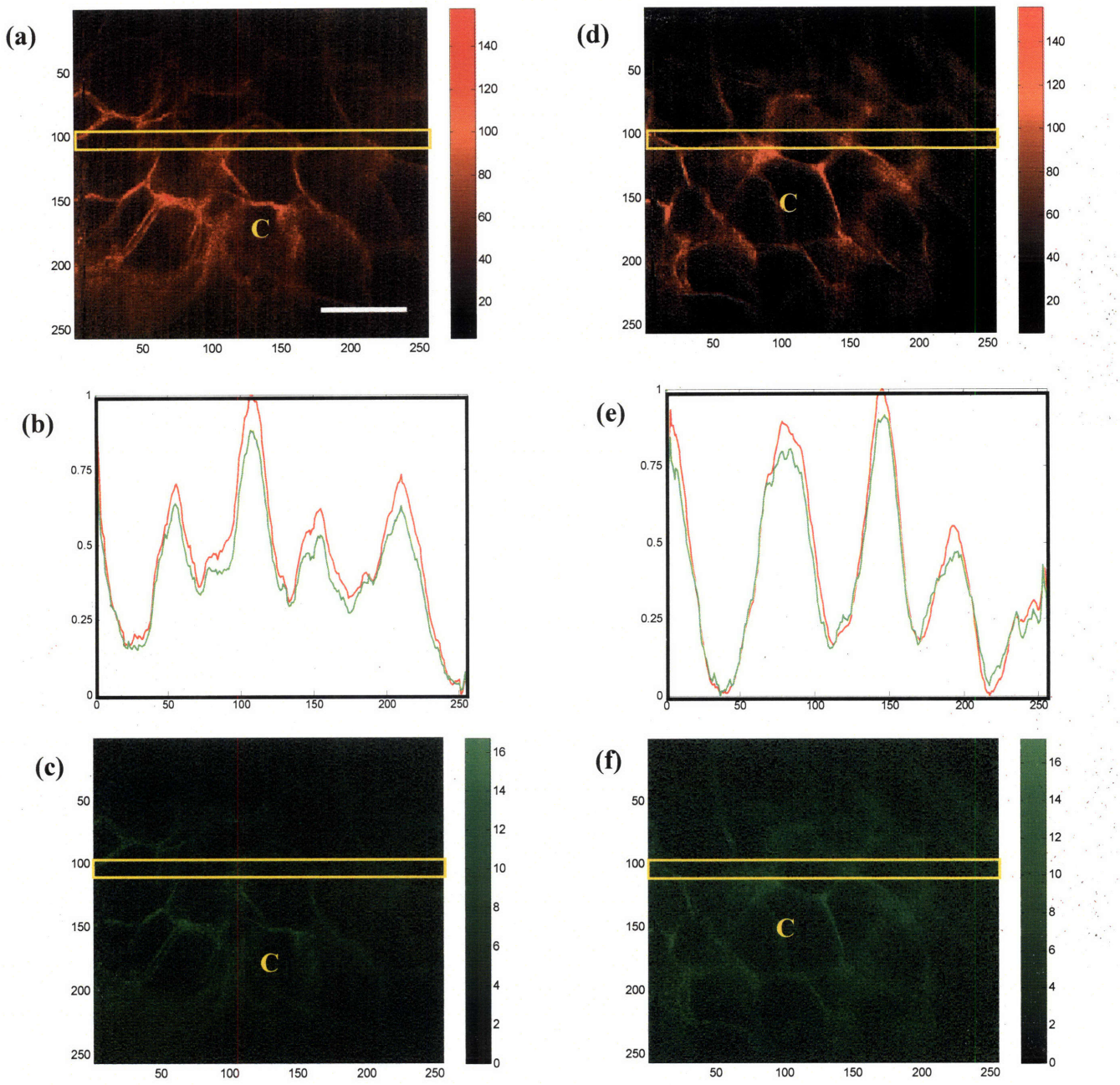

Figure 5-5. Dual-channel TPM skin images of p-FTS at z=3 μm that were exposed to solution (iii, 1 wt% SCI): (a) – SRB fluorescence (red channel), (c) – skin autofluorescence (green channel), with the linear fluorescence intensity deconstruction regions marked by the yellow rectangles. The red and the green lines in (b) represent the normalized SRB fluorescence and skin autofluorescence spectra, respectively. Figures (d), (f), and (e) are the analogous figures for p-FTS samples exposed to solution (iv, PBS Control). The color scale bars indicate an increase in SRB intensity for the red channel images (a) and (d), and an increase in skin autofluorescence intensity for the green channel images (c) and (f), as the color progresses from a low value close to zero (black) to a high value (red/green). Key: C – corneocyte, white line in (a) – 25 μm.

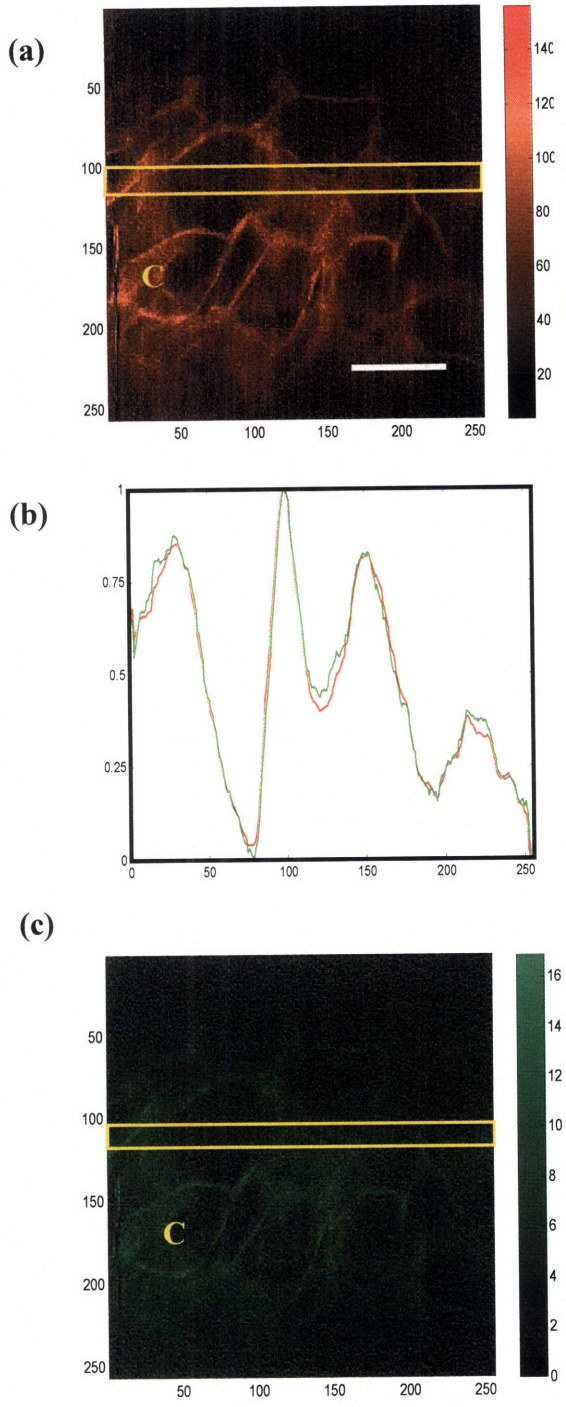

Figure 5-6. Dual-channel TPM skin images of p-FTS samples at z=3μm that were exposed to solution (v, 10 wt% Glycerol): (a) – SRB fluorescence (red channel), (c) – skin autofluorescence (green channel), with the linear fluorescence intensity deconstruction regions are marked by the yellow rectangles. The red and the green lines in (b) represent normalized SRB fluorescence and skin autofluorescence spectra, respectively. The color scale bars indicate an increase in SRB intensity for the red channel image (a), and an increase in skin autofluorescence intensity for the green channel image (c), as the color progresses from a low value close to zero (black) to a high value (red/green). Key: C – corneocyte, white line in (a) – 25 μm.

5.4.3. Analysis of the Aqueous Pore Pathway Characteristics Using SRB Intensity Profiles as a Function of SC Depth in the Context of a Hindered-Transport Model

The five SRB fluorescence intensity profiles corresponding to solutions (i)-(v) are plotted as a function of the skin barrier depth (z) in *Figure 5-7*. One can clearly see that the SRB fluorescence intensity count induced at the SC surface (z=0) by aqueous contacting solutions (i)-(v) follows the order (from the highest to the lowest): (i) > (ii) > (iii) > (iv) > (v). Specifically, for all these five contacting solutions, the aqueous contacting solution with 1 wt% SDS induces the highest SRB-skin partition coefficient.[35] Interestingly, the SRB-skin partition coefficient induced by the 1 wt% SDS aqueous contacting solution is significantly reduced, by more than three times, when 10 wt% Glycerol is added to the solution (see *Figure 5-7 and Table 5-1*). This provides additional evidence that Glycerol mitigates the ability of SDS to interact strongly with the SC surface, thereby reducing skin permeability. In addition, the 1 wt% SDS aqueous contacting solution induces significantly *deeper* penetration of SRB into the skin relative to aqueous contacting solutions (ii)-(v) (see *Figure 5-7*). Note that a similar observation was made in Section 5.4.1 when comparing the color scale bars associated with *Figure 5-2 (b)* to those associated with *Figures 5-2 (d) and (f), and with Figures 5-3 (b) and (d).*

[35] Note that the SRB-skin partition coefficient between the donor contacting solution and the skin, ϕ, is proportional to the SRB fluorescence intensity count induced at the SC surface (z=0) (see Section 5.3.1).

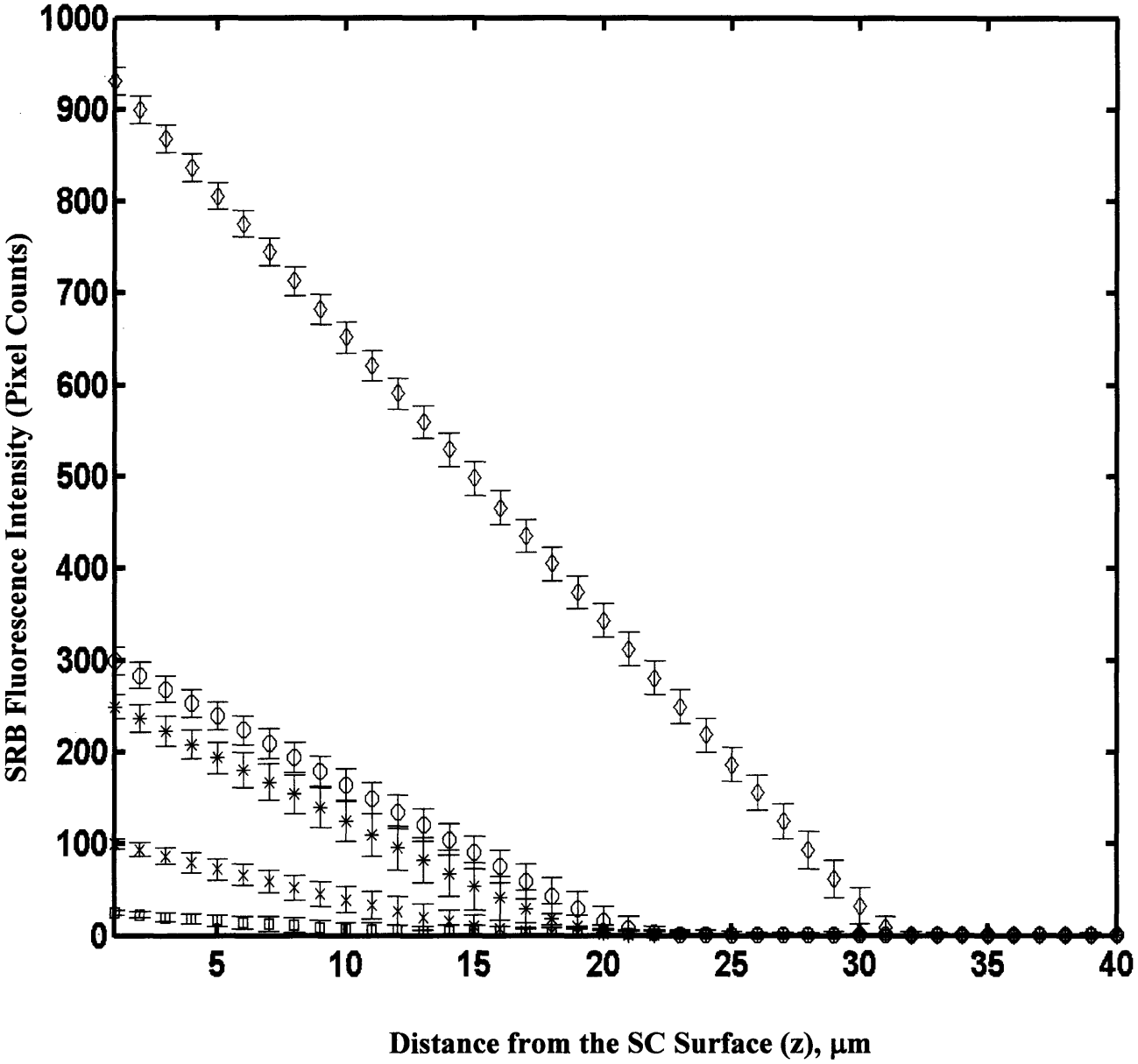

Figure 5-7. Quantification of the SRB probe intensity in units of pixel count as a function of the skin barrier depth (z) from the skin surface (z = 0) for p-FTS samples exposed to aqueous contacting solutions (i)-(v). The error bars represent standard errors based on 6 skin imaging sites on 7 p-FTS samples. Key: ◊ – SDS (1 wt%), ○ – SDS (1 wt%)+Glycerol (10 wt%), * – SCI (1 wt%), × – PBS Control, and □ – Glycerol (10 wt%).

Therefore, adding 10 wt% Glycerol to a 1 wt% aqueous SDS contacting solution not only reduces the SRB-skin partition coefficient, but it also reduces the depth to which SDS can drive SRB into the skin. Both of these findings provide evidence of the ability of the humectant, Glycerol, to mitigate SDS-induced skin barrier perturbation. Aqueous contacting solutions (iii)-(v) lead to significantly smaller values of SRB-skin partition coefficients and SRB-skin penetration depths, relative to contacting solution (i) containing 1 wt% SDS.

The enhancements in the intercepts and in the slopes of the SRB fluorescence intensity profiles induced by aqueous contacting solutions (i)-(v) were evaluated relative to the PBS control, that is, relative to aqueous contacting solution (iv).[36] These results are reported in *Table 5-1*. Using an average aqueous pore radius corresponding to the PBS control ($r_{pore,C}$) of 20±3Å (see *Table 5-1* and Chapter 2) in the context of the theoretical model presented in Section 5.3.1, $r_{pore,E}$ values (denoted as r_{pore} in *Table 5-1*) induced by aqueous contacting solutions (i), (ii), (iii), and (v) were determined, and are reported in *Table 5-1*. These r_{pore} values are in excellent agreement with the r_{pore} values reported in Chapters 2, 3, and 4.

[36] Note that the enhancement in the intercept induced by aqueous contacting solutions (i)-(v) relative to the control (aqueous contacting solution (iv)) is equal to the enhancement in the overall SRB partition coefficient, $(E_i)_\Phi$ (see Section 5.3.1). In addition, note that the $(E_i)_\Phi$ values were used to determine $r_{pore,E}$ values by inputting $r_{pore,c}$ = 20±3Å (see Section 5.3.1).

Table 5-1. Enhancements in the slopes and intercepts of the SRB fluorescence intensity profiles as a function of skin barrier depth, and the corresponding theoretically computed aqueous pore characteristics (the porosity-to-tortuosity ratio, ε/τ, and the average pore radius, r_{pore}) induced by aqueous contacting solutions (i), (ii), (iii), and (v) relative to aqueous contacting solution (iv, the control).

Aqueous Contacting Solution	E(Slope)	E(Intercept)	E(ε/τ)*	r_{pore}
(i) 1 wt% SDS	6.5±1.5	9.3±0.9	6.5±1.5	34±5
(ii) 1 wt% SDS+10 wt% Glycerol	3.1±1.2	2.8±0.7	3.1±1.2	19±6
(iii) 1 wt% SCI	2.5±1.3	2.4±0.6	2.5±1.3	28±5
(iv) PBS Control	1	1	1	20±3**
(v) 10 wt% Glycerol	0.5±0.2	0.3±0.2	0.5±0.2	13±5

* Note that E(Slope) = E(ε/τ), as discussed in Section 5.3.1.

** This r_{pore} value, induced by aqueous contacting solution (iv), was determined previously using Log P-Log R measurements in the context of a hindered-transport aqueous porous pathway model (see Chapter 2), and has been utilized as an input to the model described in Section 5.3.1 to determine the r_{pore} values induced by aqueous contacting solutions (i), (ii), (iii), and (v).

The findings reported here indicate that: (a) an aqueous contacting solution of 1 wt% SDS (a harsh surfactant) induces the largest ε/τ value relative to the other four aqueous contacting solutions considered, (b) an aqueous contacting solution of 1 wt% SCI (a mild surfactant) induces a r_{pore} value that is closer to that induced by an aqueous contacting solution of 1 wt% SDS, while inducing a significantly smaller ε/τ value, (c) adding 10 wt% Glycerol to the 1 wt% SDS aqueous contacting solution significantly reduces the r_{pore} and ε/τ values, and (d) an aqueous contacting solution of 10 wt% Glycerol induces significantly smaller r_{pore} and ε/τ values than does the PBS control.

5.5. Conclusions

The TPM skin visualization studies reported in this chapter revealed that SDS induces corneocyte damage by rupturing corneocyte envelopes and denaturing keratins. This may further induce the creation of intra-corneocyte penetration pathways once SDS "opens-up" the cross-linked keratin structure of the corneocytes. Therefore, a group of such damaged adjacent corneocytes, taken together, may exhibit a large number of intra-corneocyte penetration pathways that may result in a localized transport region (LTR). A simultaneous quantitative analysis of the red and the green channel TPM skin images showed that an aqueous contacting solution of 1 wt% SDS+10 wt% Glycerol does not significantly induce corneocyte damage or LTR formation. Therefore, taken together with the results presented in Chapter 2, these dual-channel TPM images provide additional evidence that adding 10 wt% Glycerol to a 1 wt% SDS aqueous contacting solution significantly mitigates the ability of SDS to penetrate into the SC and interact with the keratins of the corneocytes and induce corneocyte damage. The dual-channel TPM images of p-FTS exposed to an aqueous 1 wt% SCI contacting solution showed a lower extent of SRB penetration into the corneocytes and into the intercellular lipid bilayers relative to the aqueous contacting solution of 1 wt% SDS. The PBS control solution induced localization of the SRB probe within the intercellular lipid bilayers surrounding the corneocytes of the SC. In addition, aqueous contacting solutions containing 10 wt% Glycerol showed the least extent of lipid bilayer perturbation, and no effect on the corneocytes of the SC, relative to the other surfactant/humectant aqueous contacting solutions considered here. This important finding is consistent with the results of the studies reported in Chapters 2 and 4, where I showed that an aqueous contacting solution of 10 wt% Glycerol reduces the porosity-to-tortuosity ratio

and the average radius of the aqueous pores through which the hydrophilic SRB probe molecules can penetrate into the SC.

For the five aqueous contacting solutions considered in this chapter, most of the SRB probe that penetrates into the skin barrier is present in the SC, and the probe intensity decays significantly as one visualizes the layers in the epidermis below the SC. I have quantified the amount of SRB that penetrated into the SC as a function of the SC depth upon contacting p-FTS separately with the five aqueous contacting solutions (i)-(v). This TPM analysis revealed that SDS enhances the probe partition coefficient the most, and that the extent of skin barrier perturbation induced by aqueous contacting solutions follows the order (from the highest to the lowest): (i) > (ii) > (iii) > (iv) > (v), which is consistent with the results of the in vitro ranking metric reported in Chapter 4.

In the next chapter, Chapter 6, I will investigate the effects of adding 10 wt% Glycerol to SDS aqueous contacting solutions on the skin aqueous pores by developing a theoretical pore size distribution model.

5.6. References

1. P.T.C.So, H.Kim, and I.E.Kochevar, Two-photon deep tissue ex vivo imaging of mouse dermal and subcutaneous structures, *Optics Express*, 3(9):p. 339-350 (1998).

2. P.T.C.So, C.Y.Dong, B.R.Masters, and K.M.Berland, Two-photon excitation fluorescence microscopy, *Annu. Rev. Biomed. Eng.* 02:p. 399-429(2000).

3. J.C.Malone, A.F.Hood, T.Conley, J.Nurnberger, L.A.Baldridge, J.L.Clendenon, K.W.Dunn, and C.L.Phillips, Three-dimensional imaging of human skin and mucosa by two-photon laser scanning microscopy, *Journal of Cutaneous Pathology*, 29:p. 453-458 (2002).

4. W.Denk, J.H.Strickler, and W.W.Webb, Two-photon laser scanning fluorescence microscopy, *Science*, 248:p. 73-76 (1990).

5. B.Yu, C.Y.Dong, P.T.So, D.Blankschtein, and R.Langer, In vitro visualization and quantification of oleic acid-induced changes in transdermal transport using two-photon fluorescence microscopy, *Journal of Investigative Dermatology,* 117:p. 16-25 (2001).

6. B.Yu, K.H.Kim, P.T.C.So, D.Blankschtein, and R.Langer, Visualization of oleic acid-induced transdermal diffusion pathways using two-photon fluorescence microscopy, *Journal of Investigative Dermatology*, 120:p. 448-455 (2003).

7. B.Yu, P.T.So, D.Blankschtein, and R.Langer, Evaluation of fluorescent probe surface intensities as an indicator of transdermal permeant distributions using wide-area two-photon fluorescence microscopy, *Journal of Pharmaceutical Science, 92*:p. 2354-2365 (2003).

8. B.Yu, K.H.Kim, P.T.C.So, D.Blankschtein, and R.Langer, Topographic heterogeneity in transdermal transport revealed by high-speed two-photon microscopy: Determination of representative skin sample sizes, *Journal of Investigative* Dermatology, 118:p. 1085-1088 (2002).

9. B.R.Masters, P.T.C.So, and E.Gratton, Multiphoton excitation fluorescence microscopy and spectroscopy of in vivo human skin, *Biophysical Journal*, 72:p. 2405-2412 (1997).

10. R.Na, I.Stender, L.Ma, and H.C.Wulf, Autofluorescence Spectrum of skin: Component bands and body site variations, *Skin Research and Technology*, 6: p. 112-117 (2000).

11. J.Kushner, "Theoretical and experimental investigations of passive and ultrasound-enhanced transdermal drug delivery", Ph.D. thesis, Department of Chemical Engineering, Massachusetts Institute of Technology, Cambridge, MA, *USA (2006).*

12. R.L.Bronaugh, and H.I.Maibach, In vitro models for human percutaneous absorption, In H.I.Maibach et al. (Eds.). Models in Dermatology, Karger, Bassel, Vol.2, p.178-188, (1985).

13. R.L.Bronaugh, R.F.Stewart, E.R.Congdon, A.L.Giles. Jr, Methods for in vitro pecutaneous absorption studies. I. Comparison with in vivo results, *Toxicol. Appli. Pharmacol*, 62:p. 474-480 (1982).

14. R.M.Adams, Occupational skin disease, in Fitzpatrick's dermatology in general medicine. New York:McGraw-Hill, Health Professions Division, c1999.

15. P.Moore, "A fundamental investigation of surfactant-induced skin irritation", Ph.D. thesis, Department of Chemical Engineering, Massachusetts Institute of Technology, Cambridge, MA, USA (2002).

16. P.Moore, S.Puvvada, and D.Blankschtein, Challenging the surfactant monomer skin penetration model: Penetration of sodium dodecyl sulfate micelles into the epidermis, *Journal of Cosmetic Science*, 54:p. 29-46 (2003).

17. P.Moore, A.Shiloach, S.Puvvada, and D.Blankschtein, Penetration of mixed micelles into the epidermis: Effect of mixing sodium dodecyl sulfate with dodecyl hexa(ethylene oxide), *Journal of Cosmetic Science*, 54:p. 143-159 (2003).

18. L.D.Rhein, F.A.Simion, R.L.Hill, R.H.Cagan, J.Mattai, and H.I.Maibach, Human cutaneous response to a mixed surfactant system: role of solution phenomena in controlling surfactant irritation, *Dermatologica*, 180:p. 18-23 (1990).

19. K.P.Ananthapadmanabhan, K.K.Yu, C.L.Meyers, and M.P.Aronson, Binding of surfactants to stratum corneum, *Journal of the Society of Cosmetic Chemists*, **47**:p. 185-200 (1996).

20. A.Di Nardo, K.Sugino, P.Wertz, J.Ademola, and H.I.Maibach, Sodium lauryl sulfate (SLS) induced irritant contact dermatitis: a correlation study between ceramides and in vivo parameters of irritation, *Contact Dermatitis*, 35:p. 86-91 (1996).

21. L.D. Rhein, "In vitro interactions: Biochemical and biophysical effects of surfactants on skin", in *Surfactants in Cosmetics*, M.M. Rieger and L.D. Rhein, Eds. (Marcel Dekker Inc, New York, 1997), pp.397-426.

22. E.Beraradesca and F.Distante, Mechanisms of Skin Irritation, *Current problems in dermatology*, 23:p. 1-8 (1995).

23. K.P.Wilhelm, M.Samblebe, and C.P.Siegers, Quantitative in vitro assessment of N-alkyl sulphate-induced cytotoxicity in human keratinocytes (HaCaT). Comparison with in vivo human irritation tests, *Br. J. Dermatol.*, 130:p. 18-23 (1994).

24. B.R.Masters, P.T.C.So, and E.Gratton, Optical Biopsy of In Vivo Human Skin: Multi-photon Excitation Microscopy, *Lasers Med Sci*, 13:p. 196-203 (1998).

25. K.H.Kim, C.Buehler, and P.T.C.So, High-speed, two-photon scanning microscope, *Applied Optics*, 38(28):p. 6004-6009 (1999).

26. G.K.Menon, and P.M.Elias, Morphologic basis for a pore-pathway in mammalian stratum corneum, *Skin Pharmacology*, 10:p. 235-246 (1997).

27. R.M.Raphael, R.E.Waugh, S.Svetina, and B.Zeks, Fractional occurrence of defects in membranes and mechanically driven interleaflet phospholipids transport, *Physical Review B*, 64(5), art. no. 05913, part 1.

28. M.S.Malghani, J.Yang, and J.Wu, Generation and growth of bilayer defects induced by ultrasound, *Journal of the Acoustic Society of America*, 103:p. 1682-1685 (1998).

29. H.Tang, S.Mitragotri, D.Blankschtein, and R.Langer, Theoretical description of transdermal transport of hydrophilic permeants: Application to low-frequency sonophoresis, *Journal of Pharmaceutical Sciences*, 90(5):p. 545-568 (2001).

30. K.D.Peck, A.H. Ghanem, and W.I.Higuchi, Hindered diffusion of polar molecules through and effective pore radii estimates of intact and ethanol treated human epidermal membrane, *Pharmaceutical Research*, 11(9):p. 1306-1314 (1994).

31. W.M.Deen, Hindered transport of large molecules in liquid-filled pores, *AIChE Journal*, 33(9):p. 1409-1425 (1987).

32. J.L.Anderson and J.A.Quinn, Restricted transport in small pores, a model for steric exclusion and hindered particle motion, *Biophysical Journal*, 14:p.130 (1974).

33. A.Tezel, A.Sens, and S.Mitragotri, Description of Transdermal transport of hydrophilic solutes during low-frequency sonophoresis based on a modified porous pathway model, *Journal of Pharmaceutical Sciences,* 92(2):p. 381-393 (2003).

34. B.Yu, "Elucidation of Chemically-Induced Transdermal Transport Processes", Ph.D. thesis, Department of Chemical Engineering, Massachusetts Institute of Technology, Cambridge, MA, USA (2002).

35. H.Schaefer, and T.E.Redelmeier, *Skin Barrier*, Basel: Karger (1996).

36. S.Mitragotri, M.E.Johnson, D.Blankschtein, and R.Langer, A theoretical analysis of partitioning, diffusion, and permeation across lipid bilayers, *Biophysical Journal*, 77:p. 1268-1283 (1999).

37. J.Kushner, D.Blankschtein, and R.Langer, Experimental demonstration of the existence of highly permeable localized transport regions in low-frequency sonophoresis, *Journal of Pharmaceutical Sciences*, 93:p. 2733–2745 (2004).

38. U.F.Pliquett, T.E.Zewert, T.Chen, R.Langer, and J.C.Weaver, Imaging of fluorescent molecule and small ion transport through human stratum comeum during high voltage pulsing: localized transport regions are involved, *Biophysical Journal*, 58:p.185-204 (1996).

39. K.P.Ananthapadmanabhan, D.J.Moore, K.Subramanyan, M.Misra, and F.Meyer, Cleansing without compromise: The impact of cleansers on the skin barrier and the technology of mild cleansing, *Dermatologic Therapy*, 17:p. 16-25 (2004).

Chapter 6

6. Aqueous Pore Size Distribution Induced by an Aqueous Surfactant Solution in the Absence and in the Presence of a Humectant

6.1. Introduction and Motivation

In Chapter 1, Section 1.4.2, I examined the existence and the nature of an aqueous pore pathway in the stratum corneum (SC). The aqueous pore pathway results from aqueous pores in the SC that align vertically and horizontally to form tortuous, cylindrical channels accessible to polar permeants, thereby making it possible for hydrophilic, polar permeants to penetrate into the SC and traverse the continuous hydrophobic, lipoidal domains within the SC. The following mechanisms were advanced in the literature to provide a physical basis for the existence of the aqueous pore pathway: (i) discrete lacunar domains between two layers of lipid headgroups in a lipid bilayer that may fill up with water upon skin hydration (1), and (ii) imperfections in the lipid bilayers, including fault dislocations or missing lipids, separation of grain boundaries, and lattice vacancies (2, 3). One, or more, of these mechanisms may act in tandem to lead to the

formation of the aqueous pores in the SC (1-4, 8, 9). Because of the inherent skin heterogeneity, the number of lacunae and defects at different SC sites is expected to be different (4-7). As a result, this variation in the number of lacunae and defects can potentially lead to a size distribution of the aqueous pores that align to form the aqueous pore pathway in the SC (8, 9). Evidence for the existence of a size distribution of aqueous pores in the SC was provided indirectly by conducting skin permeability studies which revealed that permeants of similar charges and hydrophobicities/hydrophilicities, but of different molecular sizes (radii), exhibit different rates of skin permeability (8-10). In particular, Tezel et al. measured different skin permeability values for hydrophilic permeants having different molecular radii, such as, Urea and Mannitol, which have hydrodynamic radii smaller than 5Å, and Dextran, which has a hydrodynamic radius larger than 20Å (8). Specifically, Tezel et al. observed an inverse correlation between the permeant hydrodynamic radius (size) and the permeant transdermal permeability, a finding that provides indirect evidence for the existence of a size distribution of aqueous pores in the SC. Indeed, the larger the molecular radius of a permeant, the fewer the number of aqueous pores that it can access in order to penetrate into and traverse the SC, and therefore, the smaller its transdermal permeability. Because there is a size distribution of aqueous pores in the SC, smaller hydrophilic permeants can access a larger number of these aqueous pores, and therefore, can exhibit higher permeabilities when compared to larger hydrophilic permeants (8-10).

In Chapter 2, we reported that SDS aqueous contacting solutions induced an average aqueous pore radius of 33±5Å, while when 10 wt% Glycerol was added to these contacting solutions, the aqueous pore radius was decreased to 20±5Å. As a result, an SDS micelle in an SDS aqueous contacting solution, having an effective hydrodynamic radius of 19.5±1Å was able

to penetrate into the SC, and induce skin barrier perturbation, by accessing aqueous pores whose average radius was significantly larger (33±5Å). On the other hand, an SDS micelle in an SDS aqueous contacting solution with 10 wt% added Glycerol, having an effective hydrodynamic radius of 18.5±1Å, was sterically hindered from penetrating into the SC because it was not able to access, to the same extent, the aqueous pores having an average radius of 20±5Å.

In this chapter, in order to gain additional mechanistic insight on the radii (sizes) of the aqueous pores induced by aqueous contacting solutions containing: (i) SDS (1-200 mM), and (ii) SDS (1-200 mM) +10 wt% added Glycerol, I developed a theoretical methodology to characterize the size distribution of aqueous pores induced by aqueous contacting solutions (i) and (ii) above. Because there is an inherent size distribution of aqueous pores in the SC, being able to characterize it in the presence of aqueous surfactant/humectant systems can lead to an accurate prediction of the contribution of surfactant in micellar form, relative to that of surfactant in monomeric form, to surfactant skin penetration, and thereby, to surfactant-induced skin barrier perturbation in the presence of humectants (see Section 6.3). For example, consider the theoretical analysis reported in Chapter 2 on the role of SDS micelles on skin barrier perturbation, in the presence and in the absence of 10 wt% added Glycerol. Although the analysis in Chapter 2 revealed that the SDS micelles did not play a significant role in SDS skin penetration in the presence of 10 wt% Glycerol, it was unable to specifically *quantify the relative contributions* of SDS in monomeric and in micellar forms to SDS skin penetration. Indeed, because there is a size distribution of aqueous pores induced by an SDS+10 wt% Glycerol aqueous contacting solution, there are *still* some aqueous pores which are sufficiently large to allow penetration of SDS micelles into the SC, even though, *on average*, the SDS micelles are sterically hindered from penetrating into the SC through the aqueous pores (see Chapter 2).

Therefore, unless one is able to characterize the size distribution of the aqueous pores induced upon exposure of the skin to the aqueous contacting solutions containing SDS+10wt% added Glycerol, one cannot accurately quantify the contribution of the SDS micelles, relative to that of the SDS monomers, to SDS skin penetration and associated skin barrier perturbation.

In determining the size distribution of the aqueous pores upon exposing skin to: (i) aqueous SDS contacting solutions, and (ii) aqueous SDS+10 wt% Glycerol contacting solutions, I have: (a) considered the SDS monomers and the SDS micelles as the two penetrating entities, and (ii) used appropriate steric pore-partition coefficients for the SDS monomers and the SDS micelles (see Section 6.2). Furthermore, in determining the aqueous pore size distribution, I have used the measured SDS *skin penetration data* reported in Chapter 2, instead of using the measured *skin permeability data* for commonly used hydrophilic permeants, such as Mannitol and ions.[37] Indeed, using the measured SDS skin penetration data to determine the size distribution of the aqueous pores has two key advantages: (i) the SDS skin penetration measurements provide a *direct* way to probe the aqueous pore size distribution, as opposed to the Mannitol skin permeability and skin electrical current measurements which provide an *indirect* way to do so, and (ii) the SDS skin penetration measurements enable the development of a model to quantify surfactant penetration into the skin, as opposed to determining only enhancements in the transdermal delivery of hydrophilic permeants, such as Mannitol and ions, upon exposing skin to surfactants. In order to develop mechanistic insight on the skin barrier perturbation induced by aqueous surfactant/humectant systems, it is essential to understand the process of surfactant skin penetration in the presence of humectants, rather than the transdermal delivery of

[37] The skin permeability of ions, in this case, of Na^+ and Cl^-, is primarily responsible for inducing an electrical current across the skin, and can therefore be determined experimentally using skin electrical current measurements (see Chapter 2).

surfactants in the presence of humectants. This follows because: (1) the skin barrier is not saturated with surfactants, and therefore, it may continue to absorb surfactants before these chemicals can actually cross the skin barrier and enter into the blood stream (11-15), (2) the in vivo erythema (skin redness) response has been shown to result from the ability of surfactants to penetrate into, and subsequently damage, the skin barrier, and not so much from their ability to diffuse into the blood stream (13-15), (3) researchers have observed that the skin penetration of surfactants is relatively large compared to their diffusion across the skin barrier and into the blood stream (15-17), and (4) I have observed that a humectant, such as Glycerol, significantly inhibits the skin penetration of surfactants, such as SDS, which in turn, minimizes the in vivo erythema response (see Chapter 2). Clearly, for our purposes here, being able to model the penetration of surfactants into the skin, which is directly responsible for surfactant-induced skin barrier perturbation, is more important than being able to model the systemic uptake of surfactants by the body, or than being able to model the skin permeation enhancement induced by surfactants.

6.2. Development of the Aqueous Pore Size Distribution Model Using Single-Parameter Exponential and Truncated Normal Distribution Functions

I investigated the size distribution of the aqueous pores in the SC induced by aqueous contacting solutions of SDS (1-200 mM) and SDS (1-200 mM) + 10 wt% added Glycerol using the SDS skin penetration data reported in Chapter 2. The SDS monomers and the SDS micelles were considered as the two skin penetrating entities having different sizes (effective

hydrodynamic radii).[38] Due to simplicity and model tractability, single-parameter distributions, specifically: (i) an exponential distribution function, and (ii) a truncated normal distribution function, were used to represent the size distribution of the aqueous pores in the SC. Below, I present the various steps involved in formulating the two aqueous pore size distribution models, including evaluating the corresponding pore size distribution parameters.

Step 1: *Use single-parameter distribution functions to model the aqueous pore size distribution in the SC (8, 9, 18).*

Using an exponential distribution function to model the size distribution of aqueous pores in the SC results in the following expression:

$$\gamma(r) = \lambda \exp(-\lambda r) \tag{1}$$

where r is the aqueous pore radius, $\gamma(r)$ is the exponential distribution function, and λ is the pore size distribution parameter characterizing the exponential distribution function. In addition, using Eq.(1), one can obtain an analytical expression for the average aqueous pore radius, $r_{pore}^{\exp}$, corresponding to the aqueous pore size distribution in Eq.(1). Specifically (30),

$$r_{pore}^{\exp} = \int_0^\infty r\gamma(r)dr = \frac{1}{\lambda} \tag{2}$$

Note that the average pore radius, calculated using Eq.(2) is, in effect, an estimate of the expected pore radius that one would find, on average, upon randomly sampling a pore radius using the expected distribution of pore radii given in Eq.(1).

Similarly, using a truncated normal distribution function to model the size distribution of aqueous pores in the SC results in the following expression:

[38] The effective hydrodynamic radius of an SDS monomer was determined using the Stokes-Einstein equation. The effective hydrodynamic radius of an SDS micelle was determined using Dynamic Light Scattering (DLS) measurements, as reported in Chapter 2.

$$\delta(r) = \frac{1}{\sigma}\sqrt{\frac{2}{\pi}}\exp(-\frac{r^2}{2\sigma^2}) \tag{3}$$

where r is the aqueous pore radius, $\delta(r)$ is the truncated normal distribution function, and σ is the pore size distribution parameter characterizing the truncated normal distribution function.[39] In addition, one can obtain an analytical expression for the average aqueous pore radius, r_{pore}^{normal}, corresponding to the aqueous pore size distribution in Eq.(3) (30). Specifically,

$$r_{pore}^{normal} = \int_0^\infty r\delta(r)dr = \sigma\sqrt{\frac{2}{\pi}} \tag{4}$$

In addition, note that the aqueous pore size distributions in Eqs. (1) and (3) satisfy the following physical constraints:

$$\int_0^\infty \gamma(r)dr = 1, r \to \infty \Rightarrow \gamma(r) \to 0 \tag{5a}$$

and

$$\int_0^\infty \delta(r)dr = 1, r \to \infty \Rightarrow \delta(r) \to 0 \tag{5b}$$

Because: (1) a hydrophilic permeant can access aqueous pores whose radii are larger than the permeant radius, and (2) Eqs.(5a) and (5b) imply that, for infinitely large hydrophilic permeants, the probability of obtaining a very large pore is infinitesimally small, it follows that none of the aqueous pores are available for penetration of such permeants into the SC. Equations (1)-(4) were used to model the size distribution and the average radius of the aqueous pores in the SC induced by aqueous contacting solutions containing: (i) SDS (1-200 mM) and (ii) SDS (1-200

[39] Note that the distribution function, $\delta(r)$, in Eq.(3) was obtained by *truncating* the normal distribution function using the restriction that the aqueous pore radii are not negative ($r \geq 0$). As a result, the pre-exponential constant in $\delta(r)$ differs from the pre-exponential constant in the conventional normal distribution function (R) (18). Furthermore, note that this pre-exponential constant factor in Eq.(3) satisfies the physical constraints imposed in Eqs.(5a) and (5b) (18).

mM)+10 wt% added Glycerol (see Chapter 2 for a discussion of the effects of contacting solutions (i) and (ii) on the aqueous pores in the SC).

Step 2: *Derive mathematical expressions for the pore size distribution parameters, λ and σ, in Eqs.(1) and (3), respectively, using experimental values for the SDS monomer / SDS micelle pore penetration ratio, $R_{mon/mic}$, in the presence and in the absence of 10 wt% Glycerol.*

In Chapter 2, a multiple linear regression (MLR) analysis of the amount of ^{14}C radiolabeled SDS that can penetrate into the epidermis from aqueous contacting solution (i) containing SDS (1-200 mM) (see above) was used to determine $R_{mon/mic}$.[40] Specifically (see Chapter 2 and (11, 31, 32)):

$$C_{skin} = \alpha C_{mon} + \beta C_{mic} \Rightarrow R_{mon/mic} = \frac{\alpha C_{mon}}{\beta C_{mic}} \quad (6)$$

where C_{skin} is the concentration of ^{14}C radiolabeled SDS in the epidermis, C_{mon} and C_{mic} are the concentrations of the SDS monomers and the SDS micelles, respectively, in the aqueous contacting solutions, α is the linear regression coefficient that quantifies the contribution of the SDS monomers to SDS skin penetration per unit monomer concentration in the aqueous contacting solution, and β is the linear regression coefficient that quantifies the contribution of the SDS micelles to SDS skin penetration per unit micelle concentration in the aqueous contacting solution.

[40] Note that $R_{mon/mic}$, which I have defined as the SDS monomer/SDS micelle pore penetration ratio, can also be interpreted as the contribution of the SDS monomer/SDS micelle ratio to SDS skin penetration. Because SDS binds strongly to the epidermis, and does not diffuse significantly across the epidermis, the penetration of SDS into the aqueous pores, rather than the transdermal diffusion of SDS through the aqueous pores, is the primary driving force that controls the amount of SDS that can penetrate into the skin from an aqueous contacting solution (see Chapter 2 and Section 6.1).

The SDS monomer / SDS micelle pore penetration ratio, $R_{mon/mic}$, can also be related to: (i) the average SDS monomer-aqueous pore partition coefficient, ϕ_{mon}, (ii) the average SDS micelle-aqueous pore partition coefficient, ϕ_{mic}, and (iii) the SDS monomer and SDS micelle skin porosities, ε_{mon} and ε_{mic}, [41] respectively, using well-accepted principles of hindered-transport theory (8, 11, 18-25). Specifically,

$$R_{mon/mic} = \frac{\phi_{mon}\varepsilon_{mon}}{\phi_{mic}\varepsilon_{mic}}\left(\frac{C_{mon}}{C_{mic}}\right) \tag{7}$$

Equation (7) describes the penetration of the SDS monomers relative to that of the SDS micelles through the aqueous pores of the SC. An SDS monomer can access an aqueous pore whose radius, r, is larger than the radius of the SDS monomer, r_{mon}. Similarly, an SDS micelle can access an aqueous pore whose radius, r, is larger than the radius of the SDS micelle, r_{mic}. Next, the SDS monomer and the SDS micelle can partition into the these aqueous pores with an average SDS monomer-aqueous pore partition coefficient, ϕ_{mon}, and an average SDS micelle-aqueous pore partition coefficient, ϕ_{mic}, respectively. In addition, note that the quantities, ε_{mon} and ε_{mic}, appear in Eq.(7) because the SC is a porous membrane where *only* the area occupied by the aqueous pores is available for penetration of an SDS monomer and an SDS micelle. The ratio C_{mon}/C_{mic} appears in Eq.(7) because the concentrations of the SDS monomers and the SDS micelles contacting the skin should be directly proportional to the extents to which they penetrate into the skin (see assumption (vi) below).

It is instructive to summarize and explain the validity of the key assumptions made in the derivation of Eq.(7): (i) steric interactions are the dominant interactions between the permeants

[41] The skin porosity is defined as the fraction of the skin cross-sectional area available for penetration of permeants that is occupied by the aqueous pores.

and the aqueous pore walls, (ii) the permeants do not 'clog' the aqueous pore entries and exits, (iii) the SDS monomer and SDS micelle-pore wall partition coefficients dominate the SDS monomer and SDS micelle pore diffusion coefficients in determining the total amount of SDS skin penetration, (iv) the concentration of the permeant in the donor compartment is high, and does not deplete with time, (v) the concentration of the permeant in the donor compartment is always much higher than that in the receiver compartment, and (vi) the SDS monomer to micelle pore penetration ratio is directly proportional to the ratio of the SDS monomer concentration to the SDS micelle concentration in the aqueous contacting solution. Moore et al. (11, 31, 32) have shown that assumption (vi) is valid. Assumptions (iv) and (v) are valid because an insignificant amount of the permeant present in the donor compartment was observed to permeate across the p-FTS samples used in the appropriate experiments (see Chapter 2). Assumption (iii) is also valid for the SDS skin penetration assays used because less than 1% of SDS present in the donor compartment permeated across the p-FTS samples into the receiver compartment, while a significantly larger amount of SDS present in the donor compartment penetrated into the p-FTS samples (see Section 6.1 and Chapter 2). Assumption (ii) is a well-accepted one in the hindered-transport literature aimed at modeling penetration and diffusion of permeants across the skin barrier (8, 9, 18-26). In addition, Tang et al. have shown that steric interactions between permeants and the aqueous pore walls are usually more significant than electrostatic and van der Waals interactions for the types of systems examined here (25).

By combining Eqs.(6) with (7), one can obtain a relationship between: (i) the linear regression coefficients, α and β, (ii) the SDS monomer and SDS micelle average aqueous-pore partition coefficients, ϕ_{mon} and ϕ_{mic} , and (iii) the SDS monomer and SDS micelle skin porosities, ε_{mon} and ε_{mic}. Specifically,

$$\frac{\alpha}{\beta} = \frac{\phi_{mon}\varepsilon_{mon}}{\phi_{mic}\varepsilon_{mic}} \tag{8}$$

Because only steric interactions are assumed to operate between the walls of the aqueous pores and the SDS monomers and the SDS micelles (see assumption (i) above), one can relate ϕ_{mon} and ϕ_{mic} to r_{mon} and r_{mic}, respectively, and to the single-parameter exponential pore size distribution, $\gamma(r)$, as follows (8, 9, 18-25):

$$\phi_{mon} = \int_{r_{mon}}^{\infty} \gamma(r)\left(1 - \frac{r_{mon}}{r}\right)^2 dr \tag{9a}$$

and

$$\phi_{mic} = \int_{r_{mic}}^{\infty} \gamma(r)\left(1 - \frac{r_{mic}}{r}\right)^2 dr \tag{9b}$$

In addition, expressions for the skin porosities associated with the SDS monomers and the SDS micelles, ε_{mon} and ε_{mic}, respectively, can be derived by assuming that only aqueous pores having a radius r which is larger than the effective hydrodynamic radius of a SDS monomer (r_{mon}) will contribute to ε_{mon}, and that only aqueous pores having a radius r which is larger than the effective hydrodynamic radius of a SDS micelle (r_{mic}) will contribute to ε_{mic} (8, 9). Specifically,

$$\varepsilon_{mon} = \int_{r_{mon}}^{\infty} \gamma(r)\frac{N_p}{A}\pi r^2 dr \tag{10a}$$

and

$$\varepsilon_{mic} = \int_{r_{mic}}^{\infty} \gamma(r)\frac{N_p}{A}\pi r^2 dr \tag{10b}$$

where (N_p/A) is the pore number density, that is, the number of aqueous pores (N_p) per unit skin area (A).

By multiplying Eqs.(9a) and (10a), dividing by the product of Eqs.(9b) and (10b), and using this result in Eq.(8), an explicit expression is obtained which relates the aqueous pore size distribution, $\gamma(r)$, to the experimentally determined linear regression coefficients, α and β. Specifically,

$$\frac{\alpha}{\beta}=\frac{\left[\int_{r_{mon}}^{\infty}\gamma(r)\left(1-\frac{r_{mon}}{r}\right)^{2}dr\right]\left[\int_{r_{mon}}^{\infty}\gamma(r)\frac{N_p}{A}\pi r^{2}dr\right]}{\left[\int_{r_{mic}}^{\infty}\gamma(r)\left(1-\frac{r_{mic}}{r}\right)^{2}dr\right]\left[\int_{r_{mic}}^{\infty}\gamma(r)(\frac{N_p}{A})\pi r^{2}dr\right]} \tag{11}$$

where all the variables were defined above.

Using the truncated normal distribution function to model the size distribution of the aqueous pores in the SC, one can obtain a similar expression for α/β, with $\gamma(r)$ replaced by $\delta(r)$ in Eq.(11). Note that Eqs.(6)-(11) were derived to determine the aqueous pore size distribution in p-FTS samples that were contacted with aqueous solutions containing SDS (1-200 mM) (contacting solution (i)). A similar analysis was carried out to determine the aqueous pore size distribution in p-FTS samples that were contacted with aqueous solutions containing SDS (1-200 mM)+10 wt% added Glycerol (contacting solution (ii)). Below, I describe how to compute λ and σ to uniquely determine $\gamma(r)$ and $\delta(r)$, in Eqs.(1) and (3), respectively.

Step 3: *Evaluate the aqueous pore size distribution parameters, λ and σ, including the average aqueous pore radii induced by aqueous contacting solutions containing SDS (1-200 mM) and SDS (1-200 mM)+10 wt% added Glycerol.*

The integrals in the numerator and the denominator of Eq.(11) were evaluated numerically for a specific value of λ (see Eq.(1)), and subsequently, Eq.(11) was solved using a trial-and-error procedure.[42] The lower limits of the integrals in Eq.(11), r_{mon} and r_{mic}, correspond to the SDS monomer and the SDS micelle radii, respectively, which were assumed to be equal to the effective hydrodynamic radii values. In Chapter 2, the SDS micelle effective hydrodynamic radius in an aqueous SDS solution was determined using Dynamic Light Scattering (DLS) measurements to be 19.5±1Å, while in an aqueous SDS solution with 10wt% added Glycerol, it was determined to be 18.5±1Å. With this in mind, for the purpose of the calculations reported here, I have used r_{mic} = 19.5Å in the absence of Glycerol, and r_{mic} = 18.5Å in the presence of 10 wt% added Glycerol. The effective hydrodynamic radius of a SDS monomer, r_{mon} , was determined to be 5Å, using the Stokes-Einstein equation (see Chapter 2 and (27)), which corresponds to the lower limit of the integral in the numerator of Eq.(11). Using the trial-and-error solution procedure discussed above, I obtained appropriate λ values characterizing the exponential aqueous pore size distributions in the absence and in the presence of 10 wt% added Glycerol. Specifically, I obtained: (i) λ_{SDS} , for p-FTS that was exposed to aqueous SDS (1-200 mM) contacting solutions, and (ii) λ_{SDS+G} , for p-FTS that was exposed to aqueous SDS (1-200 mM)+10 wt% added Glycerol contacting solutions.

In addition, using the truncated normal distribution function to model the size distribution of the aqueous pores in the SC, I obtained an equation similar to Eq.(11), with $\gamma(r)$ replaced by $\delta(r)$. Subsequently, I used the trial-and-error solution procedure discussed above to obtain

[42] Given this value of λ, the ratio of the integrals was compared to the ratio, α/β, and the error was computed. If this error was within a pre-specified error tolerance level (10^{-6}), then this value of λ was identified as the solution to Eq.(11). However, if the error was not within the pre-specified error tolerance level, a new value of λ was specified, and the recursive solution procedure was continued until the error was within the pre-specified error tolerance level.

appropriate σ values characterizing the truncated normal aqueous pore size distributions in the absence and in the presence of 10 wt% added Glycerol. Specifically, I obtained: (i) σ_{SDS}, for p-FTS that was exposed to aqueous SDS (1-200 mM) contacting solutions, and (ii) σ_{SDS+G}, for p-FTS that was exposed to aqueous SDS (1-200 mM) +10 wt% added Glycerol contacting solutions.

The average aqueous pore radii corresponding to the exponential pore size distributions, induced by aqueous contacting solutions (i) and (ii), $r^{exp}_{pore,SDS}$ and $r^{exp}_{pore,SDS+G}$, were then calculated using the λ_{SDS} and λ_{SDS+G} values determined above, respectively, in Eq.(2). In addition, the average aqueous pore radii corresponding to the truncated normal pore size distributions, induced by aqueous contacting solutions (i) and (ii), $r^{normal}_{pore,SDS}$ and $r^{normal}_{pore,SDS+G}$, were calculated using the σ_{SDS} and σ_{SDS+G} values determined above, respectively, in Eq.(4).

Step 4: *Evaluate the changes in the skin porosity and pore partition coefficient associated with the SDS micelles induced upon adding 10 wt% Glycerol to aqueous contacting solutions containing SDS (1-200 mM).*

In Chapter 2, I observed that upon adding 10 wt% Glycerol to aqueous solutions containing SDS (1-200 mM), the SDS-induced normalized porosity-to-tortuosity ratio, ε/τ, of the aqueous pores in the SC decreased from 7±1 to 3±1, which is a decrease of more than 57%. Furthermore, the decrease in the normalized ε/τ ratio was attributed to a reduction in the SDS-induced porosity, ε, upon adding 10 wt% Glycerol to aqueous SDS contacting solutions (see Chapter 2 and (8, 9, 11, 25, 31)). Therefore, it is reasonable to anticipate a decrease in the skin

porosity to SDS micelles upon adding 10 wt% Glycerol to an aqueous SDS contacting solution.[43] Using the exponential distribution function to model the size distribution of the aqueous pores, one can now determine the ratio of the skin porosity associated with the SDS micelles induced by aqueous contacting solution (i), relative to aqueous contacting solution (ii), denoted as E_{ε}^{exp}. Specifically, in terms of the single-parameter exponential aqueous pore size distribution (see Eq.(10b)),

$$E_{\varepsilon}^{\exp} = \frac{\varepsilon_{mic,SDS}^{\exp}}{\varepsilon_{mic,SDS+G}^{\exp}} = \frac{\int_{mic,SDS}^{\infty} \left(\frac{N_p}{A}\right)_{SDS} \gamma(r)_{SDS}\, \pi r^2 dr}{\int_{mic,SDS+G}^{\infty} \left(\frac{N_p}{A}\right)_{SDS+G} \gamma(r)_{SDS+G}\, \pi r^2 dr} \tag{12}$$

where $\varepsilon_{mic,SDS}^{\exp}$ is the skin porosity associated with the SDS micelles induced by aqueous contacting solution (i), $\varepsilon_{mic,SDS+G}^{\exp}$ is the skin porosity associated with the SDS micelles induced by aqueous contacting solution (ii), $r_{mic,SDS}$ is the SDS micelle radius in aqueous contacting solution (i), $r_{mic,SDS+G}$ is the SDS micelle radius in aqueous contacting solution (ii), $\gamma(r)_{SDS}$ is the exponential pore size distribution induced by aqueous contacting solution (i), and $\gamma(r)_{SDS+G}$ is the exponential pore size distribution induced by aqueous contacting solution (ii). In addition, $(N_p/A)_{SDS}$ is the number of pores per unit skin area (A) induced by aqueous contacting solution (i), and $(N_p/A)_{SDS+G}$ is the number of pores per unit skin area (A) induced by aqueous contacting solution (ii). Note that because $(N_p/A)_{SDS} \neq (N_p/A)_{SDS}$, one cannot directly evaluate E_{ε}^{exp} by computing the definite integrals in the numerator and denominator of Eq.(12).

[43] A similar analysis carried out for the SDS monomers in Chapter 2 indicates that the addition of 10 wt% Glycerol to the aqueous contacting solutions containing SDS (1-200 mM) does not prevent SDS monomers from contributing to SDS skin penetration. Indeed, in *Table 6-1*, one can observe that the values of α_{SDS} and α_{SDS+G} are similar (see Eq.(6)).

In order to calculate E_{ε}^{exp}, I have obtained explicit relationships relating: (a) changes in the skin porosity, E_{ε}^{exp}, and the pore partition coefficient, $E_{\phi}^{\exp}$, to (b) linear regression coefficients that quantify the contribution of the SDS micelles to SDS skin penetration per unit SDS micelle concentration in the aqueous contacting solutions (i) and (ii), β_{SDS+G} and β_{SDS+G}, respectively (see Eq.(6)). Specifically, upon comparing the contribution of the SDS micelles to SDS skin penetration in aqueous contacting solution (i) relative to that in aqueous contacting solution (ii), I obtain:

$$\frac{\beta_{SDS} C_{mic}^{SDS}}{\beta_{SDS+G} C_{mic}^{SDS+G}} = \frac{\varepsilon_{mic,SDS}^{\exp} \phi_{mic,SDS}^{\exp}}{\varepsilon_{mic,SDS+G}^{\exp} \phi_{mic,SDS+G}^{\exp}} \left(\frac{C_{mic}^{SDS}}{C_{mic}^{SDS+G}} \right) \Rightarrow \frac{\beta_{SDS}}{\beta_{SDS+G}} = \left(E_{\varepsilon}^{\exp} \right) \left(E_{\phi}^{\exp} \right) \qquad (13)$$

where $\phi_{mic,SDS}^{\exp}$ is the average SDS micelle-aqueous pore partition coefficient induced by aqueous contacting solution (i), $\phi_{mic,SDS+G}^{\exp}$ is the average SDS micelle-aqueous pore partition coefficient induced by aqueous contacting solution (ii), C_{mic}^{SDS} is the concentration of SDS micelles in aqueous contacting solution (i), and C_{mic}^{SDS+G} is the concentration of SDS micelles in aqueous contacting solution (ii), and $E_{\phi}^{\exp} = \phi_{mic,SDS}^{\exp} / \phi_{mic,SDS+G}^{\exp}$. Therefore, if one can determine $E_{\phi}^{\exp}$, then one can determine $E_{\varepsilon}^{\exp}$ using Eq.(13) (recall that $\beta_{SDS} / \beta_{SDS+G}$ in Eq.(13) can be determined experimentally using an MLR analysis of the ^{14}C radiolabeled SDS skin penetration data upon contacting p-FTS to aqueous contacting solutions (i) and (ii)).

Using Eq.(9b) to express $\phi_{mic,SDS}^{\exp}$ and $\phi_{mic,SDS+G}^{\exp}$ in terms of $\gamma(r)_{SDS}$ and $\gamma(r)_{SDS+G}$, respectively, it follows that:

$$E_{\phi}^{\exp} \equiv \frac{\phi_{mic,SDS}^{\exp}}{\phi_{mic,SDS+G}^{\exp}} = \frac{\int_{mic,SDS}^{\infty} \gamma(r)_{SDS} \left(1 - \frac{r_{mic,SDS}}{r}\right)^2 dr}{\int_{mic,SDS+G}^{\infty} \gamma(r)_{SDS+G} \left(1 - \frac{r_{mic,SDS+G}}{r}\right)^2 dr} \tag{14}$$

Therefore, upon determining $\gamma(r)_{SDS}$, $\gamma(r)_{SDS+G}$, $r_{mic,SDS}$, and $r_{mic,SDS+G}$ (see above), Eq.(14) can be used to determine $E_{\phi}^{\exp}$. Once $E_{\phi}^{\exp}$ is determined in this manner, Eq.(13) can then be used to determine $E_{\varepsilon}^{\exp}$. In addition, equations similar to Eqs.(13) and (14) can be derived in the case of the truncated normal distribution function (see Eq.(3)) to determine the ratio of the skin porosity associated with the SDS micelles induced by aqueous contacting solution (i) relative to the skin porosity associated with the SDS micelles induced by aqueous contacting solution (ii), denoted as E_{ε}^{normal}. To derive this equation, one only needs to replace $\gamma(r)_{SDS}$ by $\delta(r)_{SDS}$ and $\gamma(r)_{SDS+G}$ by $\delta(r)_{SDS+G}$ in Eqs.(13) and (14). [44] These results are discussed next in Section 6.3.

6.3. Evaluation of the Aqueous Pore Size Distributions Induced by SDS in the Absence and in the Presence of 10 wt% Added Glycerol

Using multiple linear regression (MLR), I determined values of α and β upon exposing p-FTS to aqueous contacting solutions containing: (i) SDS (1-200 mM), that is, α_{SDS} and β_{SDS}, and (ii) SDS (1-200 mM) + Glycerol (10 wt%), that is, α_{SDS+G} and β_{SDS+G}, as discussed in Section 6.2 (see also *Table 6-1* below). The ratio α/β which quantifies the contribution of the SDS

[44] Note that $\gamma(r)_{SDS}$ appears in the term $[\phi_{mic,SDS}^{\exp} \varepsilon_{mic,SDS}^{\exp}]$, and $\gamma(r)_{SDS+G}$ appears in the term $[\phi_{mic,SDS+G}^{\exp} \varepsilon_{mic,SDS+G}^{\exp}]$ in Eq.(13).

monomers relative to that of the SDS micelles to SDS skin penetration (see Section 6.2) increases by more than six times when 10 wt% Glycerol is added to the SDS aqueous contacting solution (see *Table 6-1*). Clearly, the addition of 10 wt% Glycerol significantly reduces the contribution of the SDS micelles to SDS skin penetration, which is consistent with my finding in Chapter 2.[45]

Table 6-1. Multiple Linear Regression (MLR) analysis of ^{14}C radiolabeled SDS skin penetration data from aqueous contacting solutions containing SDS (1-200 mM) (i) and SDS (1-200 mM)+Glycerol (10 wt%) (ii).

	Aqueous Contacting Solutions	
	(i) SDS (1-200 mM)	(ii)SDS (1-200 mM)+Glycerol (10 wt%)
α	5.228×10^{-3}	4.477×10^{-3}
β	1.256×10^{-3}	1.699×10^{-4}
α/β	4.163	26.360
R^2	9.641×10^{-1}	9.707×10^{-1}

Using the α/β values for aqueous contacting solutions containing SDS (1-200 mM) and SDS (1-200 mM) + 10 wt% added Glycerol, in the context of the trial-and-error solution procedure discussed in Section 6.2, I determined the following values for the exponential pore size distribution parameter, λ (see *Table 6-2)*: (a) $\lambda_{SDS} = 0.04$ for aqueous contacting solution (i), and (b) $\lambda_{SDS+G} = 0.10$ for aqueous contacting solution (ii).

[45] In Chapter 2, the addition of 10 wt% Glycerol to SDS aqueous contacting solutions did not result in a statistically significant reduction in the contribution of the SDS monomers to SDS skin penetration, while the contribution of the SDS micelles was significantly reduced. Therefore, it follows that the ratio of the contribution of the SDS monomers to the contribution of the SDS micelles to SDS skin penetration is significantly increased in the presence of 10 wt% Glycerol in the SDS aqueous contacting solutions.

In addition, the following values were determined for the truncated normal pore size distribution parameter, σ : (a) $\sigma_{SDS} = 34$ for aqueous contacting solution (i), and (b) $\sigma_{SDS+G} = 18$ for aqueous contacting solution (ii). The resulting aqueous pore size distributions, $\gamma(r)$ and $\delta(r)$, are plotted in *Figures 6-1 and 6-2*, respectively. Clearly, as shown in both figures, the addition of 10 wt% Glycerol to an aqueous SDS contacting solution induces a shift in the size distribution of aqueous pores induced by the aqueous SDS contacting solution – from larger to smaller pores, a finding that is consistent with the conclusions reached in Chapter 2 on the effect of 10 wt% added Glycerol on SDS-induced skin barrier perturbation. Indeed, because the addition of 10 wt% Glycerol to an aqueous SDS contacting solution results in smaller aqueous pores, relative to those found in an aqueous SDS contacting solution with no added Glycerol, the SDS micelles are sterically hindered from penetrating into the skin through the smaller aqueous pores, and as a result, cannot effectively contribute to SDS-induced skin barrier perturbation. Nevertheless, as *Figures 6-1* and *6-2* show, because of the existence of a size distribution of aqueous pores, some of the aqueous pores are sufficiently large to allow SDS micelle skin penetration, even when 10 wt% Glycerol is added to an aqueous SDS contacting solution. In order for our findings here to be consistent with those in Chapter 2, the number of such aqueous pores should be significantly reduced in the presence of 10 wt% Glycerol, such that the contribution of the SDS micelles to SDS skin penetration is also significantly reduced. To verify this claim, using the exponential pore distribution function, $\gamma(r)$, in *Figure 6-1*, I computed the percentage of aqueous pores that are larger in size than the size of an SDS micelle, and hence, allow penetration of SDS micelles into the skin.

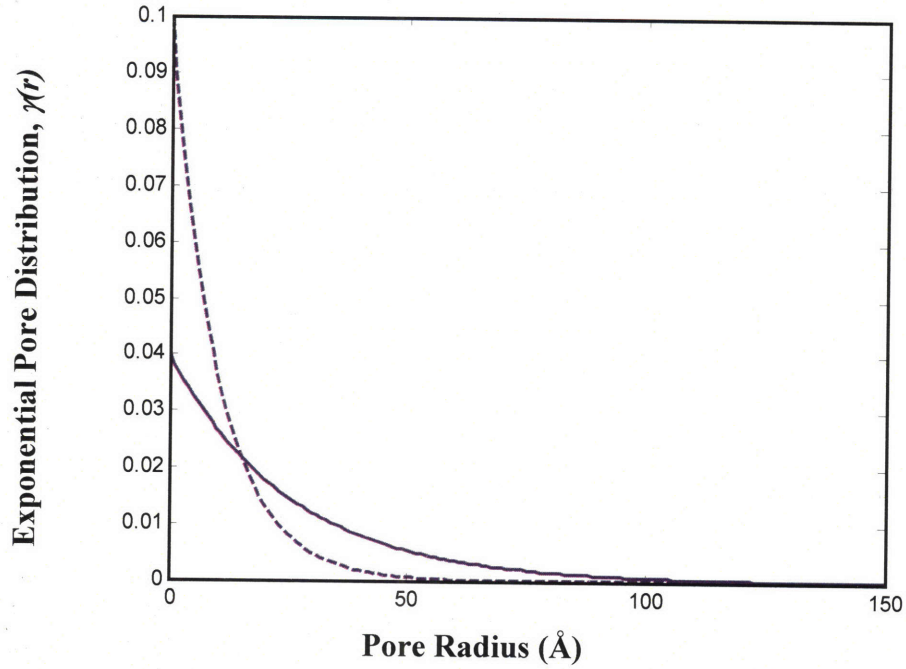

Figure 6-1. Size distribution of aqueous pores using the exponential pore distribution function induced in p-FTS exposed to the SDS (1-200 mM) (solid line) and the SDS (1-200 mM)+Glycerol (10 wt%) (dashed line) aqueous contacting solutions.

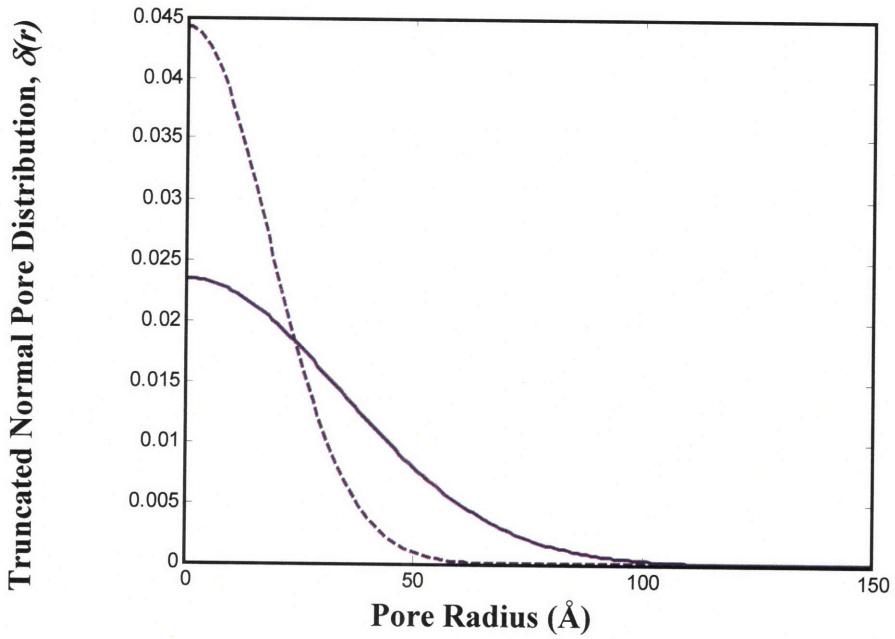

Figure 6-2. Size distribution of aqueous pores using the truncated normal pore distribution function induced in p-FTS exposed to the SDS (1-200 mM) (solid line) and the SDS (1-200 mM)+Glycerol (10 wt%) (dotted line) aqueous contacting solutions.

Specifically, using the values of λ_{SDS} and λ_{SDS+G} obtained earlier (see above), the area under the curves for ($r_{mic,SDS}<r<\infty$) corresponding to aqueous contacting solutions (i), and for ($r_{mic,SDS+G}<r<\infty$) corresponding to aqueous contacting solutions (ii), were computed numerically (see Eq.(15) below).

$$\eta_{SDS}^{\exp} = \int_{r_{mic,SDS}}^{\infty} \lambda_{SDS} \exp(-\lambda_{SDS} r) dr = \exp(-\lambda_{SDS} r_{mic,SDS}) = 46\% \qquad (15)$$

$$\eta_{SDS+G}^{\exp} = \int_{r_{mic,SDS+G}}^{\infty} \lambda_{SDS+G} \exp(-\lambda_{SDS+G} r) dr = \exp(-\lambda_{SDS+G} r_{mic,SDS+G}) = 16\%$$

where $\eta_{SDS}^{\exp}$ is the percentage of aqueous pores induced by SDS (1-200 mM) that are larger in size than the size of an SDS micelle in an aqueous SDS solution, and $\eta_{SDS+G}^{\exp}$ is the percentage of aqueous pores induced by SDS (1-200 mM)+10 wt% added Glycerol that are larger in size than the size of an SDS micelle in an aqueous SDS solution containing 10 wt% added Glycerol. In addition, a similar analysis conducted using the truncated normal pore size distribution yields $\eta_{SDS}^{normal} = 57\%$ and $\eta_{SDS+G}^{normal} = 30\%$ (see *Table 6-2*). Therefore, the addition of 10 wt% Glycerol to an aqueous SDS contacting solution reduces the fraction of aqueous pores available for SDS micelle penetration by: (i) *65%* ($=1-\eta_{SDS+G}^{\exp}/\eta_{SDS}^{\exp}$) for aqueous pores in the SC that are modeled using an exponential pore size distribution function, and (ii) *47%* ($=1-\eta_{SDS+G}^{normal}/\eta_{SDS}^{normal}$) for aqueous pores in the SC that are modeled using a truncated normal pore size distribution function.

Using Eq.(2), along with $\lambda_{SDS} = 0.04$ and $\lambda_{SDS+G} = 0.10$ (see above), the average aqueous pore radii corresponding to the exponential pore distribution functions are: (i) $r_{pore,SDS}^{\exp} = 25\text{Å}$ for

SDS (1-200 mM), and (ii) $r^{exp}_{pore,SDS+G} = 10\text{Å}$ for SDS (1-200 mM)+10 wt% added Glycerol (see *Table 6-2*). Similarly, using Eq.(4), along with $\sigma_{SDS} = 34$ and $\sigma_{SDS+G} = 18$ (see above), the average aqueous pore radii using the truncated normal pore distribution functions are: (i) $r^{normal}_{pore,SDS} = 27\text{Å}$ for SDS (1-200 mM), and (ii) $r^{normal}_{pore,SDS+G} = 14\text{Å}$ for SDS (1-200 mM)+10 wt% added Glycerol (see *Table 6-2*). These results clearly indicate that the addition of 10 wt% Glycerol to an SDS aqueous contacting solution results, on average, in aqueous pores having a smaller radius. Furthermore, these results also indicate that the aqueous pores induced by SDS (1-200 mM), on average, have radii larger than the size of an SDS micelle. However, when 10 wt% Glycerol is added to the SDS (1-200 mM) aqueous solution, the aqueous pores, on average, have radii which are smaller than the size of an SDS micelle, a key finding that supports the hypothesis put forward in Chapter 2 on how Glycerol may minimize SDS-induced skin barrier perturbation – specifically, Glycerol reduces the size of the aqueous pores induced by aqueous SDS contacting solutions such that SDS micelles, *on average*, are sterically hindered from penetrating into the SC through the aqueous pores, and thereby, from inducing skin barrier perturbation.

Using the values of λ_{SDS} and λ_{SDS+G} reported above, along with $\beta_{SDS} = 1.256\times10^{-3}$ and $\beta_{SDS+G} = 1.699\times10^{-4}$ (see *Table 6-1*), in Eqs.(13) and (14), I obtained: (i) $E^{exp}_{\varepsilon} = 1.2$, *and (ii)* $E^{exp}_{\phi} = 6.16$. These results show that the addition of 10 wt% Glycerol to an aqueous SDS contacting solution reduces the skin porosity associated with the SDS micelles by 17% (=1-$1/E^{exp}_{\varepsilon}$) and the SDS micelle-aqueous pore partition coefficient by 84% (=1-$1/E^{exp}_{\phi}$).

A similar calculation carried out using the truncated normal pore distribution function yielded the following results: (i) $E_{\varepsilon}^{normal}=1.9$, *and (ii)* $E_{\phi}^{normal}=3.89$. [46] Therefore, these results indicate that the addition of 10 wt% Glycerol to an aqueous SDS contacting solution reduces the skin porosity associated with the SDS micelles by 47% (=1-1/E_{ε}^{normal}) and the SDS micelle-aqueous pore partition coefficient by 74% (=1-1/E_{ϕ}^{normal}). Taken together, the exponential and truncated normal distribution functions, which were used to model the size distribution of aqueous pores in the SC, indicate that upon adding 10 wt% Glycerol to an aqueous contacting solution containing 1-200 mM SDS, the SDS micelles are sterically-hindered from partitioning into the aqueous pores, and that the low SDS micelle-aqueous pore partition coefficient is primarily responsible for the low SDS micelle skin penetration and associated skin barrier perturbation.

Table 6-2. Summary of the aqueous pore size distribution characteristics induced by aqueous contacting solutions containing SDS (1-200 mM) (i) and SDS (1-200 mM)+Glycerol (10 wt%) (ii).

	Aqueous Contacting Solutions	
	(i) SDS (1-200 mM)	(ii)SDS (1-200 mM)+ Glycerol (10 wt%)
λ	0.04	0.10
σ	34	18
r_{pore}^{exp}	25	10
r_{pore}^{normal}	27	14
η_{pore}^{exp}	0.46	0.16
η_{pore}^{normal}	0.57	0.30

[46] Note that $E_{\varepsilon}^{exp} \times E_{\phi}^{exp}=1.2\times 6.16=7.39=\beta_{SDS}/\beta_{SDS+G}$, and $E_{\varepsilon}^{normal} \times E_{\phi}^{normal}=1.9\times 3.89=7.39=\beta_{SDS}/\beta_{SDS+G}$.

6.4. Testing the Validity of the Aqueous Pore Size Distribution Functions

In this section, I have conducted tests to determine the validity of using the single-parameter, exponential and truncated normal distribution functions to model the size distribution of aqueous pores in the SC. For this purpose, I computed the product of the Mannitol skin permeability, P, and the average electrical skin resistivity, R, using these distribution functions in the context of an appropriately modified hindered-transport aqueous porous pathway model. This type of analysis can prove unambiguously that if the exponential and the truncated normal distribution functions can accurately *predict* the experimentally determined P×R quantity (see Chapter 2), then, these distribution functions can also appropriately model the size distribution of the aqueous pores in the SC.

To carry out the analysis outlined above, I have modified the theoretical model developed by Tang et al. (25) by utilizing the single-parameter, exponential pore size distribution function, as described in Eqs.(1) and (2), instead of an average aqueous pore radius. Tang et al. have used average values for: (1) the diffusional hindrance parameters that can describe the transport of the permeant, and the ion, respectively, and (2) the porosity of the skin aqueous pores (25). In Eq.(16) below, *average values* for (1) and (2) have been replaced by their *expected values* using the single-parameter, exponential pore size distribution function. In addition, the following assumptions were made: (i) the ions and the hydrophilic permeant access similar aqueous pores based on their sizes in traversing the SC (8, 9, 23-26), and (ii) the tortuosities experienced by the ion and the permeant in traversing the aqueous pores are similar (23-25). This yields:

$$PR = \frac{\int_{per}^{\infty} \gamma(r) H(\kappa)_{per}\, dr}{\int_{ion}^{\infty} \gamma(r) H(\kappa)_{ion}\, dr} \left(\frac{\int_{per}^{\infty} \left(\frac{N_p}{A} \right) \gamma(r) \pi r^2 dr}{\int_{ion}^{\infty} \left(\frac{N_p}{A} \right) \gamma(r) \pi r^2 dr} \right) \left(\frac{D_P^{\infty}}{D_i^{\infty}} \right) \left[\frac{k_B T}{2 z^2 F c_i e_0} \right] \tag{16}$$

where P is the Mannitol skin permeability, R is the average skin electrical resisitivity, D_p^{∞} = 0.672×10^{-5} cm^2/s is the infinite-dilution diffusion coefficient of Mannitol at 25°C, r_{per}=4.44Å is the hydrodynamic radius of Mannitol, D_{ion}^{∞}=1.33×10^{-5} cm^2/s is the infinite-dilution diffusion coefficient of the Na^+ ions in the PBS electrolyte at 25°C, and r_{ion}=2.2Å is the hydrodynamic radius of the Na^+ ion. Note that all these constants were reported previously by Tang et al. (25). In addition, k_B=1.38×10^{-23} J/K is the Boltzmann constant, T=298 K, F=9.6485×10^4 C/mol is the Faraday constant, z = 1 (in the PBS electrolyte solution, since NaCl is the dominant electrolyte), c_{ion} = 0.137 M is the concentration of the Na^+ ions in the PBS electrolyte, e_0 =1.6×10^{-19} C, $\kappa = r_{per/ion}/r$, and $H(\kappa)_{per}$ and $H(\kappa)_{ion}$ are the diffusional hindrance parameters associated with the transport of the permeant and the ion through the aqueous pores in the SC, respectively. Note that Deen et al. (19) have provided expressions for $H(\kappa)_{per}$ and $H(\kappa)_{ion}$ (see Chapter 2). In addition, note that Eq.(16) can be further simplified as follows:

$$\left(\frac{PR}{C} \right) = \frac{\int_{per}^{\infty} \gamma(r) H(\kappa)_{per}\, dr}{\int_{ion}^{\infty} \gamma(r) H(\kappa)_{ion}\, dr} \left(\frac{1 + (1 + r_{per}\lambda)^2}{1 + (1 + r_{ion}\lambda)^2} \right) \frac{\exp(-\lambda r_{per})}{\exp(-\lambda r_{ion})} \tag{17}$$

where $C = \left(\frac{D_P^{\infty}}{D_i^{\infty}} \right) \left[\frac{k_B T}{2 z^2 F c_i e_0} \right]$, $\int \lambda r^2 \exp(-\lambda r) dr = \frac{\exp(-\lambda r)}{\lambda^3} \left[1 + (1 + r\lambda)^2 \right]$ (30), and λ is the exponential pore size distribution parameter (see Eq.(1)).

In addition, by replacing $\gamma(r)$ by $\delta(r)$ in Eq.(16), an expression can be obtained relating *PR/C* to $\delta(r)$. The definite integrals in the expression involving $\delta(r)$ were evaluated numerically using $\sigma_{SDS} = 34$ and for $\sigma_{SDS+G} = 18$ (see *Table 6.2*), which represent the truncated normal pore size distribution functions for (i) SDS (1-200 mM) aqueous contacting solutions, and (ii) SDS(1-200 mM)+10 wt% added Glycerol aqueous contacting solutions (see Section 6.3). The expressions involving $\gamma(r)$ in Eq.(17) were evaluated numerically using $\lambda_{SDS} = 0.04$ and for $\lambda_{SDS+G} = 0.10$ (see *Table 6-2*), which characterize the exponential pore size distribution functions in p-FTS contacted with aqueous solutions (i) and (ii), respectively (see Section 6.3). Carrying out these analyses, it was possible to obtain estimates for *PR/C* (see *Table 6-3*). A close agreement between the experimentally determined and the theoretically predicted *PR/C* values will serve as validation of the single-parameter exponential and truncated normal pore size distributions, $\gamma(r)$ and $\delta(r)$, that were assumed in Eqs.(1) and (3) in Section 6.2.

Table 6-3. Comparison of the theoretically predicted *PR/C* values, using the single-parameter exponential and truncated normal distribution functions to model the size distribution of aqueous pores in the SC, with the experimentally determined *PR/C* values.

Aqueous Contacting Solutions	SDS (1-200 mM)	SDS (1-200 mM) + Glycerol (10 wt%)
$\gamma(r)$ (Exponential) ,r in Å	$0.04\exp(-0.04r)$	$0.1\exp(-0.1r)$
$\delta(r)$ (Truncated Normal) , r in Å	$0.02\exp(-r^2/2312)$	$0.04\exp(-r^2/648)$
PR/C [experimental]	0.73±0.11	0.55±0.09
PR/C [predicted by γ (r)]	0.64	0.44
Error [γ(r) prediction]*	12.3%	18.2%
PR/C [predicted by δ(r)]	0.66	0.5
Error [δ (r) prediction] **	9.6%	9.1%

* Note that the error in the $\gamma(r)$ prediction was calculated using the following relation: Error [γ (r) prediction] = abs[$(PR/C)_{expt} - (PR/C)_{exp}$] / $(PR/C)_{expt}$.

** Note that the error in the $\delta(r)$ prediction was calculated using the following relation: Error [δ(r) prediction] = abs[$(PR/C)_{expt} - (PR/C)_{normal}$] / $(PR/C)_{expt}$.

The results in *Table 6-3* show that: (i) the errors in predicting the *PR/C* values using both pore size distribution functions are less than 20% (8, 18, 19, 23, 25, 26), which lends validity to the modeling of the size distribution of aqueous pores in the SC using the single-parameter, exponential and truncated normal distribution functions, and (ii) the errors in predicting the *PR/C* values for (i) aqueous contacting solutions containing SDS (1-200 mM) and (ii) aqueous contacting solutions containing SDS(1-200 mM)+10wt% added Glycerol are lower for the truncated normal distribution function than for the exponential distribution function. Therefore,

this result indicates that the truncated normal distribution function, $\delta(r)$, models more accurately the size distribution of aqueous pores in the SC of p-FTS contacted with aqueous solutions (i) and (ii) than does the exponential distribution function, $\gamma(r)$.

6.5. Comparison of the Aqueous Pore Size Distribution Models with an Average Aqueous Pore Radius Model

It is instructive to compare the single-parameter, exponential and truncated normal aqueous pore size distribution models with an average aqueous pore radius model that uses an average pore radius, r_{pore}^{avg}, and the skin porosity, ε, as the two parameters in describing the ^{14}C radiolabeled SDS skin penetration data from aqueous contacting solutions containing SDS (1-200 mM) and SDS(1-200 mM)+10 wt% added Glycerol. Note that the average aqueous pore radius model does not allow for the use of separate skin porosities associated with the SDS monomers and the SDS micelles (see Chapter 2).[47] Because: (1) the ratio of the contribution of the SDS monomers to SDS skin penetration per unit SDS monomer concentration to the contribution of the SDS micelles to SDS skin penetration per unit SDS micelle concentration is equal to the ratio of the SDS monomer-aqueous pore partition coefficient to the SDS micelle-aqueous pore partition coefficient (see Section 6.2), and (2) the SDS monomer-aqueous pore partition coefficient is equal to $\left(1-\frac{r_{mon,SDS}}{r_{pore,SDS}^{avg}}\right)^2$, while the SDS micelle-aqueous pore partition

[47] This reflects the fact that the skin porosity associated with the SDS monomers is assumed to be the same as that associated with the SDS micelles (see Chapter 2).

coefficient is equal to $\left(1-\frac{r_{mic,SDS}}{r_{pore,SDS}^{avg}}\right)^2$, which account for steric interactions between the SDS monomer / SDS micelle and the aqueous pore wall (8, 18-26), the key equations corresponding to the average aqueous pore radius model are given by:

$$\left(\frac{\alpha}{\beta}\right)_{SDS}=\frac{\left(1-\frac{r_{mon,SDS}}{r_{pore,SDS}^{avg}}\right)^2}{\left(1-\frac{r_{mic,SDS}}{r_{pore,SDS}^{avg}}\right)^2},\left(\frac{\alpha}{\beta}\right)_{SDS+G}=\frac{\left(1-\frac{r_{mon,SDS+G}}{r_{pore,SDS+G}^{avg}}\right)^2}{\left(1-\frac{r_{mic,SDS+G}}{r_{pore,SDS+G}^{avg}}\right)^2} \tag{18}$$

where $r_{pore,SDS}^{avg}$ is the average aqueous pore radius induced by aqueous SDS (1-200 mM) contacting solutions, $r_{pore,SDS+G}^{avg}$ is the average aqueous pore radius induced by aqueous SDS (1-200 mM)+10 wt% added Glycerol contacting solutions, and all the other variables were defined previously. In addition, because the skin porosity induced by aqueous SDS (1-200 mM) contacting solutions, ε_{SDS}, is not equal to the skin porosity induced by aqueous SDS (1-200 mM)+10 wt% added Glycerol contacting solutions ε_{SDS+G} *(that is,* $\varepsilon_{SDS} \neq \varepsilon_{SDS+G}$*)*, $\beta_{SDS}/\beta_{SDS+G}$ has an explicit dependence on $\varepsilon_{SDS}/\varepsilon_{SDS+G}$. Specifically,

$$\left(\frac{\beta_{SDS}}{\beta_{SDS+G}}\right)=\frac{\left(1-\frac{r_{mic,SDS}}{r_{pore,SDS}}\right)^2\varepsilon_{SDS}}{\left(1-\frac{r_{mic,SDS+G}}{r_{pore,SDS+G}}\right)^2\varepsilon_{SDS+G}} \tag{19}$$

where all the variables were defined previously.

Using the values of α_{SDS}, α_{SDS+G}, β_{SDS}, and β_{SDS+G} listed in *Table 6-1*, along with Eqs.(18) and (19), the average aqueous pore radii and the enhancements in the skin porosity were calculated and are given by: (i) $r^{avg}_{pore,SDS}$ = 32Å, (ii) $r^{avg}_{pore,SDS+G}$ = 22Å, (iii) $E^{avg}_{\varepsilon} = \varepsilon_{SDS}/\varepsilon_{SDS+G}$ = 1.23, and (iv) $E^{avg}_{\phi} = \phi_{SDS}/\phi_{SDS+G}$ = 6.03. Therefore, these results indicate that adding 10 wt% Glycerol to aqueous SDS (1-200 mM) contacting solutions leads to: (i) a significant reduction in the average aqueous pore radius, and (ii) a more significant reduction in the SDS micelle-aqueous pore partition coefficient in comparison to the reduction in the skin porosity associated with the SDS micelles.[48] In addition, the average aqueous pore radii estimates using the average pore radius model are very close to the aqueous pore radii estimates of 33±5Å in SDS (1-200 mM) aqueous contacting solutions and 20±5Å in SDS (1-200 mM)+10 wt% added Glycerol aqueous contacting solutions, calculated using Mannitol skin permeability and average skin electrical resistivity values in the context of a hindered-transport aqueous porous pathway model, as reported in Chapter 2. The average aqueous pore radii estimates obtained using the average pore radius model are also in reasonable agreement (see *Table 6.2*) with the average aqueous pore radii estimates obtained using the single-parameter, exponential and truncated normal pore size distribution functions for p-FTS exposed to SDS (1-200 mM) and to SDS(1-200 mM)+10 wt% added Glycerol.

Next, using $r^{avg}_{pore,SDS}$, $r^{avg}_{pore,SDS+G}$, and E^{avg}_{ε}, the average *PR/C* value, $(PR/C)_{avg}$ was predicted, and then compared to the experimentally determined *PR/C* value (see Section 6.4). Specifically,

---

[48] One can observe that the reduction in the SDS micelle-aqueous pore partition coefficient upon adding 10 wt% Glycerol is equal to $(1\text{-}1/E^{avg}_{\phi})$ = 0.834, and the reduction in the skin porosity associated with the SDS micelles upon adding 10 wt% Glycerol is equal to $(1\text{-}1/E_{\varepsilon}^{avg})$ = 0.187.

$$\left(\frac{PR}{C}\right)_{avg} = E_{\varepsilon}^{avg}\,\frac{H(\kappa)_{SDS}}{H(\kappa)_{SDS+G}} \tag{20}$$

where all the quantities were defined previously. Note that Eq.(20) is based on similar assumptions as those leading to Eq.(16). Using Eq.(20), the $(PR/C)_{avg}$ values predicted by the average aqueous pore size model are: (i) 0.71 for SDS (1-200 mM) aqueous contacting solutions, which deviates by 2.8% from the experimental value of 0.73±0.11, and (ii) 0.59 for SDS (1-200 mM)+10 wt% added Glycerol aqueous contacting solutions, which deviates by 7.3% from the experimental value of 0.55±0.09 (see *Table 6-3*). Therefore, from *Table 6-3* and Eq.(20), the following order of accuracy in predicting the experimentally determined *PR/C* value is obtained (from the most accurate to the least accurate):

$$(PR/C)_{avg} > (PR/C)_{normal} > (PR/C)_{exp}$$

It is interesting to note that the average pore radius model turns out to be more accurate than the single-parameter exponential and truncated normal pore size distribution models in predicting *PR/C*. This probably reflects the fact that the size distribution of aqueous pores in the SC can be better described using several permeants exhibiting a range of permeant radii, rather than using only the two skin permeants considered here – an SDS monomer and an SDS micelle (see Section 6.6).

6.6. Conclusions

^{14}C radiolabeled SDS skin penetration data were analyzed in the context of: (a) a single-parameter, exponential distribution function, and (b) a single-parameter, truncated normal distribution function, to model the size distribution of aqueous pores in the SC of p-FTS exposed

to aqueous contacting solutions containing SDS (1-200 mM) and SDS (1-200 mM)+10 wt% added Glycerol. The analysis using both (a) and (b) above showed that the addition of 10 wt% Glycerol to an aqueous SDS contacting solution significantly shifts the pore size distribution – from larger to smaller pores, resulting in reduced average aqueous pore radii, from 25Å to 10Å for (a), and from 27Å to 14Å for (b). The results of this analysis corroborate the findings reported in Chapter 2 – that Glycerol reduces aqueous pore sizes, which in turn, sterically hinders SDS micelles from penetrating into the SC through these aqueous pores. As a result, the SDS micelle contribution to SDS skin penetration is significantly reduced, which is responsible for mitigating SDS-induced skin barrier perturbation in the presence of 10 wt% added Glycerol. The pore size distribution models considered in this chapter also show that Glycerol has a stronger effect on the SDS micelle-aqueous pore partition coefficient than on the skin porosity associated with the SDS micelles.

The aqueous pore size distribution models (a) and (b) above were also used to independently *predict* the experimentally measured *PR/C* values, where *P* is the Mannitol skin permeability, *R* is the average skin electrical resistivity, and *C* is a constant that depends on the transport characteristics of the permeants (in the present case, the hydrophilic permeant Mannitol and the ions). Both models were found to satisfactorily predict the experimentally determined *PR/C* values (errors < 20%). However, the single-parameter, truncated normal distribution functions *[$\delta(r)=0.02\exp(-r^2/2312)$ for SDS (1-200 mM) aqueous contacting solutions and $\delta(r)=0.04\exp(-r^2/648)$* for *SDS (1-200 mM)+10 wt% added Glycerol aqueous contacting solutions]* performed better in comparison to the exponential distribution functions [$\gamma(r)=0.04\exp(-0.04r)$ *for SDS (1-200 mM) aqueous contacting solutions and* $\gamma(r)= 0.1\exp(-0.1r)$ for *SDS (1-200 mM)+10 wt% added Glycerol aqueous contacting solutions*]. This finding

indicates that a single-parameter, truncated normal distribution function more closely approximates the actual size distribution of aqueous pores in the SC of p-FTS exposed to aqueous contacting solutions of SDS (1-200 mM) and of SDS (1-200 mM)+10 wt% added Glycerol. Finally, an average aqueous pore radius model was developed using similar assumptions involved in developing models (a) and (b), the critical difference being the absence of a size distribution of aqueous pores. The average aqueous pore radius model could predict the experimentally determined *PR/C* value more accurately than either model (a) or (b). This analysis shows that an average aqueous pore radius model can satisfactorily describe the transport of small hydrophilic permeants (Mannitol and ions) through the SC of p-FTS exposed to aqueous contacting solutions (i) and (ii), relative to the single-parameter, exponential and truncated normal aqueous pore size distribution models. Therefore, in order to obtain a more accurate description of the size distribution of the aqueous pores in the SC, a two-parameter distribution function may be considered, with the additional requirement of conducting numerous transdermal permeability studies with a large number of hydrophilic permeants whose molecular radii should span a wide range, for example 2Å to 100Å. These hydrophilic permeants, whose molecular radii are significantly different from each other, can span a greater window of the size distribution of aqueous pores in the SC than was possible using solely the SDS monomers and the SDS micelles, which have molecular radii of 5Å and 19.5Å, respectively, in an aqueous solution.

In the final chapter, Chapter 7, I summarize the main conclusions of the studies conducted in this thesis, and also discuss future research directions in the area of skin barrier perturbation induced by aqueous surfactant/humectant systems.

6.7. References

1. G.K.Menon and P.M.Elias, Morphologic basis for a pore-pathway in mammalian stratum corneum, *Skin Pharmacology*, 10:p. 235-246 (1997).

2. R.M.Raphael, R.E.Waugh, S.Svetina, and B.Zeks, Fractional occurrence of defects in membranes and mechanically driven interleaflet phospholipids transport, *Physical Review B*, 64(5), art. no. 05913, part 1.

3. M.S.Malghani, J.Yang, and J.Wu, Generation and growth of bilayer defects induced by ultrasound, *Journal of the Accoustic Society of America*, 103:p. 1682-1685 (1998).

4. R.Scheuplein and I.Blank, Permeability of the skin, *Physiol. Rev.*, 51:p. 702-747 (1971).
5. P.M.Elias, Lipids and the epidermal permeability barrier, *Arch. Dermatol. Res.*, 270:p. 95-117 (1981).
6. P.W.Wertz and D.E.Downing, "Stratum corneum: biological and biochemical considerations", in *Transdermal Drug Delivery: Developmental issues and research initiatives*. J.Hadgraft and R.H.Guy, Eds. (Marcel Dekker, Inc. 1989), pp. 1-22.
7. R.L.Bronaugh and H.I.Maibach, "In vitro models for human percutaneous absorption", in *Models in Dermatology*. H.I.Maibach et al., Eds. (Karger, Bassel, 1985), Vol. 2, pp. 178-188.
8. A.Tezel, A.Sens, and S.Mitragotri, Description of transdermal transport of hydrophilic solutes during low-frequency sonophoresis based on a modified porous pathway model, *J. Pharm. Sci.*, 92:p. 381-393 (2003).

9. J.Kushner, "Theoretical and experimental investigations of passive and ultrasound-enhanced transdermal drug delivery", Ph.D. thesis, Department of Chemical Engineering, Massachusetts Institute of Technology, Cambridge, MA, USA (2006).
10. R.O.Potts and R.H.Guy, Predicting skin permeability, *Pharm. Res.*, 9:p. 663–669 (1992).
11. P.Moore, "A fundamental investigation of surfactant-induced skin irritation", Ph.D. thesis, Department of Chemical Engineering, Massachusetts Institute of Technology, Cambridge, MA, USA (2002).
12. P.M.Elias and K.R.Feingold, Skin as an organ of protection, in *Fitzpatrick's dermatology in general medicine*. New York:McGraw-Hill, Health Professions Division, c1999.
13. L.D.Rhein, In vitro interactions: Biochemical and biophysical effects of surfactants on skin. In: *Surfactants in Cosmetics* (M.M.Rieger and L.D.Rhein, eds), p. 397-426. Surfactant Science Series, Marcel Dekker, Inc., Vol. 68 (1997).
14. G.Imokawa, Surfactant mildness. In: *Surfactants in Cosmetics* (M.M.Rieger and L.D.Rhein, eds), p. 427-471. Surfactant Science Series, Marcel Dekker, Inc., Vol. 68 (1997).
15. J.A.Faucher and E.D.Goddard, Interaction of keratinous substrates with sodium lauryl sulfate II. Permeation through stratum corneum, *Journal of the Society for Cosmetic Chemists*, 29:p. 339-352 (1978).
16. E.Beraradesca and F.Distante, Mechanisms of skin irritation, *Current problems in dermatology*, 23:p. 1-8 (1995).
17. K.P.Ananthapadmanabhan, K.K.Yu, C.L.Meyers, and M.P.Aronson, Binding of surfactants to stratum corneum, *Journal of the Society of Cosmetic Chemists*, 47:p. 185-200 (1996).

18. W.M.Deen, C.R.Bridges, B.M.Brenner, and B.D.Myers, Heteroporous model of glomerular size selectivity: application to normal and nephritic humans, *Am. J. Physiol.*, 249:p. 374-389 (1985).

19. W.M.Deen, Hindered transport of large molecules in liquid-filled pores, *AIChE Journal*, 33:p. 1409-1425 (1987).

20. J.L.Anderson and J.A.Quinn, Restricted Transport in Small Pores, A model for steric exclusion and hindered particle motion, *Biophysical Journal*, 14:p. 130 (1974).

21. F.G.Smith and W.M.Deen, Electrostatic effects on the partitioning of spherical colloids between dilute bulk solution and cylindrical pores, *Journal of Colloid and Interface Science*, 91:p. 571-590 (1983).

22. F.G.Smith and W.M.Deen, Electrostatic double-layer interactions for spherical colloids in cylindrical pores, *Journal of Colloid and Interface Science*, 78:p. 444-465 (1980).

23. K.D.Peck, A.H. Ghanem, and W.I.Higuchi, Hindered diffusion of polar molecules through and effective pore radii estimates of intact and ethanol treated human epidermal membrane, *Pharmaceutical Research*, 11(9):p. 1306-1314 (1994).

24. K.D.Peck, A.H.Ghanem, and W.I.Higuchi, The effect of temperature upon the permeation of polar and ionic solutes through human epidermal membrane, *Journal of Pharmaceutical Sciences*, 84(8):p. 975-982 (1995).

25. H.Tang, S.Mitragotri, D.Blankschtein, and R.Langer, Theoretical Description of Transdermal Transport of Hydrophilic Permeants: Application to Low-Frequency Sonophoresis, *J. Pharm. Sci.*, 90(5):p. 545-568 (2001).

26. S.Mitragotri, Modeling skin permeability to hydrophilic and hydrophobic solutes based on four permeation pathways, *Journal of Controlled Release*, 86:p. 69-92 (2003).

27. A.Einstein, *Investigation on the Theory of Brownian Movement*, New York: Dover, 58, (1956).

28. R.H.Perry and D.W.Green, *Chemical Engineering Handbook*, New York: McGraw-Hill (1973).

29. D.R.Lide, Editor, *CRC Handbook of Chemistry and Physics*, 75th edition, Boca Raton FL: CRC Press (1994).

30. H.B.Dwight, Tables of Integrals and Other Mathematical Data, 4th edition, New York: Macmillan (1961).

31. P.Moore, S.Puvvada, and D.Blankschtein, Challenging the surfactant monomer skin penetration model: Penetration of sodium dodecyl sulfate micelles into the epidermis, *Journal of Cosmetic Science*, 54:p. 29-46 (2003).

32. P.Moore, A.Shiloach, S.Puvvada, and D.Blankschtein, Penetration of mixed micelles into the epidermis: Effect of mixing sodium dodecyl sulfate with dodecyl hexa (ethylene oxide), *Journal of Cosmetic Science*, 54:p. 143-159 (2003).

Chapter 7

7. Conclusions and Future Research Directions

The primary objective of this thesis was to develop a mechanistic understanding, including quantification, of: (i) how aqueous surfactant solutions, once in contact with the skin, can induce skin barrier perturbation, and (ii) how the phenomenon of surfactant-induced skin barrier perturbation can be effectively mitigated through the addition of humectants to the aqueous surfactant solutions contacting the skin. This objective was accomplished using an integrated analysis involving the following studies: (a) use of diffusion cell bioengineering assays to determine the transdermal fluxes of: (i) ions (through skin electrical current/resistivity measurements), (ii) a hydrophilic model permeant (through Mannitol skin permeability measurements), and (iii) radiolabeled surfactants (through skin radioactivity measurements) upon contact of the skin with surfactant/humectant systems, (b) use of two-photon fluorescence microscopy (TPM) imaging to visualize and quantify the skin morphological modifications that result from contact of the skin with surfactant/humectant systems, and (c) use of theoretical models to determine the nature and the extent of skin barrier perturbation induced by surfactant/humectant systems contacting the skin. The fundamental understanding gained from studies (a)-(c) above on the effects of surfactant/humectant systems on the skin barrier can, in turn, be utilized to design surfactant-based skin care formulations that do not induce an

appreciable extent of skin barrier perturbation. Based on the fundamental understanding gained, I developed an in vitro ranking metric of the effect of surfactant/humectant systems on the skin barrier. This ranking metric was then validated using in vivo patch tests that are capable of quantifying the extent of clinical erythema (skin redness) and skin dryness induced by these surfactant/humectant systems.

In this Chapter, Section 7.1 summarizes the main results and conclusions of the thesis. Section 7.2 discusses potential future research directions in the field of skin barrier perturbation induced by surfactant/humectant systems. Finally, Section 7.3 discusses the potential fundamental and practical impact of this thesis.

7.1. Thesis Summary

Humectants, such as Glycerol, have been shown to mitigate surfactant-induced skin barrier perturbation in vivo. In Chapter 2, a mechanistic investigation of the effect of anionic surfactant (Sodium Dodecyl Sulfate, SDS) micelles contacting the skin from an aqueous solution containing Glycerol (a well-known humectant) on the skin barrier was carried out. When the skin was contacted with an aqueous SDS solution, SDS penetrated into the skin and disrupted this barrier. It is well-established, both in vitro and in vivo, that the SDS skin penetration is dose-dependent, and that it increases with an increase in the total SDS concentration above the Critical Micelle Concentration (CMC) of SDS. However, when Glycerol was added at a concentration of 10 wt% to the aqueous SDS contacting solution, I observed, through in vitro quantitative skin radioactivity assays using ^{14}C radiolabeled SDS, that the dose-dependence in SDS-skin penetration was almost completely eliminated. To rationalize this observation, which may be related to the ability of Glycerol to mitigate SDS-induced skin barrier perturbation in vivo, I

hypothesized that the addition of 10 wt% Glycerol may hinder the ability of the SDS micelles to penetrate into the skin barrier through aqueous pores that exist in the stratum corneum (SC).

To test this hypothesis, I conducted in vitro Mannitol skin permeability and average skin electrical resistivity measurements upon exposure of the skin to: (i) an aqueous SDS contacting solution, and (ii) an aqueous SDS+10 wt% Glycerol contacting solution, both in the context of a hindered-transport aqueous porous pathway model of the SC. My in vitro studies demonstrated that the addition of 10 wt% Glycerol: (1) reduces the average aqueous pore radius resulting from exposure of the skin to the aqueous SDS contacting solution from 33±5Å to 20±5Å, such that a SDS micelle of radius 18.5±1Å (as determined using dynamic light scattering measurements) experiences significant steric hindrance and cannot penetrate into the SC, and (2) reduces the porosity-to-tortuosity ratio in the SC by more than 50%, thereby further reducing the ability of the SDS micelles to penetrate into the SC and perturb the skin barrier.

Certain anionic surfactants like Sodium Cocoyl Isethionate (SCI) are clinically mild to the skin barrier, and do not induce erythema or skin dryness. In Chapter 3, I investigated the effect of SCI, which is an important surfactant ingredient in mild, syndet (synthetic detergent) cleansing bars, on the skin barrier. In vitro and in vivo studies have demonstrated that SCI is mild and less damaging to the skin barrier than soaps and surfactants such as SDS. As we saw in Chapter 2, SDS forms small micelles in aqueous solutions contacting the skin relative to the aqueous pores in the SC, and as a result, the SDS micelles can contribute to SDS skin penetration and induce skin barrier perturbation. In Chapter 3, I investigated the well-known skin mildness of SCI by examining the size of the SCI micelles relative to that of the skin aqueous pores.

For this purpose, I conducted in vitro Mannitol skin permeability and average skin electrical resistivity measurements upon exposure of the skin to an aqueous SCI contacting solution in the context of a hindered-transport aqueous porous pathway model of the SC. These in vitro studies demonstrated that a SCI micelle of radius $33.5 \pm 1 Å$ (as determined using dynamic light scattering measurements) experiences significant steric hindrance and cannot penetrate into the SC through aqueous pores that have an average radius of $29 \pm 5 Å$. This inability of the SCI micelles to contribute to SCI skin penetration and associated skin barrier perturbation is responsible for the observed skin mildness of SCI. Through in vitro quantitative skin radioactivity assays using ^{14}C radiolabeled SCI and pig full-thickness skin (p-FTS), I showed conclusively that SCI skin penetration is *dose independent*, an important finding which provides additional evidence that the *larger* SCI micelles cannot penetrate into the SC through the *smaller* aqueous pores that exist in the SC, and therefore, cannot induce skin barrier perturbation.

Macroscopic measurements, such as average skin electrical resistivity (R) and Mannitol skin permeability (P), in the context of a hindered-transport theory, can be effectively used to *rank* certain chemicals, such as surfactants and humectants commonly encountered in skin-care formulations, based on their ability to perturb the aqueous porous pathways in the SC. The development of this methodology can potentially: (i) reduce, or eliminate altogether, several costly and time consuming testing operations, such as, human and animal testing and trial-and-error screening, and (ii) simultaneously screen and rank many surfactants and humectants for use in skin-care formulations, thereby significantly speeding up the effort and time required to bring new skin-care formulations to the market. In Chapter 4, I developed such an in vitro *ranking metric* using enhancements in the skin electrical current induced by aqueous surfactant/humectant contacting solution – the enhancer, relative to an in vitro PBS aqueous

contacting solution – the control. The results of the in vitro ranking metric was then analyzed using P and R measurements, in the context of a hindered-transport aqueous porous pathway model, to shed light on the enhancements in average pore radius and the pore number density. For this study, I considered aqueous solutions of the following chemicals: (1) humectants – Glycerol and Propylene Glycol, (2) surfactants – SDS (anionic) and $C_{12}E_6$ (nonionic), and (3) a control – PBS (Phosphate Buffered Saline). Utilizing the in vitro ranking metric, I obtained the following ranking order, from the *mildest* to the *harshest*, for the surfactants and the humectants considered above, based on their ability to perturb the aqueous pores in the SC: Glycerol < Propylene Glycol < PBS < $C_{12}E_6$ < SDS.

To substantiate the findings above and to establish the validity of the ranking metric, in vivo *soap chamber measurements* were carried out using aqueous solutions of the surfactants and the humectants described above.[49] Specifically, a patch containing an appropriate treatment solution was applied to the volar forearm of a human volunteer for five hours. Subsequently, the patches were removed and the test site rinsed with water and dried with a towel. Finally, a clinical assessment of erythema (skin redness) was conducted using a chromameter, visual skin dryness was assessed by an expert grader, and transepidermal water loss (TEWL) measurements were conducted using an evaporimeter. These measurements were performed at baseline (no exposure to test formulations), and then again, after the application of the patches, and deviations from the baseline measurements were reported. These in vivo soap chamber measurements showed excellent agreement with the ranking results obtained using the in vitro ranking metric for the aqueous surfactant and humectant contacting solutions considered. In addition, in vivo soap chamber measurements were also carried out for SDS+Glycerol aqueous contacting

[49] The in vivo soap chamber patch studies were conducted by the research group of Dr. Gary Grove of CyberDERM Clinical Studies, in collaboration with Dr. Sidney Hornby of Neutrogena/J&J (see Chapter 4).

solutions. These in vivo measurements indicated that adding Glycerol to a SDS aqueous contacting solution significantly minimizes SDS-induced in vivo skin barrier perturbation, a result which is consistent with the results that I reported in Chapter 2. Specifically, Glycerol reduced the size of the aqueous pores in the SC relative to that of the SDS micelles, such that SDS in micellar form was not able to contribute to SDS skin penetration, which in turn, minimized SDS-induced skin barrier perturbation.

Chapter 5 described the results of an in vitro visualization study of physical SC perturbations induced by aqueous contacting solutions of surfactants and humectants relative to an aqueous control solution (PBS). For this purpose, I carried out two-photon fluorescence microscopy (TPM) imaging studies of p-FTS exposed to aqueous contacting solutions containing: (i) SDS (an anionic surfactant which is a harsh skin agent), (ii) SCI (an anionic surfactant which is a mild skin agent), (iii) Glycerol (a humectant which is a skin beneficial agent), (iv) SDS+Glycerol (a surfactant/humectant mixture), and (v) PBS (the control). TPM is a non-invasive, three-dimensional imaging technique based on two-photon induced nonlinear excitations of fluorophores. TPM has the capability for deep-tissue imaging (up to several hundred micrometers) and reduced photo-damage, which are extremely desirable characteristics for the imaging of opaque and highly scattering tissues, such as, skin (1).

The TPM visualization studies were carried out using Sulforhodamine B (SRB), which is a hydrophilic fluorescent probe that emits a fluorescent signal in the red spectrum. The p-FTS samples were exposed to aqueous contacting solutions (i)-(v) separately, and subsequently, were contacted with aqueous SRB solutions. Following these SRB exposures, the p-FTS samples were dried and visualized using the TPM apparatus. Using a filter set in the TPM apparatus, the emission wavelengths resulting from the presence of SRB in the skin (probe fluorescence) were

collected by the red channel, while the emission wavelengths resulting from the inherent fluorophores present in the skin (skin autofluorescence) were collected by the green channel. Since there is minimal wavelength overlap between the red and the green channels, a quantification of the SRB spatial distribution relative to the SC morphology in the same skin sample, at precisely the same skin spatial locations, was achieved using this technique of dual-channel (the green channel and the red channel) TPM. *Hence, the skin inherent structural features, as delineated in the green channel, provided a fingerprint relative to the probe spatial distribution, as delineated in the red channel.*

The results of this TPM visualization study revealed that SDS induces corneocyte damage (which is expected because SDS has the potential to denature keratins). Intra-corneocyte penetration pathways may be created once SDS "opens-up" the cross-linked keratin structure of the corneocytes through keratin denaturation. Therefore, a group of such damaged adjacent corneocytes, taken together, may exhibit a large number of intra-corneocyte penetration pathways that may result in a localized transport region, LTR. A simultaneous quantitative analysis of the red and the green channel TPM images showed that solution (iii) did not significantly induce corneocyte damage. Therefore, taken together with the results presented in Chapter 2, these dual-channel TPM images provide additional evidence that adding Glycerol to a SDS aqueous contacting solution significantly minimizes the ability of SDS in micellar form to penetrate into the SC and interact with the keratins of the corneocytes and induce corneocyte damage. The dual-channel TPM images of p-FTS exposed to aqueous contacting solutions (ii), (iii), and (v) showed: (a) low SRB penetration into the corneocytes, and consequently, low extent of corneocyte damage, and (b) localization of the SRB probe within the lipid bilayers surrounding the corneocytes of the SC. Of all the five aqueous contacting solutions (i)-(v)

considered in this study, p-FTS exposed to aqueous contacting solution (iii), that is, Glycerol, showed the least extent of SRB probe penetration. This important finding is consistent with the results of the studies reported in Chapters 2 and 4, where I showed that an aqueous contacting solution of Glycerol reduces the porosity-to-tortuosity ratio and the average radius of the aqueous pores through which the hydrophilic SRB probe molecules can penetrate into the SC.

For the five aqueous contacting solutions considered above, most of the SRB probe that penetrates into the skin barrier is present in the SC, and the probe intensity decays significantly as one visualizes the layers in the epidermis below the SC. I have quantified the amount of probe that penetrated into the SC as a function of the SC depth upon contacting p-FTS separately with the five aqueous contacting solutions. This TPM analysis revealed that SDS enhances the probe partition coefficient the most, and that the extent of skin barrier perturbation induced by these chemicals follows the order: (iii) < (v) < (ii) < (iv) < (i), which is consistent with the results of the in vitro ranking metric reported in Chapter 4.

In Chapter 6, I focused my efforts on a quantitative determination and prediction of how surfactants may penetrate into the skin barrier, both in the absence and in the presence of humectants, thereby damaging this barrier. There is evidence that the aqueous pores present in the SC have a size distribution, which may determine how surfactants such as SDS may penetrate into the SC. Recently, Mitragotri et al. attempted to characterize the skin aqueous pore size distribution, in the presence of strong enhancers such as ultrasound, using hydrophilic transdermal permeants of different hydrodynamic radii, such as, Urea and Mannitol, which have hydrodynamic radii which are less than 5Å, as well as Dextran which has a hydrodynamic radius which is larger than 20Å (2). I investigated the size distribution of the aqueous pores in the SC induced by aqueous contacting solutions of SDS and of SDS+10 wt% Glycerol. For this purpose,

I utilized the skin penetration data of SDS in the presence and in the absence of Glycerol, as reported in Chapter 2. The SDS monomers and the SDS micelles were considered as the two skin penetrating species having different effective hydrodynamic radii. The effective hydrodynamic radius of the SDS monomers was determined using the Stokes-Einstein theory. The effective hydrodynamic radius of the SDS micelles was determined in Chapter 2. Due to simplicity and model tractability, a (i) single-parameter exponential distribution function and a (ii) single-parameter truncated normal distribution function (12) were used to represent the pore size distribution of the aqueous pores in the SC induced by SDS and by SDS+ 10 wt% Glycerol aqueous contacting solutions. The pore size distribution parameter for each of these distributions was obtained through a numerical, non-linear integral solution for the SDS monomer-skin partition coefficient and for the SDS micelle-skin partition coefficient, which were, in turn, deduced using a multiple linear regression analysis of the SDS skin penetration data in the presence and in the absence of 10 wt% Glycerol (see Chapter 6). The average pore radii induced by these aqueous contacting solutions were computed as the *means* of the pore size distributions. The next part of the analysis involved establishing the validity of these distributions. For this purpose, I computed the product of the Mannitol skin permeability, P, and the average electrical skin resistivity, R, using these distributions in the context of an appropriately modified hindered-transport aqueous porous pathway model. This analysis proved unambiguously that the pore size distributions derived from the SDS skin penetration data, both in the absence and in the presence of 10 wt% Glycerol, could correctly *predict* the experimentally determined P×R quantity, thereby establishing the validity of these single-parameter distribution functions used in this analysis. In addition, the aqueous pore size distribution analysis, as applied to the SDS skin penetration data in the absence and in the presence of 10 wt% Glycerol, was found to be superior

when compared to an equivalent analysis using average aqueous pore radii values (see Chapter 6 for additional details).

The pore size distributions induced by SDS and by SDS+10 wt% Glycerol aqueous contacting solutions, which were obtained using the analysis outlined above, were significantly different from each other. Adding 10 wt% Glycerol to the SDS aqueous contacting solution induced a shift in these single-parameter pore size distributions – from larger to smaller pores. In fact, upon adding 10 wt% Glycerol to a SDS aqueous contacting solution: (i) the *mean* pore radius calculated using the single-parameter exponential distribution function decreased from 25Å to 10Å, a reduction of 60%, and (ii) the *mean* pore radius calculated using the single-parameter truncated normal distribution function decreased from 27Å to 14Å, a reduction of 47%. Using an average pore radius analysis based on the hindered-transport aqueous porous pathway model (see Chapter 2), I had previously shown that the average pore radii values induced by SDS and by SDS+10 wt% Glycerol are equal to 33Å and 20Å, respectively. The observed difference in the average versus the mean (expected) pore radii values clearly shows that one needs to use the pore size distribution analysis developed here to gain deeper insight into the sizes of the aqueous pores induced by SDS and by SDS+10 wt% Glycerol aqueous contacting solutions. For example, the pore size distribution analysis conducted using the single-parameter exponential distribution function suggests that less than 10% of the SDS micelles can penetrate into p-FTS that was exposed to a SDS+10 wt% Glycerol aqueous contacting solution through the aqueous pores. This is because less than 10% of the aqueous pores have pore radii which are larger than the average SDS micelle hydrodynamic radius in p-FTS exposed to this contacting solution. On the other hand, more than 45% of the SDS micelles can penetrate into p-FTS that was exposed to a SDS aqueous contacting solution, because more than 45% of these

aqueous pores have pore radii which are larger than the effective SDS micelle hydrodynamic radius.

7.2. Future Research Directions

In this section, I discuss potential future research directions aimed at gaining additional insight on the effect of surfactants and humectants on the skin barrier. Some of the proposed research directions involve generalizations of the experimental and the theoretical studies pursued as part of this thesis, while others involve exploring exciting new avenues.

7.2.1. Location of Surfactants in the Skin Barrier

Although we can currently measure the total amount of surfactant, for example, of ^{14}C radiolabeled SDS, that penetrates into the SC, we still do not know the specific location of the surfactant within the SC. Using two-photon fluorescence microscopy, along with the image analysis procedure developed in Chapter 5, I have *indirectly* visualized the effect of surfactants, such as SDS and $C_{12}E_6$, on the lipid bilayers and on the corneocytes of the SC by determining the location of the fluorescent probe (SRB) in the SC that was previously exposed to the aqueous SDS and $C_{12}E_6$ contacting solutions. Furthermore, I have also visualized the effect of the aqueous SDS contacting solution on the SC in the presence of 10 wt% Glycerol.

Using a *fluorescent* surfactant, one could study *directly* the location of the fluorescent surfactant in the SC, as opposed to indirectly visualizing the effect of a surfactant on the SC by studying the location of the fluorescent probe in the SC. However, identifying such a fluorescent surfactant is not without challenges. For example, some of the common Rhodamine-based fluorescent dyes that could be attached to a surfactant molecule may be too large to enable the

surfactant to remain surface active. Additional research should be directed at synthesizing fluorescent surfactant heads or tails, using smaller fluorescent dyes, for example, benzene. Preliminary studies should be conducted to ensure that the fluorescent surfactant does indeed remain surface active, and retains its ability to form micelles at concentrations above the CMC. The next phase of these studies should focus on determining the wavelength at which the surfactant shows fluorescent characteristics. Once known, the appropriate filter may be used in the TPM apparatus to determine the fluorescent surfactant intensity, and thereby, its concentration within the SC (see Chapter 5 for additional details).

The benefits of conducting the study proposed above are clear. One can determine directly how the surfactant partitions, and thereby modifies the structure of the SC, once it has penetrated into the SC, by directly visualizing its location in the SC. Furthermore, such a study may also shed light on how surfactants affect the transport pathways in the SC (lipoidal versus aqueous pore). One may also be able to visualize if a harsh fluorescent surfactant can rupture the corneocyte envelopes and expose keratins within the corneocytes that may then be denatured, thereby eliciting skin barrier perturbation and possibly erythema (see Chapter 4). If the presence of humectants such as Glycerol does not alter the surfactant fluorescent properties, then, one may also be able to *directly* visualize the ability of Glycerol to mitigate the surfactant-induced rupture of the corneocyte envelopes, as was shown *indirectly* through the TPM studies reported in Chapter 5.

7.2.2. Penetration of Surfactants into the Skin Barrier as a Function of the Humectant Concentration in the Contacting Solution

In Chapter 2, I studied the effect of increasing the concentration of SDS in an aqueous contacting solution containing 10 wt% Glycerol. It was observed that at a concentration of 10 wt%, Glycerol does not significantly alter the micellization characteristics of SDS or the micellar solution properties, such as the viscosity. Therefore, at 10 wt%, the ability of Glycerol to mitigate SDS-induced skin barrier perturbation is due to its effect on the SC, specifically by reducing the average pore radius and the porosity-to-tortuosity ratio of the aqueous pores in the SC. However, certain skin-care formulations contain Glycerol at high concentrations, such as 40 wt% (3). At these high concentrations, not only will Glycerol directly impact the skin barrier, but it may also significantly increase the viscosity of the contacting micellar solution, which should further mitigate the extent of surfactant-induced skin barrier perturbation by decreasing the ability of the surfactant to penetrate into the SC from a highly viscous contacting solution. Future research should focus on conducting in vitro and in vivo surfactant-skin penetration studies that can determine the amount of SDS in the epidermis as a function of the concentration of Glycerol (in the range 1 to 40 wt%) in the contacting solution. In addition, these studies can be extended to include other humectants of interest in cosmetic science, such as, Propylene Glycol and Sorbitol.

7.2.3. Penetration of Humectants into the Skin Barrier

Humectant-skin penetration studies by Okamoto et al. have shown that an increase in the amount of Glycerol absorbed by the SC correlates with an increase in the extent of skin moisturization as determined using an evaluation of the skin surface electrical conductance

measured with a high-frequency impedance meter (4). Future research should focus on a systematic investigation of the beneficial impact of humectants on the skin barrier as a function of their concentration in the epidermis. In vitro studies, similar to those discussed in Chapter 4, can be conducted by exposing skin to contacting solutions of radiolabeled humectants such as Glycerol and Propylene Glycol at different concentrations, and subsequently, by assaying for the skin radioactivity to determine the amount of radiolabeled humectant that has penetrated into the epidermis. In addition, in order to determine the amount of humectant that has penetrated into the epidermis in vivo, repeated tape-strippings can be carried out on skin exposed to these contacting solutions of non-radiolabeled humectants. The weight of the collected epidermis can be estimated from a measurement of the weight of a sheet of adhesive tape before and after tape-stripping (4). The humectant can then be extracted from the epidermis on the tape using methanol, and subsequently analyzed using gas chromatography (4).

The studies proposed in this section can reveal if there is a *critical* concentration of humectant in the epidermis which is required for the humectant to beneficially impact the skin barrier, as well as if this critical humectant concentration is different for different humectants.

7.2.4. Effect of Other Additives on Surfactant-Skin Penetration

In Chapter 2, I examined how humectants such as Glycerol affect the extent of SDS-skin penetration. Moore et al. have shown that: (i) a nonionic polymer such as PEO (5), and (ii) a nonionic surfactant such as $C_{12}E_6$ (6), can reduce the amount of SDS that can penetrate into the epidermis by *increasing* the size of the SDS micelles relative to that of the skin aqueous pores, as well as by *reducing* the SDS monomer concentration in the micellar solution contacting the skin. Other additives, for example, cationic polymers such as Poly Vinyl Pyrrolidone (PVP), can be

expected to dramatically reduce the monomer concentration of an anionic surfactant like SDS, as well as to form polymer-surfactant complexes that are too large to penetrate into the epidermis, thereby minimizing the amount of SDS that can penetrate into the epidermis (11). However, one of the main challenges associated with mixing a positively-charged (cationic) polymer like PVP with a negatively-charged (anionic) surfactant like SDS in aqueous solution is the precipitation of the polymer-surfactant complexes that form due to charge neutralization (see below). Preliminary studies that I have conducted with proteins, such as zein which: (i) has positively-charged sites that bind to negatively-charged surfactants like SDS at pH=7-7.4, and (ii) exhibits cooperative binding with the SDS micelles to form protein-surfactant complexes that are soluble in water (22), have shown that there is a dramatic reduction in the penetration of SDS into the skin. In addition to polymers and proteins, other additives of interest are oils, which have been shown to improve the mildness characteristics of surfactant-based skin care formulations (7). It is not clear how the addition of oils mitigates surfactant-induced skin barrier perturbation, although possible mechanisms may include: (i) swelling of surfactant micelles by incorporation of the oil in the hydrophobic micelle cores, thereby preventing penetration of surfactant in micellar form into the skin, and/or (ii) forming an occlusive oil coating on the surface of the SC, thereby minimizing surfactant-skin interactions (7, 11).

As discussed above, one of the main challenges in designing oppositely-charged polymer/protein-surfactant systems is preventing the precipitation of the resulting complexes in aqueous solution. This may be achieved by tuning the solution properties, including the temperature, the viscosity, and the charge density of the complexes. Once a suitable non-precipitating surfactant-additive system is identified, in vitro surfactant skin penetration studies can be conducted, similar to those reported in Chapter 2. Furthermore, (i) in vitro studies that use

the penetration of radiolabeled surfactants into the skin (see Chapter 2), and (ii) in vivo studies that use tape-strippings followed by surfactant extraction with methanol (see Section 7.2.3), can be utilized to determine the amount of surfactant that has penetrated into the skin from contacting solutions containing the appropriate surfactant-additive systems (4).

7.2.5. Penetration of *Charged* Surfactant Micelles into the Skin Barrier in the Presence of Humectants

The hindered-transport aqueous porous pathway model presented in Chapter 2, and the pore size distribution model presented in Chapter 6, did not account for electrostatic repulsions between the negatively-charged SDS micelles and the skin aqueous pore walls, which are also negatively charged (8-10). Indeed, in this case, it was sufficient to consider the Debye-Hückel screening length[50] which was much smaller than the average skin aqueous pore radius (see Chapter 2), which indicated that steric effects should dominate any potential electrostatic effects. However, positively-charged skin permeants, for example, micelles consisting of the cationic surfactant Cetyl Trimethyl Ammonium Bromide (CTAB), may experience an electrostatic attraction with the negatively-charged skin aqueous pore walls at salt concentrations where the Debye-Hückel screening length may become comparable to the average skin aqueous pore radius.[51] Moore et al. have observed that tuning the ionic strength of the surfactant solution and the charge density of the surfactant micelles may lead to electrostatic interactions of the surfactant micelles with the skin aqueous pore walls, which can in turn play a significant role in controlling the penetration of charged surfactants into the skin (11). The role of humectants like

[50] The Debye-Hückel screening length is the length scale associated with the screening of electrostatic interactions between the ions (or between the charged permeants) and the negatively-charged skin aqueous pore walls.

[51] In fact, the negatively-charged SDS micelles may experience an electrostatic *repulsion* with the negatively-charged skin aqueous pore walls at salt concentrations where the Debye-Hückel screening length may become comparable to the average skin aqueous pore radius.

Glycerol, which may affect surfactant solution properties, for example, the solution dielectric constant,[52] at high Glycerol concentrations of 40 wt%, may result in less effective screening, and consequently, in stronger electrostatic interactions between the surfactant micelles and the negatively-charged skin aqueous pore walls.

Future research should focus on conducting experiments that can determine the skin penetration ability of an anionic surfactant like SDS and of a cationic surfactant like CTAB under a systematic variation of the ionic strength of the contacting solution, in the presence and in the absence of Glycerol. This will allow determining the effect of the contacting solution ionic strength on the skin penetration ability of these surfactants. Through Dynamic Light Scattering (DLS) measurements, one can determine the effective hydrodynamic radius of the surfactant micelles in the presence and in the absence of Glycerol (see Chapter 2), and analyze the skin penetration results using an *electrostatic* hindered-transport theory (13-15; see also Section 7.2.7). Such a study may indicate how factors other than the steric size of the surfactant micelles, for example, the micellar charge density, control the ability of charged micelles to access and traverse the skin barrier through the aqueous pores that exist in the skin. Furthermore, the study proposed above can also determine the effect that humectants like Glycerol may exhibit on the ability of charged surfactant micelles to penetrate into the epidermis and induce skin barrier perturbation.

[52] At 25°C, the dielectric constant of water is 78.3, and that of Glycerol is 42.5. Therefore, the higher the concentration of Glycerol in the aqueous contacting solution, the lower is the solution dielectric constant (29). This, in turn, should lead to an increase of the electrostatic interactions, since they are inversely proportional to the magnitude of the dielectric constant (18).

7.2.6. Effect of the Solution pH on Surfactant-Induced Skin Barrier Perturbation in the Presence of Humectants

The ionic charge of many surfactants, such as carboxylate and zwitterionic surfactants, is affected by the solution pH. A change in the pH of the contacting solution can lead to: (i) a change in the micelle shape and aggregation number, and consequently, in the size, of the surfactant micelles present in the contacting solution, and (ii) a change in the CMC, and consequently, in the surfactant monomer concentration (11). Furthermore, tuning the pH of the contacting solution can directly impact the skin barrier. Robbins and Fernee (19) examined the effect of pH on surfactant-induced swelling of isolated epidermis for: (i) the anionic surfactants, SDS and Linear Alkyl Benzenesulfonate (LAS), and (ii) the cationic surfactant Dodecyl Trimethyl Ammonium Bromide (DTAB). Their results showed that for the anionic surfactants, swelling decreased as the solution pH was reduced from a value of 9 (basic) to a value of 3 (acidic). However, the cationic surfactant exhibited an inverse relation between the solution pH values and the extent of epidermal swelling. Ananthapadmanabhan et al. (20) found a direct effect of the solution pH on the SC protein swelling and lipid rigidity, both of which increased as the solution pH was increased from 6.5 (acidic) to 10 (basic).

Therefore, it would be interesting to study the effect of the solution pH on the barrier properties of the skin. Future research should focus on conducting in vitro and in vivo skin barrier measurements, including skin electrical current and transepidermal water loss (TEWL), upon exposing skin to the following aqueous contacting solutions: (i) SDS (1-200 mM), (ii) SDS (1-200 mM)+Glycerol (10 wt%), (iii) Glycerol (10 wt%), and (iv) PBS Control. These measurements should be carried out at acidic (pH=5-6), neutral (pH=7), and basic (pH=9-10)

solution conditions to determine an experimental correlation between the solution pH and surfactant-induced skin barrier perturbation in the presence of humectants.

7.2.7. Developing Models to Incorporate Electrostatic Interactions between the Charged Surfactant Micelles and the Skin Aqueous Pores

The generalized hindered-transport aqueous porous pathway model presented in Chapter 6 incorporates a pore-size distribution to appropriately model the variation in aqueous pore radii induced by SDS and by SDS+10 wt% Glycerol aqueous solutions contacting the skin. However, this model does not incorporate electrostatic interactions between the charged surfactant micelles and the charged skin aqueous pores. Below, I discuss the development of a preliminary model that takes into account electrostatic interactions between a charged permeant and the charged aqueous pore walls in the SC. To test the new model, future research may focus on conducting in vitro skin penetration measurements where the skin is contacted with an aqueous solution containing charged mixed micelles consisting of two surfactants, for example, of the anionic SDS and the nonionic $C_{12}E_6$ surfactants (11). In this case, the micelle charge density can be controlled by tuning the composition of the resulting mixed micelles. In addition, SDS and $C_{12}E_6$ may be radiolabeled with different radioactive tracers, for example, ^{14}C and ^{3}H, such that the amounts of each surfactant in the skin can be measured using dual-radiolabeled skin radioactivity assays (12). Therefore, by measuring the amounts of ^{14}C radiolabeled SDS and ^{3}H radiolabeled $C_{12}E_6$ that have penetrated into the epidermis from aqueous contacting solutions containing charged mixed micelles of tunable charge densities, one can implement the new model presented below to determine the electrostatic interactions between the charged mixed micelles and the charged skin aqueous pore walls.

Deen, and later Zydney (13-17), developed a comprehensive theory to evaluate the permeant *i*-pore partition coefficient ϕ_i between the skin aqueous pores and the aqueous permeant *i* contacting solution. The theory for permeant partitioning into the aqueous pores can predict ϕ_i using molecular characteristics such as the size, the shape, and the electric charge of permeant i and of the aqueous pores. In our case, the permeant is a charged mixed micelle partitioning into the SC through the aqueous pores. The model discussed below uses the following assumptions (16): (i) the center-line approximation, which neglects the effect of variations in the radial position of the permeant on the diffusional hindrance parameter $H(\gamma_i)$, where *'i'* refers to the permeant (see Chapter 2), (ii) the ions are modeled as solid charged spheres of known surface charge density or surface potential, (iii) a known surface charge density or surface potential of the aqueous pores, and (iv) the permeant molecules are modeled as spherical and the pores as cylindrical.

The theoretical analysis incorporates axisymmetric positions of the sphere, and the linearized form of the Poisson—Boltzmann equation is used. Analytical expressions for the potential energy of interaction are obtained, and subsequently used to calculate the equilibrium permeant-pore partition coefficient. The key modeling equation relates the dimensionless interaction energy between the charged permeant and the charged pore wall, V, to the permeant and the pore molecular characteristics, including the permeant and the pore surface charge densities and their sizes (16). Specifically,

$$V = \frac{\left[\frac{4\pi\tau\gamma_i^4 e^{\tau\gamma_i} S_0}{1+\tau\gamma_i}\right]\sigma_s^2 + \left[\frac{4\pi^2\gamma_i^2}{I_1(\tau)}\right]\sigma_s\sigma_c + \left[\frac{\pi^2 h(\tau\gamma_i)}{\tau^2 I_1^{\,2}(\tau)}\right]\sigma_c}{\left[\pi\tau(1+\tau\gamma_i)e^{-\tau\gamma_i} - S_0 h(\tau\gamma_i)\right]} \quad (1)$$

where, I_1 *is the* first-order modified spherical Bessel function of the first kind, $h(\tau\gamma_i) = (1+\tau\gamma_i)e^{-\tau\gamma_i} - (1-\tau\gamma_i)e^{\tau\gamma_i}$, $S_0 = \frac{\pi}{2}\left(\frac{\pi}{\tau}\right)^{1/2} e^{-2\tau}\left[\tau + \frac{15}{16} - \frac{39}{512\tau}\right]$, σ_s is the constant surface charge density of the permeant modeled as a hard sphere, σ_c is the constant surface charge density of the pore wall with the pore modeled as a hollow cylinder, δ is the Debye-Hückel screening length, γ_i is the ratio of the permeant radius, r_i, to the average pore radius, r, and $\tau = \frac{r}{\delta}$.

The dimensional interaction energy, *E(0)*, is related to the dimensionless interaction energy, *V*, in Eq.(1) as follows (15, 16):

$$E(0) = \frac{r\varepsilon}{4\pi}\left[\frac{RT}{F}\right]^2 V \quad (2)$$

where ε is the dielectric constant, R is the universal gas constant, T is the temperature in K, and F is the Faraday unit of charge. All the other quantities appearing in Eq.(2) have already been defined.

Using the center-line approximation, one can write:

$$E(z) = E(0)\exp(\tau z) \quad (3)$$

where $z = r/r_p$ is the dimensionless radial position of the sphere center, and $0 \le z \le 1-\gamma_i$, which accounts for the excluded-volume interactions.

The permeant *i*-pore partition coefficient, ϕ_i, which is the ratio of the concentration of permeant *i* in the pore, C_i^p, to the concentration of permeant *i* in the dilute bulk solution, C_i^∞,can then be evaluated as follows (63, 65):

$$\phi_i = \frac{C_i^p}{C_i^\infty} = 2\int_0^{1-\gamma_i} e^{[-E(z)/kT]} z dz \qquad (4)$$

Equation (4) indicates that in the case of weak electrostatic interactions for which $V \approx 0$, and hence, $E(0) \approx 0$ and $E(z) \approx 0$ (see Eqs.(2) and (3)), the permeant *i*-pore partition coefficient, ϕ_i, is equal to $(1-\gamma_i)^2$, which is the expression resulting from steric interactions that was used in Chapter 2.

The calculation of the pore radius, r_{es}, reflecting the effects of both the long-range electrostatic (e) and the short-range steric (s) interactions, involves an iterative procedure, as illustrated in the flow chart presented in *Figure 7-1*, and discussed in detail below.

Once the pore radius, r_s, is determined based solely on steric considerations (see the appendix in Chapter 2), one can use this r_s value as an input in τ to determine the dimensionless interaction energy, V, using Eq.(1), for both the permeant *i* and for the ion. Subsequently, using Eqs.(2) and (3), one can determine the dimensional interaction energy, $E(z)$, for both the permeant *i* and for the ion. Having determined the two $E(z)$ values in this manner, one can then perform a numerical integration, according to Eq.(4), using a Simpson's algorithm, to determine the pore-partition coefficients of permeant *i* and ion.

The next step in the calculation involves using the corrected permeant-pore partition coefficient value, ϕ_{es} (accounting for both the electrostatic and the steric interactions), to evaluate the diffusional hindrance parameters, $H(\gamma)_{es}$ for permeant i and for the ion, and hence, to recalculate the pore radius, r_{es}, which now accounts for both the steric and the electrostatic interactions. If the two pore radii values, that is, r_s and r_{es}, calculated in this manner (one based solely on steric considerations and the other based on both electrostatic and steric considerations) are sufficiently close in magnitude (one needs to assign a reasonable preset tolerance value *(tol)* for this comparison, see *Figure 7-1*), then, one may conclude that the electrostatic interactions are not important. However, if this difference is significant, then, it is clear that the electrostatic interactions are important for the system considered (either for permeant i or for the ion, or for both), and therefore, need to be accounted for. The calculation will then involve an iterative procedure in which the pore-partition coefficients of permeant i and of the ion, computed considering both the electrostatic and the steric interactions, ϕ_{es}, should be used to recalculate the pore radius, r_{es}, with the iterative procedure continuing until the pore radii values obtained from the previous and from the current iterations are sufficiently close, within the reasonable preset tolerance value, *tol* (see *Figure 7-1*).

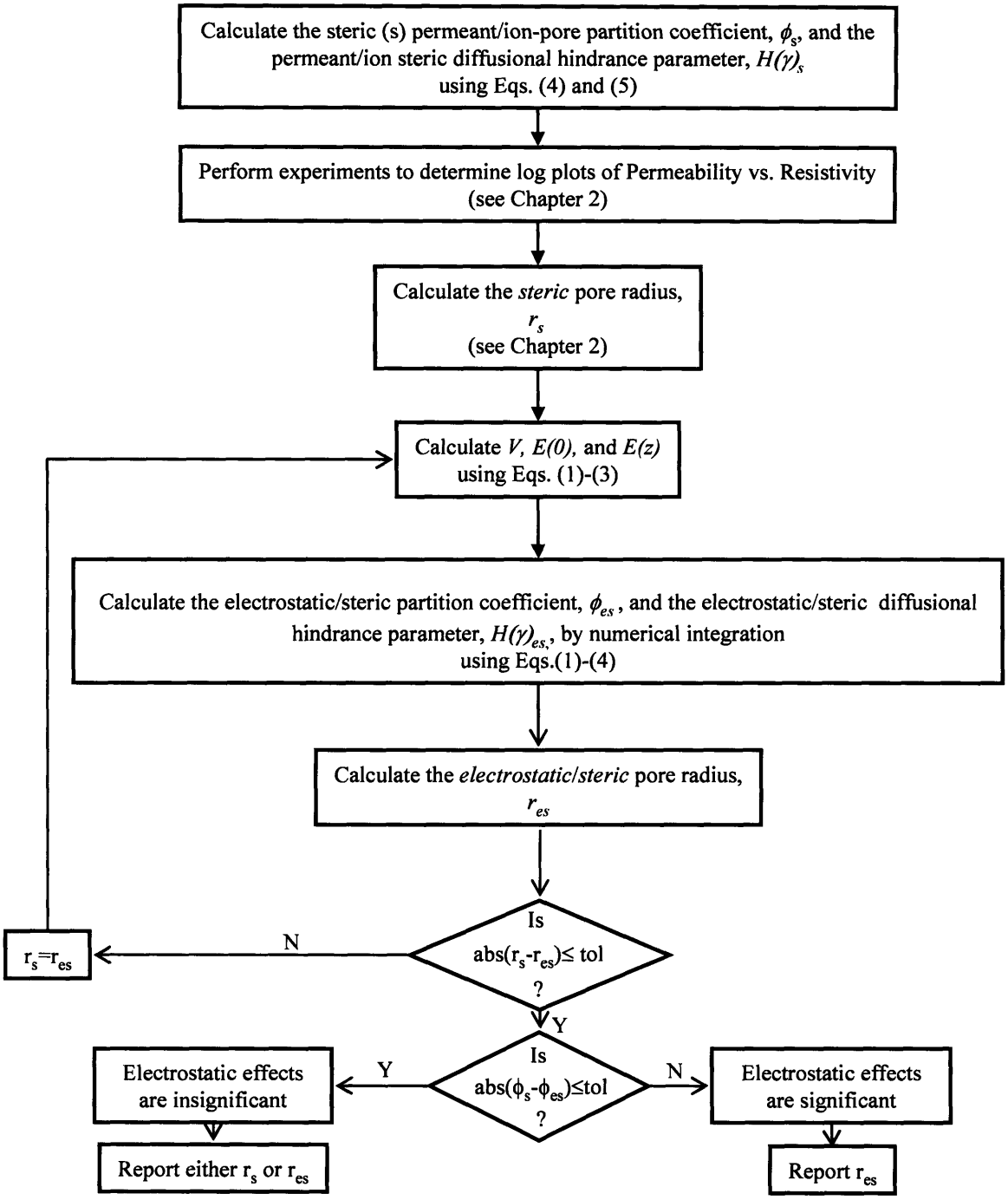

Figure 7-1. Flow Chart of the iteration procedure to determine the skin aqueous pore radius which accounts for both electrostatic and steric interactions between the charged permeant/ion and the charged pore wall. Note that 'tol' denotes the tolerance for error, which is an input to the trial-and-error solution procedure.

7.3. Impact of this Thesis

The fundamental understanding of surfactant-induced skin barrier perturbation in the presence of humectants developed in this thesis is of particular relevance to the cosmetic industry in enabling the formulation of milder, non-drying, skin care products that contain surfactants and humectants. Specifically, at appropriate concentrations, humectants such as Glycerol can mitigate SDS-induced skin barrier perturbation, and associated erythema (skin redness) and skin dryness, by 'closing' aqueous pores through which SDS micelles penetrate into the epidermis. In fact, cosmetic formulators can apply the fundamental knowledge gained in this thesis to design surfactant-based skin care formulations that contain humectants such that the surfactant present in micellar form does not penetrate into the skin and induce erythema and skin dryness, thereby: (i) enhancing consumer experience of their products, and (ii) capturing market share in a rapidly growing $50B market.[53]

The novel two-photon fluorescence microscopy studies that visualize, as well as quantify, skin morphology upon exposure of the skin to surfactant/humectant systems (see Chapter 5), has the potential to be developed into a high-throughput in vivo imaging tool for the screening of new skin-care formulations that can: (i) reduce or eliminate altogether costly and time consuming testing operations used presently by the cosmetic industry, such as, human and animal testing and trial-and-error screening, and (ii) simultaneously screen the skin-mildness potential of many skin-care formulations, thereby significantly speeding up the effort and time required to bring new skin-care formulations to the market.

[53] Note that according to Colin A. Houston & Associates, Inc. (CAHA), a consulting firm in Brewster, NY, the size of the North American market for cosmetic products, ranging from hair-care, skin-care, shaving gels, and cosmeceuticals, was $50B in 2002. Furthermore, with the revival of the US economy in the period 2002-2006, this market has expanded rapidly, both in the size and competitiveness of its products.

In addition to the practical impact on the formulation of mild skin-care products which is the central goal of cosmetic science, this thesis has also advanced fundamental research carried out in the investigative dermatology and related health disciplines through the development of a fundamental microscopic and macroscopic understanding of the skin barrier and its response to the exposure to surfactants in the absence and in the presence of humectants. This fundamental understanding has been achieved by bringing together concepts and methodologies from diverse research areas, including: (i) surfactant physical chemistry in the presence and in the absence of humectants, (ii) aqueous pore size distribution and hindered-transport models of the skin barrier, (iii) two-photon microscopy visualization and quantification of images of the skin morphology, and (iv) in vitro and in vivo bio-engineering assays to quantitatively determine modifications in the skin barrier morphology that result from exposure of the skin to surfactants in the absence and in the presence of humectants.

It is my hope that the fundamental advances made in this thesis on the effect of surfactants and humectants on the skin barrier will stimulate the development of exciting new in vitro and in vivo methods to characterize surfactant-induced skin barrier perturbation in the absence and in the presence of humectants.

7.4. References

1. B. Yu, C.-Y. Dong, P.T.C. So, D. Blankschtein, and R. Langer, In vitro visualization and quantification of oleic acid induced changes in transdermal transport using two-photon fluorescence microscopy, *Journal of Investigative Dermatology*, 117: p. 16-25 (2001).
2. A.Tezel, A.Sens, and S.Mitragotri, Description of transdermal transport of hydrophilic solutes during low-frequency sonophoresis based on a modified porous pathway model, *J. Pharm. Sci.*, 92:p. 381-393 (2003).
3. D.S.Orth and Y.Appa, "Glycerine: a natural ingredient for moisturizing skin", in Dry skin and moisturizers: chemistry and function, M.Loden and H.I.Maibach, Eds. (CRC Press, Boca Raton, 2000), pp. 213-228.
4. T.Okamoto, H.Inoue, S.Anzai, and H.Nakajima, Skin-moisturizing effect of polyols and their absorption into the human stratum corneum, Preprint of the Annual Scientific Meeting for the *Society of Cosmetic Chemists*, NY (1997).
5. P.Moore, S.Puvvada, and D.Blankschtein, Challenging the surfactant monomer skin penetration model: Penetration of sodium dodecyl sulfate micelles into the epidermis, *Journal of Cosmetic Science*, 54:p. 29-46 (2003).
6. P.Moore, A.Shiloach, S.Puvvada, and D.Blankschtein, Penetration of mixed micelles into the epidermis: Effect of mixing sodium dodecyl sulfate with dodecyl hexa (ethylene oxide), *Journal of Cosmetic Science*, 54:p. 143-159 (2003).
7. G.Imokawa, S.Akasaki, Y.Minematsu, and M.Kawai, Importance of intercellular lipids in water-retention properties of the stratum corneum: Induction and recovery study of surfactant dry skin, *Dermatological Research*, 281: p. 45-51 (1989).

8. S.M.Sims, W.I.Higuchi, and V.Srinivasan, Skin alteration and convective solvent flow effects during iontophoresis: I. Neutral solute transport across human skin, *International Journal of Pharmaceutics*, 69:p. 109-121(1991).
9. S.K.Li, A.H.Ghanem, and W.I.Higuchi, Pore Charge distribution considerations in human epidermal membrane electroosmosis, *Journal of Pharmaceutical Sciences*, 88:p. 1044-1049 (1999).
10. S.K.Li, A.H.Ghanem, K.D.Peck, and W.I.Higuchi, Characterization of the transport pathways induced during low to moderate voltage iontophoresis in human epidermal membrane, *Journal of Pharmaceutical Science*, 87: p. 40-48 (1998).
11. P.Moore, "A fundamental investigation of surfactant-induced skin irritation", Ph.D. thesis, Department of Chemical Engineering, Massachusetts Institute of Technology, Cambridge, MA, USA (2002).
12. J.Kushner, "Theoretical and experimental investigations of passive and ultrasound-enhanced transdermal drug delivery", Ph.D. thesis, Department of Chemical Engineering, Massachusetts Institute of Technology, Cambridge, MA, USA (2006).
13. W.M.Deen, Hindered transport of large molecules in liquid-filled pores, *AIChE Journal*, 33:p. 1409-1425 (1987).
14. J.L.Anderson and J.A.Quinn, Restricted Transport in Small Pores, A model for steric exclusion and hindered particle motion, *Biophysical Journal*, 14:p. 130 (1974).
15. F.G.Smith and W.M.Deen, Electrostatic effects on the partitioning of spherical colloids between dilute bulk solution and cylindrical pores, *Journal of Colloid and Interface Science*, 91:p. 571-590 (1983).

16. F.G.Smith and W.M.Deen, Electrostatic double-layer interactions for spherical colloids in cylindrical pores, *Journal of Colloid and Interface Science*, 78:p. 444-465 (1980).

17. W.D.Munch, L.P.Zestar, J.L.Anderson, Rejection of polyelectrolytes from microporous membranes, *Journal of Membrane Science*, 5:p. 77-102 (1979).

18. N.S.Pujar and A.L.Zydney, Charge regulation and electrostatic interactions for a spherical particle in a cylindrical pore, *Journal of Colloid and Interface Science*, 192:p. 338-349 (1997).

19. C.R.Robbins and K.M.Fernee, Some observations on the swelling of human epidermal membrane, *J. Soc. Cosmet. Chem.*, 34:p. 21-34 (1983).

20. K.P.Ananthapadmanabhan, A.Lips, C.Vincent, F.Meyer, S.Caso, A.Johnson, K.Subramanyan, M.Vethamuthu, G.Rattinger, and D.J.Moore, pH-induced alterations in stratum corneum properties, *International Journal of Cosmetic Science*, 25:p. 103-112 (2003).

21. D.R.Lide, Editor, CRC handbook of chemistry and physics, 75th edition, Boca Raton FL: CRC Press (1994).

22. P.Moore, S.Puvvada, and D.Blankschtein, Role of surfactant polar head structure in protein-surfactant complexation: Zein protein solubilization by SDS and by SDS/$C_{12}E_n$ surfactant solutions, *Langmuir*, 19:p. 1009-1016 (2003).